AEROSOL DYNAMICS
IN AN
URBAN ATMOSPHERE

Thesis by
Thomas William Peterson

In Partial Fulfillment of the Requirements

for the Degree of

Doctor of Philosophy

California Institute of Technology

Pasadena, California

1978

(Submitted August 10, 1977)

ACKNOWLEDGEMENTS

I would like to thank my advisor, Dr. John Seinfeld, for his guidance and encouragement, and for proposing the topics considered in this work. I am grateful for the opportunity to have worked in his group, and am indebted to him for the instrumental role he has played in my career.

I would also like to thank all the friends and colleagues who have selflessly contributed to my work and my stay here at Cal Tech. In particular, I would like to thank Dr. Sheldon Friedlander and his research group, for sharing with me their considerable knowledge in air pollution aerosols; Dr. T. E. Ramabhadran and Freddy Gelbard, for their collaboration on the material in Chapters III and IV; and my officemates Sudarshan Kumar and Ken Bencala, for their friendship and for the many times they have discussed my work with me.

I am forever grateful to Lenore Kerner, for so masterfully typing much of this manuscript, and to my mother, Jane Peterson, for typing the remainder of this thesis in less than a week.

Throughout my work, I have been unfailingly encouraged by my wife Shannon, who has always managed to provide the proper perspective on both my successes and failures. I am fortunate to have her as a friend and partner.

Finally, I am grateful to my parents, even more for their direction on matters of the spirit than for the many sacrifices they have made on my behalf.

ABSTRACT

This work examines three aspects of modeling the dynamic behavior of an atmospheric aerosol distribution. First, a steady state, three-dimensional solution of the atmospheric diffusion equation including settling, deposition, and first order removal is presented. The solution is applied to the prediction of airborne concentrations of gaseous and particulate pollutants in the case in which gases are converted to secondary particulate matter. The conversion of sulfur dioxide, nitrogen oxides, and hydrocarbons to particulate sulfate, nitrate, and organics in the Los Angeles atmosphere and urban plume is analyzed.

Second, the dynamic behavior of aerosol size distributions under the influence of coagulation and growth by heterogeneous condensation of gaseous species is studied. Analytical solutions are obtained to the integro-differential equation governing the aerosol size distribution density function. Two modes of coagulation (constant and linear coagulation kernels) and two modes of condensation (growth independent of particle volume and linearly dependent on particle volume) are considered. Also included are simplified mechanisms for nucleation and removal of aerosol particles. The interaction of these mechanisms on aerosol size distributions is elucidated.

Finally, a detailed study of heterogeneous condensation on and reaction within an aerosol particle is undertaken. All important mechanisms governing the transfer of pollutants from the gas to the particulate phase are discussed, and the general framework for describing heterogeneous reaction within the particle is constructed. The model is then used to describe growth and composition change of a marine aerosol exposed to SO_2, NH_3 and H_2SO_4.

TABLE OF CONTENTS

TABLE OF CONTENTS
(continued)

TABLE OF CONTENTS
(continued)

TABLE OF CONTENTS
(continued)

LIST OF FIGURES

LIST OF FIGURES
(continued)

LIST OF FIGURES
(continued)

LIST OF FIGURES
(continued)

LIST OF TABLES

LIST OF TABLES
(continued)

CHAPTER I
INTRODUCTION

Atmospheric pollutants in an urban airshed exist in both gaseous and particulate phases. In addition to direct emissions of both phases of pollutants (primary pollutants), there exist transformation processes from one gaseous pollutant to another and from gaseous to particulate pollutants (secondary pollutants). Considerable work has been done on the development of mathematical models describing the relationship between sources and ambient levels of gaseous pollutants, including the complex chemistry describing the formation of secondary gaseous pollutants. The development of models describing the evolution of atmospheric aerosols is the next step in the process of attempting to understand the physics and chemistry of the polluted atmosphere.

In this Introduction we present the dynamic equation governing aerosol behavior, with emphasis on application to an urban airshed, and discuss the mechanism that each term represents. In so doing, the work that has been undertaken and described in this thesis can be put in proper perspective in relation to a full dynamic model governing the entire system.

The derivation of the general dynamic equation has been presented elsewhere (Chu and Seinfeld, 1975) and shall not be repeated here. The general dynamic equation governs the size-composition distribution function for the atmospheric aerosol. Since there exist no experimental means for measuring

this distribution function, the equation governing an integral moment of the general equation, the particle size distribution function, will be presented and discussed here.

If $n(D_p,\underset{\sim}{r},t)$ is the distribution of particles by particle diameter ($\mu m^{-1}cm^{-3}$), then the general dynamic equation governing $\bar{n}(D_p,\underset{\sim}{r},t)$, the mean size distribution function*, is

$$\frac{\partial \bar{n}}{\partial t} + \sum_{i=1}^{3} \frac{\partial}{\partial r_i}\left(\bar{u}_i \bar{n}\right) + \frac{\partial}{\partial D_p}\left(\bar{I}_o \bar{n}\right) - u_s \frac{\partial \bar{n}}{\partial r_3} =$$

$$\sum_{i=1}^{3} \frac{\partial}{\partial r_i}\left(K_{ii}\frac{\partial \bar{n}}{\partial r_i}\right) + \int_0^{D_p/2^{1/3}} \beta\left((D_p^3 - \tilde{D}_p^3)^{1/3}, \tilde{D}_p\right) \cdot$$

$$\bar{n}\left[(D_p^3 - \tilde{D}_p^3)^{1/3},\underset{\sim}{r},t\right] \cdot \bar{n}(\tilde{D}_p,\underset{\sim}{r},t) \frac{D_p^2}{(D_p^3-\tilde{D}_p^3)^{2/3}} d\tilde{D}_p$$

$$- \int_o^{\infty} \beta(D_p,\tilde{D}_p)\, \bar{n}(D_p,\underset{\sim}{r},t)\, \bar{n}(\tilde{D}_p,\underset{\sim}{r},t)\, d\tilde{D}_p + S_o(D_p,t) + S_1(D_p,\underset{\sim}{r},t) \qquad \text{(Eq. 1)}$$

where

K_{ii} = Turbulent diffusivity in i^{th} direction, $cm^2 sec^{-1}$
I_o = Rate of change of aerosol particle diameter from condensation, $\mu m/sec$
r_i = Spatial variable in i^{th} direction, m
S_o = Rate of homogeneous nucleation, $\mu m^{-1}cm^{-3}sec^{-1}$
S_1 = Rate of particulate sources, $\mu m^{-1}cm^{-3}sec^{-1}$
$\bar{u}_i$ = mean velocity in i^{th} direction, m sec^{-1}
u_s = settling velocity, m sec^{-1}

The terms on the left-hand side of Eq. (1) represent accumulation, convection, growth by condensation and settling, respectively. The terms on the right-hand side represent

*All terms involving products of turbulent fluctuating components of wind and the distribution function have been neglected.

turbulent diffusion (Brownian diffusion has been neglected), coagulation, nucleation and particulate sources, respectively. With appropriate boundary conditions Eq.(1) represents the most general form of the dynamic equation for an aerosol the chemical composition of which is a unique function of its size, spatial position, and time.

If Eq.(1), with appropriate boundary conditions, could be solved numerically for conditions typifying a general urban airshed, the aerosol model would be complete. Our understanding of many components of the model is inadequate, however, the most important components being primary particulate emissions inventories, the chemical mechanisms of gas-to-particle conversion and rates of homogeneous nucleation. A preliminary step in proceeding toward a general urban aerosol model requires both a closer examination of the system as a whole and a more detailed look at the specific mechanisms present in Eq.(1).

Figure 1 is a diagram describing the interaction between gaseous and particulate pollutants. The additional complexity of the particulate system over the gaseous system becomes readily apparent. From primary emissions of gaseous pollutants, the chemical composition and size of an aerosol particulate is altered by diffusion and condensation of condensable vapor species and by absorption of primary gaseous pollutants. Once absorbed, dissolved vapors may participate in heterogeneous reactions. This process of condensation or

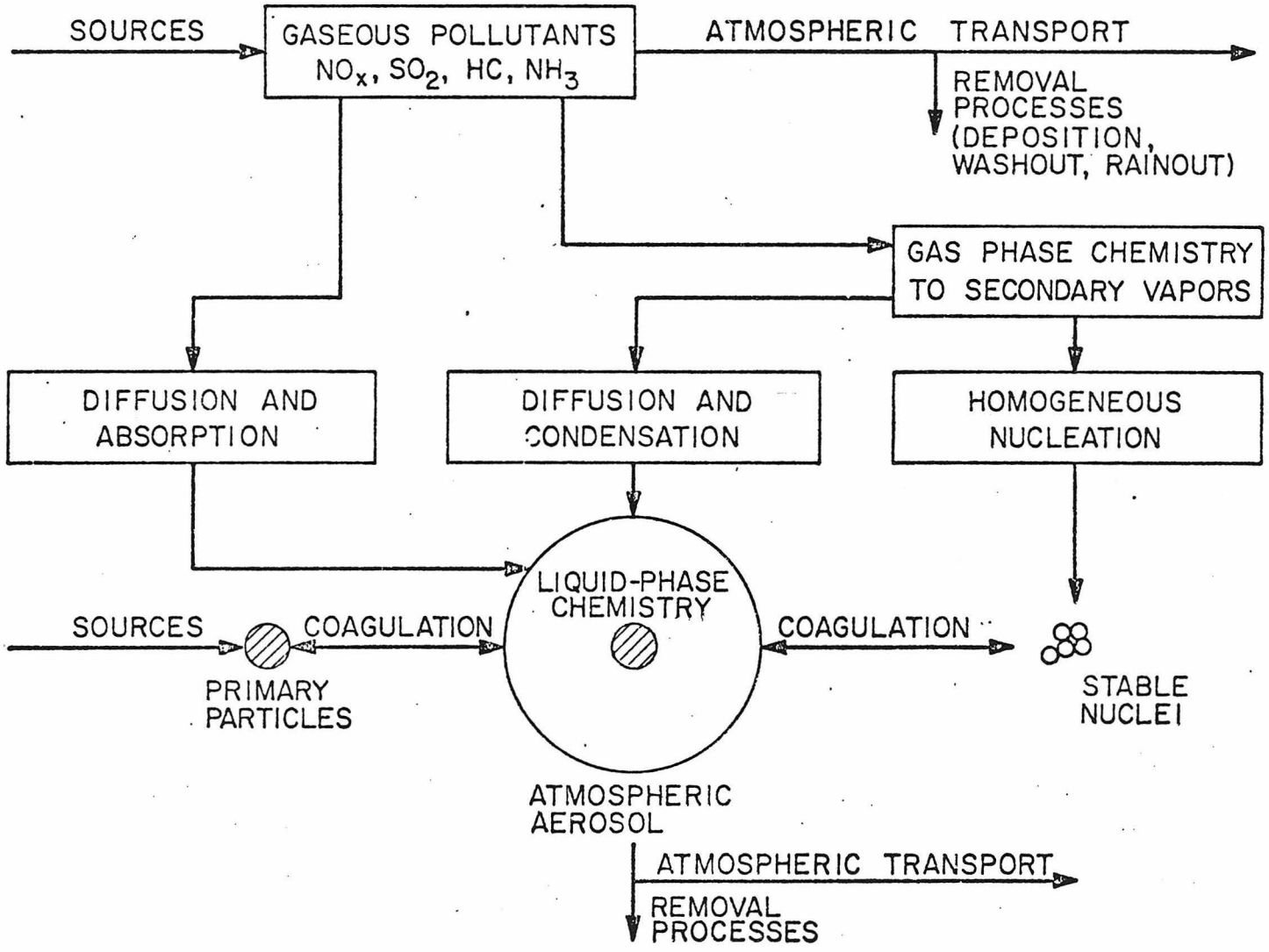

Figure 1

Interaction between Gaseous and Particulate Pollutants

absorption takes place on primary aerosols, background particles such as soil dust and marine aerosol, stable nuclei formed by homogeneous nucleation, or on particles formed by coagulation of any of the above particulate species.

This dynamic process of chemical change, particle growth by condensation and coagulation, and removal and replenishment of particulates takes place as the aerosol mass is transported through an urban airshed. Additional physical removal mechanisms (deposition, settling, washout and rainout) affect the aerosol distribution.

The distribution of aerosols in an atmosphere or smog chamber is affected by different mechanisms, depending upon the aerosol number concentration, the gaseous compounds present and whether the system of interest is open or closed. For example,the description of the evolution of an aerosol distribution in the immediate vicinity of a particulate source must include the coagulation mechanism, whereas the description of an "aged" aerosol far downwind from primary sources can safely neglect coagulation. Similarly, a smog chamber model must include wall losses, whereas an atmospheric model can ignore this term. Table 1 outlines various aerosol/particulate systems that would be of interest to mathematically model, and the important mechanisms for each system.

Before any system can be described in detail, the first and most important step to take is to close all mass and energy balances on the system. In the atmosphere, ambient conditions are such that the isothermal assumption,

TABLE 1

Aerosol Systems of Interest

SYSTEM	IMPORTANT MECHANISMS
Smog Chamber	Condensation, Coagulation, Nucleation, Wall Losses
Power Plant Plume	Convection, Diffusion, Condensation, Coagulation, Nucleation, Sources, Deposition & Settling, Washout & Rainout
Atmosphere	
a.) Near Particulate Sources	Condensation, Coagulation, Nucleation, Sources, Deposition & Settling, Washout & Rainout
b.) Far From Particulate Sources	Convection, Diffusion, Condensation, Sources, Deposition & Settling, Washout & Rainout

while strictly incorrect, can be made without introducing significant errors. Hence, the mass or material balance is the important equation to be considered first.

Chapter II is concerned with such a material balance on gas phase and particulate pollutants. In this chapter, we try to answer the following question: By utilizing simple mechanisms for source, conversion and removal rates in the general mass balance equation for particulate pollutants and gaseous precursors, can we account for the ambient levels of these pollutants measured in the Los Angeles air basin?

Figure 2 outlines the relationship of this work to the processes described in the general dynamic equation. The processes within the dashed line are replaced by a simple model of gas-to-particle conversion with no particle size dependence. As can be seen, we consider the full system, but certain detailed descriptions of the general equation are replaced with "black box" substitutes. These surrogate representations seek to describe the salient features of the mechanism involved while ignoring the detail of the mechanism. In the case of Chapter II, the mechanisms of gas-to-particle conversion are replaced by a simple first order rate of conversion from gaseous pollutants to total particulate mass. By retaining the basic mechanisms of advection, diffusion and removal of both gases and particulates, the question of accountability for reported ambient levels of pollutants can be answered.

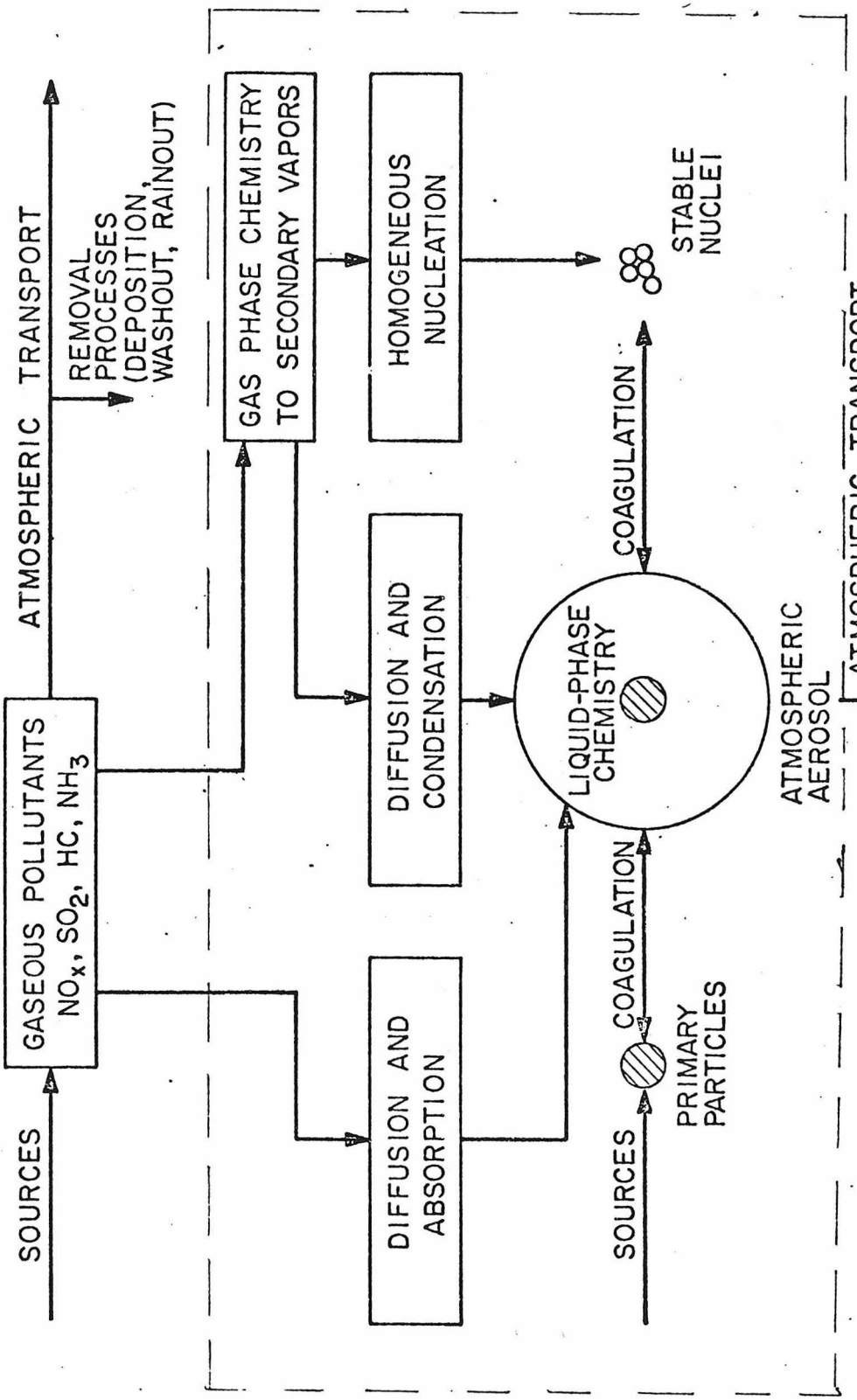

Figure 2

Specific Problem considered in Chapter II

The primary complication in dealing with particulate pollutants over gaseous pollutants is the addition of physical as well as chemical mechanisms affecting the composition and size of the particle. In Chapters III and IV, we derive analytic solutions to the spatially homogeneous general dynamic equation for certain idealized representations of the important mechanisms. The area enclosed by a solid line in Figure 3 represents this work. Again, a surrogate model for the area within the dashed line is utilized. Here, idealized models for the particle growth by condensation are proposed. Mechanistic models are also employed for the processes of coagulation, nucleation and removal.

These analytic solutions are valuable in two ways. First, they provide insight into the intrinsic response of an aerosol particle size distribution to the various mechanisms. Each mechanism (coagulation, condensation, nucleation and removal) affects the time evolution of the distribution in a manner more characteristic of the general mechanism than of the specific details of that mechanism, and these analytic solutions reflect this behavior. Second, the analytic solutions provide a valuable tool for testing numerical solutions of the homogeneous general dynamic equation. Any description of realistic condensation and coagulation processes within the general dynamic equation will require numerical solution of the equation, and these analytic solutions can be used to test the accuracy of the numerical routines.

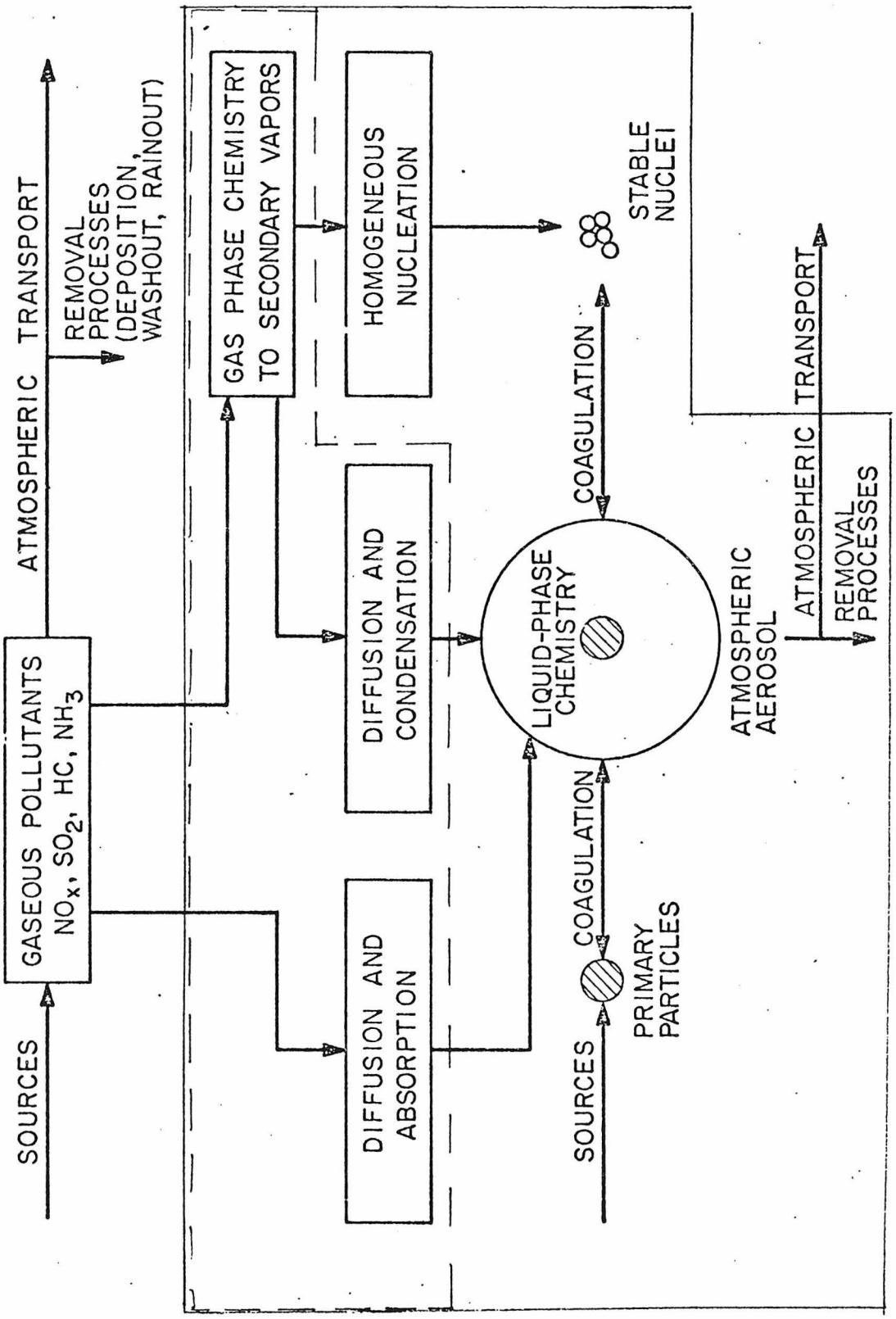

Figure 3

Specific Problem considered in Chapters III and IV

Finally a close examination of the detail of aerosol growth by condensation is undertaken. While Chapters II - IV have utilized representations of this process, Chapter V studies the problem of heterogeneous condensation and liquid phase reaction for a single aerosol droplet. In Figure 4, we see that only a small portion of the total general dynamic equation is considered. However, we have attempted to include in this formulation the details of all suspected processes involved in the mechanism of condensation and reaction of an aerosol droplet.

The inclusion of the detailed processes of particle growth (as discussed in Chapter V) in the complete atmospheric aerosol size distribution calculation will be difficult numerically, particularly if simultaneous coagulation and condensation with heterogeneous reaction are to be modelled. The logical extension of the work of Chapter V would be to the general dynamic equation neglecting coagulation, which, from Table 1, would adequately describe the particle size distribution of an aerosol far from primary sources. The numerical solution of such an equation would involve the independent solution of a discretized size distribution in much the same manner as the simple aerosol particle is treated in Chapter V. Inclusion of primary aerosols, continuous sources and removal mechanisms (in addition to transport processes) can also be made.

This thesis does not attempt to solve the general dynamic equation for an atmospheric aerosol, as given by Eq.1. Rather, we attempt to complete the preliminary steps necessary

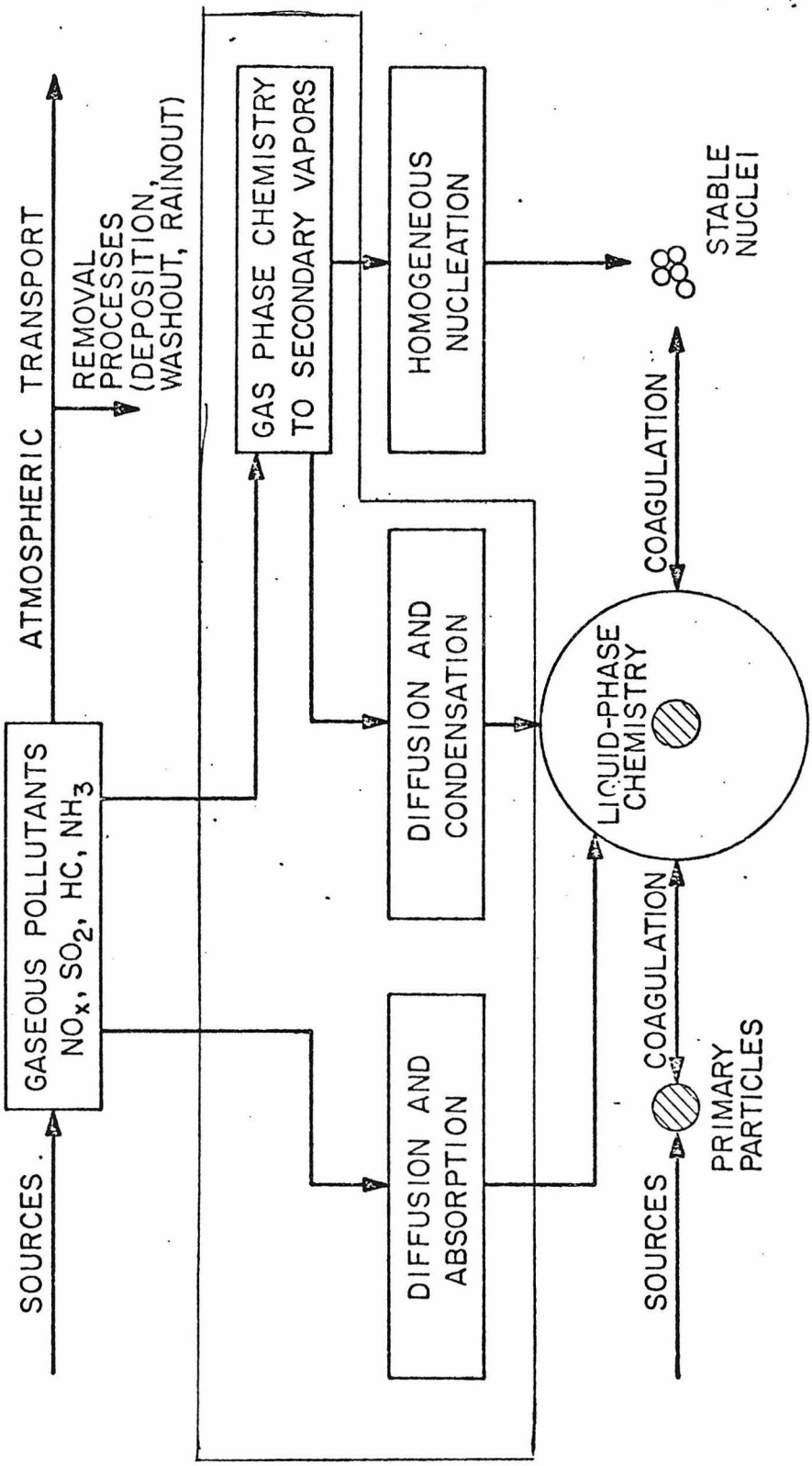

Figure 4

Specific Problem considered in Chapter V

before proceeding to the more general problem. First, we perform a general material balance on particulate pollutants and their gas phase precursors. Second, we derive analytic solutions for special cases of the spatially homogeneous general dynamic equation with idealized mechanisms for condensation, coagulation, nucleation and removal. Finally, we study in detail the problem of heterogeneous condensation and chemical reaction of a single aerosol droplet. Table 2 outlines the material found in each Chapter, and the objectives we attempt to achieve by this work.

TABLE 2

Thesis Outline

CHAPTER	DESCRIPTION	OBJECTIVE
II	Material balance of particulate pollutants and gas phase precursors	Account for measured ambient levels of gaseous and particulate pollutants in Los Angeles Air Basin, using simple mechanisms for conversion, transport and removal.
III-IV	Analytic solution to the spatially homogeneous size distribution function including condensation and coagulation (Ch. III) and condensation, coagulation, nucleation and removal (Ch. IV).	Determine characteristics of particle size distribution function as it is influenced by the mechanisms of condensation, coagulation, nucleation and removal. Provide exact solutions against which numerical routines to solve general dynamic equation can be tested.
V	Heterogeneous condensation on and reaction within an aerosol particle.	Study the processes of growth and chemical change of an aerosol particle. Establish a framework for general growth calculations.

REFERENCES

Chu K.J. and Seinfeld J.H. (1975) Formulation and Initial Application of a Dynamic Model for Urban Aerosols. Atmos. Env. 9,375-402.

CHAPTER II

TRANSPORT, INTERCONVERSION AND REMOVAL OF GASEOUS AND PARTICULATE AIR POLLUTANTS*

*Accepted for publication, Atmospheric Environment, 1977

INTRODUCTION

Most available mathematical models for the steady state or dynamic behavior of air pollutants apply to gaseous pollutants (either chemically inert or reactive) or to particulate matter that may be considered as chemically inert. One of the important atmospheric phenomena that requires elucidation is the conversion of air pollutants from gaseous to particulate form. For example, of particular interest is the so-called urban plume, wherein sulfur dioxide is converted to particulate sulfate, nitrogen oxides to particulate nitrate, and hydrocarbons to particulate organic material. Several recent studies have been reported in which measurements (usually airborne) have been carried out downwind of large urban complexes in order to obtain material balances on gaseous and particulate pollutants (Haagenson and Morris, 1974; Stampfer and Anderson, 1975; Breeding et al., 1975, 1976). A goal of these studies is to determine the relative roles of transport, conversion of gaseous to particulate pollutants, and removal on the overall pollutant material balance downwind of a major urban source.

In the analysis of urban plume data it is desirable to have a mathematical model capable of describing the behavior of both gaseous and particulate pollutants and their interrelations. Eventually such a model would include both gaseous and particulate phases with detailed treatments of gas phase and particulate phase chemistry, as well as size distributions of the particles. However, before attempting to develop a model of full complexity, it is desirable to formulate a "first order" model, one that contains all the major mechanisms influencing the airborne concentrations of gaseous and particulate pollutants but one that does not include the details of atmospheric chemistry and particle size distributions. The processes to

be included are advection, turbulent diffusion, conversion of gaseous species to particulate material, settling, deposition, washout and rainout. Such a "first order" model is in essence a material balance, designed to provide estimates of the fraction of pollutants that still remain airborne at a certain distance downwind of a city, the fraction that has been removed by deposition and gas to particle conversion. The object of this study is to develop and test such a model. It is hoped that the model presented here will subsequently prove to be a convenient tool in the analysis of airborne urban plume pollutant flux measurements.

Although a dynamic model is desirable, a steady state model will enable one to assess if all the major mechanisms are accounted for in analyzing data on urban pollutant fluxes. We will restrict our attention to scales of transport over which the atmospheric diffusion equation is applicable, that is, to problems on the mesoscale. We do not consider "long range" transport because of the recognized inadequacy of the atmospheric diffusion equation in describing macroscale transport. (For consideration of long range transport, the reader is referred to Bolin and Persson, 1975). There exist a variety of numerical models (numerical solutions of the atmospheric diffusion equation) capable of simulating the transport and removal of air pollutants, for example Belot et al. (1976). However, there is considerable attractiveness in an analytical model that does not require numerical solution of the atmospheric diffusion equation. In previous work of this nature, Heines and Peters (1973) have presented analytic steady state solutions for gas phase pollutants with no deposition or depletion due to reaction. Scriven and Fisher (1975) have presented a solution to the steady-state, two-dimensional atmospheric diffusion equation including deposition and first-order removal.

In this work we present a new solution to the steady-state, three-dimensional atmospheric diffusion equation including settling, deposition, and first-order removal and conversion of gaseous to particulate pollutants. The main purpose of the model is to enable the carrying out of overall material balance calculations for the gaseous and particulate phases in the urban atmosphere and in the urban plume. The first half of the study is devoted to the development of the model. The second half is concerned with the application of the model to the Los Angeles atmosphere and to the Los Angeles urban plume. Such a gas-particle material balance has not been carried out previously for Los Angeles. Specifically, we will analyze the conversion of sulfur dioxide, nitrogen oxides, and hydrocarbons to particulate sulfate, nitrate, and organics, respectively, in the Los Angeles atmosphere. A study of this type not only provides estimates of the relative roles of transport and removal mechanisms but also is a necessary prerequisite to more detailed modeling studies involving gases and particles.

FORMULATION OF THE MODEL

The mean concentration $c(x,y,z)$ of a gaseous pollutant or of a primary particulate pollutant under conditions in which the mean wind is aligned with the x-axis and in which a first-order removal process exists can be described by the atmospheric diffusion equation (Monin and Yaglom, 1971),

$$\bar{u} \frac{\partial c}{\partial x} - w_s \frac{\partial c}{\partial z} = \frac{\partial}{\partial y}\left(K_H \frac{\partial c}{\partial y}\right) + \frac{\partial}{\partial z}\left(K_V \frac{\partial c}{\partial z}\right) - kc \qquad (1)$$

where $\bar{u}$ is the mean wind speed in the x-direction, w_s is the settling velocity (non-zero if c represents the concentration of particulate matter), K_H and K_V are the horizontal and vertical eddy diffusivities, and k is the first-order rate constant for removal of the species. The term kc may account for conversion of gaseous pollutants to particulate material (as long as the process may be represented approximately as first-order) or for the removal of either gases or particles by rainout and washout.

We consider the following boundary conditions to (1). The source is taken to be a point source of strength Q_1 (g sec^{-1} located at $x = 0$, $y = 0$, $z = z_s$. (From the solution for this elevated point source we can construct solutions for all other types of sources of interest.) Thus, the $x = 0$ boundary condition is

$$c(0,y,z) = \frac{Q_1}{\bar{u}} \delta(y)\delta(z-z_s) \qquad x = 0 \tag{2}$$

where $\delta(\cdot)$ is the Dirac delta function.

At infinite lateral distance the concentration approaches zero,

$$c(x,y,z) = 0 \qquad y \to \pm \infty \tag{3}$$

There is assumed to exist an elevated inversion base at $z = H_a$ which inhibits vertical turbulent mixing,

$$\frac{\partial c}{\partial z} = 0 \qquad z = H_a \tag{4}$$

Finally, the pollutant may be removed across a layer at height $z = z_a$ through deposition with a deposition velocity v_d,

$$K_V \frac{\partial c}{\partial z} + w_s c = v_d c \qquad z = z_a \tag{5}$$

We note that we select the lower boundary condition at z_a, the height corresponding to that at which a deposition velocity may have been measured. (A typical value of z_a is one meter.) For simplicity we shall assume that K_H and K_V may be taken as constants. The problems associated with this assumption are well known (Monin and Yaglom, 1971). Nevertheless, it is not deemed necessary for our purposes to include the additional complication of spatially dependent K_H and/or K_V.

It is convenient to cast the problem in dimensionless form. To do so we define the dimensionless spatial variables,

$$X = \frac{K_V x}{\bar{u}H^2} \qquad Y = \frac{y}{H} \qquad Z = \frac{z-z_a}{H} \tag{6}$$

where $H = H_a - z_a$. In addition, we define the dimensionless concentration as

$$C = \frac{\bar{u}H^2 c}{Q_1} \tag{7}$$

With these definitions, (1)-(5) become

$$\frac{\partial C}{\partial X} - W\frac{\partial C}{\partial Z} = \beta\frac{\partial^2 C}{\partial Y^2} + \frac{\partial^2 C}{\partial Z^2} - \alpha C \tag{8}$$

$$C(0,Y,Z) = \delta(Y)\delta(Z-Z_s) \tag{9}$$

$$C(X,Y,Z) = 0 \qquad Y \to \pm\infty \tag{10}$$

$$\frac{\partial C}{\partial Z} = 0 \qquad Z = 1 \tag{11}$$

$$\frac{\partial C}{\partial Z} = (N - W)C \qquad Z = 0 \tag{12}$$

where $W = w_s H/K_V$, $\beta = K_H/K_V$, $\alpha = kH^2/K_V$, and $N = v_d H/K_V$. N represents the dimensionless deposition velocity (or mass transfer coefficient).

The details of the solution are given in the Appendix. The solution of (8) - (12) is

$$C(X,Y,Z) = \frac{1}{2\sqrt{\beta\pi X}}\exp(-\alpha X)\exp\left(-\frac{Y^2}{4\beta X}\right)\exp\left(-\frac{WZ}{2}\right)\cdot$$

$$\left\{\sum_{n=1}^{\infty} a_n \Phi_n^{(1)}(Z)\exp\left(-\mu_n^{(1)}X\right) + \sum_{m=1}^{M} c_m \Phi_m^{(2)}(Z)\exp\left(-\mu_m^{(2)}X\right)\right\} \tag{13}$$

where

$$\Phi_n^{(1)}(Z) = \cos(\gamma_n Z) + \delta_n \sin(\gamma_n Z) \tag{14}$$

$$\Phi_m^{(2)}(Z) = \exp(\theta_m Z) - \tau_m \exp(-\theta_m Z) \tag{15}$$

$$\mu_n^{(1)} = \gamma_n^2 + (W/2)^2 \tag{16}$$

$$\mu_m^{(2)} = (W/2)^2 - \theta_m^2 \tag{17}$$

$$\delta_n = (N - W/2)/\gamma_n \tag{18}$$

$$\tau_m = \frac{N-W/2-\theta_m}{N-W/2+\theta_m} \tag{19}$$

$$a_n = \frac{\exp(WZ_s/2)[\cos(\gamma_n Z_s)+\delta_n \sin(\gamma_n Z_s)]}{\frac{1}{2}(1+\delta_n^2)+(1-\delta_n^2)\sin(2\gamma_n)/4\gamma_n+\delta_n \sin^2\gamma_n/\gamma_n} \tag{20}$$

$$c_m = \frac{\exp(WZ_s/2)[\exp(\theta_m Z_s)-\tau_m \exp(-\theta_m Z_s)]}{(\exp(2\theta_m)-1+\tau_m^2(1-\exp(-2\theta_m)))/2\theta_m-2\tau_m} \tag{21}$$

and where the eigenvalue relations are

$$\frac{\tan\gamma_n}{\gamma_n} = \frac{N - W}{\gamma_n^2 + \frac{W}{2}(N - \frac{W}{2})} \qquad n = 1,2,\ldots \tag{22}$$

and

$$\exp(2\theta_m) = \left(\frac{N-W/2-\theta_m}{N-W/2+\theta_m}\right)\left(\frac{W/2+\theta_m}{W/2-\theta_m}\right) \qquad m = 1,2,\ldots, M \tag{23}$$

The finite sum (m = 1 to M) in (13) arises from the finite number (M) of roots of (23), whereas the infinite sum in (13) arises from the infinite number of roots of (22). Whereas (20) and (21) are analytically exact, their inclusion in the solution (13) does not yield a convergent expansion because the coefficients arise from the eigenfunction expansion of the delta function, $\delta(Z-Z_s)$. For computational purposes it is necessary to approximate the delta function by a more well-behaved function and then represent this function by an eigenfunction expansion. This procedure and the resultant equations for a_n and c_m are given in the Appendix.

Equation (13) can be extended to include L point sources, each of strength Q_i located at (X_i, Y_i, Z_s), $i = 1,2,\ldots, L$,

$$C(X,Y,Z) = \frac{1}{2\sqrt{\beta\pi}} \exp\left(-\frac{WZ}{2}\right) \sum_{i=1}^{L} \hat{Q}_i \, U(X-X_i) \exp\left[-\frac{(Y-Y_i)^2}{4\beta(X-X_i)}\right] \frac{\exp(-\alpha(X-X_i))}{\sqrt{X-X_i}} \cdot$$

$$\left\{ \sum_{n=1}^{\infty} a_n \Phi_n^{(1)}(Z) \exp(-\mu_n^{(1)}(X-X_i)) + \sum_{m=1}^{M} c_m \Phi_m^{(2)}(Z) \exp(-\mu_m^{(2)}(X-X_i)) \right\} \qquad (24)$$

where $\hat{Q}_i = Q_i/Q_1$, and $U(X-X_i)$ is the unit step function,

$$U(X-X_i) = \begin{cases} 0 & X < X_i \\ \\ 1 & X \geq X_i \end{cases} \qquad (25)$$

For L area sources, each of strength q_i (g $m^{-2} sec^{-1}$) located in the rectangular regions, $X_{ia} \leq X \leq X_{ib}$, $Y_{ia} \leq Y \leq Y_{ib}$, the mean concentration is given by

$$C(X,Y,Z) = \frac{1}{2} \exp\left(-\frac{WZ}{2}\right) \sum_{i=1}^{L} \hat{q}_i U(X-X_{ia}) \cdot$$

$$\left\{ \sum_{n=1}^{\infty} a_n \Phi_n^{(1)}(Z) \left[I_n^{(1)} - I_n^{(2)} \right] + \sum_{m=1}^{M} c_m \Phi_m^{(2)}(Z) \left[I_m^{(3)} - I_m^{(4)} \right] \right\} \qquad (26)$$

where $\hat{q}_i = q_i/q_1$ and

$$I_n^{(1)} = I(\alpha+\mu_n^{(1)}, (Y-Y_{ia})/2\sqrt{\beta}) \qquad (27)$$

$$I_n^{(2)} = I(\alpha+\mu_n^{(1)}, (Y-Y_{ib})/2\sqrt{\beta}) \qquad (28)$$

$$I_m^{(3)} = I(\alpha+\mu_m^{(2)}, (Y-Y_{ia})/2\sqrt{\beta}) \qquad (29)$$

$$I_m^{(4)} = I(\alpha+\mu_m^{(2)}, (Y-Y_{ib})/2\sqrt{\beta}) \qquad (30)$$

and if $X_{ia} < X \leq X_{ib}$,

$$I(A,B) = \frac{1}{A}\left\{\exp\left(-A(X-X_{ia})\right) \operatorname{erf}\left(B/\sqrt{X-X_{ia}}\right)\right\}$$
$$- \frac{1}{2A}\left\{\exp\left(2B\sqrt{A}\right) \operatorname{erfc}\left(\sqrt{A(X-X_{ia})} + B/\sqrt{X-X_{ia}}\right)\right.$$
$$\left. + \exp\left(-2B\sqrt{A}\right) \operatorname{erfc}\left(-\sqrt{A(X-X_{ia})} + B/\sqrt{X-X_{ia}}\right)\right\} \qquad (31)$$

whereas if $X > X_{ib}$,

$$I(A,B) = \frac{1}{A}\left\{\exp\left(-A(X-X_{ib})\right) \operatorname{erf}\left(B/\sqrt{X-X_{ib}}\right) - \exp\left(-A(X-X_{ia})\right) \operatorname{erf}\left(B/\sqrt{X-X_{ia}}\right)\right\}$$
$$+ \frac{1}{2A}\left\{\exp(2B\sqrt{A})\left[\operatorname{erfc}\left(\sqrt{A(X-X_{ib})} + B/\sqrt{X-X_{ib}}\right)\right.\right.$$
$$\left. - \operatorname{erfc}\left(\sqrt{A(X-X_{ia})} + B/\sqrt{X-X_{ia}}\right)\right]$$
$$\left. + \exp(-2B\sqrt{A})\left[\operatorname{erfc}\left(-\sqrt{A(X-X_{ib})} + B/\sqrt{X-X_{ib}}\right) - \operatorname{erfc}\left(-\sqrt{A(X-X_{ia})} + B/\sqrt{X-X_{ia}}\right)\right]\right\} \qquad (32)$$

where $C(X,Y,Z)$ is the dimensionless concentration based on the area source strength q_1, that is $C(X,Y,Z) = cK_V/q_1H$. If the area source is at ground level, Z_s is set equal to zero in (20) and (21).

Finally, of interest is the solution for an elevated vertical area source, wherein the flux of pollutant from an area in the $x = 0$ plane is specified. This problem may arise in the modeling of an urban plume, where the city is represented as an area source in the $x = 0$ plane that is situated at the downwind end of the area. If the pollutant flux Q_1 (g sec^{-1}) through an area defined by $-b \leq y \leq b$ and $z_1 \leq z \leq z_2$ is specified, then the boundary condition analogous to (2) is

$$c(0,y,z) = \frac{Q_1 U(b+y)U(b-y)U(z-z_1)U(z_2-z)}{2\bar{u}b(z_2-z_1)} \tag{33}$$

In dimensionless form, (33) becomes

$$C(0,Y,Z) = \frac{U(B+Y)U(B-Y)U(Z-Z_1)U(Z_2-Z)}{2B(Z_2-Z_1)} \tag{34}$$

where $Z_1 = (z_1-z_a)/H$, $Z_2 = (z_2-z_a)/H$, and $B = b/H$.

The solution of (8), (10)-(12) and (34) is

$$C(X,Y,Z) = \frac{1}{4B}\exp(-\alpha X)\exp\left(-\frac{WZ}{2}\right)\left\{\operatorname{erf}\left(\frac{B-Y}{2\sqrt{\beta X}}\right) + \operatorname{erf}\left(\frac{B+Y}{2\sqrt{\beta X}}\right)\right\}.$$

$$\left\{\sum_{n=1}^{\infty} \bar{a}_n \Phi_n^{(1)}(Z)\exp\left(-\mu_n^{(1)}X\right) + \sum_{m=1}^{M} \bar{c}_m \Phi_m^{(2)}(Z)\exp\left(-\mu_m^{(2)}X\right)\right\} \tag{35}$$

where $\bar{a}_n = I_1/I_2$, $\bar{c}_m = I_3/I_4$ and

$$I_1 = \frac{1}{\left(\left(\frac{W}{2}\right)^2+\gamma_n^2\right)(Z_2-Z_1)}\left\{\exp\left(\frac{WZ_2}{2}\right)\left[\frac{W}{2}\left(\cos(\gamma_n Z_2) + \delta_n \sin(\gamma_n Z_2)\right)\right.\right.$$

$$\left. + \gamma_n\left(\sin(\gamma_n Z_2) - \delta_n\cos(\gamma_n Z_2)\right)\right] - \exp\left(\frac{WZ_1}{2}\right)\left[\frac{W}{2}\left(\cos(\gamma_n Z_1) + \delta_n \sin(\gamma_n Z_1)\right)\right.$$

$$\left.\left. + \gamma_n\left(\sin(\gamma_n Z_1) - \delta_n\cos(\gamma_n Z_1)\right)\right]\right\} \tag{36}$$

$$I_2 = \frac{1}{2}(1+\delta_n^2) + \frac{(1-\delta_n^2)}{4\gamma_n}\sin(2\gamma_n) + \frac{\delta_n}{\gamma_n}\sin^2\gamma_n \tag{37}$$

$$I_3 = \frac{1}{(Z_2-Z_1)}\left\{\frac{1}{\frac{W}{2}+\theta_m}\left[\exp\left(\left(\frac{W}{2}+\theta_m\right)Z_2\right) - \exp\left(\left(\frac{W}{2}+\theta_m\right)Z_1\right)\right]\right.$$

$$\left. - \frac{\tau_m}{\frac{W}{2}-\theta_m}\left[\exp\left(\left(\frac{W}{2}-\theta_m\right)Z_2\right) - \exp\left(\left(\frac{W}{2}-\theta_m\right)Z_1\right)\right]\right\} \tag{38}$$

$$I_4 = \frac{1}{2\theta_m}\left[\exp(2\theta_m)-1 + \tau_m^2\left(1 - \exp(-2\theta_m)\right)\right] - 2\tau_m \qquad (39)$$

SECONDARY PARTICULATE MATTER

The model developed in the previous section is applicable to gaseous pollutants (with W = 0) and to primary particulate pollutants. Analyses of airborne particulate matter have established that a substantial fraction of the particulate matter often cannot be attributable to primary particulate sources but rather is the consequence of conversion of gaseous species to the particulate phase. Obviously sulfate represents one important example of the gas-to-particle conversion. Let us denote by c_p the airborne concentration of a secondary species (such as sulfate) in the particulate phase. Then, we can write the steady state material balance for this species by analogy to (1) as

$$\bar{u}\frac{\partial c_p}{\partial x} - w_s\frac{\partial c_p}{\partial z} = K_H\frac{\partial^2 c_p}{\partial y^2} + K_V\frac{\partial^2 c_p}{\partial z^2} + \nu_g kc - k_p c_p \qquad (40)$$

where ν_g is the mass ratio of the secondary particulate species to the primary gaseous species which is being converted, and k_p is the first-order rate constant for removal of particulate matter by washout and rainout. In writing (40) in this way, the rate constant k_p is taken to represent only the gas-to-particle conversion process and not other scavenging processes.

Since it is assumed that there are no direct sources of the secondary particulate matter, the boundary conditions for (40) are

$$c_p(0,y,z) = 0 \qquad (41)$$

$$c_p(x,y,z) = 0 \qquad y \to \pm\infty \tag{42}$$

$$\frac{\partial c_p}{\partial z} = 0 \qquad z = H_a \tag{43}$$

$$K_V \frac{\partial c_p}{\partial z} + w_s c_p = v_{d_p} c_p \qquad z = z_a \tag{44}$$

where v_{d_p} is the deposition velocity of the particulate matter.

Equations (40)-(44) can be made dimensionless in the same manner as before, where we use the gaseous emission rate Q_1 in the definition of C_p (since there is no direct emission in this case). The result is

$$\frac{\partial C_p}{\partial X} - W \frac{\partial C_p}{\partial Z} = \beta \frac{\partial^2 C_p}{\partial Y^2} + \frac{\partial^2 C_p}{\partial Z^2} + \nu_g \alpha C - \alpha_p C_p \tag{45}$$

$$C_p(0,Y,Z) = 0 \tag{46}$$

$$C_p(X,Y,Z) = 0 \qquad Y \to \pm\infty \tag{47}$$

$$\frac{\partial C_p}{\partial Z} = 0 \qquad Z = 1 \tag{48}$$

$$\frac{\partial C_p}{\partial Z} = (N_p - W)\, C_p \qquad Z = 0 \tag{49}$$

where $\alpha_p = k_p H^2/K_V$ and $N_p = v_{d_p} H/K_V$.

It is not possible to obtain readily an analytic solution of (45) because of the presence of $C(X,Y,Z)$ accounting for the coupling between the gaseous and particulate phases. Therefore, in studying the behavior of C_p it is necessary to resort to approximate techniques. We define

$$C_p'(X,Z) = \int_{-\infty}^{\infty} C_p(X,Y,Z)\, dY \tag{50}$$

$$\bar{C}_p(X) = \int_0^1 \int_{-\infty}^{\infty} C_p(X,Y,Z)\, dYdZ \tag{51}$$

$$\bar{C}(X) = \int_0^1 \int_{-\infty}^{\infty} C(X,Y,Z)\, dYdZ \tag{52}$$

C_p', $\bar{C}_p$, and $\bar{C}$ each have an important physical interpretation. The total flow G_g(g sec^{-1}) of a gaseous pollutant through the plane at any x is given by

$$G_g = \int_{z_a}^{H_a} \int_{-\infty}^{\infty} \bar{u}c(x,y,z)\, dydz \tag{53}$$

In dimensionless form (the concentration is based on the source strength Q_1) (53) becomes

$$\bar{C}(X) = \frac{G_g}{Q_1} = \int_0^1 \int_{-\infty}^{\infty} C(X,Y,Z)\, dYdZ \tag{54}$$

Thus, $\bar{C}(X)$ is the ratio of the mass flow of pollutant at any X to the source strength. $\bar{C}_p(X)$ can be similarly interpreted. C_p', $\bar{C}_p$, and $\bar{C}$ are also related to the fraction of pollutant lost by deposition, reaction, or rainout and washout. The total mass of pollutant removed by deposition between 0 and x is given by

$$M_d = \int_0^X \int_{-\infty}^{\infty} v_d c(x',y,0)\, dydx' \tag{55}$$

which in dimensionless form becomes

$$M_d/Q_1 = N \int_0^X C'(X',0)\, dX' \tag{56}$$

Similarly, the fraction of the pollutant removed by first-order reaction, M_k/Q_1, is given by

$$M_k/Q_1 = \alpha \int_0^X \bar{C}(X')\, dX' \tag{57}$$

Equivalent relationships can be written for the particulate matter.

If we assume that we can relate $C_p'(X,0)$ and $C_p'(X,1)$ to $\bar{C}_p(X)$ in the following approximate way,

$$C_p'(X,0) = f_o \bar{C}_p(X) \tag{58}$$

$$C_p'(X,1) = f_1 \bar{C}_p(X) \tag{59}$$

then one obtains the following equation governing $\bar{C}_p(X)$,

$$\frac{d\bar{C}_p}{dX} + K\bar{C}_p = \nu_g \alpha \bar{C}(X) \tag{60}$$

$$\bar{C}_p(0) = 0 \tag{61}$$

where $K = N_p f_o - W f_1 + \alpha_p$. The solution of (60) subject to (61) is

$$\bar{C}_p(X) = \nu_g \alpha \exp(-KX) \int_0^X \exp(K\xi)\bar{C}(\xi)\, d\xi \tag{62}$$

For L point sources of gaseous pollutant, (62) becomes

$$\bar{C}_p(X) = \nu_g \alpha \sum_{i=1}^{L} \hat{Q}_i U(X-X_i) \left\{ \sum_{n=1}^{\infty} \frac{a_n \Gamma_n^{(1)}}{K-(\alpha+\mu_n^{(1)})} \left[\exp\left(-(\alpha+\mu_n^{(1)})(X-X_i)\right) - \exp\left(-K(X-X_i)\right) \right] + \sum_{m=1}^{M} \frac{c_m \Gamma_m^{(2)}}{K-(\alpha+\mu_m^{(2)})} \left[\exp\left(-(\alpha+\mu_m^{(2)})(X-X_i)\right) - \exp\left(-K(X-X_i)\right) \right] \right\} \tag{63}$$

where

$$\Gamma_n^{(1)} = \frac{\left[\exp\left(-\frac{W}{2}\right)\left[\gamma_n(\sin\gamma_n - \delta_n\cos\gamma_n) - \frac{W}{2}(\cos\gamma_n + \delta_n\sin\gamma_n)\right] + \frac{W}{2} + \delta_n\gamma_n\right]}{\left(\frac{W}{2}\right)^2 + \gamma_n^2} \tag{64}$$

and

$$\Gamma_m^{(2)} = \frac{\exp\left(\theta_m - \frac{W}{2}\right) - 1}{\theta_m - \frac{W}{2}} - \frac{\tau_m\left[1 - \exp\left(-(\theta_m + \frac{W}{2})\right)\right]}{\theta_m + \frac{W}{2}} \tag{65}$$

The assumptions of (58) and (59) are difficult or impossible to establish experimentally, and no direct means of estimating the values of f_o and f_1 exist. However, as will be discussed later, the scaling of the solution and the values of the particulate deposition velocities cause the solution for $\bar{C}_p(X)$ to be quite insensitive to the values of f_o and f_1. If this were not the case then it would be necessary to consider another means of obtaining a closed form solution for $\bar{C}_p(X)$.

For L area sources, (62) can also be evaluated. For $X_{ia} \leq X \leq X_{ib}$, the solution is

$$\bar{C}_p(X) = \nu_g\alpha \sum_{i=1}^{L} \hat{q}_i U(X-X_{ia})(Y_{ib}-Y_{ia})\left\{\frac{1-\exp(-K(X-X_{ia}))}{K}\left[\sum_{n=1}^{\infty}\frac{a_n\Gamma_n^{(1)}}{\alpha+\mu_n^{(1)}} + \sum_{m=1}^{M}\frac{c_m\Gamma_m^{(2)}}{\alpha+\mu_m^{(2)}}\right]\right.$$
$$- \sum_{n=1}^{\infty}\frac{a_n\Gamma_n^{(1)}}{\alpha+\mu_n^{(1)}}\left[\frac{\exp(-(\alpha+\mu_n^{(1)})(X-X_{ia})) - \exp(-K(X-X_{ia}))}{K-(\alpha+\mu_n^{(1)})}\right]$$
$$\left. - \sum_{m=1}^{M}\frac{c_m\Gamma_m^{(2)}}{\alpha+\mu_m^{(2)}}\left[\frac{\exp(-(\alpha+\mu_m^{(2)})(X-X_{ia})) - \exp(-K(X-X_{ia}))}{K-(\alpha+\mu_m^{(2)})}\right]\right\} \tag{66}$$

and for $X \geq X_{ib}$, the solution is

$$\bar{C}_p(X) = \nu_g \alpha \sum_{i=1}^{L} \hat{q}_i U(X-X_{ia})(Y_{ib}-Y_{ia}) \Bigg\{ \frac{1-\exp(-K(X_{ib}-X_{ia}))}{K} \Bigg(\sum_{n=1}^{\infty} \frac{a_n \Gamma_n^{(1)}}{\alpha+\mu_n^{(1)}}$$

$$+ \sum_{m=1}^{M} \frac{c_m \Gamma_m^{(2)}}{\alpha+\mu_m^{(2)}} \Bigg) + \sum_{n=1}^{\infty} \frac{a_n \Gamma_n^{(1)}}{\alpha+\mu_n^{(1)}} \frac{1}{K-(\alpha+\mu_n^{(1)})} \Bigg(\Big(1-\exp(-(\alpha+\mu_n^{(1)})(X_{ib}-X_{ia}))\Big) \cdot$$

$$\Big(\exp(-(\alpha+\mu_n^{(1)})(X-X_{ib})) - \exp(-K(X-X_{ib}))\Big) - \Big(\exp(-(\alpha+\mu_n^{(1)})(X_{ib}-X_{ia}))$$

$$- \exp\Big(-K(X_{ib}-X_{ia})\Big)\Bigg)$$

$$+ \sum_{m=1}^{M} \frac{c_m \Gamma_m^{(2)}}{\alpha+\mu_m^{(2)}} \frac{1}{K-(\alpha+\mu_m^{(2)})} \Bigg[\Big(1-\exp(-(\alpha+\mu_m^{(2)})(X_{ib}-X_{ia}))\Big) \cdot$$

$$\Big(\exp(-(\alpha+\mu_m^{(2)})(X-X_{ib})) - \exp(-K(X-X_{ib}))\Big) - \Big(\exp(-(\alpha+\mu_m^{(2)})(X_{ib}-X_{ia}))$$

$$- \exp(-K(X_{ib}-X_{ia}))\Big)\Bigg]\Bigg\} \qquad (67)$$

Finally, for the elevated vertical area source in the X = 0 plane, $\bar{C}_p(X)$ is given by

$$\bar{C}_p(X) = \nu_g \alpha \Bigg\{ \sum_{n=1}^{\infty} \frac{\bar{a}_n \Gamma_n^{(1)}}{K-(\alpha+\mu_n^{(1)})} \Big[\exp\Big(-(\alpha+\mu_n^{(1)})X\Big) - \exp(-KX)\Big]$$

$$+ \sum_{m=1}^{M} \frac{\bar{c}_m \Gamma_m^{(2)}}{K-(\alpha+\mu_m^{(2)})} \Big[\exp\Big(-(\alpha+\mu_m^{(2)})X\Big) - \exp(-KX)\Big]\Bigg\} \qquad (68)$$

Equation (68) is of the same form as (63) for a single point source at X = 0, with $\bar{a}_n$ and $\bar{c}_m$ replacing a_n and c_m in (63).

Figure 1 shows $\bar{C}(X)$ vs. X for a hypothetical point source located at X = 0.01, and for α = N = 1. (As will be seen later, the parameters for SO_2

produce values of α and N of order one.) Figure 1 delineates the various contributions to the decay of the species. For these parameter values both deposition and conversion are important, with deposition more efficient near the source where ground-level concentrations are highest.

GASEOUS AND PARTICULATE POLLUTANT MATERIAL BALANCES IN THE LOS ANGELES AIRSHED

The atmospheric aerosol in the Los Angeles airshed is a complex mixture of primary and secondary pollutants. The particulate matter can be characterized as either natural or anthropogenic in origin, with the anthropogenic aerosol being either primary or secondary. Our objective in the remainder of this work is to apply the model just developed to analyze the conversion of gaseous species to secondary particulate matter in the Los Angeles airshed. The basic question to be faced is - can we account for the observed levels of secondary particulate matter, in particular, sulfates, nitrates, and organics, on the basis of the simple first-order gas-to-particle conversion mechanism used in the current model. Such a gross material balance is a necessary prerequisite to more detailed modeling studies of gas/aerosol interactions.

We wish to stress again that the main purpose of the model developed here is to enable the carrying out of overall order-of-magnitude gaseous and particulate material balances in urban atmospheres and in the urban plume. As a steady state model it cannot be used for day-to-day calculations. Nevertheless, it is a tool that can enable one to assess the relative roles of transport, settling, deposition, and gas-to-particle conversion in the urban atmosphere and downwind.

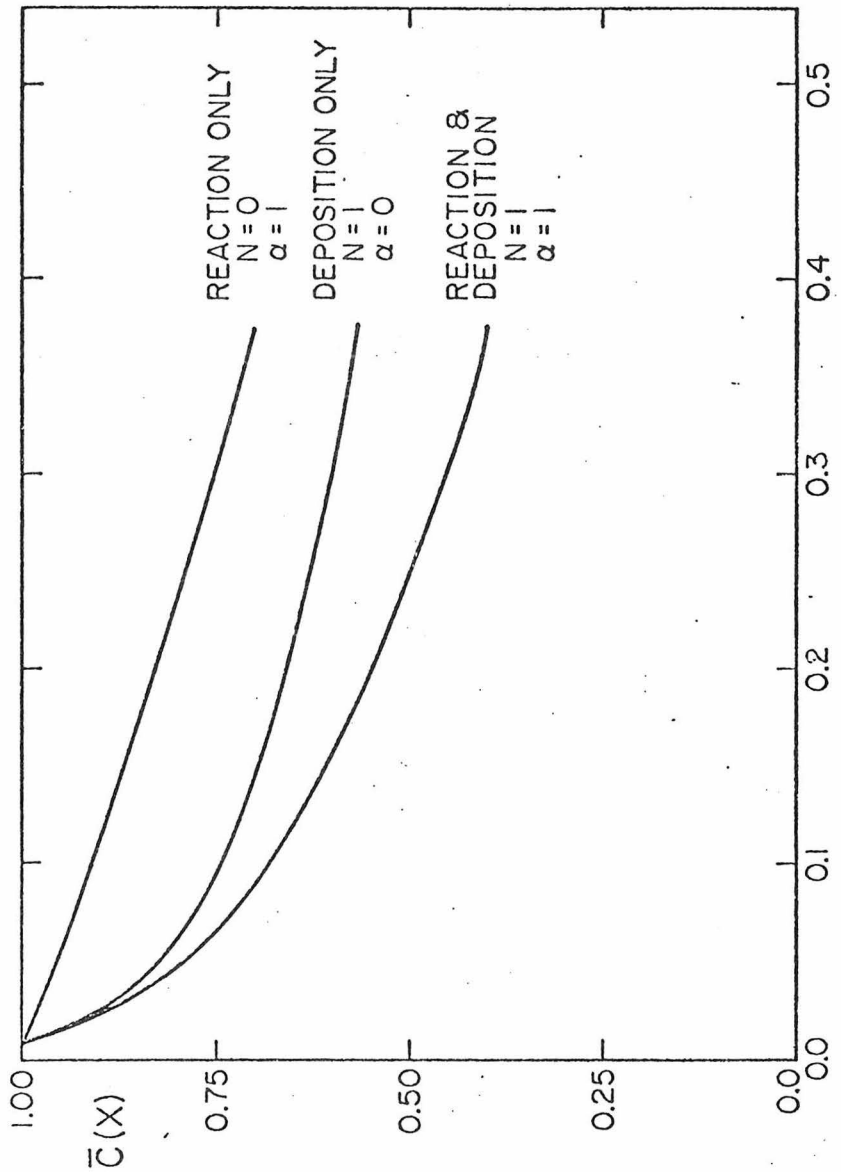

FIGURE 1

Relative Rates of Removal of a Gaseous Pollutant by Reaction and Surface Deposition

The important mechanisms of gas-to-particle conversion in Los Angeles and other urban atmospheres are:

1. Sulfate formation from SO_2
2. Nitrate formation from NO_x ($NO + NO_2$)
3. Particulate organic formation from certain gaseous hydrocarbons.

Whereas sulfates, nitrates and organics do not represent all the constituents of secondary aerosol, they do represent three of the most important species.

The application of the model developed can take either of two forms. First, a cartesian coordinate system can be situated over an airshed such that the x-direction coincides with the average direction of the prevailing wind. Alternatively, a trajectory approach can be taken, wherein the x-direction is defined by the average wind direction at any point, and the y- and z-directions are defined as the directions normal to the x-direction at any point. In such an approach a wind trajectory is "straightened out" and the model is applied as if the trajectory were straight. The trajectory approach was chosen for this application. Obviously, attempting to characterize the "average" meteorology (wind speed and direction, eddy diffusivities, mixing depth, etc.) of the Los Angeles airshed by a few constant parameters is a gross oversimplification. However, because our main objective is to compute the transformation of gaseous species to particulate species over the Basin, a trajectory approach is favored since a full grid-type model is not necessary. Rainout and washout were assumed to be unimportant in this study.

Figure 2 shows the South Coast Air Basin with the selected trajectory superimposed. The prevailing daytime wind can be roughly represented as a sea breeze emanating from the southwest and following the basin contours into the eastern desert region. Figure 2 also shows this trajectory as it appears "straightened out," with the locations of many of the cities within the basin appropriately marked. Also shown on Figure 2 are the three regions of emissions strengths, to be described below.

Table 1 lists the necessary meteorological and transport parameters. The area shown in Figure 2 was chosen because it encompasses a large portion of the heavily polluted region, and many pollutant sources are uniformly distributed throughout this region. We will consider the year 1972 for the simulation.

The emissions of SO_2, NO_x and hydrocarbons are divided into three regions, which are labeled in Figure 2. Region I is predominated by industrial emissions along the coastal areas, from refineries, utilities and chemical plants. Region II is predominated by high-density hydrocarbon and NO_x emissions from mobile sources. Region III encompasses the eastern portion of the basin, wherein emissions are somewhat lower than in the western portion.

An extensive gaseous pollutant emissions inventory has been compiled for 1972 for the Los Angeles basin by TRW (1974). Hunter and Helgeson (1975) and Bartz et al. (1974) have compiled emissions inventories for stationary sources of SO_x and NO_x, respectively, for the year 1974. All provide emissions rates as a function of location, but the spatial resolution of the inventories of Bartz et al. (1974) and Hunter and Helgeson (1975) is more detailed than that found in the inventory by TRW (1974). The source strengths of SO_2, NO_x, and hydrocarbon emissions utilized in this simulation were compiled in the following manner:

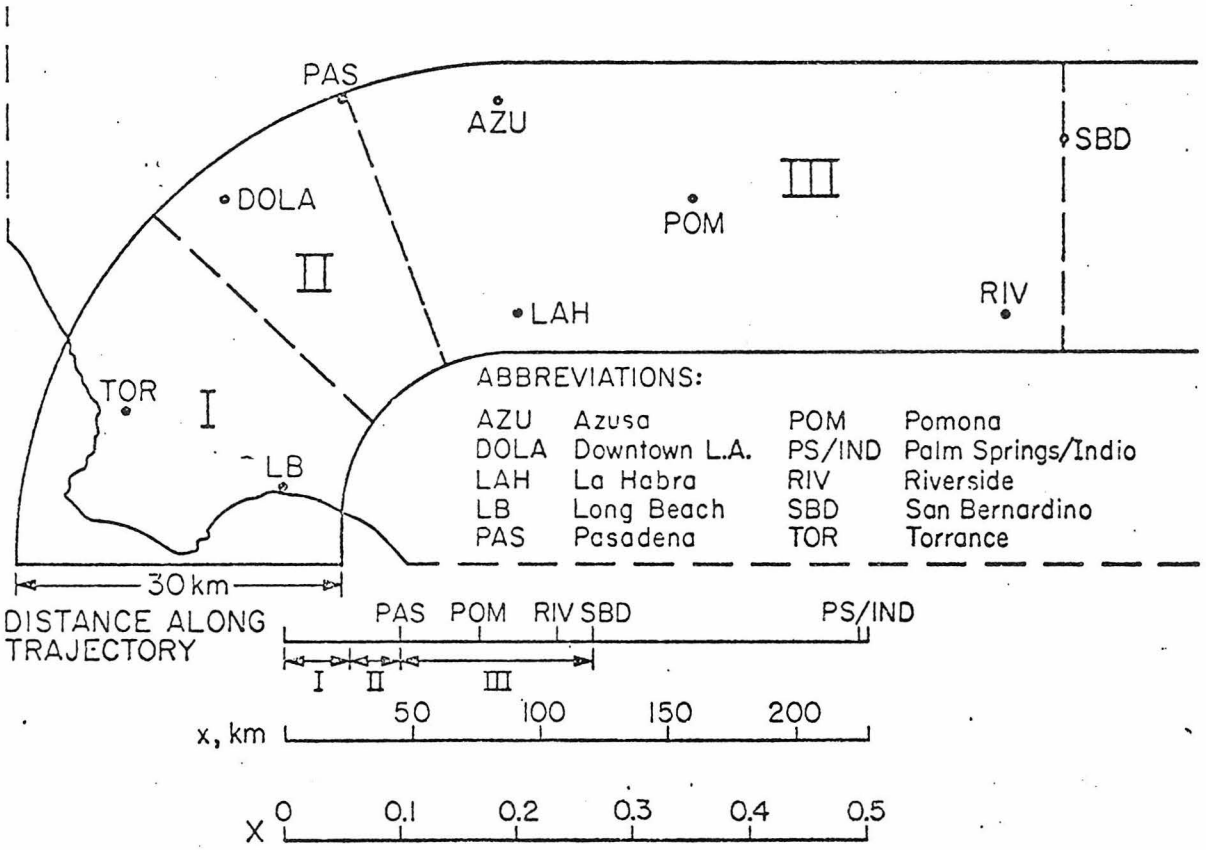

FIGURE 2

South Coast Air Basin with Superimposed Trajectory Representing Typical Daytime Wind Flow Conditions

Table 1. Meteorological Parameters for Los Angeles Trajectory Simulation

Parameter	Value	Source
$\bar{u}$	2.25 m sec^{-1}	ARB (1972)
z_a	1 m	
H_a	1000 m	ARB (1972), Holzworth (1972)
K_V	5 m^2/sec	
K_H/K_V	10	

I. SO_2

a) Total emissions of SO_2 from stationary sources within the trajectory is obtained from TRW (1974).

b) The relative spatial distribution of stationary SO_2 emissions is assumed to be the same as that reported by Hunter and Helgeson (1975).

c) Mobile sources of SO_2 are neglected.

II. NO_x

a) Total emissions of NO_x from stationary and mobile sources within the trajectory are obtained from TRW (1974).

b) The relative spatial distribution of stationary NO_x emissions is assumed to be the same as that reported by Bartz et al. (1974).

c) The relative spatial distribution of mobile NO_x emissions is scaled to traffic count data within each region.

III. Hydrocarbons

a) Total hydrocarbon emissions within the trajectory are obtained from TRW (1974).

b) Since over 90% of all hydrocarbon emissions are auto-related (including petroleum marketing) the relative spatial distribution is scaled to traffic count data within each region.

The emission strengths in the three regions are presented in Table 2. A uniform area source for each pollutant in each region is assumed for simplicity.

SO_2/Sulfate

In the portion of the Los Angeles basin shown in Figure 2, SO_2 emissions are characterized by a coastal area of significant emissions, and a basin-

Table 2. Primary Pollutant Emission Strengths

Region	Area source strength ($kg\ km^{-2} day^{-1}$)		
	SO_2^*	NO_x (as N)	OAHP[+]
I	254	138	19
II	27	180	48
III	18.2	28	6.4

*Elevated sources; z_s = 100 m

[+]Organic aerosol hydrocarbon precursors

wide area of significantly smaller emissions. Since nearly all SO_2 sources are industrial in nature, an emission height of 100 m was assumed for all sources. Table 2 gives the SO_2 source strengths, and Table 3 lists the parameters used in the SO_2/sulfate simulation. For the first order rate constant for conversion of SO_2 to sulfate in Los Angeles, Roberts and Friedlander (1975) report values ranging from 0.05 to 0.15 hr^{-1}, with 0.08 hr^{-1} the average value.

NO_x/Nitrate

All particulate nitrate is assumed to originate from gaseous NO_x. Of the three systems considered, namely SO_2/sulfate, NO_x/nitrate, and organic aerosol precursors and aerosol, the least is known about the details of the conversion of NO_x to nitrate. Although the conversion of SO_2 to sulfate is a complex process that may be heterogeneous and/or homogeneous in nature, the rate of conversion is frequently reported as a first-order reaction in SO_2, and ranges for the first-order rate constant are well established. Likewise, the conversion of NO_x to nitrate may also be heterogeneous and/or homogeneous in nature, however very few studies exist in which conversion rates of NO_x to nitrate have been measured.

Based on the assumption that NO_2 is the only gaseous reactant from which particulate nitrate is formed, a possible mechanism is

$$HO + NO_2 + M \rightarrow HONO_2 + M$$

Demerjian et al. (1974) report a rate constant for this reaction of 1.5×10^{-2} $ppm^{-2}min^{-1}$. Assuming [M] = 10^6 ppm and an [OH] = 10^{-7} ppm (Calvert, 1976), a pseudo-first order rate of NO_2 depletion would be $k \simeq 0.09$ hr^{-1}.

Table 3. Parameters for Los Angeles Trajectory Simulation

Parameter	SO_2/Sulfate	NO_x/Nitrate	OAHP/OA
v_d, cm sec^{-1}	0.7[a,b]	0.5[d]	0.2[d]
w, cm sec^{-1}	0	0	0
k, hr^{-1}	0.08[c]	0.03[e]	4.0[f]
v_{d_p}, cm sec^{-1}	0.03[c]	0.03[h]	0.03[h]
w_p, cm sec^{-1}	0.03[c]	0.03[h]	0.03[h]
ν_g	1.5[g]	4.43[g]	2.0[g]
f_o	0.5[h]	0.5[h]	0.5[h]
f_1	0.1[h]	0.1[h]	0.1[h]

[a]Owers and Powell (1974)

[b]Garland et al. (1974)

[c]Roberts and Friedlander (1975)

[d]Hill (1971)

[e]Clark et al. (1976)

[f]Japar et al. (1974)

[g]Calculated

[h]Assumed

However, $HONO_2$, the product of the first reaction, is still in the gas phase, and hence only under the situation of instantaneous gas/particle conversion of $HONO_2$ would the overall rate be as fast as 0.09 hr^{-1}. It is unlikely that this is the case because of the relatively high vapor pressure of $HONO_2$.

Clark et al. (1976) have measured rates of formation of sulfate and nitrate in ambient air, and the effects of SO_2 levels on these rates. Although an apparent inverse relationship definitely exists between initial SO_2 concentration and nitrate formation, it is worthwhile to attempt a correlation of their data*. Table 4 shows the data of Clark et al. (1976). Runs suffixed by the letter B were runs "doped" with SO_2, and probably yield artificially low rates of nitrate formation. It is found that the rate of nitrate formation versus the product $[O_3][NO_2]$ yields a linear relationship for the doped runs. Assuming this linear relationship holds for undoped samples as well, a second order rate of NO_2 depletion of 0.3 ppm^{-1} hr^{-1} is estimated from run 9A. A pseudo-first order rate of NO_2 depletion of 0.03 hr^{-1} is obtained by assuming an average ozone level of 0.1 ppm. Lower by a factor of three than the rate predicted by the first mechanism, $k = 0.03\ hr^{-1}$ is intuitively more reasonable since it is based on <u>measured particulate</u> nitrate formation, as opposed to gaseous $HONO_2$ formation. In spite of its completely empirical nature, we shall employ the rate reported by Clark et al. (1976) in this study.

Table 2 gives the NO_x source strengths and Table 3 the parameters used in the NO_x/nitrate simulation.

*Although nitrite formation is also reported, its rate in comparison to nitrate formation (generally $\approx$ 0.01 times as fast) is negligible.

Table 4. Nitrate Formation Data of Clark et al. (1976)

Run No.	O_3 (ppm)	NO_2 (ppm)	$d[NO_3^-]/dt$ ($\mu g\ m^{-3} hr^{-1}$)	$-d[NO_2]/dt$ ($ppm\ hr^{-1}$)	k' ($ppm^{-1} hr^{-1}$)
6B	0.013	0.106	0.76	3.0×10^{-4}	0.218
9A	0.022	0.175	3.2	12.65×10^{-4}	0.328
9B	0.022	0.175	1.5	5.93×10^{-4}	0.154
10B	0.021	0.111	1.2	4.74×10^{-4}	0.203

Hydrocarbons/Particulate Organics

Hydrocarbon emission inventories are the most difficult to compile of those for gaseous pollutants because of the variety of sources and because hydrocarbons are a class of pollutants. Hydrocarbons differ in their reactivity to other atmospheric species. Often cited as a mechanism for particulate organic formation is the reaction of certain olefinic species with ozone (Hidy and Burton, 1975; O'Brien et al. 1975ab). It has been postulated that cyclic olefins and straight chain diolefins containing six or more carbon atoms, when reacting with ozone, are converted to species having extremely low vapor pressures that condense rapidly on existing particles. For the purpose of this study we are interested only in emissions of those hydrocarbons that are aerosol organic precursors. An emission inventory for these hydrocarbons has not been carried out. It is therefore necessary to estimate the emissions of those olefinic species. Henceforth we refer to the gaseous precursors as organic aerosol hydrocarbon precursors (OAHP).

Hydrocarbon emissions from auto exhaust and evaporated gasoline, the two largest hydrocarbon sources in 1972, have been estimated (TRW, 1974). From Maynard and Sanders (1969) and Mayrsohn et al. (1975) an extensive analysis of the composition of commercial grade gasoline can be obtained. Estimates of the hydrocarbon composition of automobile exhaust are available (Neligan et al., 1961; McEwen, 1966). Based on estimated hydrocarbon emission rates from automobile exhaust and evaporative losses, and estimates of organic aerosol precursor concentrations of 0.5 percent and 4-5 percent in gasoline and exhaust, respectively, we obtain a total organic aerosol precursor emission rate for each region in Figure 2. Table 2 lists the source strengths for the cyclic and di-olefin aerosol precursors.

It is necessary to estimate a first-order reaction rate constant for conversion of cyclic and di-olefins to organic aerosol. Assuming the aerosol

precursor hydrocarbons to consist of a mixture of cyclopentene and cyclohexene, an average second-order rate constant for reaction with ozone is 40 $ppm^{-1}hr^{-1}$. If an average ozone level is taken to be 0.1 ppm, a first-order rate constant of 4.0 hr^{-1} is obtained. Since adipic acid, a common organic constituent of particulate matter (Hidy and Burton, 1975; O'Brien et al., 1975 ab), has a molecular weight about twice that of its precursor, cyclohexene, we select $\nu_g = 2$. Table 3 gives the necessary parameters for the simulation.

A final comment concerning the consequences of the approximations of (58 and 59) is necessary. The parameters f_0 and f_1 appear only in the definition of K (below (61)), and only as products of particulate deposition and settling terms. Knowing (from the scaling of the equations) that both f_0 and f_1 must be order one, that N_p and W are of order 10^{-2}, and that the range of X is approximately $0 \leq X \leq 0.5$, the term $\exp[-K(X-X_i)]$ in (63) is very nearly one, regardless of choice of f_0 and f_1. This observation was verified computationally by selection of widely varying values of f_0 and f_1.

Material Balance Results

Figure 3 presents the dimensionless ground-level concentrations of SO_2, gaseous nitrogen and organic aerosol hydrocarbon precursors (OAHP). The numerical factors necessary to convert the dimensionless concentrations to values in $\mu g\ m^{-3}$ for each of the three primary pollutants are given in the caption to Figure 3. It should be noted that the factor given for gaseous nitrogen converts the dimensionless concentration C(X,0,0) for nitrogen to that for NO_2.

Particulate pollutant concentrations are presented first in terms of the gas/particle distribution factor, defined as the ratio of the particulate flow rate to the sum of gaseous and particulate flow rates for each pollutant pair, that is

$$f_s = \frac{G_{s(part)}}{G_{s(part)} + G_{s(gas)}} \tag{69}$$

$$f_n = \frac{G_{n(part)}}{G_{n(part)} + G_{n(gas)}} \tag{70}$$

$$f_c = \frac{G_{c(part)}}{G_{c(part)} + G_{c(gas)}} \tag{71}$$

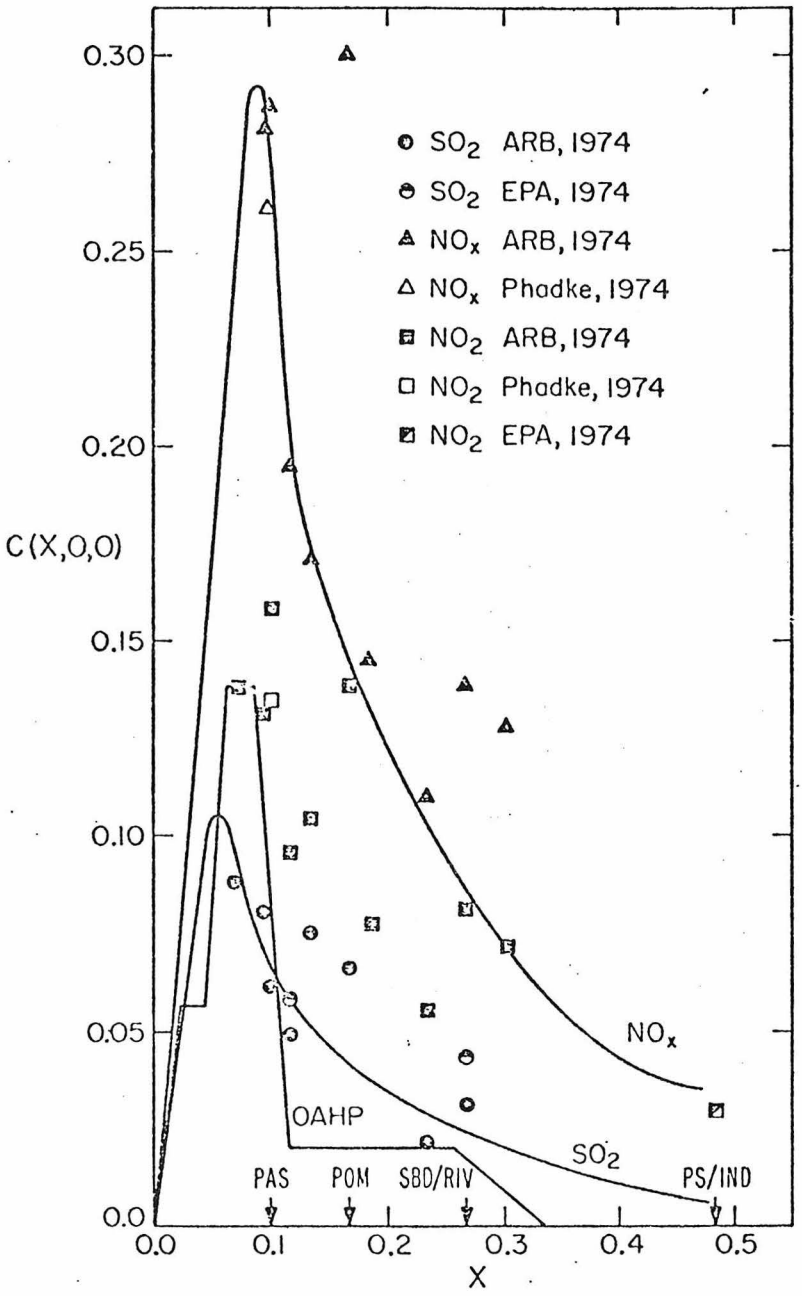

FIGURE 3

Ground-level Concentrations of Gaseous Pollutants as a Function of Dimensionless Distance Along the Trajectory. The Factors 588, 1050, and 44 convert SO_2, N (as NO_2), and OAHP Concentrations, respectively, as shown to $\mu g\ m^{-3}$.

where G_i is the flow rate of species i crossing a plane at X ($g\ sec^{-1}$). The subscripts s, n and c refer to sulfur, nitrogen and hydrocarbons, respectively. Thus $G_{s(gas)}$ and $G_{s(part)}$ are the flow rates of sulfur in gaseous and particulate forms, respectively, their sum representing the total flow of airborne sulfur at X.

Figure 4 shows the gas/particle distribution factors, f_s, f_n and f_c along the trajectory. The dimensionless particulate flow rates $\bar{C}_p(X)$, which when combined with the dimensionless gas flow rates $\bar{C}(X)$ yield the gas/particle distribution factors, are shown in Figure 5. The factors to convert the dimensionless flow rates to dimensional form are given in the caption of Figure 5. If we assume that sulfates, nitrates and organics constitute all of the secondary particulate matter, then we can determine the weight fractions of the three constituents as a function of X. These weight fractions are shown in Figure 6.

The results shown in Figures 3-6 represent the predictions of the model as applied to a "trajectory" across the South Coast Air Basin. Although the trajectory in Figure 2 is more representative of daytime conditions than of those over a 24-hour period, for simplicity we have employed daily average emission rates rather than attempting to estimate daytime emission rates. (As we have noted, the main object of the model developed here is to afford the ability to perform overall gas/particle material balance calculations. A model intended for day to day prediction will obviously need to include provisions for time-varying sources and meteorology.) In spite of its shortcomings in representing actual atmospheric phenomena, it is nevertheless of interest to compare the predictions of the model to available atmospheric data. The predictions in Figures 3 and 4 are in a form amenable to data comparison. Because the source emission rates used were based on yearly average estimates for 1972, it was felt that the most appropriate data with which to compare the predictions are yearly average concentrations for 1972. Consequently, on Figures 3 and 4 data points are included from a number of sources that represent the 1972 yearly averages of one-hour average data. Although the data base of Phadke et al. (1974) is presumably the same as that collected and reported by the ARB (1974), there are discrepancies in the NO_2 and NO_x data at Pasadena, and hence both are shown. Similar discrepancies are noted and reported between the SO_2 data of the ARB (1974) and EPA (1974) at La Habra and San Bernardino.

Sample predictions of SO_2 and the corresponding measured values include 38 $\mu g\ m^{-3}$ (predicted) vs. 35 $\mu g\ m^{-3}$ (measured) at Pasadena, 24 vs. 39 $\mu g\ m^{-3}$

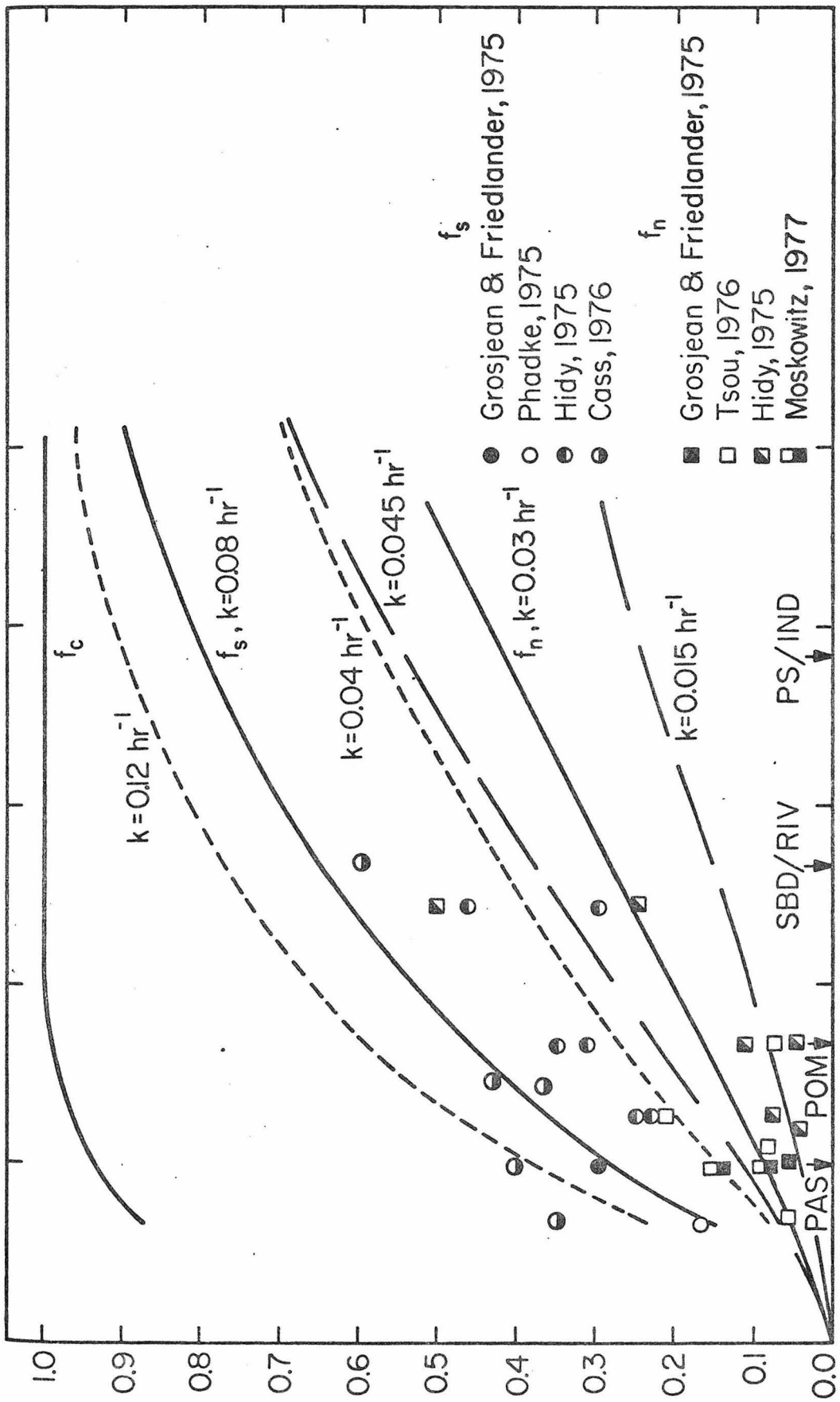

Figure 4

Gas-particle Distribution Factors as a Function of Dimensionless Distance Along the Trajectory.

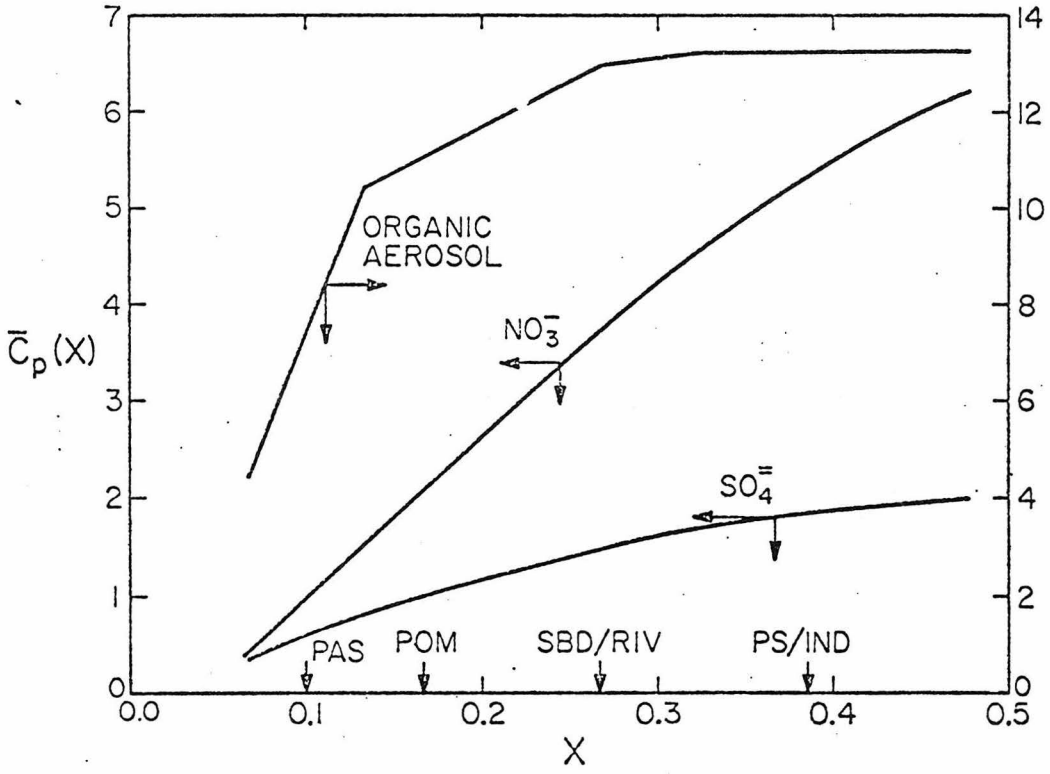

FIGURE 5
Particulate Flow Rates as a Function of Dimensionless Distance Along the Trajectory. The Factors 119.2, 191.2 and 11.9 convert the $SO_4^=$, NO_3^-, and organic aerosol dimensionless flow rates, respectively, as shown to kg min^{-1}.

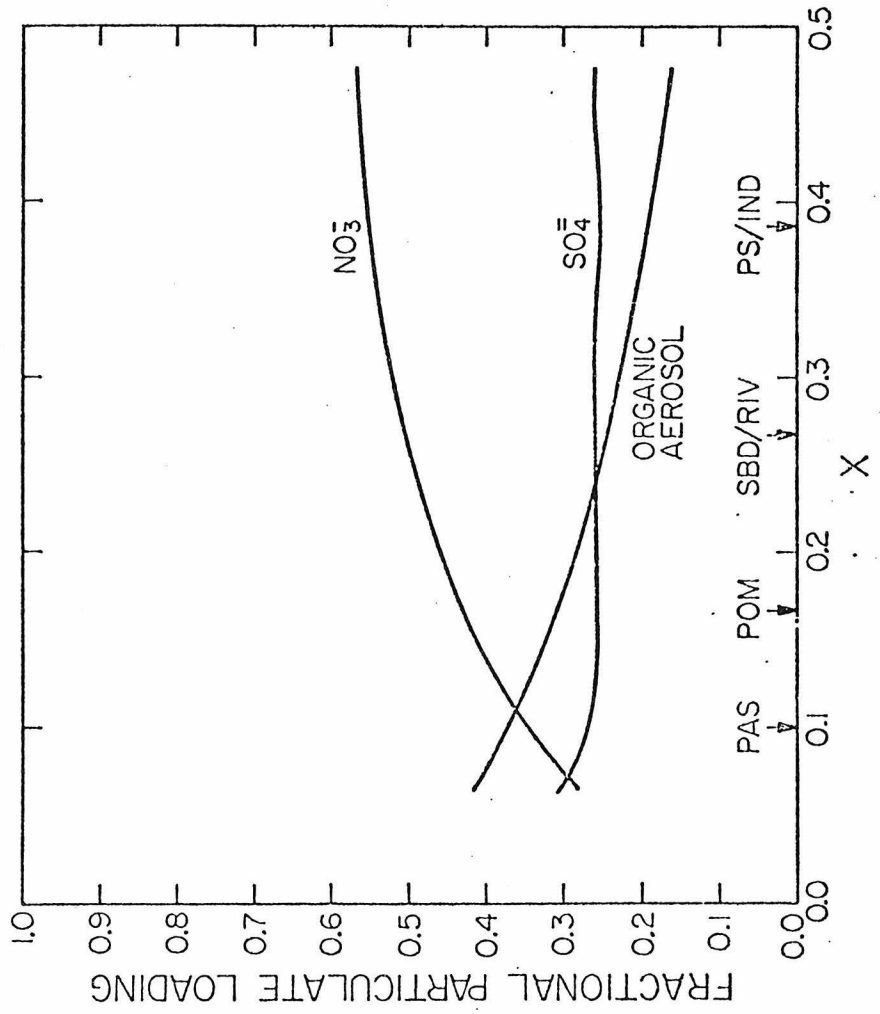

FIGURE 6

Fraction of the Total Secondary Aerosol Attributable to Sulfate, Nitrate, and Organics as a Function of Dimensionless Distance Along the Trajectory.

at Pomona, and 14.7 vs. 13-18 μg m^{-3} at San Bernardino/Riverside. Although an arithmetic mean SO_2 level is not reported for Indio, data samples taken there and reported by EPA (1974) suggest values in the 13-20 μg m^{-3} range. This compares to predicted levels of about 3 μg m^{-3}. A possible explanation is that since the values reported at San Bernardino, Riverside, Palm Springs and Indio are below the detection limit of 0.01 ppm (26 μg m^{-3}) of the monitoring equipment, reported values may be different than those actually observed.

Predicted levels of total oxides of nitrogen compare remarkably well with the data. Sample predictions and corresponding measured values include 289 μg m^{-3} (predicted) vs. 275-300 μg m^{-3} (measured) as NO_2 at Pasadena, 210 vs. 204 μg m^{-3} at La Habra, 184 vs. 180 μg m^{-3} at Azusa, and 108 vs. 118 μg m^{-3} at Riverside. The only truly anomalous results are those reported at Pomona, where reported NO_x levels reach 323 μg m^{-3} as NO_2 compared to predictions of about 152 μg m^{-3} as NO_2. However, the data reported at nearby Ontario of 152 μg m^{-3} (the level predicted in Pomona) suggests one of the two readings may be in error.

Also plotted in Figure 3 are reported levels of NO_2 throughout the Los Angeles basin. It is evident that near the eastern portion of the basin, a substantial portion of the NO emitted upwind has been photochemically oxidized to NO_2.

The organic aerosol hydrocarbon precursor (OAHP) concentrations in Figure 3 reach steady state almost immediately as the trajectory passes over regions of varying source strengths. This is due to the rapid rate of conversion to particulate organics. Few measurements of ambient levels of specific OAHP species have been measured, but Stephens and Burleson (1969) report cyclopentene concentrations (a known aerosol precursor) of about

5 ppb in early morning samplings in the Riverside area. Assuming these early morning samples would compare to those taken in early morning Los Angeles before considerable reaction has taken place, the predictions from the simulation yield levels of 2.4 to 6 $\mu g\ m^{-3}$ OAHP, or 1-2 ppb as cyclopentene.

The gas/particle distribution factors f_s, f_n and f_c are shown in Figure 4. The sources of data for these factors (or for particulate sulfate and nitrate loadings, which can be converted to f_s and f_n) are Grosjean and Friedlander* (1975), Hidy (1975), Phadke et al. (1975), Cass (1976), Tsou (1976) and Moskowitz (1977). Hidy (1975) reports particulate loadings in two ways. First, gas/particle distribution factors f_s and f_n are presented directly as calculated from their aerosol and gas phase data. Second, average 2-hour mass concentrations of sulfate and nitrate are presented for readings taken at various locations in the basin. The factors f_s and f_n are plotted directly, whereas the sulfate and nitrate concentrations are compared to average SO_2 and NO_x levels reported by the ARB (1974) to obtain other estimates of f_s and f_n. These data are also plotted in Figure 4. Table 5 lists the sources of data plotted in this figure, as well as the type of data reported. "Snapshot" data are data taken over short periods of time, or even for a single day. Yearly average data, obviously, are data collected periodically and averaged over a year. The latter data are the more realistic values against which the transport model should be compared. The predictions of sulfate factor f_s agree reasonably well with data, although the scatter in the data is quite large. Predictions of f_n, on the other hand, seem to be slightly higher than the data. A simple explanation for this result is that, for purposes of computing nitrate formation only, the gaseous nitrate predicted in the model is assumed to be entirely NO_2, since the model does not

*It should be noted that the gas/particle distribution factors defined by Grosjean and Friedlander (1975) are based on measured ground-level concentrations whereas our definition is based on the integrated flux from the ground to the inversion base. If vertical concentration and wind profiles are roughly flat, the two definitions should approximately coincide.

Table 5. Sources of Particulate Data

Data Reported	Reference	Type of Data
f_S, f_N	Grosjean and Friedlander (1975)	Snapshot, summer 1973
f_S, f_N	Hidy (1975)	Snapshot, summer 1972, 1973
f_S	Phadke et al. (1975)	Yearly average, 1972
f_S	Cass (1976)	Multi-year averages, 1972-1974
f_N	Tsou (1976)	Snapshot, summer 1974
f_N	Moskowitz (1977)	Snapshot, summer 1976

discriminate between NO and NO_2. Since gaseous nitrogen exists as both NO and NO_2, a higher rate of nitrate formation is predicted. Also, since NO_x is found in such large concentrations and f_n is generally less than 0.1, a "large" change in f_n (say, by 50%, to values less than 0.05) will yield only small changes in the NO_x predictions of Figure 3. Obviously, the approximate nature of the nitrate formation rate that we have derived from the data of Clark et al. (1976) is a contributor to any lack of agreement between predictions and data.

The organic gas/particle distribution factor f_c, as defined here on the basis of organic aerosol hydrocarbon precursors only, cannot be readily compared to data. The rapid rate of conversion of precursors to aerosol organics leads to values of f_c above 0.9 almost from the inception of the trajectory.

The most interesting aspect of Figure 5 is the relative behavior of the particulate mass fluxes. The sharper, nearly linear variation of organic aerosol indicates that the particulate organic level is closely tied to the hydrocarbon precursor emissions because of rapid conversion. Sulfates, on the other hand, require an initiation period wherein SO_2 levels build up to a point where an appreciable conversion rate to sulfate is established. Even though the assumed rate of nitrate formation is slower than the sulfate formation rate, the emissions levels (and consequently the gaseous concentrations) of NO_x produce a particulate nitrate flux that increases more rapidly than the sulfate flux.

Consistent behavior is noted past the point at which emissions are discontinued. Particulate organics, their sources terminated, level off immediately and slowly decrease due to deposition. Sulfates, still accompanied by SO_2, increase somewhat but level off quickly. Nitrates continue to increase because of the large quantities of NO_x still predicted in the air parcel.

Figure 6 shows the fractional loading for each of three particulate components. As with Figure 4, cautious interpretation is again necessary in comparison of predictions with data. Grosjean and Friedlander (1975) report that, in most samples taken from the Pasadena area, nitrates have a higher mass loading than sulfates, and organics have higher mass loading than either sulfates or nitrates. Considering that primary organic aerosol can contribute to the total measured organic aerosol (whereas the model predicts only secondary aerosol levels) the simulation results are roughly equivalent to measured results.

SUMMARY AND CONCLUSIONS

A steady-state mathematical model based on the atmospheric diffusion equation has been developed for estimating the conversion of gaseous to particulate pollutants, including deposition and settling, downwind of pollutant sources. An analytical solution of the atmospheric diffusion equation in three dimensions for wind speed and eddy diffusivities independent of height is the basis of the model. The model enables one to perform material balance calculations, the main purpose being to determine the relative roles of conversion and removal in governing gaseous and particulate concentration levels. The model has been applied to the prediction of gaseous and particulate pollutant material balances in the Los Angeles airshed and downwind.

With regard to Los Angeles, the following areas in need of further study were delineated as a result of the calculation:

1) Detailed study is needed of the mechanisms of conversion of NO_x to nitrate in urban atmospheres.

2) The specific hydrocarbons that are organic aerosol precursors need further identification; their emission rates from urban sources require elucidation; and the specific mechanisms for their conversion to particulate organics require study.

ACKNOWLEDGMENT

This work was supported by National Science Foundation Grant AEN76-04179.

REFERENCES

Air Resources Board, State of California (1972) The State of California Implementation Plan for Achieving and Maintaining the National Ambient Air Quality Standards.

Air Resources Board, State of California (1974) Ten Year Summary of California Air Quality Data: 1963-1972.

Bartz D. R., Arledge K. W., Gabrielson J. E., Hays L. G. and Hunter S. C. (1974) Control of Oxides of Nitrogen from Stationary Sources in the South Coast Air Basin, State of California Air Resources Board Rpt. ARB 2-1471.

Belot Y., Baille A. and Delmas J. L. (1976) Modele Numerique De Dispersion Des Polluants Atmospheriques en Presence De Couverts Vegetaux. Atmospheric Environment 10, 89-98.

Bolin B. and Persson C. (1975) Regional Dispersion and Deposition of Atmospheric Pollutants with Particular Application to Sulfur Pollution Over Western Europe. Tellus 27(3), 281-310.

Breeding R. J., Haagenson P. L., Anderson J. A., Lodge J. P., Jr. and Stampfer J. F., Jr. (1975) The Urban Plume as Seen at 80 and 120 km by Five Different Sensors. J. Appl. Met. 14, 204-216.

Breeding R. J., Klonis H. B., Lodge J. P., Jr., Pate J. B., Sheesley D.C., Englert T. R. and Sears D. R. (1976) Measurements of Atmospheric Pollutants in the St. Louis Area. Atmospheric Environment, 10, 181-194.

Calvert J. G. (1976) Hydrocarbon Involvement in Photochemical Smog Formation in Los Angeles Atmosphere. Env. Sci. Technol. 10(3), 256-262.

Carslaw H. S. and Jaeger J. C. (1959) Conduction of Heat in Solids. Clarendon Press, Oxford.

Cass G. R. (1976) Baseline Air Quality Characterization: Sulfate Air Quality in the South Coast Air Basin. Environmental Quality Laboratory, Calif. Inst. of Technol., Pasadena, Calif.

Clark W. E., Landis D. A. and Harker A. B. (1976) Measurements of the Photochemical Production of Aerosols in Ambient Air Near a Freeway for a Range of SO_2 Concentrations. Atmospheric Environment 10, 637-644.

Courant R., and Hilbert D. (1953) Methods of Mathematical Physics, Vol. I Interscience Publishers, New York.

Demerjian K. L., Kerr J. A. and Calvert J. G. (1974) The Mechanism of Photochemical Smog Formation. Adv. in Env. Sci. and Tech. 4, (J. N. Pitts and R. L. Metcalf, eds.) Wiley-Interscience, New York, 1-262.

Environmental Protection Agency (1974) Air Quality Data - 1972 Annual Statistics. EPA Rpt. 450/2-74-001.

Garland J. A., Atkins D.H.F., Readings C. J. and Caughey S. J. (1974) Deposition of Gaseous Sulphur Dioxide to the Ground. Atmospheric Environment 8, 75-79.

Grosjean D. and Friedlander S. K. (1975) Gas-Particle Distribution Factors for Organic and Other Pollutants in the Los Angeles Atmosphere. J. Air Poll. Cont. Assoc. 25(10), 1038-1044

Haagenson P. L. and Morris A. L. (1974) Forecasting the Behavior of the St. Louis, Missouri, Pollutant Plume. J. Appl. Met. 13, 901-909.

Heines T. S. and Peters L.K. (1973) The Effect of a Horizontal Impervious Layer Caused by a Temperature Inversion Aloft on the Dispersion of Pollutants in the Atmosphere. Atmospheric Environment 7, 39-48.

Hidy G. M. and Burton C. S. (1975) Atmospheric Aerosol Formation by Chemical Reactions. Int. J. Chem. Kinetics. Symposium 1, 509-541.

Hidy G. M. (1975) Characterization of Aerosols in California (ACHEX) State of California Air Resources Board.

Hill A. C. (1971) Vegetation: A Sink for Atmospheric Pollutants, J. Air Poll. Cont. Assoc. 21(6), 341-346.

Holzworth G. (1972) Mixing Heights, Wind Speeds and Potential for Urban Air Pollution Throughout the Contigious United States. EPA Rpt AP-101.

Hunter S. C. and Helgeson N. L. (1975) Control of Oxides of Sulfur from Stationary Sources in the South Coast Air Basin. State of California Air Resources Board Rpt. ARB 4-421.

Japar S. M., Wu C. H. and Niki H. (1974) Rate Constants for the Reaction of Ozone with Olefins in the Gas Phase. J. Phys. Chem. 78(23), 2318.

Maynard J. B. and Sanders W. N. (1969) Determination of the Detailed Hydrocarbon Composition and Potential Atmospheric Reactivity of Full-Range Motor Gasolines. J. Air Poll. Cont. Assoc. 19(7), 505-510.

Mayrsohn H. M., Kuramoto M., Crabtree J. H., Sothern R. D. and Mant S. H. (1975) Hydrocarbon Composition of Los Angeles Gasolines. State of California Air Resources Board.

McEwen D. J. (1966) Automobile Exhaust Hydrocarbon Analysis by Gas Chromatograph. Anal. Chem. 38, 1047.

Monin A. S. and Yaglom A. M. (1971) Statistical Fluid Mechanics. MIT Press, Cambridge, Mass.

Moskowitz A. H. (1977) Particle Size Distribution of Nitrate Aerosols in the Los Angeles Air Basin. EPA Rpt. EPA-600/3-77-053.

Neligan R. E., Mader P. P. and Chambers L. A. (1961) Exhaust Composition in Relation to Fuel Combustion. J. Air Poll. Cont. Assoc. 11, 178-186.

O'Brien R. J., Holmes J. R. and Bockian A. H. (1975a) Formation of Photochemical Aerosol from Hydrocarbons: Chemical Reactivity and Products. Env. Sci. Technol. 9(6), 568.

O'Brien R. J., Crabtree J. H., Holmes J. R., Hoggan M. C. and Bockian A. H. (1975b) Formation of Photochemical Aerosol from Hydrocarbons: Atmospheric Analysis. Env. Sci. Technol. 9(6), 577.

Owers M. J. and Powell A. W. (1974) Deposition Velocity of Sulfur Dioxide on Land and Water Surfaces Using a ^{35}S Tracer Method. Atmospheric Environment 8, 63-67.

Phadke, M.S., Tiao G. C., Grupe M., Liu S. T. and Wu S. (1974) Los Angeles Aerometric Data on Oxides of Nitrogen 1957-1972. Tech. Rpt. 395, Dept. of Statistics, U. Wisconsin, Madison.

Phadke, M. S., Tiao G. C., Grupe M., Wu S. C., Krug A. and Liu S. T. (1975) Los Angeles Aerometric Data on Sulfur Dioxide, Particulate Matter and Sulfate 1955-1972. Tech. Rpt. 410, Dept. of Statistics, U. Wisconsin, Madison.

Roberts P. T. and Friedlander S. K. (1975) Conversion of SO_2 to Sulfur Particulate in the Los Angeles Atmosphere. Env. Health Perspectives, 10, 103-108

Scriven R. A. and Fisher B. E. A. (1975) The Long Range Transport of Airborne Material and Its Removal by Deposition and Washout - I. General Considerations and II. The Effect of Turbulent Diffusion. Atmospheric Environment 9, 49-68.

Stampfer J. F., Jr. and Anderson J. A. (1975) Locating the St. Louis Urban Plume at 80 and 120 km and Some of its Characteristics. Atmospheric Environment 6, 743-757.

Stephens E. R. and Burleson F. R. (1969) Distribution of Light Hydrocarbons in Ambient Air. J. Air Poll. Cont. Assoc. 19(12), 929-936.

TRW (1974) A Particulate Implementation Plan for the Los Angeles Region. TRW Corp., Redondo Beach, Calif.

Tsou G. (1976) Data Collected by California Air Resources Board, Unpublished.

APPENDIX

From Equation (8) and the boundary conditions of Equations (9)-(12), the following separation of variables transformation is proposed:

$$C(X,Y,Z) = \theta_1(X,Y)\theta_2(X,Z)\exp(-\alpha X) \tag{A-1}$$

Substitution into (8) and separation of terms yields

$$\beta \frac{\partial^2\theta_1}{\partial Y^2} - \frac{\partial\theta_1}{\partial X} = \rho_1\theta_1 \tag{A-2}$$

$$\frac{\partial\theta_2}{\partial X} - W \frac{\partial\theta_2}{\partial Z} - \frac{\partial^2\theta_2}{\partial Z^2} = \rho_1\theta_2 \tag{A-3}$$

where ρ_1 is an undetermined constant. Transformation of θ_1 and θ_2 in (A-2) and (A-3) respectively by

$$\theta_1(X,Y) = \Lambda_1(X,Y)\exp(-\rho_1 X) \tag{A-4}$$

$$\theta_2(X,Z) = \Lambda_2(X,Z)\exp(\rho_1 X) \tag{A-5}$$

yields

$$C(X,Y,Z) = \Lambda_1(X,Y)\Lambda_1(X,Z)\exp(-\alpha X) \tag{A-6}$$

where Λ_1 and Λ_2 are given by

$$\beta \frac{\partial^2\Lambda_1}{\partial Y^2} = \frac{\partial\Lambda_1}{\partial X} \tag{A-7}$$

and

$$\frac{\partial^2\Lambda_2}{\partial Z^2} + W \frac{\partial\Lambda_2}{\partial Z} = \frac{\partial\Lambda_2}{\partial X} \tag{A-8}$$

with boundary conditions

$$\Lambda_1(X,Y) = 0 \qquad Y \to \pm\infty \tag{A-9}$$

$$\Lambda_1(X,Y) = \delta(Y) \qquad X = 0 \tag{A-10}$$

$$\Lambda_2(X,Z) = \delta(Z-Z_s) \qquad X = 0 \tag{A-11}$$

$$\frac{\partial \Lambda_2}{\partial Z} = 0 \qquad Z = 1 \tag{A-12}$$

$$\frac{\partial \Lambda_2}{\partial Z} = (N-W)\Lambda_2 \qquad Z = 0 \tag{A-13}$$

The solution of (A-7) is (Carslaw and Jaeger, 1959)

$$\Lambda_1(X,Y) = \frac{1}{2\sqrt{\beta\pi X}} \exp\left(\frac{-Y^2}{4\beta X}\right) \tag{A-14}$$

The solution of (A-8) is obtained by separation of variables,

$$\Lambda_2(X,Z) = \Omega_1(X)\Omega_2(Z) \tag{A-15}$$

which, when substituted into (A-8) yields the two equations

$$\frac{\partial \Omega_1}{\partial X} = \rho_2 \Omega_1 \tag{A-16}$$

$$\frac{\partial^2 \Omega_2}{\partial Z^2} + W \frac{\partial \Omega_2}{\partial Z} = \rho_2 \Omega_2 \tag{A-17}$$

Equation (A-16) requires $\rho_2 = -k_n^2$, and boundary conditions (A-12) and (A-13) transform to

$$\frac{\partial \Omega_2}{\partial Z} = (N-W)\Omega_2 \qquad Z = 0 \tag{A-18}$$

$$\frac{\partial \Omega_2}{\partial Z} = 0 \qquad Z = 1 \tag{A-19}$$

Solution for Ω_2 involves the roots, m, or the indicial equation of (A-17), given by

$$m = -\frac{W}{2} \pm \sqrt{\left(\frac{W}{2}\right)^2 - k_n^2} \tag{A-20}$$

Depending upon the sign of the quantity $[(W/2)^2-k_n^2]$, there will be solutions of the form

$$\Omega_{2_n} = \exp\left(-\frac{WZ}{2}\right)\left\{a_n \cos(\gamma_n Z) + b_n \sin(\gamma_n Z)\right\} \tag{A-21}$$

if $(W/2)^2 < k_n^2$

$$\Omega_{2_m} = \exp\left(-\frac{WZ}{2}\right)\left\{c_m \exp(\theta_m Z) + d_m \exp(-\theta_m Z)\right\}$$

if $(W/2)^2 > k_n^2$ (A-22)

By application of (A-18) and (A-19), γ_n and θ_m are determined, as are the relationships of b_n and d_m to a_n and c_m, respectively. The eigenvalues γ_n and θ_m are given by (22) and (23). As outlined in Courant and Hilbert (1953), θ_m can have only a finite number of roots of (23). The final form for Λ_2 is

$$\Lambda_2(X,Z) = \exp\left(-\frac{WZ}{2}\right)\left\{\sum_{n=1}^{\infty} a_n \Phi_n^{(1)}(Z) \exp\left(-\mu_n^{(1)} X\right) + \sum_{m=1}^{M} c_m \Phi_m^{(2)}(Z) \exp\left(-\mu_m^{(2)} X\right)\right\} \tag{A-23}$$

where $\Phi_n^{(1)}$, $\Phi_m^{(2)}$, $\mu_n^{(1)}$ and $\mu_m^{(2)}$ are given by (14-17), respectively.

Since $\Lambda_2(X,Z)$ arises from a Sturm-Liouville equation, the $\Phi_n^{(1)}(Z)$ and $\Phi_m^{(2)}(Z)$ are orthogonal with weighting function exp(WZ/2). The coefficients a_n and c_m are determined by applying the condition (A-11) to (A-23). The solutions are given by (20) and (21) respectively. If, however, a rational function approximation to the delta function $\delta(Z-Z_s)$ is used, such as

$$\delta(Z-Z_s) \approx b\ U(Z-Z_s)\exp(-a(Z-Z_s)) \tag{A-24}$$

where

$$b = \frac{a}{1-\exp(-a(1-Z_s))}, \tag{A-25}$$

$U(Z-Z_s)$ is the unit step function, and a is an arbitrarily large number, then a_n and c_m are given by

$$a_n = I_1/I_2 \tag{A-26}$$

$$c_m = I_3/I_4 \tag{A-27}$$

where

$$\begin{aligned} I_1 = \frac{b}{\left(\frac{W}{2}-a\right)^2+\gamma_n} \Bigg[& \exp\left(\frac{W}{2} - a(1-Z_s)\right)\Bigg\{\left(\frac{W}{2} - a\right)\left(\cos\gamma_n + \delta_n \sin\gamma_n\right) + \\ & \gamma_n(\sin\gamma_n - \delta_n\cos\gamma_n)\Bigg\} \\ & - \exp\left(\frac{WZ_s}{2}\right)\Bigg\{\left(\frac{W}{2} - a\right)\left(\cos(\gamma_n Z_s) + \delta_n \sin(\gamma_n Z_s)\right) \\ & + \gamma_n\left(\sin(\gamma_n Z_s) - \delta_n\cos(\gamma_n Z_s)\right)\Bigg\}\Bigg] \end{aligned} \tag{A-28}$$

$$I_3 = b\left[\frac{\exp(W/2-a(1-Z_s)+\theta_m) - \exp\left((W/2+\theta_m)Z_s\right)}{W/2-a+\theta_m}\right.$$

$$\left. - \tau_m\left(\frac{\exp(W/2-a(1-Z_s)-\theta_m)-\exp\left((W/2-\theta_m)Z_s\right)}{W/2-a-\theta_m}\right)\right] \qquad \text{(A-29)}$$

and I_2 and I_4 are given by (37) and (39). The final form for C(X,Y,Z) is given by (13).

The approach to the solution for an elevated vertical area source is identical to that just taken. However, boundary conditions (A-10) and (A-11) are replaced by

$$\Lambda_1(X,Y) = U(Y+B)U(B-Y)/2B \qquad X = 0 \qquad \text{(A-30)}$$

and

$$\Lambda_2(X,Z) = U(Z-Z_1)U(Z_2-Z)/(Z_2-Z_1) \qquad X = 0 \qquad \text{(A-31)}$$

respectively.

Solution for Λ_1 becomes (Carslaw and Jaeger, 1959)

$$\Lambda_1(X,Y) = \frac{1}{4B}\left\{\text{erf}\left(\frac{B-Y}{2\sqrt{\beta X}}\right) + \text{erf}\left(\frac{B+Y}{2\sqrt{\beta X}}\right)\right\} \qquad \text{(A-32)}$$

Again, Λ_2 is solved by separation, with boundary conditions (A-18) and (A-19) on Ω_2 unchanged. Hence $\Lambda_2(X,Z)$ in (A-23) is changed only by the values of the constants a_n and c_m. By applying (A-31) to (A-23) the solutions for a_n and c_m are given by (36-39).

CHAPTER III

DYNAMICS

OF

AEROSOL COAGULATION AND CONDENSATION*

*This Chapter appears in the Journal of the American Institute of Chemical Engineers, 22(5),840-851, 1976.

SCOPE

The growth of aerosols results from a variety of physical and chemical phenomena. For atmospheric aerosols the most important phenomena are coagulation and heterogeneous condensation. Because of the strong dependence of aerosol properties, such as light scattering, on particle size, it is desirable to understand in as much detail as possible how a size distribution evolves under the influence of these two processes. The size distribution of an aerosol is described by its size distribution density function, which is governed in general by a partial integro-differential equation. For simulations of atmospheric aerosol dynamics including turbulent transport and dispersion, numerical solution of the equation will ultimately be necessary. However, analytical solutions for certain limiting cases of a spatially homogeneous aerosol can be valuable in understanding the qualitative structure of the behavior in more complex situations. The object of this work, therefore, is to obtain analytical solutions to the general equation governing the size distribution density function of an aerosol undergoing simultaneous coagulation and condensation. Beyond their utility in understanding atmospheric aerosol dynamics, the solutions should be helpful in describing the dynamic behavior of any particulate system in which coagulation and condensation are taking place.

CONCLUSIONS AND SIGNIFICANCE

Analytical solutions are obtained to the general dynamic equation governing the size distribution density function of an aerosol undergoing simultaneous growth by coagulation and heterogeneous condensation. The solutions elucidate the influences of simultaneous coagulation and condensation on the evolving size distribution of an aerosol. Because of the complexity of actual coagulation and condensation kinetics, it is necessary to assume simple functional forms for these processes to enable analytical investigation of the dynamics. Consequently, coagulation constants independent of particle volume and dependent on the sum of the particle volumes, and condensation rates independent of particle volume and linearly dependent on particle volume are considered. A dimensionless group Λ representing the ratio of the characteristic time for condensation to that for coagulation is introduced. When $\Lambda << 1$, for example, coagulation occurs much more rapidly than condensation, and size distributions tend to exhibit the broadening characteristic of coagulation. A linear coagulation rate introduces a marked broadening in size distributions relative to a constant coagulation rate at the same value of Λ. On the other hand, for a constant coagulation rate the upper end of the size spectrum fills out more rapidly with a linear condensation rate than with a constant condensation rate. Size spectra for actual condensation growth processes can be envisioned to lie between those of the two extremes considered here. Based on an estimated value of Λ, information on the nature of the physical processes taking place can be ascertained for an aerosol for which an evolving size distribution is available.

INTRODUCTION

The dynamic behavior of a population of small particles is a subject of interest in fields as wide ranging as atmospheric physics, crystallization, and colloid chemistry. In all such systems, particles grow through collisions and coalescence with other particles (coagulation) and through accretion of material in the medium containing the particles. In the case of particles in a gas, growth of particles by accretion of vapor molecules is termed heterogeneous condensation. The evolution of the size distribution of an aerosol will depend on the relative importance of the various growth mechanisms present.

The description of the dynamics of the size distribution of an aerosol resulting from coagulation and condensation involves a partial integro-differential population balance equation which generally can only be solved numerically. Because of the extreme computational difficulties inherent in attempting to solve this equation, virtually no solutions were reported until recently (Middleton and Brock, 1976). Analytical solutions of the aerosol population balance equation are available for certain special cases of pure coagulation (Scott, 1968) and pure condensation (Brock, 1972). No solutions have been obtained for the case in which coagulation and condensation occur simultaneously, yet this is often a situation of importance.

The object of this work is to obtain analytical solutions to the general equation governing the size distribution of an aerosol undergoing simultaneous coagulation and condensation. Although the equation considered is of a general nature, the results will be most applicable to atmospheric aerosols. Through the solutions it is hoped to elucidate the interplay between the two growth processes. In the next section we develop carefully the basic equation for simultaneous coagulation and condensation of a homogeneous aerosol.

FUNDAMENTAL EQUATION GOVERNING AEROSOL SIZE DISTRIBUTIONS

A spatially homogeneous aerosol of uniform chemical composition can be fully characterized by the number densities of particles of various sizes as a function of time. Define $n_k(t)$ as the number density (cm^{-3}) of particles containing k monomers, where a monomer can be considered as a single molecule of the species comprising the particle. The basic processes that influence $n_k(t)$ are coagulation and evaporation (the loss of single molecules from a k-mer). We specifically neglect processes in which a k-mer spontaneously dissociates into two particles, of sizes $\tilde{k}$ and $k-\tilde{k}$, if $\tilde{k} > 1$. (Homogeneous nucleation, the process by which original stable particles are formed, is included within the definition of coagulation.)

The dynamic equation governing $n_k(t)$, $k \geq 2$, can be written as

$$\frac{dn_k}{dt} = \frac{1}{2} \sum_{j=1}^{k-1} \beta_{j,k-j}\, n_j n_{k-j} - \sum_{j=1}^{\infty} \beta_{k,j}\, n_k n_j - q_k n_k + q_{k+1}\, n_{k+1} \qquad (1)$$

where $\beta_{k,j}$ is the collision rate (frequency factor) between particles of sizes k and j ($cm^3 sec^{-1}$), and q_k is defined as the frequency with which monomers will escape from a k-mer (sec^{-1}). The first two terms on the right hand side of (1) express the rate of change of n_k as a result of collisional (coagulation) processes, and the last two terms describe the contribution of monomer evaporation.

Equation (1) is a rigorous representation of the kinetics of a system of particles undergoing simultaneous coalescense and evaporation. It proves to be convenient, however, to represent the process of accretion of monomers by other particles in a manner analogous to that of evaporation

Thus, we define $p_k n_k$ as the rate of gain of (k+1)-mers due to collision of a k-mer with a monomer, where p_k (sec^{-1}) is the frequency with which a monomer collides with a k-mer. This is the process we commonly refer to as heterogeneous condensation. With this modification, (1) becomes

$$\frac{dn_k}{dt} = \frac{1}{2} \sum_{j=2}^{k-2} \beta_{j,k-j}\, n_j n_{k-j} - \sum_{j=2}^{\infty} \beta_{k,j}\, n_k n_j$$

$$+ p_{k-1}\, n_{k-1} - (p_k + q_k)\, n_k + q_{k+1}\, n_{k+1} \qquad (2)$$

where $p_k = \beta_{1,k}\, n_1$.

In this formulation it is assumed that the smallest "particle" is of size k = 2. No distinction has yet been made among the processes of coagulation, homogeneous nucleation, and heterogeneous condensation. In reality, there is a minimum number of monomers in a stable nucleus, call it k_o, and generally $k_o >> 2$. In the presence of a supersaturated vapor, stable clusturs at size k_o will form continuously at a rate given by the classical theory of homogeneous nucleation. Let us denote the rate of formation of stable clusters containing k_o monomers from homogeneous nucleation as $r_o(t)$. Then coagulation and heterogeneous condensation of vapor on particles of size $k \geq k_o$ become distinct processes in (2). Changing the smallest size stable particle from 2 to k_o, (2) becomes

$$\frac{dn_k}{dt} = \frac{1}{2} \sum_{j=k_o}^{k-k_o} \beta_{j,k-j}\, n_j n_{k-j} - \sum_{j=k_o}^{\infty} \beta_{k,j}\, n_k n_j$$

$$+ p_{k-1}\, n_{k-1} - (p_k + q_k) n_k + q_{k+1}\, n_{k+1} + r_o(t)\delta_{k_o} \qquad (3)$$

$$k = k_o,\ k_o + 1,\ \ldots$$

where δ_{k_o} is the Kronecker delta function.

Although (3) is still a rigorous representation of the system, it is impractical to deal with discrete equations because of the enormous range of k. Thus, it is customary to replace the discrete number density $n_k(t)(cm^{-3})$ by the continuous size distribution density function $n(v,t)(\mu m^{-3}\ cm^{-3})$, where $v = k\Delta v$, Δv being the volume associated with a monomer. Thus, $n(v,t)dv$ is defined as the number of particles per cm^3 having volumes in the range v to v + dv. If we let $v_o = k_o \Delta v$, then (3) becomes in the limit of a continuous distribution of sizes

$$\frac{\partial n(v,t)}{\partial t} = \frac{1}{2}\int_{v_o}^{v-v_o} \beta(v-\tilde{v},\tilde{v})n(v-\tilde{v},t)n(\tilde{v},t)\,d\tilde{v} - \int_{v_o}^{\infty} \beta(v,\tilde{v})n(v,t)n(\tilde{v},t)\,d\tilde{v}$$

$$- \frac{\partial}{\partial v}(\alpha_o(v)n(v,t)) + \frac{\partial^2}{\partial v^2}(\alpha_1(v)n(v,t)) + r_o(t)\delta(v-v_o) \qquad (4)$$

where

$$\alpha_o(v) = \Delta v(p_k - q_k) \qquad (5)$$

$$\alpha_1(v) = \frac{\Delta v^2}{2}(p_k + q_k) \qquad (6)$$

Since $p_k - q_k$ is the frequency with which a k-mer experiences a net gain of one monomer, $\alpha_o(v)$ is the rate of change of the volume of a particle of size $v = k\Delta v$. The sum $p_k + q_k$ is the total frequency with which monomers enter and leave a k-mer. $\alpha_1(v)$ assumes the role of a diffusion coefficient for the size spectrum. α_o and α_1 can be computed from kinetic theory. Brock (1972), however, has obtained relations for α_o and α_1 based on a continuous size distribution which provide additonal insight into their nature. Considering only condensational growth, if

if we let $m(\tilde{v},t)$ represent the size distribution density of the small condensing nuclei, then the evolution of $n(v,t)$ is described by

$$\frac{\partial n(v,t)}{\partial t} = \int_0^{\tilde{v}_m} \beta(v-\tilde{v},\tilde{v})n(v-\tilde{v},t)m(\tilde{v},t)d\tilde{v} - \int_0^{\tilde{v}_m} \beta(v,\tilde{v})n(v,t)m(\tilde{v},t)d\tilde{v} \qquad (7)$$

where the condensing species are assumed to have volumes such that $\tilde{v} << v$, and where $\tilde{v}_m$ is the largest volume of the condensing species. Taking advantage of the fact that $\tilde{v}/v << 1$, the first integrand can be expanded in a Taylor series to yield

$$\frac{\partial n(v,t)}{\partial t} = -\frac{\partial}{\partial v}(\alpha_0(v,t)n(v,t)) + \frac{\partial^2}{\partial v^2}(\alpha_1(v,t)n(v,t)) \qquad (8)$$

where

$$\alpha_0(v,t) = \int_0^{\tilde{v}_m} \beta(v,\tilde{v})\tilde{v}\, m(\tilde{v},t)\, d\tilde{v} \qquad (9)$$

$$\alpha_1(v,t) = \frac{1}{2}\int_0^{\tilde{v}_m} \beta(v,\tilde{v})\tilde{v}^2\, m(\tilde{v},t)\, d\tilde{v} \qquad (10)$$

For $v>>\tilde{v}$ it is reasonable to assume that $\beta(v,\tilde{v}) = \beta(v)$, namely that the collision rate depends only on the volume of the particle. If, in addition, we assume that all condensing nuclei are of a uniform size $\tilde{v}_1 \leq \tilde{v}_m$, then $m(\tilde{v},t) = M\,\delta(\tilde{v}-\tilde{v}_1)$, and

$$\alpha_0(v) = \beta(v)\tilde{v}_1\, M \qquad (11)$$

$$\alpha_1(v) = \frac{1}{2}\beta(v)\tilde{v}_1^2\, M \qquad (12)$$

where M is the monomer number density, assumed to be constant.

Brock (1972) has suggested that the term in (8) involving α_1 can ordinarily be neglected. A quantitative criterion for judging the importance of that term can be readily developed. To do so we introduce the following variables, $\eta = v/v_0$, $\varepsilon = \tilde{v}_1/v_0$, and $\alpha_0^* = \alpha_0/v_0$. A common functional form for α_0(see later) is $\alpha_0^* = \alpha\eta^\gamma$, where $0 \leq \gamma \leq 1$. Using this form for α_0^*, together with the relation $\alpha_1 = \frac{1}{2}\tilde{v}_1\alpha_0$ from (11) and (12), (8) becomes

$$\frac{1}{\alpha}\frac{\partial n}{\partial t} = \eta^{\gamma-1}(\eta+\varepsilon\gamma)\frac{\partial n}{\partial \eta} + \gamma\eta^{\gamma-2}\left(\eta + \frac{1}{2}\varepsilon(\gamma-1)\right)n + \frac{1}{2}\varepsilon\eta^\gamma\frac{\partial^2 n}{\partial \eta^2} \tag{13}$$

It is evident that $\eta >> \varepsilon\gamma$ and so (13) reduces to

$$\frac{1}{\alpha}\frac{\partial n}{\partial t} = \eta^\gamma\frac{\partial n}{\partial \eta} + \gamma\eta^{\gamma-1}n + \frac{1}{2}\varepsilon\eta^\gamma\frac{\partial^2 n}{\partial \eta^2} \tag{14}$$

In order for the last term on the right hand side of (14) to be of comparable importance to the first term on the right hand side, it is necessary that

$$\frac{\partial^2 n}{\partial \eta^2} \Big/ \frac{\partial n}{\partial \eta} \geq O(\varepsilon^{-1}) \tag{15}$$

For most actual distributions this condition is not satisfied, and it is therefore justified to neglect the term involving α_1 in the general dynamic equation for n.

In (4) a stable particle has been assumed to have a lower limit of volume of v_0. From the standpoint of the solution of (4) it is advantageous to replace the lower limits v_0 of the coagulation integrals by zero. Ordinarily this does not cause any difficulty since the initial distribution $n(v,0) = n_0(v)$ may be specified as zero for $v < v_0$, and no particles of volume $v < v_0$ can be produced for $t > 0$. Homogeneous nucleation provides a

steady source of particles of size v_0, according to the rate defined by $r_0(t)$. Subsequently, we shall neglect homogeneous nucleation as its inclusion is not central to our purpose here. Thus, the equation with which we shall deal is

$$\frac{\partial n(v,t)}{\partial t} = \frac{1}{2}\int_0^v \beta(v-\tilde{v},\tilde{v})n(v-\tilde{v},t)n(\tilde{v},t)\,d\tilde{v} - \int_0^\infty \beta(v,\tilde{v})n(v,t)n(\tilde{v},t)\,d\tilde{v}$$

$$- \frac{\partial}{\partial v}(\alpha_0(v)n(v,t)) \qquad (16)$$

The initial and boundary conditions are

$$n(v,0) = n_0(v) \qquad (17)$$

$$n(0,t) = 0 \qquad (18)$$

DESCRIPTION OF COAGULATION AND CONDENSATION PROCESSES

In order to define completely the physical problem it is necessary to specify functional forms for the coagulation constant $\beta(v,\tilde{v})$ and the rate of growth by heterogeneous condensation, $\alpha_0(v)$. General expressions for $\beta(v,\tilde{v})$ and $\alpha_0(v)$ for cases of actual interest are highly nonlinear functions of v(and $\tilde{v}$)(Hidy and Brock, 1970), necessitating numerical solution of (16). Numerical solutions of (16) are, in fact, so difficult to carry out that none were reported until recently (Middleton and Brock, 1976). Clearly, the addition of spatial variation to n along with the associated turbulent transport terms in (16) makes the evaluation of n virtually intractable. Therefore, as a prelude to such detailed numerical studies it is valuable to examine certain special cases of coagulation and condensation, which, while mathematically tractable, still retain important elements of realism with respect to the rigorously established forms of β and α_0.

Analytical solutions for these special cases will enable us to examine how coagulation and condensation interact to influence an evolving size distribution. In this section, therefore, we propose functional forms of β and α_o for subsequent use in (16).

Coagulation

Coagulation of particles in a suspension may occur through a variety of mechanisms, such as Brownian motion, turbulent diffusion, laminar shear, etc. (Hidy and Brock, 1970). For atmospheric particles two mechanisms of interest are Brownian motion and turbulent diffusion.

The form of β for Brownian coagulation depends on the sizes of the two particles. When one particle is in the continuum regime, the coagulation frequency factor is given by the Smoluchowski equation,

$$\beta(v,\tilde{v}) = \frac{2k\theta}{3\mu}\,(v^{1/3} + \tilde{v}^{1/3})\left(\frac{1}{v^{1/3}} + \frac{1}{\tilde{v}^{1/3}}\right) \tag{19}$$

In the early stages of coagulation of a monodisperse aerosol, β given by (19) is essentially a constant, β_o. Fuchs (1964) has suggested that β_o is a good approximation to β if the Knudsen numbers ($Kn = 2\lambda/d_p$) of both particles are less than 0.1 even for a polydisperse aerosol, where λ is the mean free path of air molecules and d_p is the particle diameter. Thus, the case of $\beta = \beta_o$ is both physically interesting and mathematically attractive.

When coagulation results from turbulent diffusion, a reasonable approximation for β is (Golovin, 1963)

$$\beta = \beta_1(v + \tilde{v}) \tag{20}$$

From a purely mathematical standpoint, the coagulation constants $\beta = \beta_0$ and $\beta = \beta_1(v + \tilde{v})$ are apparently the only two physically realistic kernels for which analytical solutions of the coagulation equation have been obtained (Scott, 1968).* Subsequently we shall confine our attention to coagulation processes for which $\beta = \beta_0$ and $\beta = \beta_1(v + \tilde{v})$.

Condensation

The coefficient $\alpha_0(v)$ represents the rate of change of the volume of a particle of volume v by condensation of material on the particle. When the Knudsen number of the particle is less than 0.1, the rate of condensation is predicted by classical continuum diffusion theory (Hidy and Brock, 1970). In that regime

$$\alpha_0(v) = \sigma v^{1/3} \tag{21}$$

where σ involves numerical and physical constants and the difference in vapor pressures of the diffusing species in the bulk gas and at the particle surface. (For sufficiently large partiles, the effect of surface curvature on the vapor pressure at the surface, the Kelvin effect, can be neglected.) If the rate determining step for condensation is a chemical reaction occurring throughout the volume of the particle, then

$$\alpha_0(v) = \sigma' v \tag{22}$$

In general, therefore, in the continuum regime condensation growth laws can be expressed in the general form

*Solutions of the coagulation equation may also be obtained for $\beta = \beta_2 v\tilde{v}$, however this kernel leads to the prediction that the total number of particles equals zero after a time $2/\beta_2 N_0 v_0^2$, where N_0 is the initial number of particles and v_0 is the initial mean volume.

$$\alpha_0(v) = \sigma v^{\gamma} \tag{23}$$

where $0 \leq \gamma \leq 1$. For the purpose of examining limiting situations of condensation growth we will henceforth confine our attention to the two cases, $\gamma = 0$ and $\gamma = 1$. These two cases represent the two extremes of condensation, growth independent of particle size, and growth linearly proportional to particle volume.

DYNAMIC BEHAVIOR OF THE SIZE DISTRIBUTION DENSITY

The object of this section is to obtain solutions to (16) for the coagulation and condensation processes outlined in the previous section. We have selected two initial conditions and three coagulation/condensation combinations for study. Specifically, we consider the following cases:*

(1) $\beta = \beta_0$, $\alpha_0 = \sigma_1 v$ (constant coagulation rate, linear condensation rate)

(2) $\beta = \beta_1 (v+\tilde{v})$, $\alpha_0 = \sigma_1 v$ (linear coagulation rate, linear condensation rate)

(3) $\beta = \beta_0$, $\alpha_0 = \sigma_0$ (constant coagulation rate, constant condensation rate)

Two initial distributions are employed, an exponential and a first order gamma distribution. We define N_0 as the initial total number of particles and ν_0 as the mean volume of the initial size distribution. Then the two initial distributions are

$$n_0(v) = \frac{N_0}{\nu_0} \exp\left(-\frac{v}{\nu_0}\right) \tag{24}$$

$$n_0(v) = \frac{N_0 v}{\nu_0^2} \exp\left(-\frac{v}{\nu_0}\right) \tag{25}$$

*The obvious fourth case, namely $\beta = \beta_1(v+\tilde{v})$, $\alpha_0 = \sigma_0$, while amenable in principle to analytical solution poses significant difficulties and a solution cannot be obtained.

The fact that $n_o(0)$ is nonzero for (24) does not cause difficulties, although it is not physically realistic at $v = 0$.

We begin by considering the behavior of the first two moments of the size distribution in each of the three cases. We then describe briefly the solutions in each of the three cases. Examination of the solutions and detailed discussion is contained in the next section.

Moments of the Distributions

The first two moments of $n(v,t)$ are $M_o(t)$, the total number of particles present, and $M_1(t)$, the total volume of particles present, defined by

$$M_o(t) = \int_o^\infty n(v,t)\, dv \tag{26}$$

$$M_1(t) = \int_o^\infty vn(v,t)\, dv \tag{27}$$

$$M_o(0) = N_o \; ; \quad M_1(0) = N_o v_o$$

Equations governing $M_o(t)$ and $M_1(t)$ for all three cases are easily obtained by integrating (16) over v from 0 to ∞ and by multiplying (16) by v and then integrating, respectively. Table 1 presents the differential equations governing M_o and M_1 and their solutions for each of the three cases.

In case (1) it is clear that the total number of particles in influenced only by coagulation, and the total volume of particles is influenced only by condensation. Since the coagulation rate is independent of particle size, the growth from condensation does not affect the total number of particles. In case (2), however, the total number of particles is influenced by both

Table 1. Moments of the Distributions, M_0 and M_1

Case	Differential equations for M_0 and M_1	M_0 and M_1	M_0 and M_1 (dimensionless)
(1) $\beta = \beta_0$ $\alpha_0 = \sigma_1 v$	$\frac{dM_0}{dt} = -\frac{\beta_0}{2} M_0^2$ $\frac{dM_1}{dt} = \sigma_1 M_1$	$M_0 = \frac{2N_0}{2+\beta_0 N_0 t}$ $M_1 = N_0 \nu_0 \exp(\sigma_1 t)$	$\frac{M_0}{N_0} = \frac{2}{2+\tau/\Lambda}$ $\frac{M_1}{N_0 \nu_0} = e^{\tau}$
(2) $\beta = \beta_1 (v+\tilde{v})$ $\alpha_0 = \sigma_1 v$	$\frac{dM_0}{dt} = -\beta_1 M_0 M_1$ $\frac{dM_1}{dt} = \sigma_1 M_1$	$M_0 = N_0 \exp\left[\frac{\beta_1 N_0 \nu_0}{\sigma_1}(1-\exp\sigma_1 t)\right]$ $M_1 = N_0 \nu_0 \exp(\sigma_1 t)$	$\frac{M_0}{N_0} = \exp\left[\frac{(1-\exp\tau)}{\Lambda}\right]$ $\frac{M_1}{N_0 \nu_0} = e^{\tau}$
(3) $\beta = \beta_0$ $\alpha_0 = \sigma_0$	$\frac{dM_0}{dt} = -\frac{\beta_0}{2} M_0^2$ $\frac{dM_1}{dt} = \sigma_0 M_0$	$M_0 = \frac{2N_0}{2+\beta_0 N_0 t}$ $M_1 = N_0 \nu_0 \left[1 - \frac{2\sigma_0}{\beta_0 N_0 \nu_0} \ln\left(\frac{2}{2+\beta_0 N_0 t}\right)\right]$	$\frac{M_0}{N_0} = \frac{2}{2+\tau/\Lambda}$ $\frac{M_1}{N_0 \nu_0} = 1 - 2\Lambda \ln\left(\frac{2}{2+\tau/\Lambda}\right)$

coagulation and condensation because in this case the coagulation rate is volume dependent. The total particle volume is still unaffected by coagulation because the condensation growth rate is a linear function of particle volume. In case (3), as in case (1), the total number of particles is affected only by coagulation because the coagulation rate is volume independent. However, because each particle grows at the same rate independent of its volume, the total particle volume depends only on the number of particles present.

The moment relations in Table 1 will prove to be very useful when we proceed to obtaining solutions for $n(v,t)$ in the three cases.

Dimensionless Groups and Evolution of M_0 and M_1

Since there are two processes taking place, there are two fundamental characteristic times, one for coagulation and one for condensation. The ratio of these two times is the basic dimensionless group of the problem. Let us define Λ as the ratio of the characteristic time for condensation to that for coagulation. The definitions of Λ in the three cases are:

(1) $$\Lambda = \frac{\sigma_1}{\beta_0 N_0}$$

(2) $$\Lambda = \frac{\sigma_1}{\beta_1 N_0 \nu_0}$$

(3) $$\Lambda = \frac{\sigma_0}{\beta_0 N_0 \nu_0}$$

If we define dimensionless times on the basis of the characteristic times for condensation as follows: (1) $\tau = \sigma_1 t$, (2) $\tau = \sigma_1 t$, (3) $\tau = \sigma_0 t/\nu_0$, then the moments M_0 and M_1 can be expressed in dimensionless form as shown in the last column of Table 1.

Figures 1-3 show the time evolution of M_0 and M_1 in the respective dimensionless forms, M_0/N_0 and $M_1/N_0 v_0$, for each of the three cases in Table 1. The dimensionless time τ is, as noted above, based on the characteristic time for condensation. Thus, the value of Λ governs the relative rates of coagulation and condensation. For example, for $\Lambda = 10$, the rate of condensation is 10 times faster than the rate of coagulation. Figures 1-3 show, therefore, the effect of widely varying condensation and coagulation rates ($\Lambda = 0.1, 1, 10$) on the number of particles and the total volume of particles.

When the volume dependence of the condensation rate is linear, i.e. $\alpha_0 = \sigma_1 v$, variation of Λ has no effect on the evolution of the total particle volume of the system. This occurs because each particle grows at a rate dependent on its volume. Thus, in Figures 1 and 2, there is only a single curve for $M_1/N_0 v_0$. The total number of particles decreases more rapidly when $\beta = \beta_1(v + \tilde{v})$ than when $\beta = \beta_0$ because coagulation becomes more efficient as particles grow when β is volume dependent. It is evident that in condensation-dominated systems ($\Lambda \geq 10$), the total number of particles is relatively insensitive to the particular coagulation mechanism. In the coagulation-dominated regime ($\Lambda \leq 0.1$), the linear coagulation mechanism is clearly more efficient in removing particles than is the constant coagulation mechanism.

In case 3 ($\alpha_0 = \sigma_0$ and $\beta = \beta_0$) M_1 is influenced by the coagulation rate. Since condensation is size independent, the overall rate of growth is dependent only on the number of particles present. The more efficient is the coagulation mechanism, the faster the number of particles is depleted, and the slower is the rate of growth by condensation. This effect is evident by the decrease in the total volume curves for decreasing Λ. The time evolution of M_0 is identical to that shown in Figure 1.

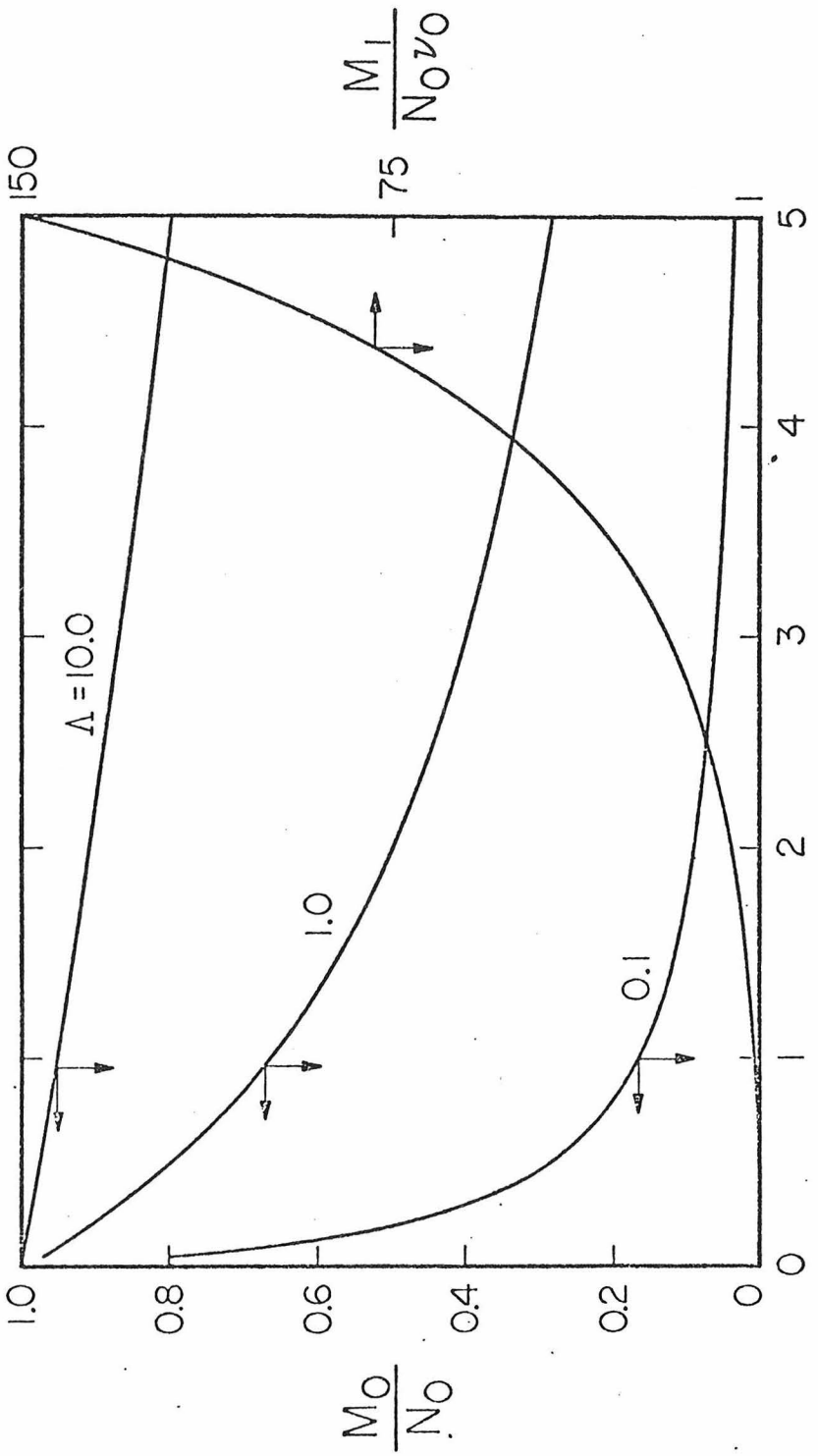

FIGURE 1

Time evolution of number and volume fraction for linear condensation and constant coagulation ($\tau = \sigma_1 t$, $\Lambda = \sigma_1/\beta_0 N_0$).

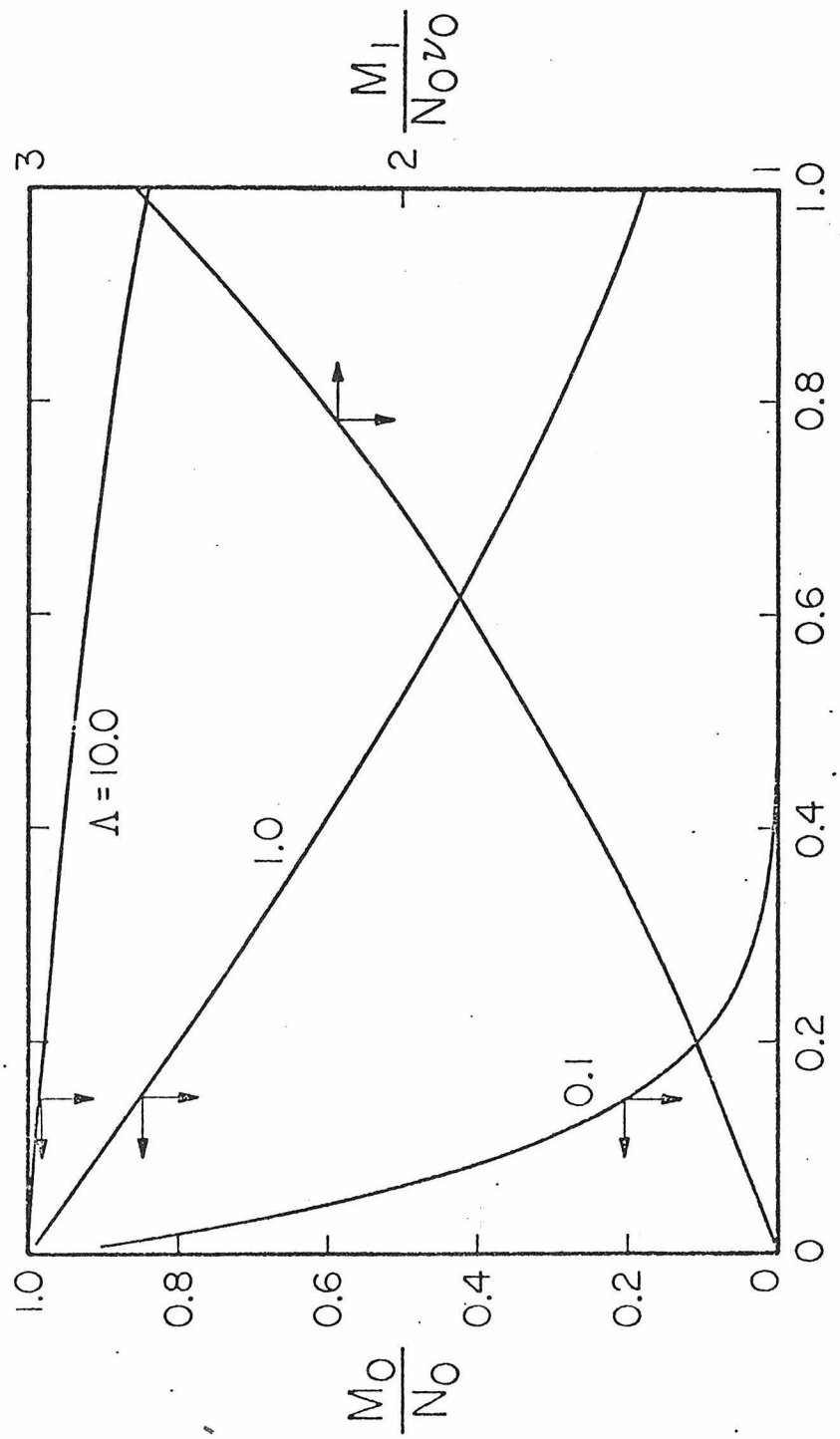

FIGURE 2

Time evolution of number and volume fraction for linear condensation and linear coagulation ($\tau = \sigma_1 t$, $\Lambda = \sigma_1/\beta_1 N_0 v_0$).

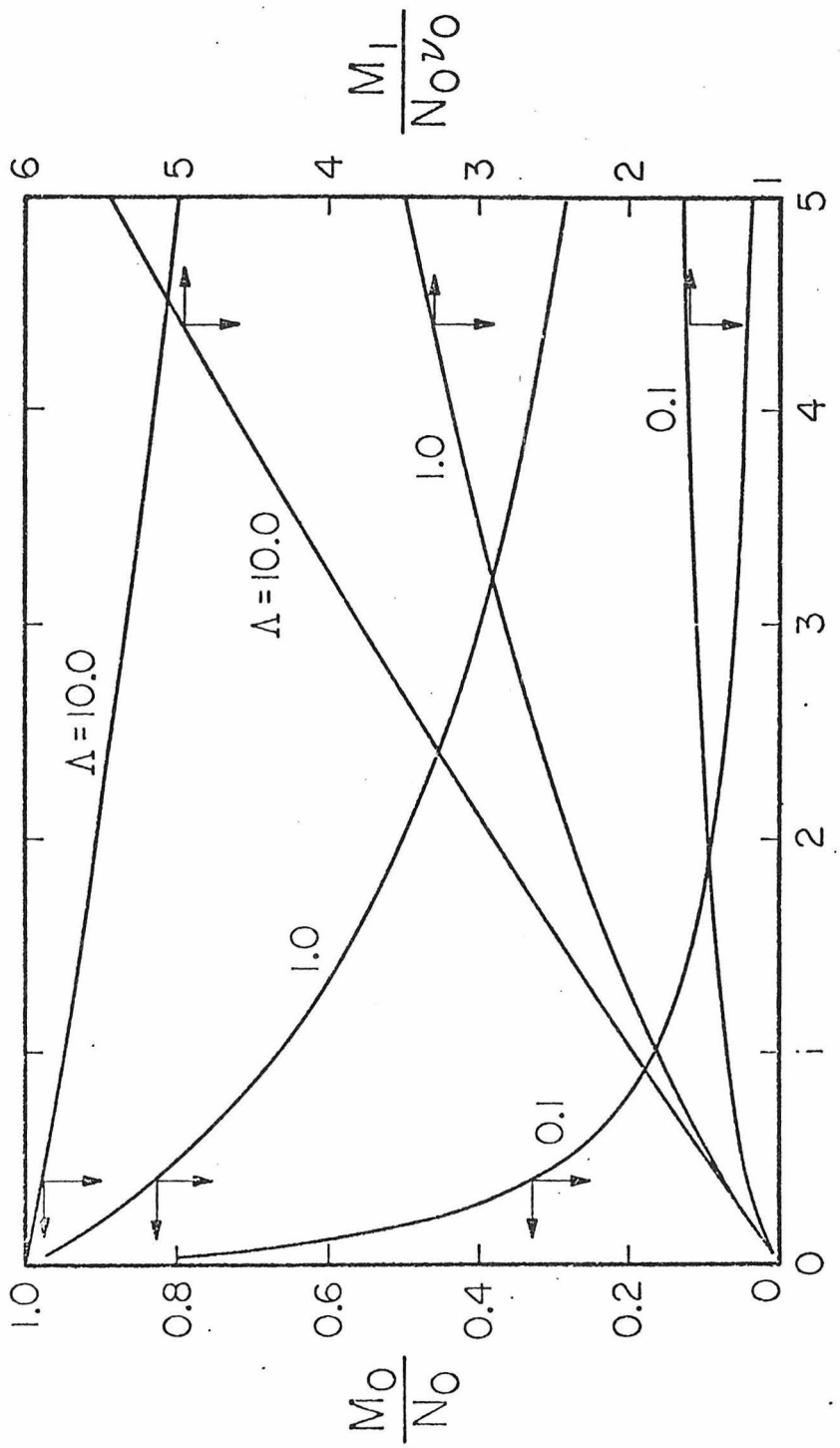

FIGURE 3

Time evolution of number and volume fraction for constant condensation and constant coagulation ($\tau = \sigma_0 t/v_0$, $\Lambda \equiv \sigma_0/\beta_0 N_0 v_0$).

Pure Coagulation and Pure Condensation

Solutions of the coagulation equation,

$$\frac{\partial n}{\partial t} = \frac{1}{2}\int_0^v \beta(v-\tilde{v},\tilde{v})n(v-\tilde{v},t)n(\tilde{v},t)d\tilde{v} - \int_0^\infty \beta(v,\tilde{v})n(v,t)n(\tilde{v},t)\, d\tilde{v} \qquad (28)$$

for the cases of $\beta = \beta_0$ and $\beta = \beta_1(v + \tilde{v})$ are given in Table 2. Solutions are presented for both coagulation constants for initial condition (24) and for $\beta = \beta_0$ for initial condition (25). The size distribution density in the two cases of pure condensation, $\alpha_0 = \sigma_0$ and $\alpha_0 = \sigma_1 v$, are, respectively,

$$n(v,t) = \begin{cases} n_0(v - \sigma_0 t) & v - \sigma_0 t > 0 \\ 0 & v - \sigma_0 t < 0 \end{cases} \qquad (29)$$

$$n(v,t) = n_0(\exp(-\sigma_1 t))\exp(-\sigma_1 t) \qquad (30)$$

Figure 4 shows the size distribution density at various times for the cases of constant ($\alpha_0 = \sigma_0$) and linear ($\alpha_0 = \sigma_1 v$) condensation rates. Figure 5 presents the same comparison for pure coagulation. In all subsequent plots the dimensionless ordinate and abscissa of Figures 4 and 5 will be used. The abscissa is the logarithm of the ratio v/v_0, whereas the ordinate is the dimensionless number density corresponding to the abscissa. We note that the ordinate of Figures 4 and 5 is related to n(v,t) by

$$n\left(\log\left(\frac{v}{v_0}\right),t\right) = 2.303v\, n(v,t) \qquad (31)$$

In Figure 4 the dimensionless times τ' and τ'' are defined for the two condensation processes. The discontinuous nature of the size distribution is evident with a constant condensation rate. Since all particles grow at the same rate, there remain at any given time, no particles of volume less

Table 2. Size Distribution Density Functions $n(v,t)$ for Pure Coagulation

Coagulation Constant β	Initial Size Distribution $n_0(v)$: $\frac{N_0}{\nu_0} \exp\left(-\frac{v}{\nu_0}\right)$	Initial Size Distribution $n_0(v)$: $\frac{N_0 v}{\nu_0^2} \exp\left(-\frac{v}{\nu_0}\right)$
β_0	$\frac{(1-T)^2}{\nu_0} N_0 \exp\left[-(1-T)\frac{v}{\nu_0}\right]$	$\frac{(1-T)^2}{\sqrt{T}} \frac{N_0}{\nu_0} \exp\left(-\frac{v}{\nu_0}\right) \sinh\left(\frac{v\sqrt{T}}{\nu_0}\right)$
$\beta_1(v + \tilde{v})$	$\frac{1-T}{\sqrt{T}} \frac{N_0}{v} \exp\left(-(1+T)\frac{v}{\nu_0}\right) I_1\left(2\sqrt{T}\frac{v}{\nu_0}\right)$	$(1-T)\frac{N_0}{\nu_0} \exp\left(-\frac{(2+T)v}{2\nu_0}\right) \sum_{k=0}^{\infty} \frac{T^k \left(\frac{v}{\nu_0}\right)^{3k+1}}{2^k (k+1)!(2k+1)!}$

$$T \equiv 1 - \frac{M_0}{N_0}$$

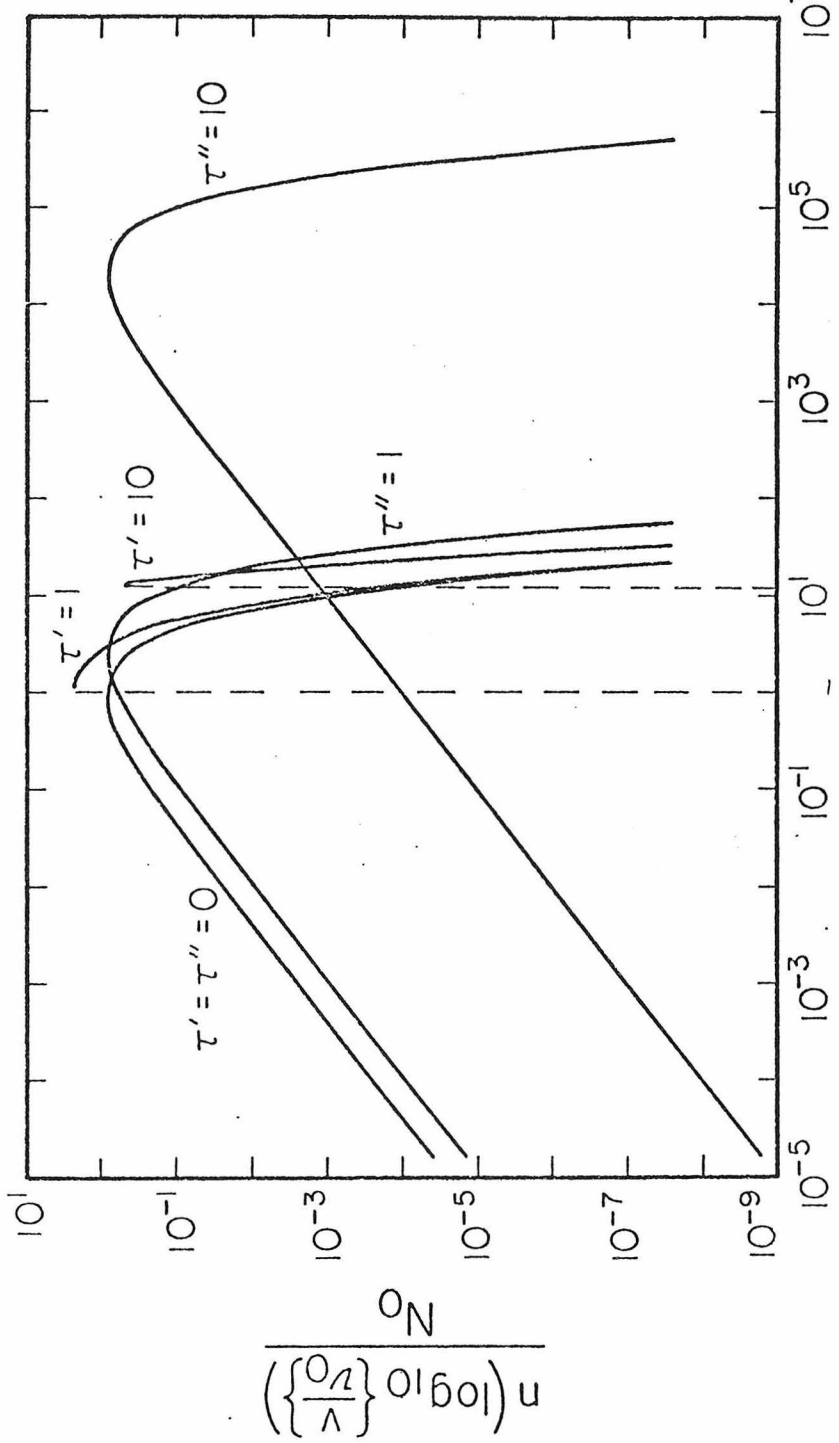

FIGURE 4

Pure condensation particle size spectra for constant condensation ($\tau' = \sigma_0 t/\nu_0$) and linear condensation ($\tau'' = \sigma_1 t$).

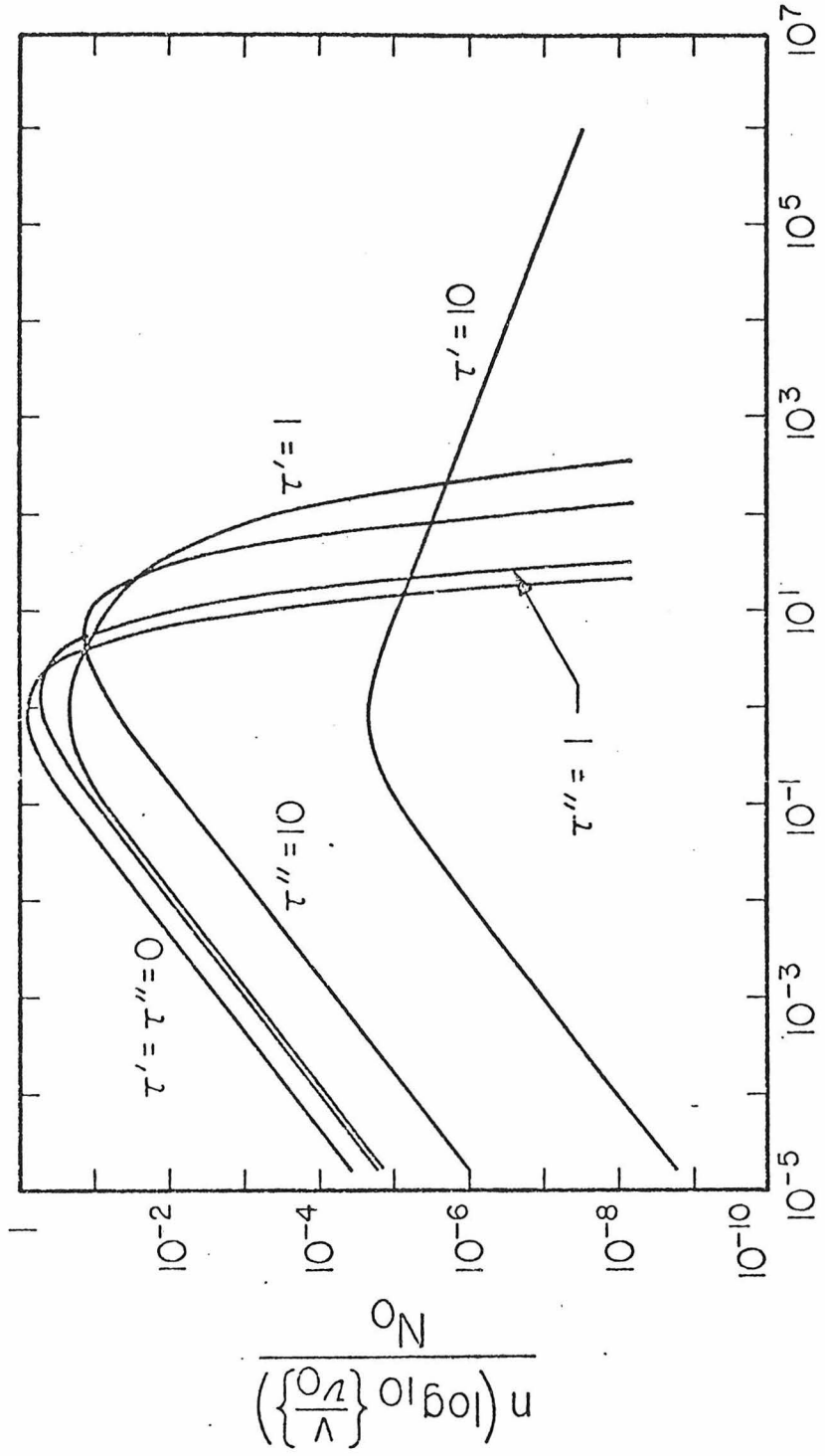

FIGURE.5

Pure coagulation particle size spectra for constant coagulation ($\tau'' = \beta_o N_o t$) and linear coagulation ($\tau' = \beta_1 N_o \nu_o t$).

than $\sigma_o t$. Also, because of the constant growth rate, the relative volume increase becomes smaller for larger particles. The size distribution becomes more and more narrow, for long times approximately centered about $v = \sigma_o t$.

The linear condensation growth rate ($\alpha_o = \sigma_1 v$) is characterized by a steady accumulation of particles in the larger sizes. However, unlike the situation of a constant condensation rate, the smaller particles are never fully depleted because of the vanishingly small growth rate for small volumes.

In Figure 5 the normalized size distributions for constant and linear coagulation rates are compared at various times. Note that the characteristic times are now based on the coagulation process. As expected, a linear coagulation rate results in a pronounced shift of the size distribution to larger sizes and a general spreading of the upper end of the size spectrum relative to that for a constant coagulation rate.

Size Distribution Density Function. Case 1.

In case (1), (16) becomes

$$\frac{\partial n(v,t)}{\partial t} + \sigma_1 \frac{\partial}{\partial v}(vn) = \frac{\beta_o}{2}\int_o^v n(v-\tilde{v},t)n(\tilde{v},t)\,d\tilde{v} - \beta_o n(v,t)M_o(t) \qquad (32)$$

The solution of (32) proceeds through Laplace transformation with respect to v to give an equation for $\bar{n}(s,t) = L[n(v,t)]$. If we define $\bar{p}(s,T) = 2\bar{n}(s,t)/(1-T)^2$, where $T = 1 - M_o/N_o$, the resulting equation for $\bar{p}(s,T)$ is

$$\frac{\partial \bar{p}}{\partial T} - 2\Lambda \frac{s}{(1-T)^2}\frac{\partial \bar{p}}{\partial s} = \frac{\bar{p}^2}{2N_o} \qquad (33)$$

Equation (33) can be solved by the method of characteristics for each of the initial conditions (24) and (25) to give, respectively,

$$\bar{p}(s,T) = \frac{2\,\frac{N_o}{\nu_o}\exp\left(-\frac{2\Lambda T}{1-T}\right)}{S + \frac{(1-T)}{\nu_o}\exp\left(-\frac{2\Lambda T}{1-T}\right)} \tag{34}$$

and

$$\bar{p}(s,T) = \frac{2N_o/\nu_o^2}{\left[s\exp\left(\frac{2\Lambda T}{1-T}\right) + \frac{1}{\nu_o}\right]^2 - \frac{T}{\nu_o^2}} \tag{35}$$

Upon inverting (34) and (35) we obtain, respectively (Roberts and Kaufman, 1966),

$$n(v,t) = \frac{N_o}{\nu_o}(1-T)^2\exp\left(-\frac{2\Lambda T}{1-T}\right)\exp\left[-\frac{v}{\nu_o}(1-T)\exp\left(-\frac{2\Lambda T}{1-T}\right)\right] \tag{36}$$

and

$$n(v,t) = \frac{N_o(1-T)^2}{\nu_o\sqrt{T}}\exp\left(-\frac{2\Lambda T}{1-T}\right)\exp\left[-\frac{v}{\nu_o}\exp\left(-\frac{2\Lambda T}{1-T}\right)\right]\sinh\left[\frac{v}{\nu_o}\sqrt{T}\exp\left(-\frac{2\Lambda T}{1-T}\right)\right] \tag{37}$$

Size Distribution Density Function. Case 2

The basic equation for $n(v,t)$ in case (2) is

$$\frac{\partial n}{\partial t} + \sigma_1\frac{\partial}{\partial v}(vn) = \frac{\beta_1}{2}\int_o^v vn(v-\tilde{v},t)n(\tilde{v},t)\,d\tilde{v} - \beta_1 n(v,t)\,[vM_o(t) + M_1(t)] \tag{38}$$

The dimensionless time which is most convenient for this case is

$$T = 1 - \frac{N_o \nu_o}{M_1(t)} = 1 - \exp \tau \tag{39}$$

Again the solution is carried out through a Laplace transform with respect to v. If we let

$$\bar{p}(s,T) = \exp\left[\frac{1}{\Lambda(1-T)}\right]\bar{n}(s,t) \tag{40}$$

then $\bar{p}(s,T)$ is governed by

$$(1-T)\frac{\partial \bar{p}}{\partial T} - \left\{s + \frac{1}{\Lambda \nu_o}\exp\left[-\frac{1}{\Lambda(1-T)}\right]\left[\exp\left(\frac{1}{\Lambda}\right) - \frac{\bar{p}}{N_o}\right]\right\}\frac{\partial \bar{p}}{\partial s} = 0 \tag{41}$$

Equation (41) is solved by the method of characteristics. In this case we consider only initial condition (24), the exponential distribution since initial condition (25) leads to an analytically intractable situation.*

$$\bar{p}(s,T) = \frac{2(1-T)(N_o/\nu_o)\exp(1/\Lambda)}{s + \frac{(1-T)(2-\omega)}{\nu_o} \pm \sqrt{\left(s + \frac{(1-T)(2-\omega)}{\nu_o}\right)^2 - \left[\frac{2(1-T)}{\nu_o}\sqrt{(1-\omega)}\right]^2}} \tag{42}$$

where

$$\omega = \exp\left[-\frac{T}{\Lambda(1-T)}\right] \tag{43}$$

The positive root in the denominator of (42) is found to lead to the physically realistic solution. Upon inverting (42) we obtain (Roberts and Kaufman, 1966)

*The resultant equation for s_o is cubic, the solution of which (in terms of s) leads to an analytically intractable inversion.

$$n(v,t) = \frac{N_o\omega}{v\sqrt{1-\omega}} \exp\left[-(1-T)(2-\omega)\frac{v}{v_o}\right] I_1\left[2(1-T)\sqrt{1-\omega}\,\frac{v}{v_o}\right] \tag{44}$$

where $I_1(\cdot)$ is the modified Bessel function of the first kind of order one.

Size Distribution Density Function. Case 3

The basic differential equation for n(v,t) in case (3) is

$$\frac{\partial n}{\partial t} + \sigma_o \frac{\partial n}{\partial v} = \frac{\beta_o}{2}\int_o^v n(v-\tilde{v},t)n(\tilde{v},t)\,d\tilde{v} - \beta_o n(v,t)M_o(t) \tag{45}$$

The dimensionless time appropriate for this case is $T = N_o/M_o - 1$. Taking Laplace transform of (45), and introducing T, we obtain

$$\frac{\partial \bar{n}(s,T)}{\partial T} + 2\left(\Lambda v_o s + \frac{1}{1+T}\right)\bar{n} = \frac{\bar{n}^2}{N_o} \tag{46}$$

where it has been assumed that n(0,t) = 0. We now let $\chi = 1 + T$, and define $\bar{p}(s,\chi) = \chi^2 \exp(2\Lambda v_o s\chi)\bar{n}(s,T)$, obtaining

$$\frac{\partial \bar{p}}{\partial \chi} = \frac{\exp(-2\Lambda v_o s\chi)}{N_o\chi^2}\,\bar{p}^2 \tag{47}$$

Integrating (47), we obtain

$$\frac{1}{\bar{p}(s,\chi)} = \frac{1}{\bar{p}(s,1)} - \frac{1}{N_o}\int_1^\chi \frac{\exp(-2\Lambda v_o s\eta)}{\eta^2}\,d\eta \tag{48}$$

which can be expressed as (Abramowitz and Stegun, p. 260, 1965)

$$\frac{1}{\bar{p}(s,\chi)} = \frac{1}{\bar{p}(s,1)} - \frac{2\Lambda v_o s}{N_o}\left[\Gamma(-1,2\Lambda v_o s) - \Gamma(-1,2\Lambda v_o s\chi)\right] \tag{49}$$

where $\Gamma(a,b)$ is the incomplete gamma function.

Noting that (Abramowitz and Stegun, p. 262, 1965)

$$E_n(z) = z^{n-1}\Gamma(1-n,z) \tag{50}$$

where $E_n(z)$ is the exponential integral of the nth kind, (49) can be written as

$$\frac{1}{\bar{p}(s,\chi)} = \frac{1}{\bar{p}(s,1)} - \frac{2\Lambda\nu_o s}{N_o}\left[\frac{E_2(2\Lambda\nu_o s)}{2\Lambda\nu_o s} - \frac{E_2(2\Lambda\nu_o s\chi)}{2\Lambda\nu_o s\chi}\right] \tag{51}$$

We note that

$$\bar{p}(s,1) = \exp(2\Lambda\nu_o s)\bar{n}_o(s) \tag{52}$$

For $n_o(v)$ given by (24) and (25)

$$\bar{p}(s,1) = \frac{N_o \exp(2\Lambda\nu_o s)}{1+s\nu_o} \tag{53}$$

and

$$\bar{p}(s,1) = \frac{N_o \exp(2\Lambda\nu_o s)}{(1+s\nu_o)^2} \tag{54}$$

respectively.

Substituting (53) or (54) into (51), and returning to $\bar{n}(s,\chi)$, we obtain

$$\bar{n}(s,\chi) = \frac{N_o \exp(-2\Lambda\nu_o s(\chi-1))/\chi^2}{1+\nu_o s-2\Lambda\nu_o s \exp(2\Lambda\nu_o s)\left[\frac{E_2(2\Lambda\nu_o s)}{2\Lambda\nu_o s} - \frac{E_2(2\Lambda\nu_o s\chi)}{2\Lambda\nu_o s\chi}\right]} \tag{55}$$

and

$$\bar{n}(s,\chi) = \frac{N_o \exp(-2\Lambda\nu_o s(\chi-1))/\chi^2}{(1+\nu_o s)^2 - 2\Lambda\nu_o s \exp(2\Lambda\nu_o s)\left[\frac{E_2(2\Lambda\nu_o s)}{2\Lambda\nu_o s} - \frac{E_2(2\Lambda\nu_o s\chi)}{2\Lambda\nu_o s\chi}\right]} \tag{56}$$

respectively.

Equations (55) and (56) cannot be readily inverted. Thus, we investigate the solution for the limiting cases $\Lambda\nu_o s \ll 1$ and $\Lambda\nu_o s\chi \ll 1$.

Physically, $\nu_o s \ll 1$ implies a solution valid in the upper end of the size spectrum, and $\Lambda \ll 1$ implies a coagulation-dominated regime. So long as χ remains of order 1, $\Lambda\nu_o s \ll 1$ implies $\Lambda\nu_o s\chi \ll 1$, and no apparent restriction on time (other than $\chi = O(1)$) is necessary. Hence, we would expect that, for $\chi = O(1)$, the solution in the regime of approximately equal condensation/coagulation rates ($\Lambda \sim 1$) will be valid only for very large particles, whereas a slightly wider spectrum will be valid under coagulation-dominated regimes ($\Lambda < 1$). Also, as condensation begins to dominate coagulation, we would expect that the solution would break down.

Employing the relationships that (Abramowitz and Stegun, p. 229-231, 1965)

$$E_2(z) = \exp(-z) - z\,E_1(z) \tag{57}$$

$$E_1(z) \cong -\gamma_1 - \ln z + z + O(z^2) \tag{58}$$

where γ_1 is Euler's constant, (55) and (56) can be simplified under the constraints on $\Lambda\nu_o s$ outlined above. Equations (55) and (56) become

$$\bar{n}(s,\chi) = \frac{N_o \exp(-2\Lambda\nu_o s(\chi-1))/\chi^2}{\left[1-2\Lambda\left(\frac{\chi-1}{\chi} - \ln\chi\right)\right]s\nu_o + \frac{1}{\chi}} \tag{59}$$

and

$$\bar{n}(s,\chi) = \frac{N_o \exp(-2\Lambda\nu_o s(\chi-1))/\chi^2}{\left\{1-(2\Lambda)^2\left[\chi -1-\ln\chi- \frac{(\chi-1)^2}{\chi}\right]\right\}(\nu_o s)^2 +\left\{1-\Lambda\left[\frac{(\chi-1)}{\chi}- \ln\chi\right]\right\}2\nu_o s+ \frac{1}{\chi}} \tag{60}$$

Equations (59) and (60) were obtained in a slightly different manner. Equation (59) was obtained by linearization of all terms involving $\Lambda\nu_o s$ and $\Lambda\nu_o s\chi$, such as the exponential and exponential integral functions found in the denominator. Equation (60), on the other hand, was obtained by quadratically approximating the same functions in the denominator. The quadratic approximation is necessary in the case of initial condition (25) in order to retain the ability to regenerate exactly the initial distribution at time t = 0. The linearization of (59) is acceptable because the inversion of initial condition (24) involves only first order terms in s. Indeed, (55) could be (and has been) solved with quadratic approximations throughout, yielding a cumbersome but slightly more accurate solution. However, the difference between the solutions obtained by the linear and quadratic approximations is marginal. Also, as will become evident, the initial condition is obtained readily from the inversion of (59), whereas reduction to the initial condition for the solution obtained by quadratic approximation to (55) can only be shown by successive application of L' Hopital's rule.

It should also be noted that there is no need to approximate the exponential found in the numerator of both equations (55) and (56). In the Laplace inversion, such a term simply shifts the solution by the value of the argument of the function.

Inversion of equations (59) and (60) yields (for $v \geq \Lambda\nu_o(\chi-1)$) (Roberts and Kaufman, 1966)

$$n(v,\chi) = \frac{(N_o/\nu_o)\exp\left[-\dfrac{\dfrac{v}{\nu_o}-2\Lambda(\chi-1)}{\chi-2\Lambda(\chi-1-\chi\ell n\chi)}\right]}{\chi[\chi-2\Lambda(\chi-1-\chi\ln\chi)]} \tag{61}$$

and

$$n(v,\chi) = \frac{N_o}{\nu_o^2}\,\frac{1}{\chi R(\chi)}\,\frac{1}{g_1-g_2}\Big[\exp(g_1(v-2\Lambda\nu_o(\chi-1))) - \exp(g_2(v-2\Lambda\nu_o(\chi-1)))\Big] \tag{62}$$

where

$$g_1 = -\frac{Q+\sqrt{Q^2-R}}{R\nu_o} \tag{63}$$

$$g_2 = -\frac{Q-\sqrt{Q^2-R}}{R\nu_o} \tag{64}$$

$$Q(\chi) = \chi - \Lambda(\chi-1-\chi\ln\chi) \tag{65}$$

$$R(\chi) = \chi - (2\Lambda)^2[\chi(\chi-1-\ln\chi) - (\chi-1)^2] \tag{66}$$

To show that (61) reduces to the initial condition (24) at $t = 0$ ($\chi = 1$) is straightforward. That (62)-(66) reduce to (25) can be shown by one application of L' Hopital's rule.

Summary of the Solutions

In Table 3 we summarize the solutions for n(v,t) in the three cases studied for the two initial conditions considered. (As noted, an analytical solution for case (2) and initial condition (25) cannot be obtained.) It is important to note that the solutions in case (3) are valid only for large volumes and for $\chi = O(1)$, i.e. $N_o/M_o \lesssim 10$. In the next section we discuss the properties of these solutions. In that section only results for initial condition (24) are exhibited. Results for initial condition (25) are qualitatively similar.

DISCUSSION OF THE SOLUTIONS

Figures 6-8 show the normalized size distribution density function for case (1), i.e. $\alpha_o = \sigma_1 v$, $\beta = \beta_o$, for $\tau = 0.1$, 1, and 10, and $\Lambda = 0.1$, 1, 10. Figures 9-11 and 12-14 present cases (2) and (3), respectively, similarly, with the exception that the maximum value of τ in case (2) is 2 rather than 10. We note that in each case τ is defined on the basis of the characteristic time for condensation. When $\Lambda = 1$, the condensation and coagulation time scales are equivalent. However, when $\Lambda = 0.1$, coagulation is ten times faster than condensation. Thus, when $\Lambda = 0.1$ and $\tau = 10$, coagulation has proceeded for 100 characteristic times while condensation has proceeded for 10. On the other hand, when $\Lambda = 10$ and $\tau = 10$, condensation has taken place for 10 characteristic times and coagulation has taken place for only one. Clearly, all combinations of τ and Λ can be viewed in terms of the time scales of the two phenomena taking place.

As Λ varies in case (1) (Figs. 6-8) from 0.1 to 10, the size distributions tend to narrow. At $\Lambda = 0.1$, coagulation is occurring rapidly, tending

Table 3. Summary of the Size Distribution Density Functions

Case	Initial condition $n_0(v) = \frac{N_0}{\nu_0} \exp\left(-\frac{v}{\nu_0}\right)$	Initial condition $n_0(v) = \frac{N_0 v}{\nu_0^2} \exp\left(-\frac{v}{\nu_0}\right)$
(1) $\alpha_0 = \sigma_1 v$, $\beta = \beta_0$	$\frac{M_0^2}{M_1} \exp\left(-\frac{M_0}{M_1} v\right)$	$\frac{M_0^2}{M_1} \frac{1}{\sqrt{1-M_0/N_0}} \exp\left(-\frac{N_0 v}{M_1}\right) \sinh\left(\sqrt{1-\frac{M_0}{N_0}} \frac{N_0 v}{M_1}\right)$
(2) $\alpha_0 = \sigma_1 v$, $\beta = \beta_1(v+\tilde{v})$	$\frac{\frac{M_0^2}{M_1} \exp\left[-\frac{M_0}{M_1}\left(\frac{2N_0}{M_0}-1\right)v\right] I_1\left(2\sqrt{1-\frac{M_0}{N_0}} \frac{N_0 v}{M_1}\right)}{\frac{M_0 v}{M_1}\sqrt{1-\frac{M_0}{N_0}}}$	
(3) $\alpha_0 = \sigma_0$, $\beta = \beta_0$	$\frac{M_0^2/M_1}{1-2\Lambda\nu_0\left(\frac{N_0-M_0}{M_1}\right)} \exp\left[-\frac{\frac{M_0}{M_1}\left(v-2\Lambda\nu_0\left(\frac{N_0}{M_0}-1\right)\right)}{1-2\Lambda\nu_0\left(\frac{N_0-M_0}{M_1}\right)}\right]$	$\frac{M_0/\nu_0^2}{R[g_1-g_2]}\left\{\exp\left[g_1\left(v-2\Lambda\nu_0\left(\frac{N_0}{M_0}-1\right)\right)\right] - \exp\left[g_2\left(v-2\Lambda\nu_0\left(\frac{N_0}{M_0}-1\right)\right)\right]\right\}$

Note: g_1, g_2, Q, and R are defined in (63)-(66).

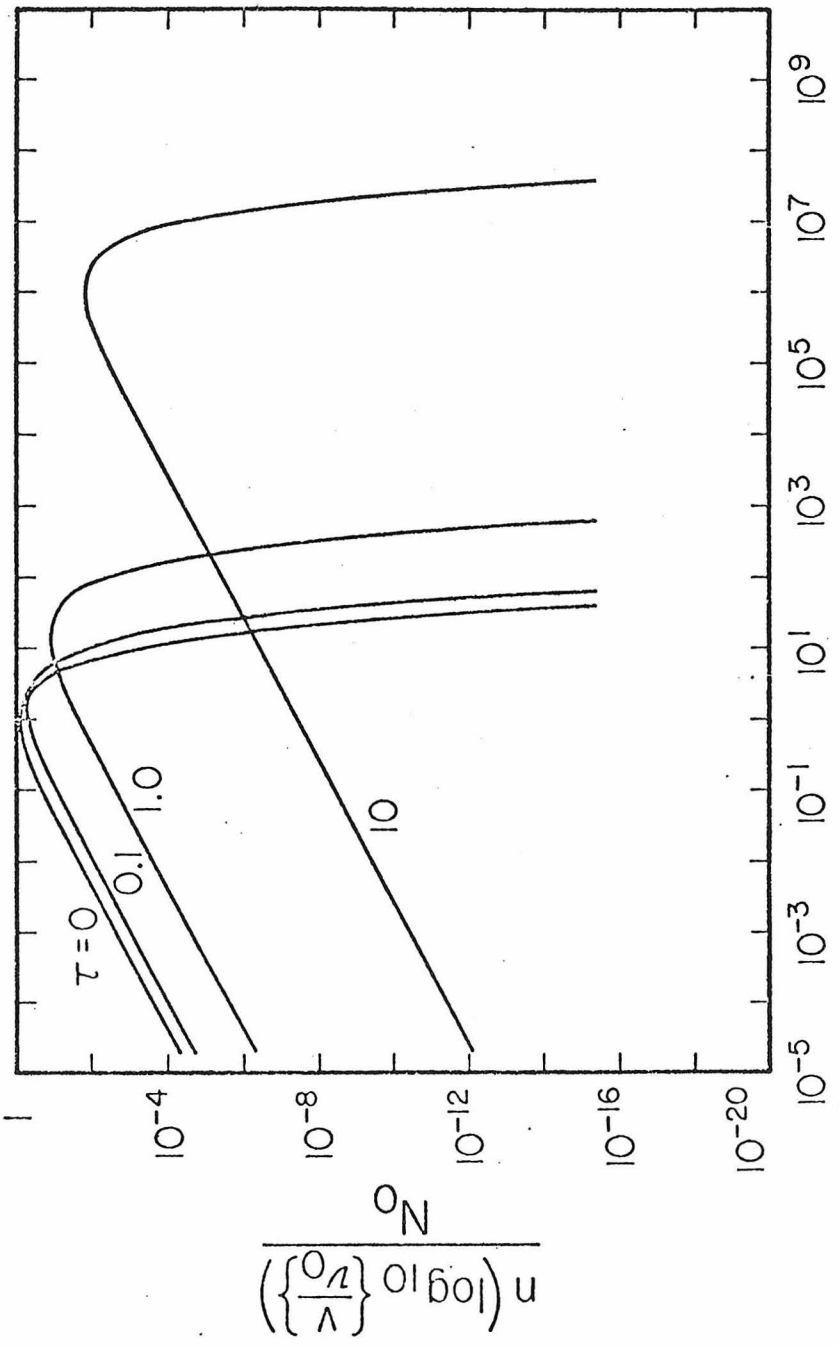

FIGURE 6.

Particle size spectra for linear condensation and constant coagulation, $\Lambda = 0.1$.

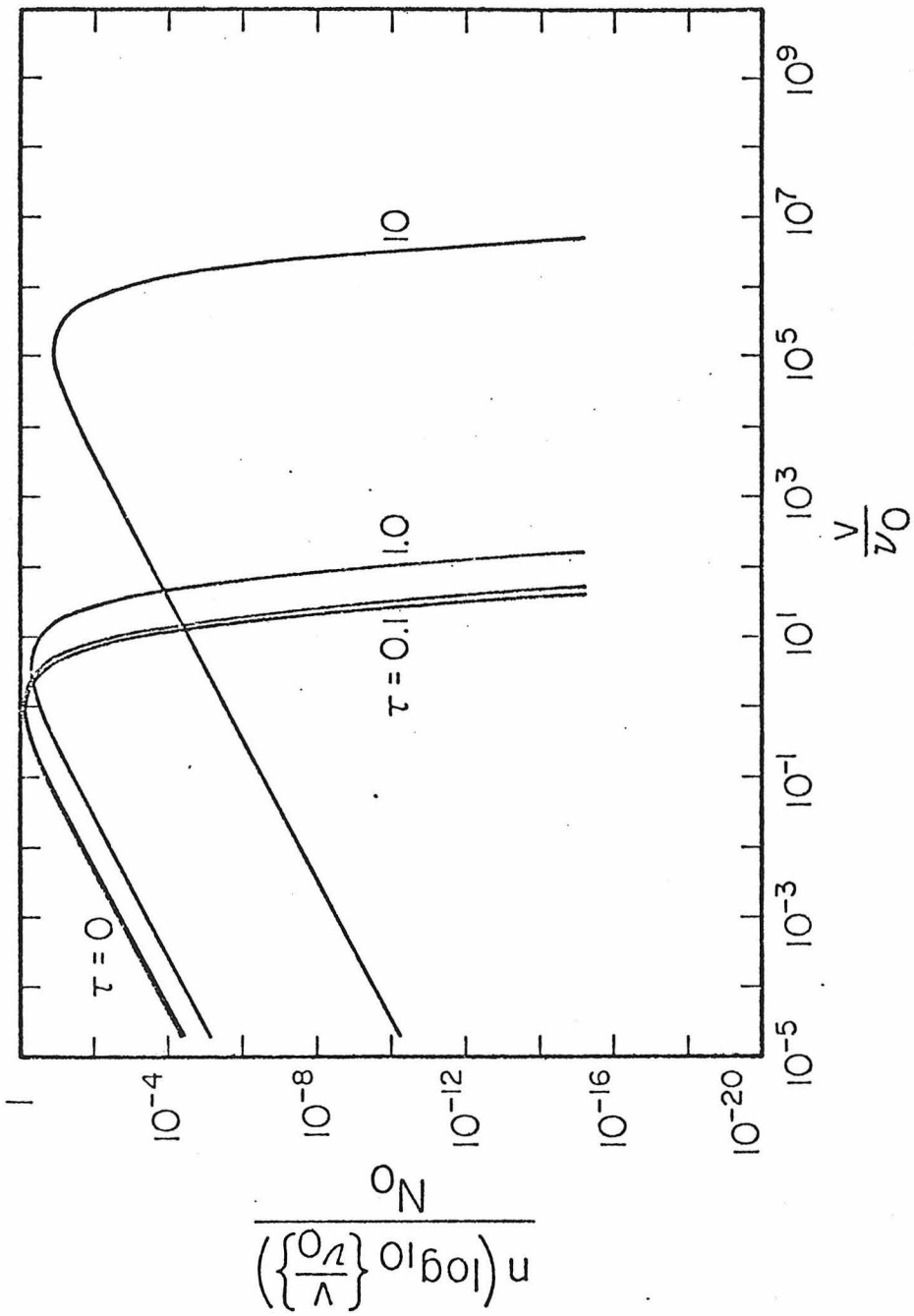

FIGURE 7

Particle size spectra for linear condensation and constant coagulation, $\Lambda = 1.0$.

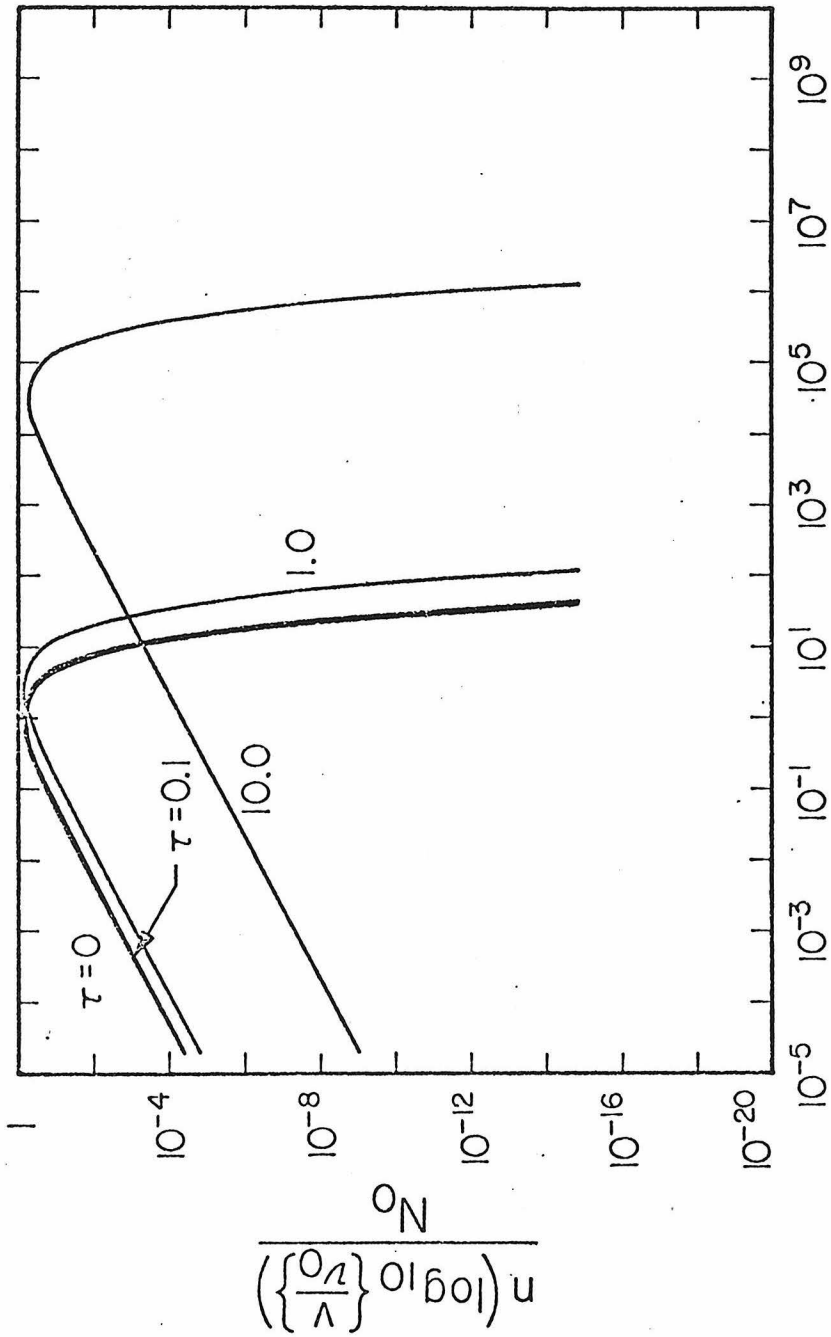

FIGURE 8

Particle size spectra for linear condensation and constant coagulation. $\Lambda = 10.0$.

to spread the upper end of the size spectrum. When $\Lambda = 10$, growth occurs mainly by condensation and the size distribution does not exhibit the broadening characteristic of coagulation growth. In case (2) (Figs. 9-11) the size distributions are significantly influenced by the value of Λ. A linear coagulation rate introduces a marked broadening in the distributions relative to a constant coagulation rate. As Λ varies from 0.1 (coagulation-dominated) to 10 (condensation-dominated) in case (2), the size distribution at $\tau = 1$ becomes markedly sharper. For $\Lambda = 0.1$, a comparison of cases (1) and (2) (Figs.6 and 9) reveals the strong influence of the volume dependence of the coagulation rate on the aerosol size distribution. The reason is, of course, that when the coagulation rate is volume-dependent, particles tend to coagulate more rapidly as they grow. (We exclude the situation in which the coagulation rate may depend inversely on volume.)

For a constant coagulation rate the upper end of the size spectrum fills out more rapidly with a linear condensation rate (Figs. 6-8) than with a constant condensation rate (Figs. 12-14). The reason is that larger particles tend to grow faster when the condensation rate is volume dependent. In addition, a constant condensation rate establishes a sharp cut-off in the lower end of the size spectrum, as already observed in Fig. 4. The cutoff volume is insensitive to Λ at any given time, since the establishment of a cutoff volume is a condensation-controlled phenomena. It is <u>not</u> independent of Λ, however. Large coagulation rates could serve to shift the cut-off volume to a point larger than expected from condensational effects alone. Finally, the "limiting solutions" for case (3) in Figs. 12-14 appear to be valid over a wider range than first expected, because of the correct prediction of the cut-off volume.

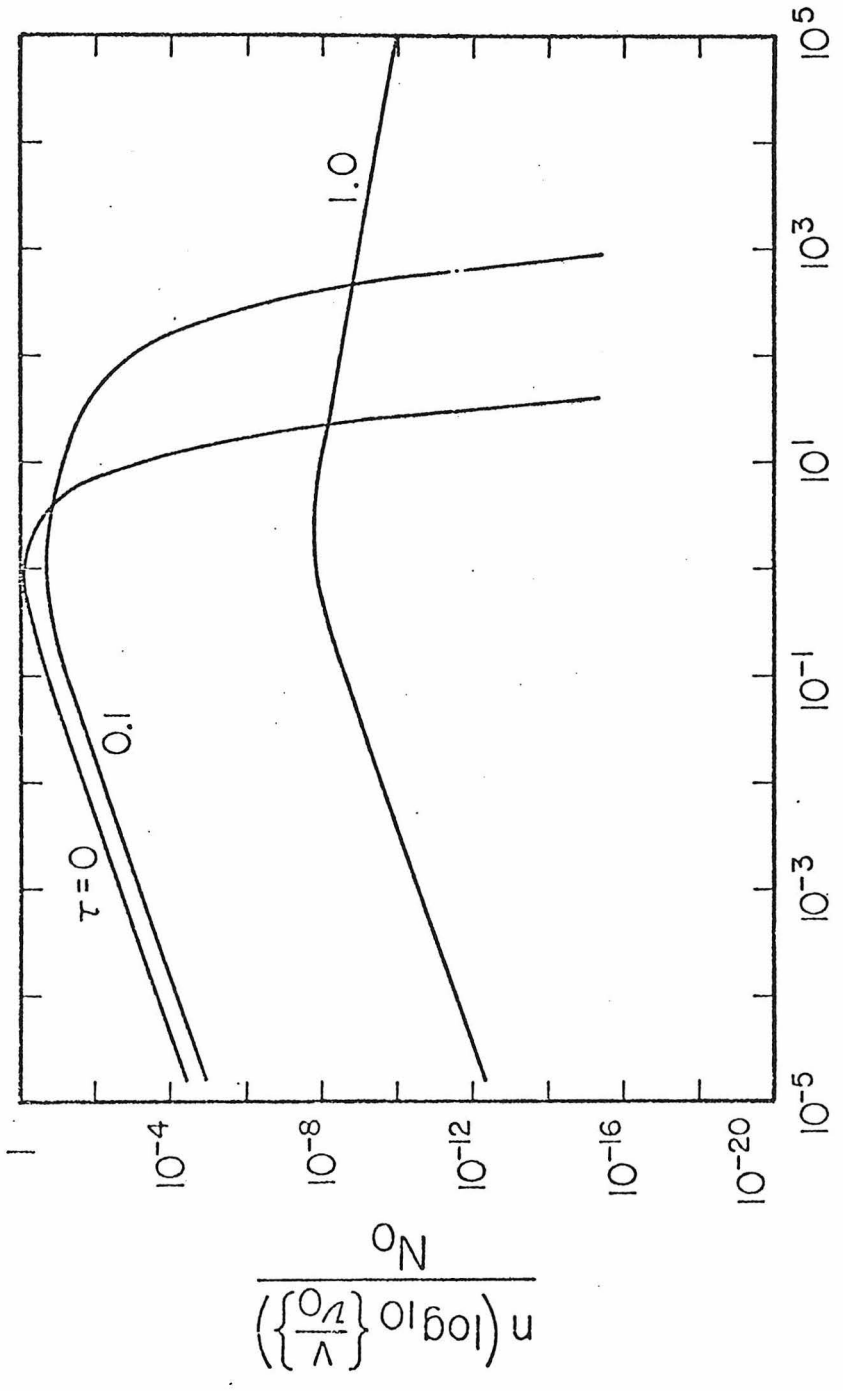

FIGURE 9

Particle size spectra for linear condensation linear coagulation. $\Lambda = 0.1$.

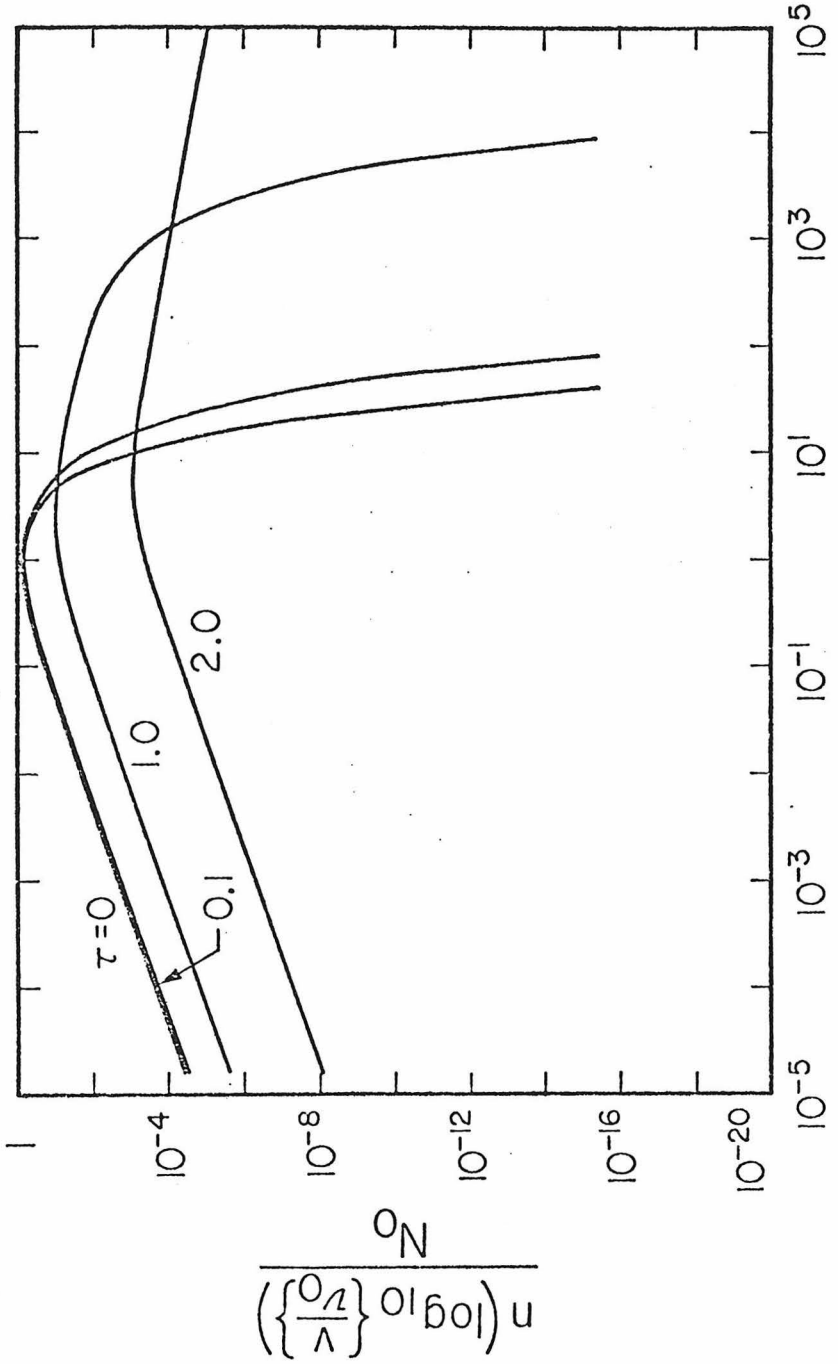

FIGURE 10

Particle size spectra for linear condensation and linear coagulation. $\Lambda = 1.0$.

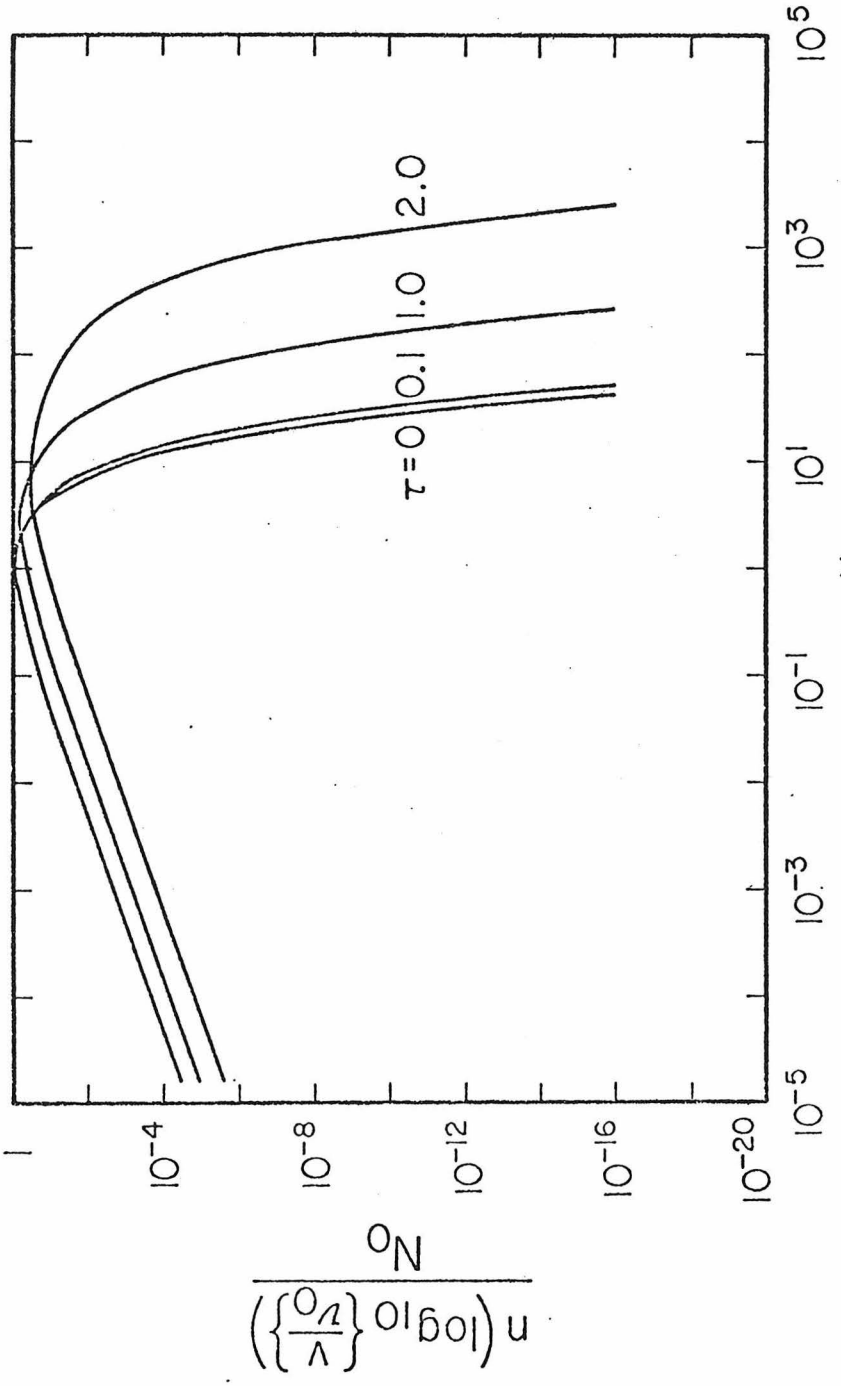

FIGURE 11

Particle size spectra for linear condensation and linear coagulation. $\Lambda = 10.0$.

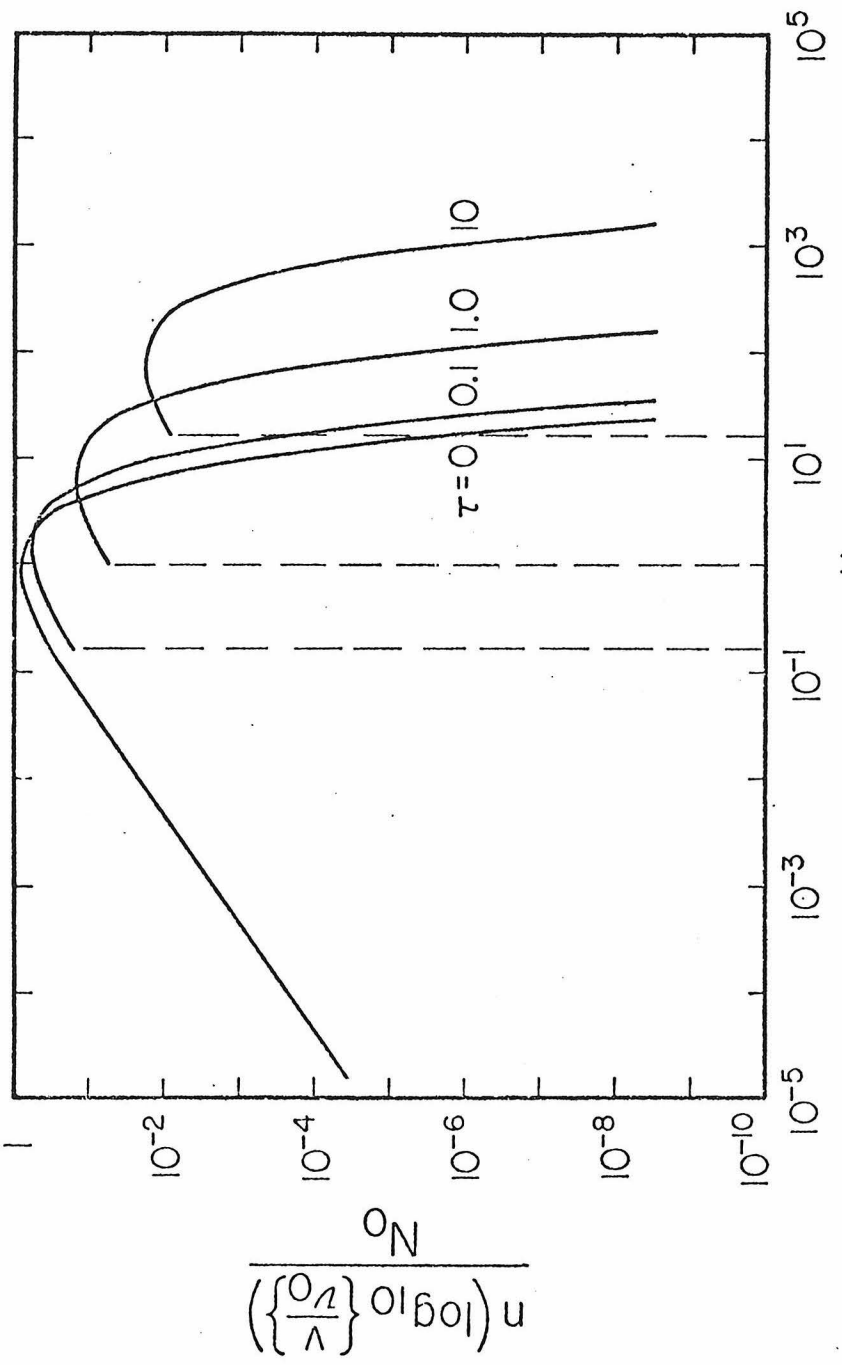

FIGURE 12

Particle size spectra for constant condensation and constant coagulation. $\Lambda = 0.1$.

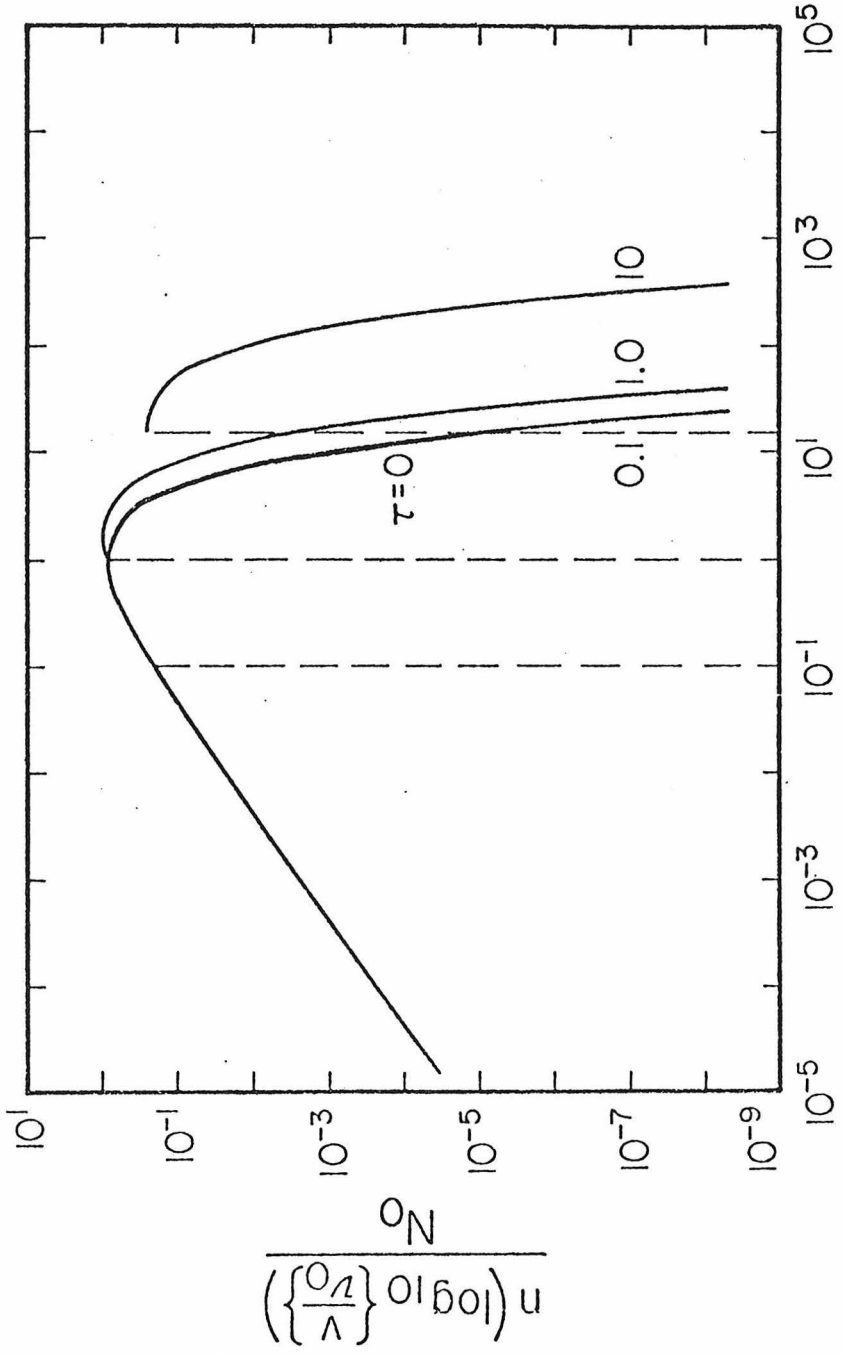

FIGURE 13
Particle size spectra for constant condensation and constant coagulation. $\Lambda = 1.0$.

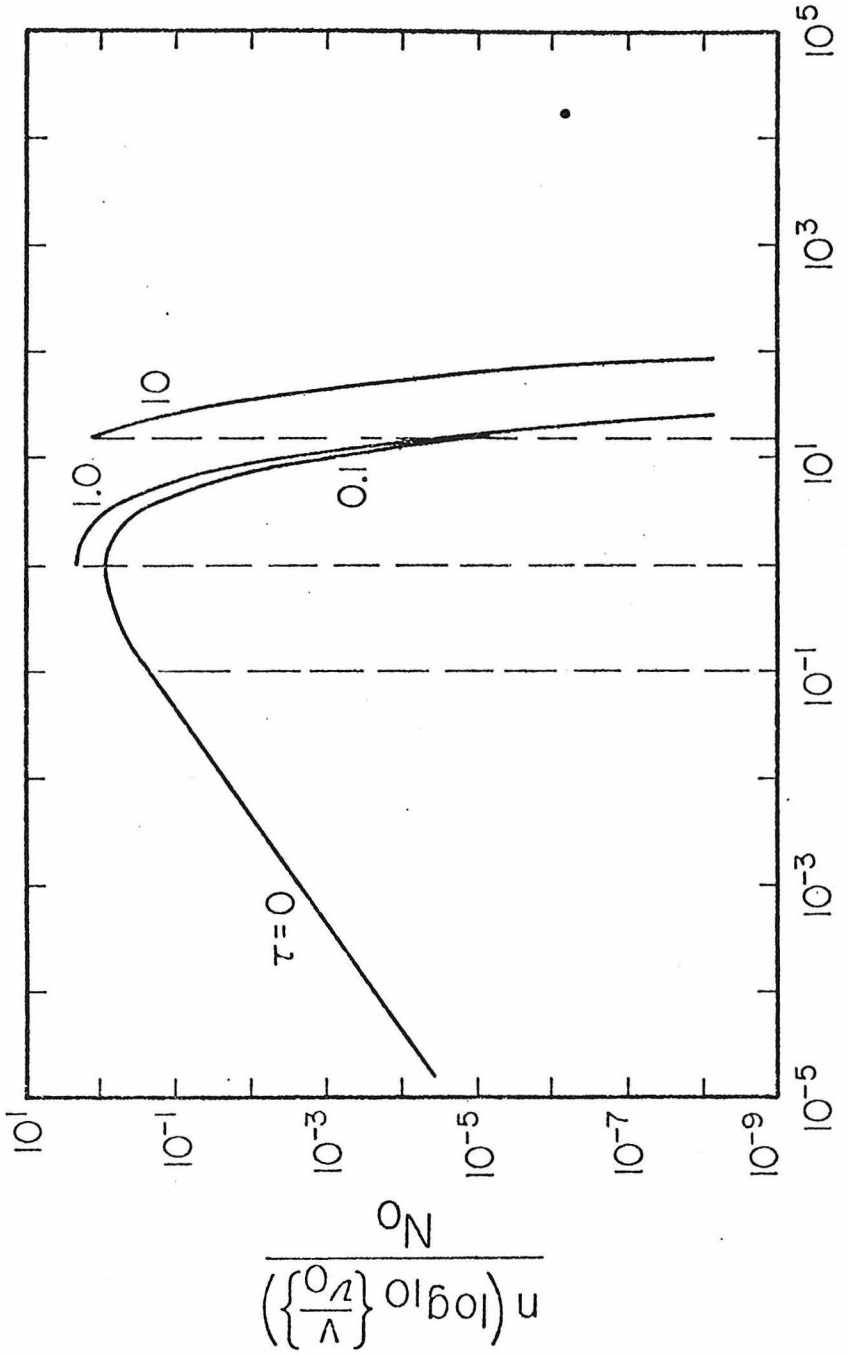

FIGURE 14

Particle size spectra for constant condensation and constant coagulation. $\Lambda = 10.0$.

We noted in the beginning that the choice of the simple functional forms for coagulation and condensation rates, while theoretically interesting in certain instances, was largely a result of their mathematical tractability. An important question, therefore, is to what extent the solutions presented here provide insight into the behavior of size spectra under more complex conditions. In studying the solutions in Table 3, similarities are evident between cases (1) and (2) and between cases (1) and (3). Of most interest is the variation in the size spectrum when the condensation rate, given generally by a function of the form $\alpha_o = \sigma v^\gamma$, varies over the range $\gamma = 1$ to $\gamma = 0$, for a fixed coagulation mechanism. Only when γ is strictly zero will sharp cut-off volume exist. As γ increases from zero, the distribution will tend to broaden, reaching a maximum in dispersion for $\gamma = 1$. Thus, size spectra for condensation growth processes in the range $0 < \gamma < 1$ can be envisioned to lie between those given in Figs. 6-8 and those in Figs. 12-14. The key aspect of analyzing actual size spectra is an estimation of Λ for the system.

SUMMARY

The dynamic behavior of an aerosol undergoing simultaneous coagulation and growth by heterogeneous condensation of vapor species has been considered. First, a criterion based on the characteristics of the size distribution was established in order that the population balance equation, as it is commonly written, can be utilized. Second, certain special cases of coagulation and condensation mechanisms, which allow analytic solution of the dynamic equation for the size distribution density function, were selected. The mechanisms, while chosen because of their attractive

mathematical nature, nonetheless encompass realistic collision and growth mechanisms for certain physical situations, such as Brownian and turbulent coagulation and volume-reaction controlled growth. The solutions obtained suggest more broadly the behavior of general aerosol populations undergoing coagulation and condensation. Thus, whereas the analytical solutions are exact for the cases considered, the qualitative features of the solutions, such as the rate of broadening of the size spectrum, should provide insight into the dynamic behavior of systems with different growth mechanisms. It is anticipated that these results will be useful in the study of particulate formation and growth in hot combustion gases and in aerosol growth in atmospheric plumes.

ACKNOWLEDGMENT

This work was supported by National Science Foundation Grant ENG 71-02486.

NOTATION

d_p	particle diameter, μm
E_n	exponential integral function of the nth kind
g_1	function defined by (63)
g_2	function defined by (64)
k	Boltzmann constant
k_o	minimum number of monomers in a stable nucleus
Kn	Knudsen number
$m(\tilde{v},t)$	size distribution density of the small condensing nuclei, m^{-3} cm^{-3}
M	constant monomer number density, cm^{-3}
$M_0(t)$	total number of particles at any time, cm^{-3}
$M_1(t)$	total volume of particles at any time, μm^3 cm^{-3}
$n(v,t)$	aerosol size distribution density, μm^{-3} cm^{-3}
n_k	number density of particles containing k monomers, cm^{-3}
$\bar{n}$	Laplace Transform of n(v,t) with respect to v
$n_o(v)$	aerosol size distribution density at t = 0, μm^{-3} cm^{-3}
N_o	total number of particles at t = 0, cm^{-3}
p_k	frequency of collision of k-mer with a monomer, sec^{-1}
q_k	frequency of escape of monomer from a k-mer, sec^{-1}
Q	function defined by (65)
R	function defined by (66)
$r_o(t)$	rate of formation of stable clusters containing k_o monomers from homogeneous nucleation, cm^{-3} sec^{-1}
s	Laplace transform variable, μm^{-3}

s_o starting value of the s-characteristic, μm^{-3}

t time, sec.

T reduced time

v particle volume μm^3

v_m largest volume of the condensing species, μm^3

Greek letters

$\alpha_o(v)$ rate of change of the volume of a particle of size v, $\mu m^3\ sec^{-1}$

$\alpha_1(v)$ diffusion coefficient for the aerosol size spectrum, $\mu m^6\ sec^{-1}$

α_o^* α_o/v_o

$\beta(v,\tilde{v})$ coagulation constant, $cm^3\ sec^{-1}$

β_o coagulation constant, $cm^3\ sec^{-1}$

β_1 coefficient in the linear coagulation constant, $cm^3\ \mu m^{-3}\ sec^{-1}$

β_2 coefficient in the quadratic coagulation, $cm^3\ \mu m^{-6}\ sec^{-1}$

$\beta_{i,j}$ collision rate between particles of sizes i and j, $cm^3\ sec^{-1}$

γ exponent in the condensation growth law, $0 \leq \gamma \leq 1$

γ_1 Euler's constant

Γ incomplete Gamma function

δ Kronecker delta function

ϵ defined as $\frac{v_1}{v_o}$

η dimensionless particle volume v/v_o

θ absolute temperature, ^{o}K

λ mean free path of air molecules, μm

Λ dimensionless group: ratio of characteristic times of condensation and coagulation

μ viscosity of air, g cm^{-1} sec^{-1}

ν_o mean volume of the initial size distribution, μm^3

σ constant in condensation growth law, $\mu m^{3(1-\gamma)}$ sec^{-1}

σ_o condensation constant for uniform growth, μm^3 sec^{-1}

σ_1 condensation constant for linear growth, sec^{-1}

τ dimensionless characteristic time for condensation

χ reduced time defined as $(1 + T)$

ω function defined by (43)

Superscript

$\bar{}$ Laplace transform variable

REFERENCES

Abramowitz, M. and I. A. Stegun, "Handbook of Mathematical Functions," U.S. National Bureau of Standards, Washington, D.C. (1965)

Brock, J. R., "Condensational Growth of Atmospheric Aerosols," J. Coll. Int. Sci., 39, No. 1, 32 (1972)

Fuchs, N. A. "The Mechanics of Aerosols," MacMillan, New York (1964)

Golovin, A. M., "The Solution of the Coagulation Equation for Raindrops, Taking Condensation into Account," Sov. Phys.-Doklady, 8, No. 2, 191 (1963)

Hidy, G. M. and J. R. Brock, "The Dynamics of Aerocolloidal Systems," Pergamon Press, Oxford (1970)

Middleton, P. and J. Brock, "Simulation of Aerosol Kinetics," submitted for publication (1976)

Roberts, G. E. and H. Kaufman, "Table of Laplace Transforms," W. B. Sanders, Philadelphia (1966)

Scott, W. T., "Analytic Studies of Cloud Droplet Coalescence I," J. Atmos. Sci., 25, 54 (1968)

CHAPTER IV

DYNAMICS

OF

SOURCE REINFORCED,

COAGULATING AND CONDENSING AEROSOLS*

*Accepted for publication, Journal of Colloid and Interface Science, 1977.

4.1 Introduction

In the previous chapter we studied the dynamic behavior of aerosol size distributions under the influence of simultaneous coagulation and condensation. For the mechanisms chosen, we were able to derive analytic solutions for three of the four combinations of constant and linear coagulation and condensation.

Two processes omitted in that formulation which also affect the aerosol size distribution are particle sources and sinks. For a spatially homogeneous aerosol undergoing growth and coagulation with particle sources and sinks the size distribution function n(v,t) is governed by the integro-differential equation,

$$\frac{\partial n}{\partial t} + \frac{\partial}{\partial v}\left[I(v,t)n\right] = \frac{1}{2}\int_0^v \beta(v-\tilde{v},\tilde{v})n(v-\tilde{v},t)n(\tilde{v},t)\,d\tilde{v} - \int_0^\infty \beta(v,\tilde{v})n(v,t)n(\tilde{v},t)\,d\tilde{v} - R(v,t) + S(v,t) \qquad (4.1)$$

where $I(v,t) = dv/dt$, the rate of growth of a particle of volume v, R(v,t) is the rate of removal of particles from the system, and S(v,t) is the rate of addition of fresh particles to the system.

In situations of practical interest, the functional forms of I, β, R and S are such that (4.1) must be solved numerically. Due to computational difficulties in solving (4.1), only a few numerical solutions have been reported in which both condensation and coagulation are included (Wadden et al. (1974), Middleton and Brock (1976)). Analytic solutions are available for certain special cases of (4.1). Golovin (1963) and Scott (1968) obtained solutions to the pure coagulation form of (4.1)

(I=R=S=0) for a few simple forms of $\beta(v,\tilde{v})$. Brock (1971, 1972) solved the pure condensation form of (4.1) (β=0) for a specific functional form of I. Drake (1976) studied the full aerosol balance equation by similarity techniques which give rise to self-preserving solutions. The previous chapter outlined analytic solutions of (4.1) for the case of simultaneous coagulation and condensation (R=S=0).

This chapter presents a full scale analytical and numerical study of (4.1). We wish to examine quantitatively the interaction among the various physical processes represented in (4.1) to elucidate the general properties of aerosol size distributions under the simultaneous influence of condensation, coagulation, removal and sources. Analytic solutions are obtained for as many cases of (4.1) as possible. For those cases for which analytical solutions could not be obtained, (4.1) was solved numerically by Gelbard (1978). As in Chapter 3, we have chosen to examine certain special cases of condensation, coagulation, removal and sources that, while mathematically tractable, still retain important elements of realism with respect to the rigorously established forms of the terms in (4.1). By placing (4.1) in dimensionless form for each form of I, β, R and S considered, the importance of each process can be measured by the value of an appropriate dimensionless group. Particularly, we wish to see how different condensation and coagulation mechanisms influence the size distribution dynamics in the presence (and absence) of removal and sources. By solving (4.1) for a range of values of the physical processes a large number of prior studies on pure coagulation, coagulation with sources and sinks, and condensation with sources and sinks become merely special cases of (4.1). Thus, we hope to provide a framework for the subsequent analysis of dynamic aerosol size distributions

in homogeneous systems. Our analysis will have applicability to the understanding of atmospheric aerosol size distributions in the presence of coagulation, condensation, sources and removal (Willeke and Whitby, 1975).

After discussing the mechanisms chosen for I, β, R and S, the solutions to the first two moments of $n(v,t)$, namely $M_0(t)$ and $M_1(t)$, are presented and discussed. The equations defining the time evolution of the total number of particles per unit volume of fluid,

$$M_0(t) = \int_0^\infty n(v,t)\, dv \tag{4.2}$$

and the total volume of particles per unit volume of fluid,

$$M_1(t) = \int_0^\infty vn(v,t)\, dv \tag{4.3}$$

are obtained from (4.1) by integrating over all volumes, or by multiplying by v and then integrating over all volumes. Much useful information regarding the time evolution of the aerosol is obtained by analyzing these moment solutions. Next, the procedures for obtaining the analytical solutions to (4.1) are presented, as is a synopsis of the cases for which analytic solutions can be obtained. Finally, the general solution to (4.1) for various cases of condensation and coagulation is presented either from analytic or numerical solutions, and the characteristics of the distributions are fully discussed.

4.2 Description of Physical Processes

It is necessary to specify the functional forms for the coagulation coefficient $\beta(v,\tilde{v})$, the growth rate $I(v,t)$, the rate of particle removal $R(v,t)$ and the rate of production of new particles $S(v,t)$. In a realistic environment, these functions would be nonlinear functions of volume and time, and would necessitate numerical solution of (4.1) in nearly all cases. It is of interest, however, to examine certain special cases of I, β, R and S that, while mathematically tractable, retain the essential properties of the functions in the more general case. We therefore seek physically realistic functional forms for I, β, R and S which will enable analytic solution of (4.1). The value of these simplified cases lies in affording an opportunity to study the behavior of the system without the need to specify a large number of physical constants.

4.2.1 Coagulation and Condensation

A complete discussion of the processes of coagulation and condensation was presented in Chapter 3. By considering the well-known functional forms for β and I, we arrived at two mathematically attractive and physically realistic forms for the coagulation and condensation mechanisms. For coagulation, our attention will be confined to $\beta=\beta_0$ and $\beta = \beta_1(v+\tilde{v})$. For condensational growth, we shall examine $I = \sigma_0$ and $I = \sigma_1 v$.

4.2.2 Removal

We will assume that removal occurs by means of a first order process with respect to the number density,

$$R(v,t) = \alpha n(v,t) \tag{4.4}$$

where, for convenience, α is taken as a constant independent of particle size. In general, α is a function of v if R represents losses by sedimentation, scavenging, or in the case of a smog chamber, diffusional wall losses. For our purposes, it is sufficient to maintain α as constant.

4.2.3 Sources

The source term S(v,t) is taken to represent the rate of formation of new particles by homogeneous nucleation. Nucleation theory (Friedlander, 1977) establishes an expression for the droplet current of particles into the system at the smallest size in the spectrum. In a continuous distribution, as described by (4.1), this source could most easily be written as

$$S(v,t) = S_0 \, \delta(v-v^*) \tag{4.5}$$

where v^* is some minimum particle volume about which nucleation occurs, and $\delta(v-v^*)$ is the dirac delta function.

Since inclusion of the delta function in (4.1) complicates both analytical and numerical solution techniques, the source rate is approximated by

$$S(v,t) = \frac{S_0}{v^*} \exp(-v/v^*) \tag{4.6}$$

where v^* is an indication of the range of particle volumes over which nucleation could occur, and S_0 is the nucleation rate in cm^{-3} sec^{-1}.

Having outlined briefly the mechanisms chosen to describe β, I, R and S, we will first derive the dimensionless form of (4.1) for each possible case. Then, as previously stated, solutions to the moment equations will be analyzed. Finally, the particle size distribution function described by (4.1) will be studied.

4.3 Dimensionless Groups

Since we have chosen to consider one mechanism to represent each of the processes of homogeneous nucleation and removal, and two mechanisms to represent each of the processes of coagulation and condensation, there will be a total of four cases of (4.1) which can be examined. Within each case, of course, are infinite combinations of values of the dimensionless parameters associated with each process. Table 4.1 summarizes the mechanisms chosen for each of the four cases.

In keeping with the emphasis we place on analysis of the dimensionless form of the governing equations, we are able to define dimensionless parameters associated with each of the mechanisms of Table 4.1. As will be shown, these parameters are the appropriate groups that arise when casting (4.1) into dimensionless form. The following groups are defined:

$$\Lambda = \frac{\text{rate of condensation}}{\text{rate of coagulation}} \tag{4.7}$$

$$\theta = \frac{\text{rate of removal}}{\text{rate of coagulation}} \tag{4.8}$$

$$\Omega = \frac{\text{rate of nucleation}}{\text{rate of coagulation}} \tag{4.9}$$

For convenience, all dimensionless groups are ratios of the rate of one particular mechanism to the rate of coagulation. We define N_o and v_o as the total number concentration and mean volume of the distribution at time t = 0 respectively.

$$N_o = \int_0^\infty n(v,0)\, dv = M_0(0) \tag{4.10}$$

$$v_o = \frac{1}{N_o} \int_0^\infty vn(v,0)\, dv = \frac{M_1(0)}{N_o} \tag{4.11}$$

Table 4.2 lists the definitions of Λ, θ and Ω for each of the four cases in terms of the parameters of the system. The dimensionless time τ is defined as a characteristic coagulation time,

$$\tau = \beta_0 N_0 t \tag{4.12}$$

for cases 1 and 3, and

$$\tau = \beta_1 N_0 \nu_0 t \tag{4.13}$$

for cases 2 and 4.

The equations for the moments M_0 and M_1 are obtained by integration of (4.1), following the procedure previously described. Since the method of solution of (4.1) for n(v,t) follows the Laplace transform technique, the equations which will provide a basis for analysis of n(v,t) will be the dimensionless form of the transformed equation for n(v,t).

4.4 Moment and Size Distribution Equations

The derivation of the moment equations is straightforward. Given the parameter definitions in Table 4.2, the definitions of τ in (4.12) and (4.13), the parameter $\Delta = v^*/\nu_0$, and the dimensionless form of the moments

$$\bar{M}_0(\tau) = M_0/N_0 \tag{4.14}$$

$$\bar{M}_1(\tau) = M_1/N_0\nu_0 \tag{4.15}$$

We can write the equations for $\frac{d\bar{M}_0}{d\tau}$ and $\frac{d\bar{M}_1}{d\tau}$ as given in Table 4.3. A derivation of these equations from (4.1) is straightforward. The

Table 4.1 Mechanisms of Coagulation, Condensation, Source and Removal

	Coagulation	Condensation	Removal	Source
Case	β	I	R	S
1	β_o	$\sigma_1 v$	αn	$\frac{S_o}{v^*} \exp\left(\frac{-v}{v^*}\right)$
2	$\beta_1(v+\tilde{v})$	$\sigma_1 v$	αn	$\frac{S_o}{v^*} \exp\left(\frac{-v}{v^*}\right)$
3	β_o	σ_o	αn	$\frac{S_o}{v^*} \exp\left(\frac{-v}{v^*}\right)$
4	$\beta_1(v+\tilde{v})$	σ_o	αn	$\frac{S_o}{v^*} \exp\left(\frac{-v}{v^*}\right)$

Table 4.2 Dimensionless Parameters

Case	Λ	θ	Ω
1	$\frac{\sigma_1}{\beta_o N_o}$	$\frac{\alpha}{\beta_o N_o}$	$\frac{S_o}{\beta_o N_o^2}$
2	$\frac{\sigma_1}{\beta_1 N_o \nu_o}$	$\frac{\alpha}{\beta_1 N_o \nu_o}$	$\frac{S_o}{\beta_1 N_o^2 \nu_o}$
3	$\frac{\sigma_o}{\beta_o N_o \nu_o}$	$\frac{\alpha}{\beta_o N_o}$	$\frac{S_o}{\beta_o N_o^2}$
4	$\frac{\sigma_o}{\beta_1 N_o \nu_o^2}$	$\frac{\alpha}{\beta_1 N_o \nu_c}$	$\frac{S_o}{\beta_1 N_o^2 \nu_o}$

Table 4.3 Equations for $\bar{M}_0$ and $\bar{M}_1$

Case	$\frac{d\bar{M}_0}{d\tau}$	$\frac{d\bar{M}_1}{d\tau}$
1	$-\frac{1}{2}\bar{M}_0^2 - \theta\bar{M}_0 + \Omega$	$(\Lambda-\theta)\ \bar{M}_1 + \Delta\Omega$
2	$-\bar{M}_0(\bar{M}_1 + \theta) + \Omega$	$(\Lambda-\theta)\ \bar{M}_1 + \Delta\Omega$
3	$-\frac{1}{2}\bar{M}_0^2 - \theta\bar{M}_0 + \Omega$	$\Lambda\bar{M}_0 - \theta\bar{M}_1 + \Delta\Omega$
4	$-\bar{M}_0(\bar{M}_1 + \theta) + \Omega$	$\Lambda\bar{M}_0 - \Theta\bar{M}_1 + \Delta\Omega$

initial conditions on $\bar{M}_0$ and $\bar{M}_1$ are

$$\bar{M}_0(0) = 1 \tag{4.16}$$

and

$$\bar{M}_1(0) = 1 \tag{4.17}$$

In deriving the dimensionless form of the population balance equation (4.1) for each case, the following definitions are required in addition to those previously defined:

$$\bar{s} = \nu_0 s \tag{4.18}$$

$$\bar{p} = \frac{1}{N_0} L\{n(v,t)\} \tag{4.19}$$

where s is the Laplace transform variable, and the Laplace operator is defined as

$$L\{n(v,t)\} = \int_0^\infty \exp(-sv)n(v,t)\, dv \tag{4.20}$$

By taking Laplace transforms of (4.1) for each of the four cases examined, and casting the resultant equations in dimensionless form, the governing equations in Table 4.4 are obtained. Details of the derivations are given in the Appendix.

Table 4.4 Dimensionless Size Distribution Equations and Their Laplace Transforms

Case	Dimensionless Equation	Laplace Transform Equation
1	$\frac{\partial \bar{n}}{\partial \tau} + \Lambda \frac{\partial}{\partial \bar{v}} [\bar{v}\bar{n}] = \frac{1}{2}\int_0^{\bar{v}} \bar{n}(\bar{v}-\tilde{v},\tau)\bar{n}(\tilde{v},\tau)d\tilde{v} - \int_0^{\infty} \bar{n}(\bar{v},\tau)\bar{n}(\tilde{v},\tau)d\tilde{v}$ $- \theta\bar{n} + \frac{\Omega}{\Delta} \exp\left(-\frac{\bar{v}}{\Delta}\right)$	$\frac{\partial \bar{p}}{\partial \tau} = \Lambda \frac{\bar{s}d\bar{p}}{\partial \bar{s}} + \frac{1}{2}\bar{p}^2 - (\bar{M}_o+\theta)\bar{p} + \frac{\Omega}{\Delta\bar{s}+1}$
2	$\frac{\partial \bar{n}}{\partial \tau} + \Lambda \frac{\partial}{\partial \bar{v}} [\bar{v}\bar{n}] = \frac{1}{2}\int_0^{\bar{v}} \bar{v}\bar{n}(\bar{v}-\tilde{v},\tau)\bar{n}(\tilde{v},\tau)d\tilde{v} - \int_0^{\infty} (\bar{v}+\tilde{v})\bar{n}(\bar{v},\tau)\bar{n}(\bar{v},\tau)d\tilde{v}$ $- \theta\bar{n} + \frac{\Omega}{\Delta} \exp\left(-\frac{\bar{v}}{\Delta}\right)$	$\frac{\partial \bar{p}}{\partial \tau} = (\Lambda\bar{s}+\bar{M}_o-\bar{p})\frac{\partial \bar{p}}{\partial \bar{s}} - (\bar{M}_1+\theta)\bar{p} + \frac{\Omega}{\Delta\bar{s}+1}$
3	$\frac{\partial \bar{n}}{\partial \tau} + \Lambda \frac{\partial \bar{n}}{\partial \bar{v}} = \frac{1}{2}\int_0^{\bar{v}} \bar{n}(\bar{v}-\tilde{v},\tau)\bar{n}(\tilde{v},\tau)d\tilde{v} - \int_0^{\infty} \bar{n}(\bar{v},\tau)\bar{n}(\tilde{v},\tau)d\tilde{v}$ $- \theta\bar{n} + \frac{\Omega}{\Delta} \exp\left(-\frac{\bar{v}}{\Delta}\right)$	$\frac{\partial \bar{p}}{\partial \tau} = \frac{1}{2}\bar{p}^2 - (\bar{M}_o+\theta+\Lambda\bar{s})\bar{p} + \frac{\Omega}{\Delta\bar{s}+1}$
4	$\frac{\partial \bar{n}}{\partial \tau} + \Lambda \frac{\partial \bar{n}}{\partial \bar{v}} = \frac{1}{2}\int_0^{\bar{v}} \bar{v}\bar{n}(\bar{v}-\tilde{v},\tau)\bar{n}(\tilde{v},\tau)d\tilde{v} - \int_0^{\infty} (\bar{v}+\tilde{v})\bar{n}(\bar{v},\tau)\bar{n}(\tilde{v},\tau)d\tilde{v}$ $- \theta\bar{n} + \frac{\Omega}{\Delta} \exp\left(-\frac{\bar{v}}{\Delta}\right)$	$\frac{\partial \bar{p}}{\partial \tau} = (\bar{M}_o-\bar{p})\frac{\partial \bar{p}}{\partial \bar{s}} - (\bar{M}_1+\theta+\Lambda\bar{s})\bar{p} + \frac{\Omega}{\Delta\bar{s}+1}$

$\bar{n} = \frac{n}{N_o/\nu_o}$ $\quad \bar{v} = \frac{v}{\nu_o}$ $\quad \bar{p} = \frac{L\{n\}}{N_o}$ $\quad \bar{s} = \nu_o s$

4.5 Solutions for the Moments $\bar{M}_0$ and $\bar{M}_1$

Analytic solutions for the moments for cases 1-3 are presented in Table 4.5. Case 4 offers no closed form analytic solution, and hence must be solved numerically. Details of the solutions are given in the Appendix.

The solutions for $\bar{M}_0$ and $\bar{M}_1$ are all functions of the parameters Λ, θ, Ω and Δ, and graphic presentation of the solutions requires assignment of numerical values to these parameters. In order to present the results in as concise a manner as possible, while still demonstrating the salient features that the solutions will possess under varying values of these parameters, values of 0.1, 1.0, and 10.0 were assigned to each of the three parameters Λ, θ, and Ω, while Δ was assumed to be constant at $\Delta = 0.01$. By plotting the temporal dependence of $\bar{M}_0$ and $\bar{M}_1$ for all combinations of these parameters, and thereby simulating situations under which the various mechanisms of coagulation, condensation, nucleation and removal dominate, we can examine the effects that these mechanisms have on the behavior of $\bar{M}_0$ and $\bar{M}_1$.

Figures 4.1-4.12 present $\bar{M}_0(\tau)$ and $\bar{M}_1(\tau)$ for various values of θ, Λ and Ω. Figures 4.1-4.3, 4.4-4.6, 4.7-4.9 and 4.10-4.12 represent cases 1, 2, 3 and 4, respectively.

4.5.1 Case 1

For case 1, constant coagulation and linear condensation, it is evident from Figures 4.1-4.3 that the rate of condensation Λ has no effect on the total number $\bar{M}_0$. If nucleation dominates removal the steady state total number is higher than the initial total number. If, however, nucleation is the same order as removal or less, the steady

Table 4.5 $\bar{M}_0(\tau)$ and $\bar{M}_1(\tau)$ in Cases 1-3

Case	$\bar{M}_0(\tau)$	$\bar{M}_1(\tau)$
1	$\bar{M}_0(\tau) = \dfrac{r_1 - r_2 F(\tau)}{1 - F(\tau)}$	$\bar{M}_1(\tau) = -\beta + (1+\beta)\exp((\Lambda-\theta)\tau)$
2	$\bar{M}_0(\tau) = \left(\dfrac{1+\beta}{\bar{M}_1+\beta}\right)^{\frac{\theta-\beta}{\Lambda-\theta}} \exp\left(\dfrac{1-\bar{M}_1}{\Lambda-\theta}\right) \cdot \left\{ 1 + \dfrac{\beta}{\Delta} \int_1^{\bar{M}_1} \dfrac{\exp\left(\frac{\xi-1}{\Lambda-\theta}\right)}{\xi+\beta} \left(\dfrac{\xi+\beta}{1+\beta}\right)^{\frac{\theta-\beta}{\Lambda-\theta}} d\xi \right\}$	$\bar{M}_1(\tau) = -\beta + (1+\beta)\exp((\Lambda-\theta)\tau)$
3	$\bar{M}_0(\tau) = \dfrac{r_1 - r_2 F(\tau)}{1 - F(\tau)}$	$\bar{M}_1(\tau) = \left(\dfrac{\bar{M}_0 - r_1}{1-r_1} \cdot \dfrac{1-r_2}{\bar{M}_0 - r_2}\right)^{\frac{2\theta}{r_1-r_2}} \cdot \left\{ 1 - 2 \int_1^{\bar{M}_0} \dfrac{\Lambda\xi + \Omega\Delta}{(\xi-r_1)(\xi-r_2)} \left(\dfrac{\xi-r_2}{1-r_2} \cdot \dfrac{1-r_1}{\xi-r_1}\right)^{\frac{2\theta}{r_1-r_2}} d\xi \right\}$

$$r_1 = -\theta + \sqrt{\theta^2 + 2\Omega}$$

$$r_2 = -\theta - \sqrt{\theta^2 + 2\Omega}$$

$$\beta = \frac{\Omega\Delta}{\Lambda - \theta}$$

$$F(\tau) = \frac{1-r_1}{1-r_2} \exp\left[-\left(\frac{r_1 - r_2}{2}\right)\tau \right]$$

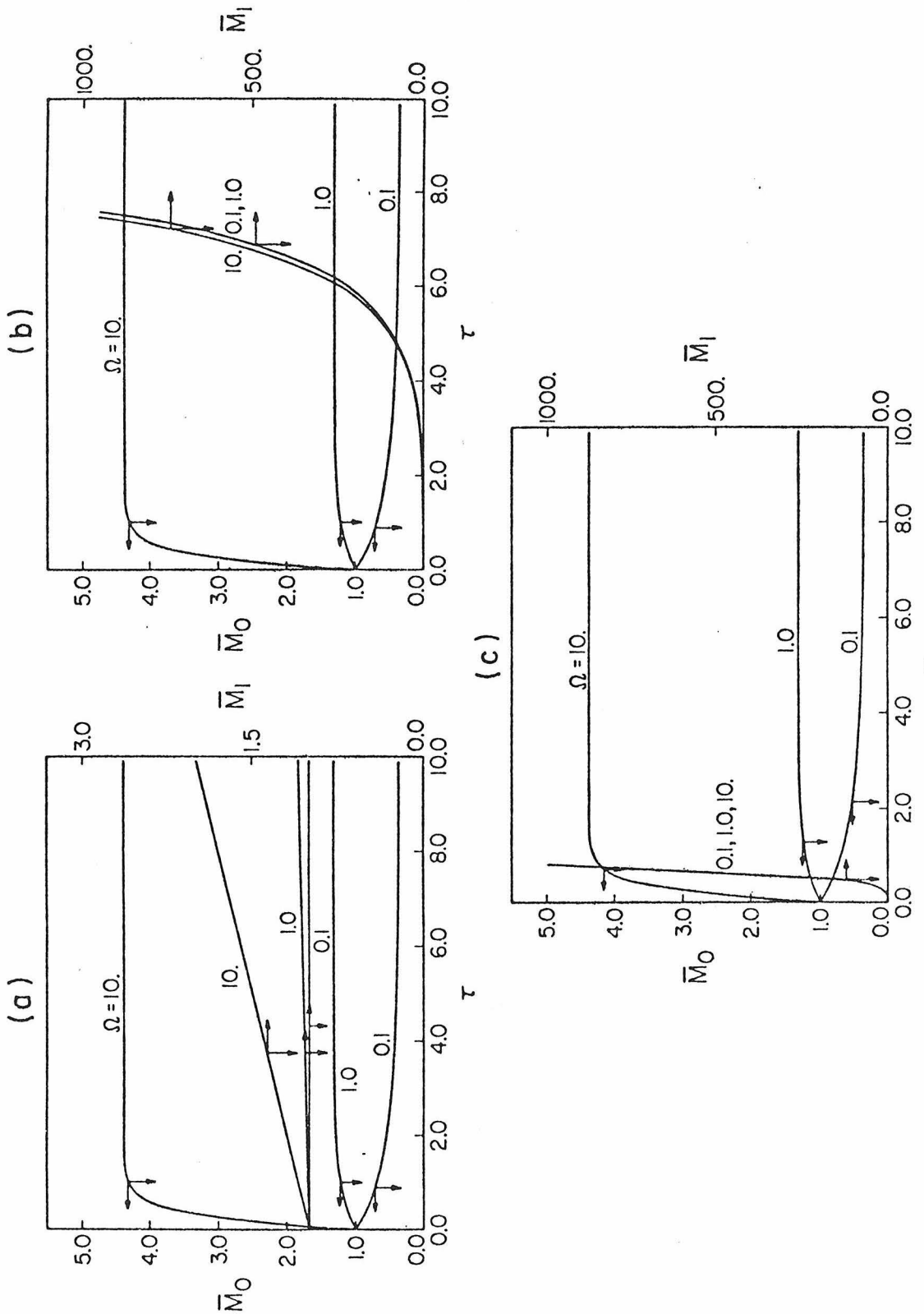

Figure 4.1

Time evolution ($\tau=\beta_0 N_0 t$) of number and volume fraction for linear condensation ($I=\sigma_1 v$) and constant coagulation ($\beta=\beta_0$), $\theta=0.1$ and (a) $\Lambda=0.1$, (b) $\Lambda=1.0$ and (c) $\Lambda=10.0$.

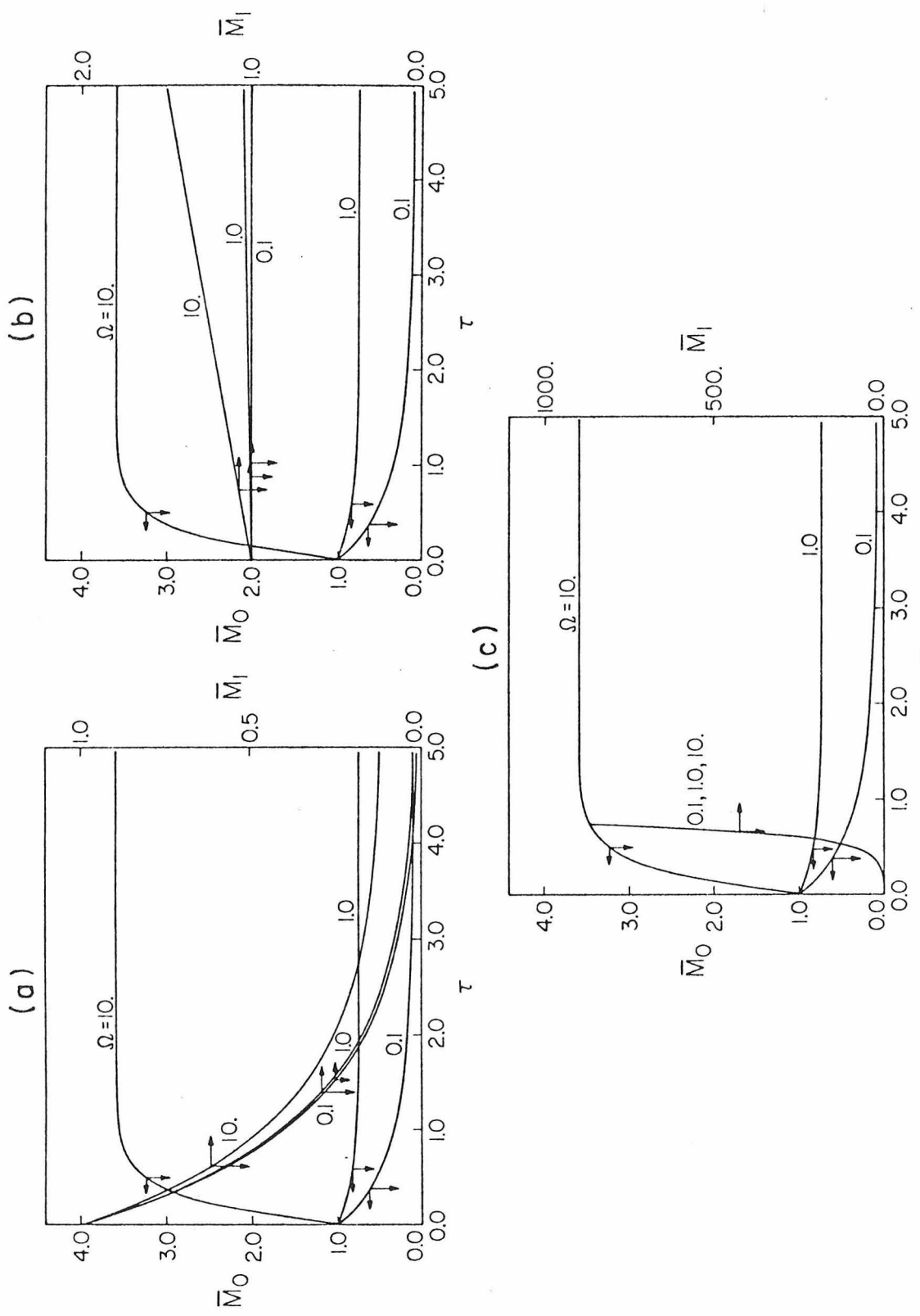

Figure 4.2

Time evolution ($\tau=\beta_o N_o t$) of number and volume fraction for linear condensation ($I=\sigma_1 v$) and constant coagulation ($\beta=\beta_o$), Θ=1.0 and (a) Λ=0.1, (b) Λ=1.0 and (c) Λ=10.0 .

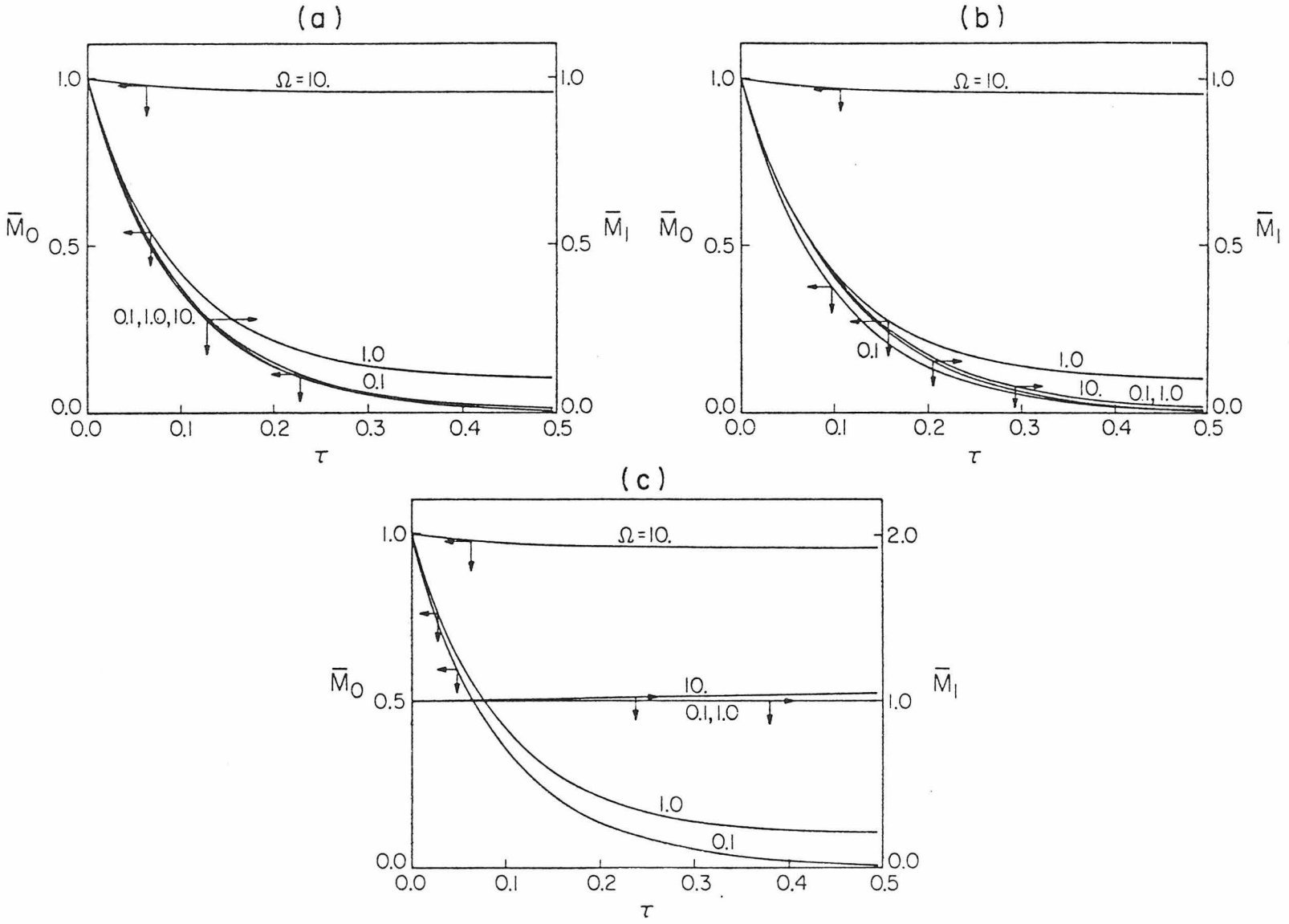

Figure 4.3

Time evolution ($\tau=\beta_o N_o t$) of number and volume fraction for linear condensation ($I=\sigma_1 v$) and constant coagulation ($\beta=\beta_o$), $\Theta=10.$ and (a) $\Lambda=0.1$, (b) $\Lambda=1.0$ and (c) $\Lambda=10.0$.

state total number is less than the initial total number. These results can be observed from the algebraic equations for $\bar{M}_0$ and $\bar{M}_1$ which result at steady state. For case 1, this yields

$$\bar{M}_{0_{ss}} = r_1 = - \theta + \sqrt{\theta^2+2\Omega} \tag{4.21}$$

$$\bar{M}_{1_{ss}} = \frac{\Delta\Omega}{\theta-\Lambda} \tag{4.22}$$

From (4.21) we see that if $\Omega > \theta + 1/2$, $\bar{M}_{0_{ss}} > M_0(0)$, and if $\Omega < \theta + 1/2$, $\bar{M}_{0_{ss}} < M_0(0)$. If $\Omega = \theta + 1/2$, the nucleation and removal processes are exactly balanced, and $\bar{M}_0$ is independent of τ. Also evident in Figures 4.1-4.3 is the fact that a steady state is reached for $\bar{M}_1$ only when the rate of removal is greater than the rate of volume addition by condensation ($\theta>\Lambda$). This is also evident from (4.22). When $\Lambda > \theta$, the condensation rate dominates the removal rate, and the total volume steadily increases. When $\Lambda = \theta$, regardless of the magnitude, the total volume increases linearly with τ, due solely to the volume addition from nucleation. This is because volume addition by condensation is exactly balanced by removal.

4.5.2 Case 2

Figures 4.4-4.6 present $\bar{M}_0(\tau)$ and $\bar{M}_1(\tau)$ for case 2, linear coagulation and linear condensation. Since coagulation, which effects the total number, is linear in volume, and total volume increases due to condensation, $\bar{M}_0$ is a function of the condensation rate Λ even though condensation obviously does not directly change the number of particles. Consideration of the solutions for $\bar{M}_0$ and $\bar{M}_1$ for long times indicates the following.

$$\left.\begin{aligned} \bar{M}_1 &\to \frac{\Delta\Omega}{\theta-\Lambda} \\ \bar{M}_0 &\to \frac{\Omega}{\theta+\frac{\Delta\Omega}{\theta-\Lambda}} \end{aligned}\right\} \text{ if } \theta > \Lambda \qquad (4.23),\ (4.24)$$

$$\left.\begin{aligned} \bar{M}_1 &\to \infty \quad \text{linearly in } \tau \\ \bar{M}_0 &\to 0 \quad \sim \text{as } 1/\tau \end{aligned}\right\} \text{ if } \theta = \Lambda \qquad (4.25),\ (4.26)$$

$$\left.\begin{aligned} \bar{M}_1 &\to \infty \quad \text{exponentially in } \tau \\ \bar{M}_0 &\to 0 \quad \sim \text{exponentially in } \tau \end{aligned}\right\} \text{ if } \theta < \Lambda \qquad (4.27),\ (4.28)$$

For a given rate of condensation (Λ = constant) the rate of increase in $\bar{M}_1$ goes from approximately exponential to linear in τ as θ increases from a small value to $\theta = \Lambda$. This behavior is reasonable, since an increased rate of removal causes a decrease in the total volume of particles in the system at any instant. Also reasonable is the observation that as removal continues to increase ($\theta>\Lambda$), $\bar{M}_1$ reaches a steady state, the magnitude of which (by(4.23)) decreases as removal increases.

An interesting effect is evident in analyzing (4.23)-(4.28) and Figures 4.4-4.6 with regard to $\bar{M}_0$. For a given rate of condensation (Λ = constant) the rate of depletion of particles <u>decreases</u> as removal increases ($\theta\to\Lambda$) until $\theta = \Lambda + \sqrt{\Delta\Omega}$. In proceeding to this point, θ has passed through $\theta = \Lambda$, where $\bar{M}_0$ changes from a function that always decays to zero to a function with a steady state value given by (4.24). As θ increases beyond $\theta = \Lambda + \sqrt{\Delta\Omega}$, the steady state value of $\bar{M}_0$ falls off approximately as $1/\theta$ for large θ, as can be seen from (4.24).

The explanation of this behavior lies in the fact that coagulation is a process linearly dependent on particle volume. As long as $\theta < \Lambda + \sqrt{\Delta\Omega}$, the nucleation and subsequent growth by condensation move particles into the larger sizes before first order removal claims them from the system. However, the coagulation process, which is second order in concentration and linear in particle volume, rapidly removes these larger particles by coagulation, even more rapidly than they would be removed by first order removal kinetics. Hence, the increase in removal rate θ only depletes the particles before they have a chance to grow to larger sizes and be removed by the more rapid coagulation process.

As θ becomes greater than $\Lambda + \sqrt{\Delta\Omega}$, the condensation process can no longer bring particles to the larger sizes for subsequent coagulation before they are removed by the first order removal mechanism. Hence, increasing the removal rate simply causes an increase in the rate of particle depletion.

Also of interest in Figures 4.4-4.6 is the modal character of $\bar{M}_0$ for selected values of θ and Λ and large values of the nucleation rate Ω. Here, $\bar{M}_0$ increases initially to a peak, and then eventually falls off to zero. This behavior only occurs when the rate of condensation Λ is greater than or equal to the rate of removal θ, and is due to the growth in particles from nucleation until such time that these nucleated particles have grown to a size where linear coagulation can remove them.

Just the opposite effect occurs for small condensation rates and larger but roughly equal rates of nucleation and removal, where $\bar{M}_0$ initially decreases to some minimum value, and then increases slowly to a steady state value. Larger particles are preferentially depleted since, although first order removal is size independent, nucleation "builds up"

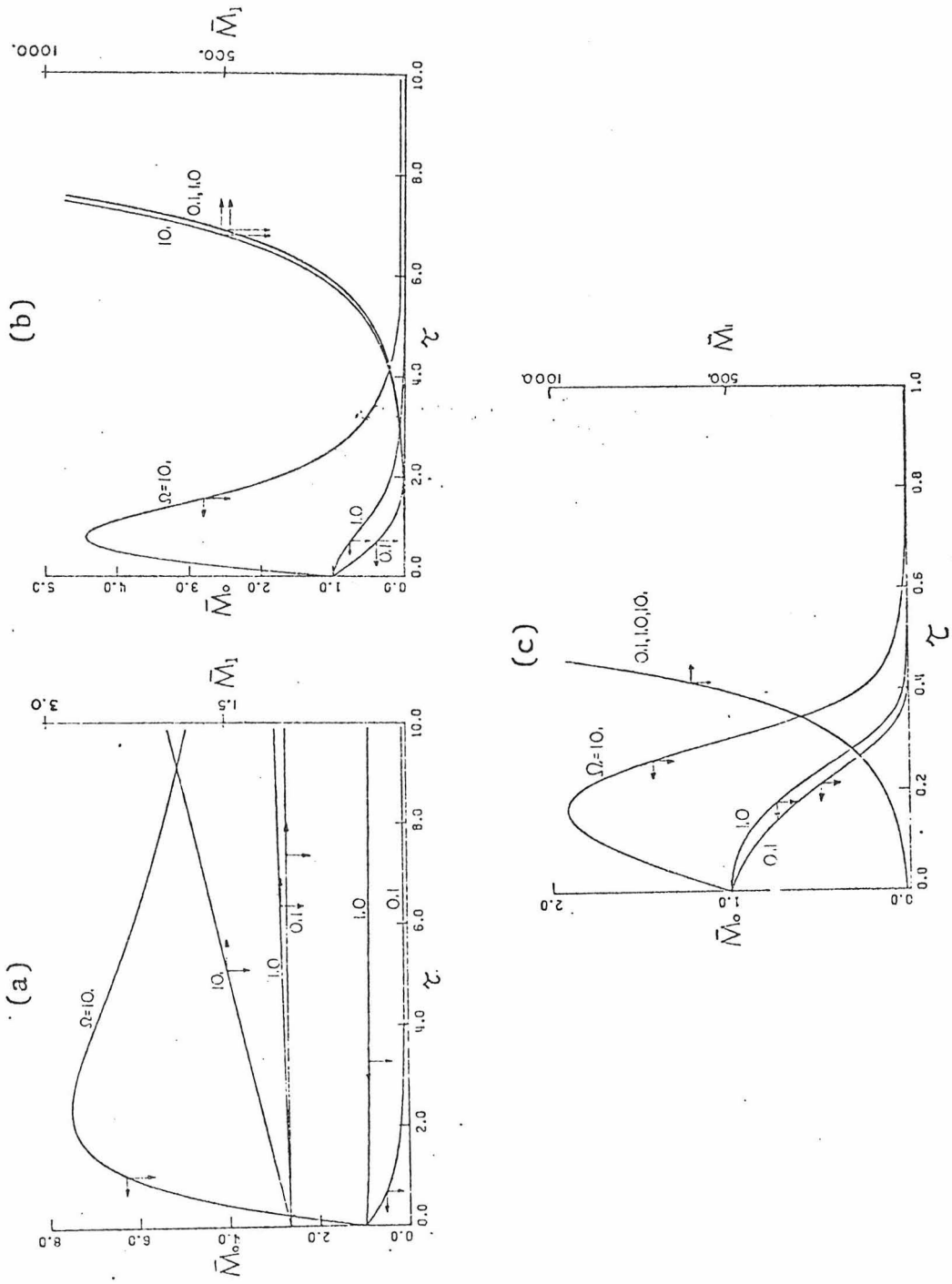

Figure 4.4

Time evolution ($\tau=\beta_1 N_o \nu_o t$) of number and volume fraction for linear condensation ($I=\sigma_1 v$) and linear coagulation ($\beta=\beta_1(v+\tilde{v})$), Θ=0.1 and (a) Λ=.1, (b) Λ=1.0 and (c) Λ=10.0 .

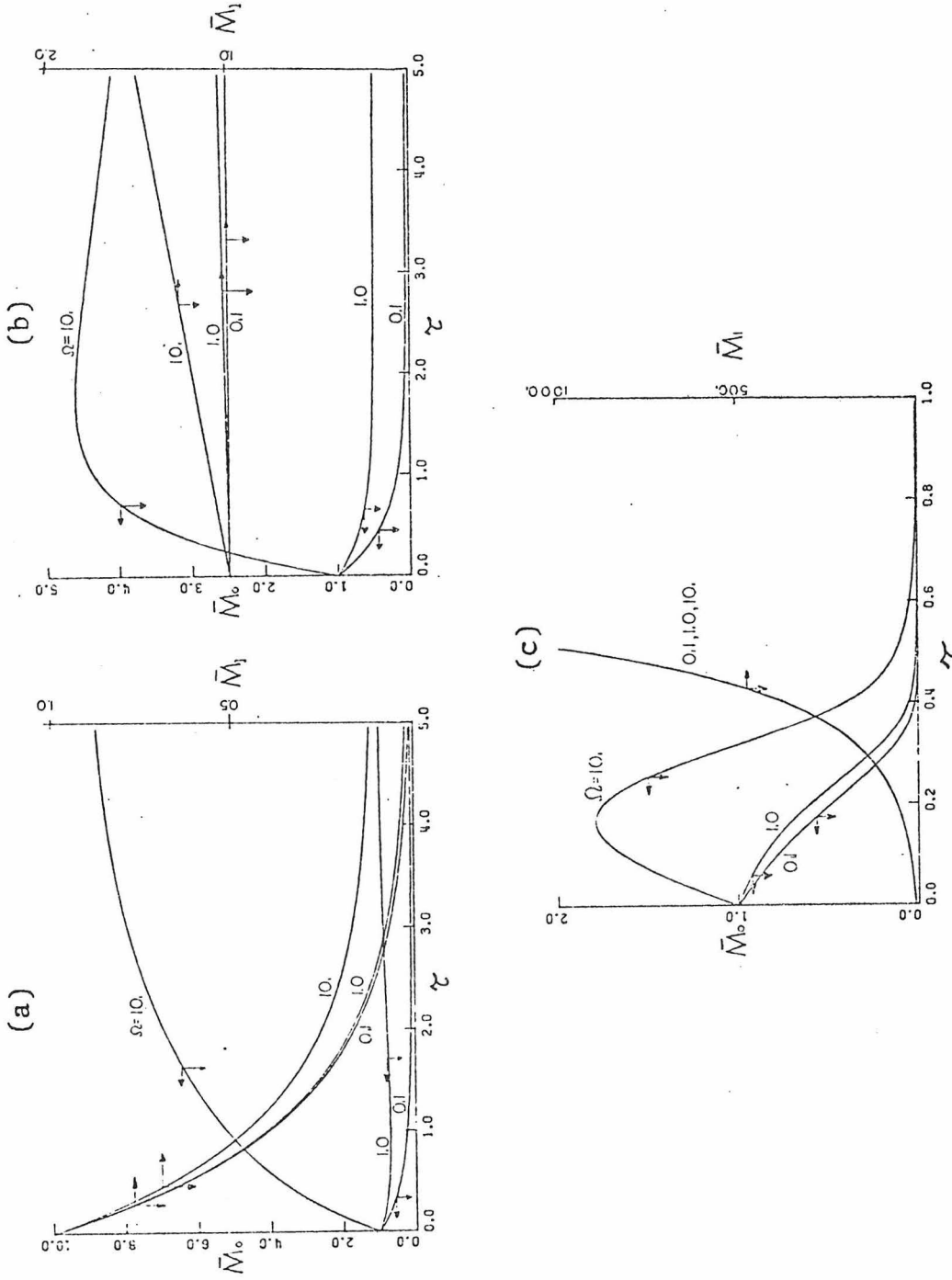

Figure 4.5

Time evolution ($\tau=\beta_1 N_o \nu_o t$) of number and volume fraction for linear condensation ($I=\sigma_1 v$) linear coagulation ($\beta=\beta_1(v+\tilde{v})$), Θ=1.0 and (a) Λ=0.1, (b) Λ=1.0 and (c) Λ=10.0 .

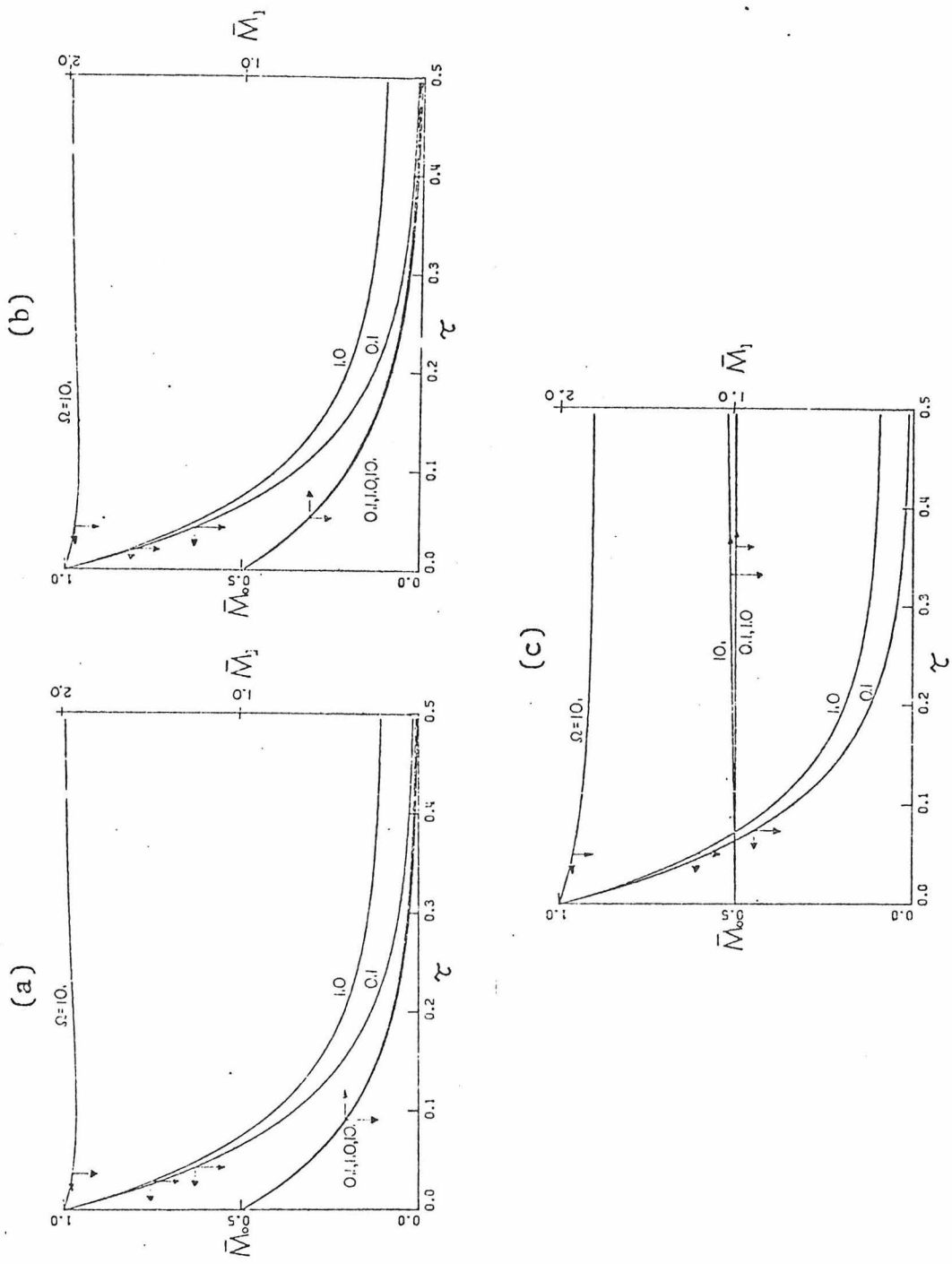

Figure 4.6

Time evolution ($\tau=\beta_1 N_o \nu_o t$) of number and volume fraction for linear condensation ($I=\sigma_1 v$) linear coagulation ($\beta=\beta_1(v+\tilde{v})$), Θ=10.0 and (a) Λ=0.1, (b) Λ=1.0 and (c) Λ=10.0 .

the lower end of the spectrum while small condensational growth prohibits their achieving larger sizes. This continues until the concentration of large particles is small enough to retard removal by coagulation, where upon the number slowly builds to a steady state value.

4.5.3 Case 3

Figures 4.7-4.9 present $\bar{M}_0(\tau)$ and $\bar{M}_1(\tau)$ for case 3, constant coagulation and constant condensation. From Table 4.3, it is obvious that $\bar{M}_0$ in case 3 is identical to that predicted in case 1, and hence no further discussion is necessary. Since condensation is particle-size independent, and hence dependent only on the number of "condensation sites," the time evolution of $\bar{M}_1$ depends on $\bar{M}_0$. When removal dominates volume addition by nucleation and growth, $\bar{M}_{1_{ss}} < M_1(0)$, and when removal is dominated by the condensation and nucleation processes, $\bar{M}_{1_{ss}} > M_1(0)$. For all values of the parameters, the steady state for $\bar{M}_1$ is given by

$$\bar{M}_{1_{ss}} = \frac{\Delta\Omega}{\theta} + \Lambda\left(\sqrt{1 + \frac{2\Omega}{\theta^2}} - 1\right) \tag{4.29}$$

Roughly speaking, the first term in (4.29) represents the volume increase due to nucleation, whereas the second term is associated with volume addition due to growth on both existing and nucleated particles.

One solution for $\bar{M}_1$ which exhibits a peak occurs for $\theta = 1$, $\Lambda = 10$ and $\Omega = 0.1$, that is, slight nucleation, an average rate of removal, and rapid condensational growth. Here, the total volume increases initially as the volume removed is more than offset by the volume addition due to rapid condensation. However, once particles have grown to larger sizes, the total volume falls off, since removal is size independent,

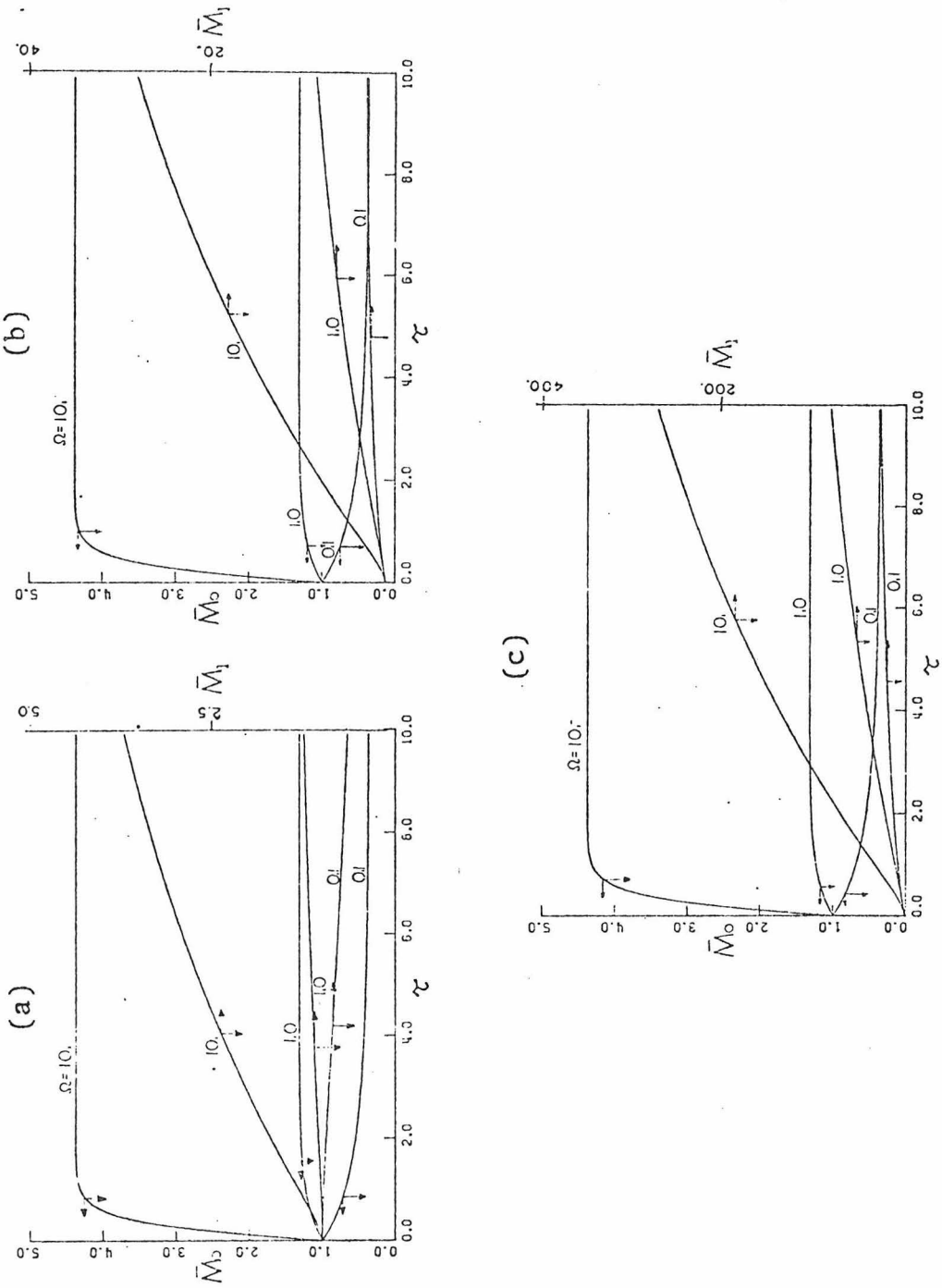

Figure 4.7

Time evolution ($\tau=\beta_o N_o t$) of number and volume fraction for constant condensation ($I=\sigma_o$) and constant coagulation ($\beta=\beta_o$), Θ=0.1 and (a) Λ=0.1, (b) Λ=1.0 and (c) Λ=10.0 .

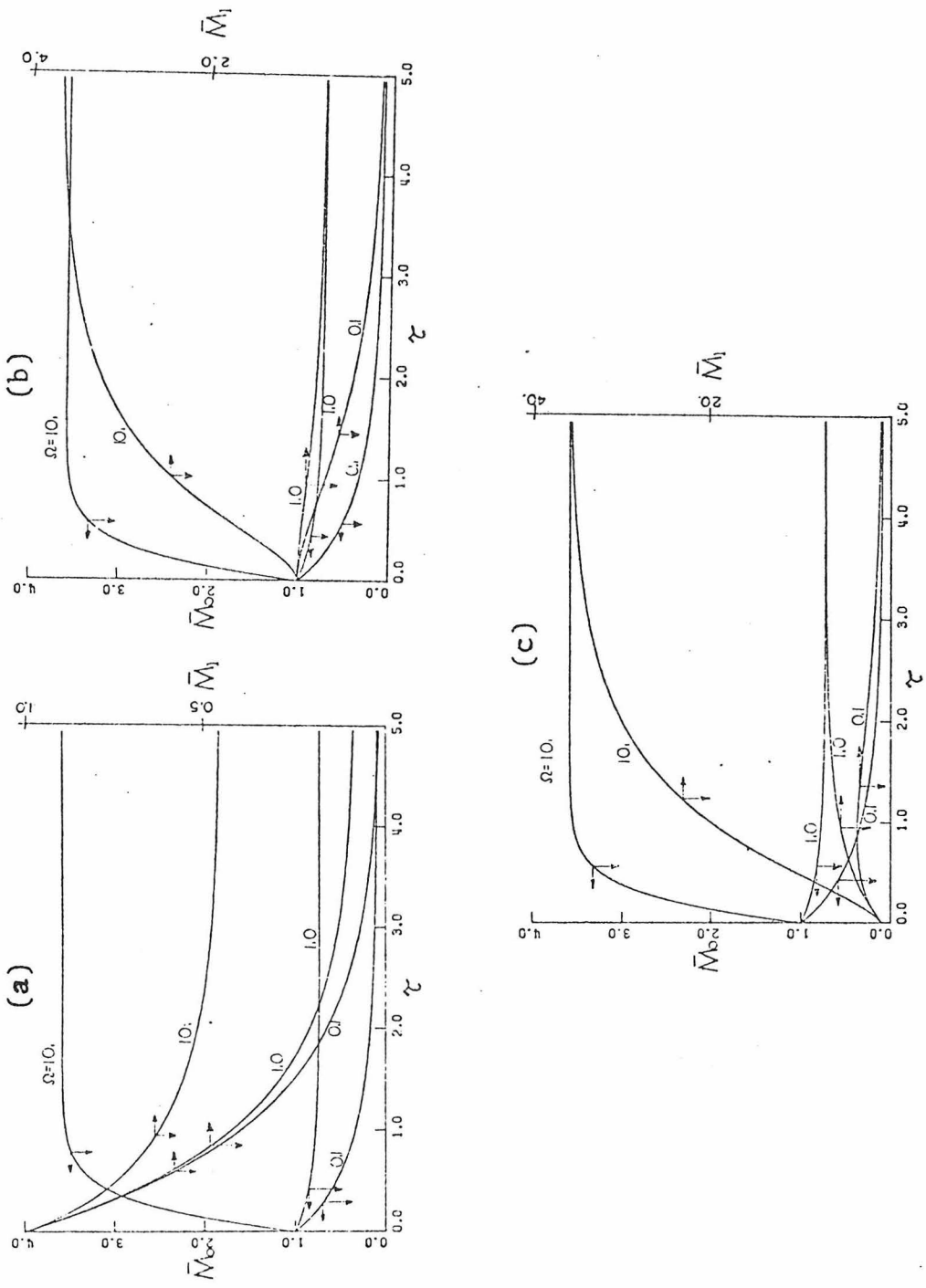

Figure 4.8

Time evolution ($\tau=\beta_o N_o t$) of number and volume fraction for constant condensation ($I=\sigma_o$) and constant coagulation ($\beta=\beta_o$), θ=1.0 and (a) Λ=0.1 (b) Λ=1.0 and (c) Λ=10.0 .

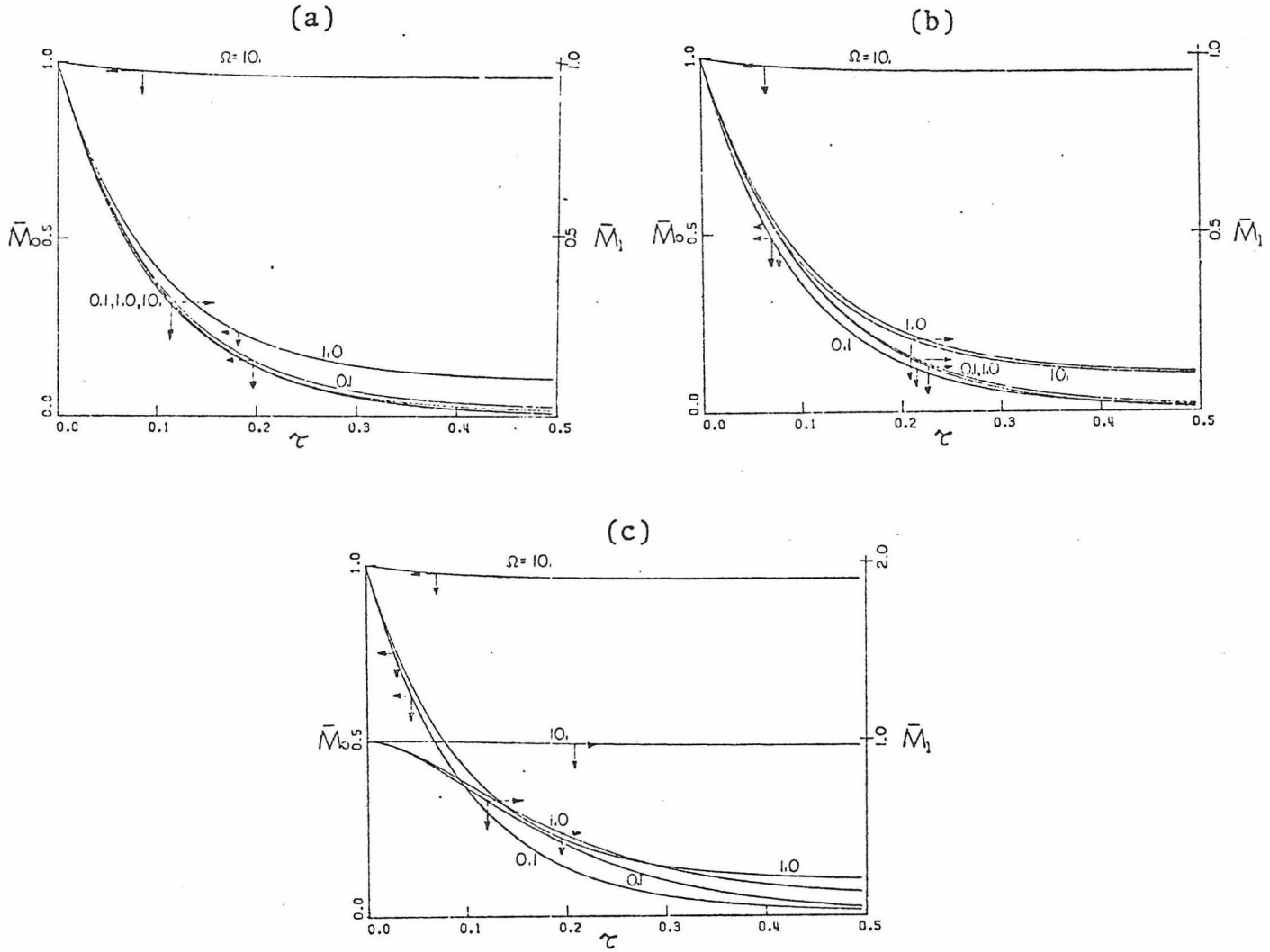

Figure 4.9

Time evolution ($\tau=\beta_o N_o t$) of number and volume fraction for constant condensation ($I=\sigma_o$) and constant coagulation ($\beta=\beta_o$), Θ=10. and (a) Λ=0.1, (b) Λ=1.0 and (c) Λ=10.0 .

and big particles as well as small particles are removed. If θ increases, volume removal always dominates and no peak occurs. If nucleation is more rapid (Ω larger), both volume and condensation site addition are sufficient to dominate removal for all times. If condensation decreases, the volume addition by condensational growth is always negated by removal. Hence, the peaked behavior of $\bar{M}_1$ occurs only for select values of the parameters.

4.5.4 Case 4

Figures 4.10-4.12 present $\bar{M}_0(\tau)$ and $\bar{M}_1(\tau)$ for case 4, linear coagulation and constant condensation. Since coagulation effects total number and condensation effects total volume, linear coagulation and constant condensation couples both mechanisms, produces the most complex case computationally and provides some of the most interesting cases to study.

For small rates of removal (θ=0.1, Figure 4.10) $\bar{M}_0$ exhibits a peak characteristic of a system whose total number increases initially due to large nucleation rates (Ω=10) but diminishes after these particles have grown due to condensation and coagulation. As condensation increases, the time at which this peak occurs decreases, as does the magnitude of the peak. For very large condensation rates (Λ=10) growth and subsequent coagulation occur so quickly that the number falls off rapidly after the peak develops. However, if the removal rate is increased, then the peak occurs once again, giving rise to the phenomenon of increased total number with increased removal rates, as seen already in case 2. This behavior is observed for all values of $\bar{M}_0$ in going from θ = 0.1 (Figure 4.10) to θ = 1.0 (Figure 4.11), but $\bar{M}_0$ decreases for increasing θ as θ goes to θ = 10. (Figure 4.12)

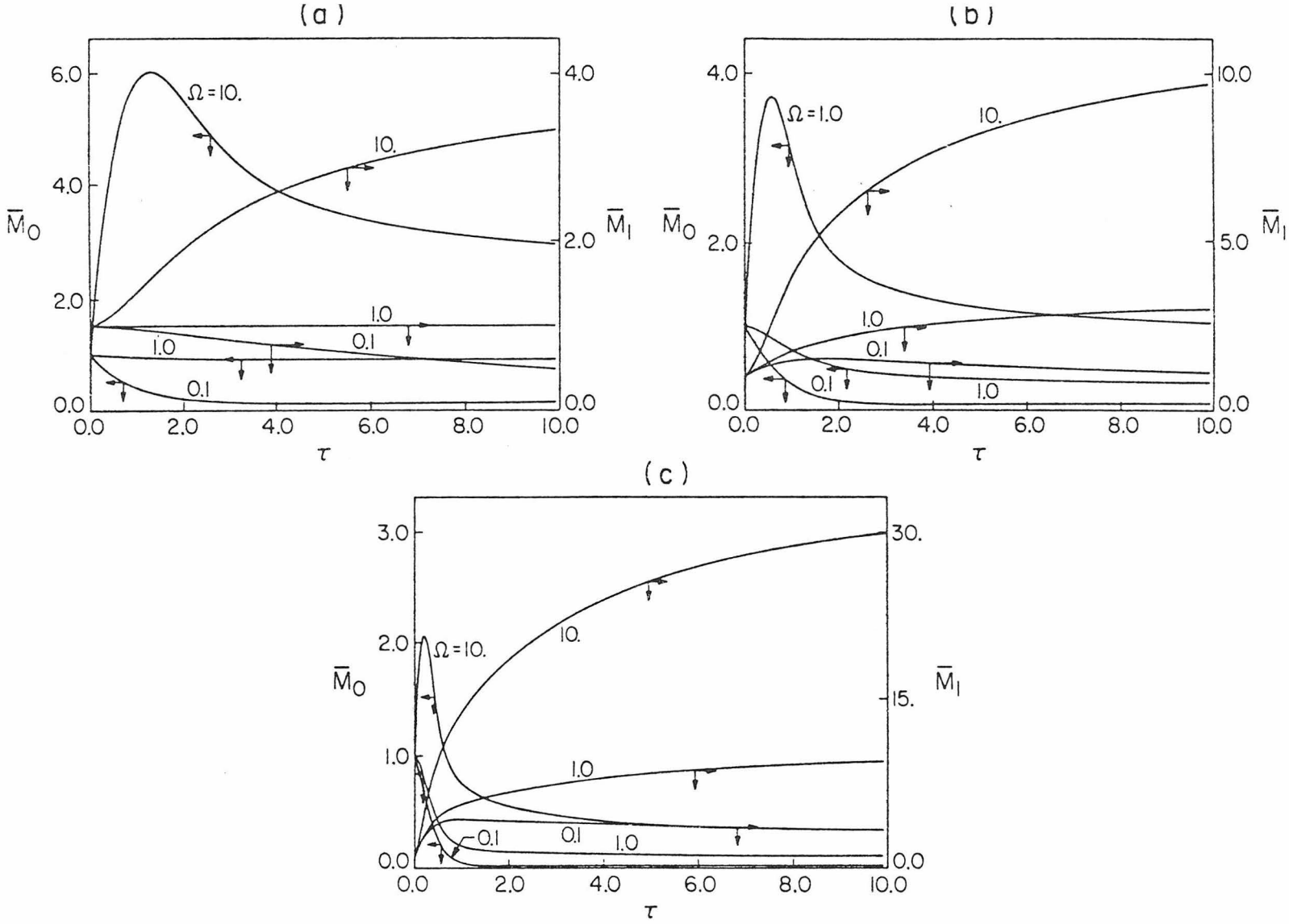

Figure 4.10

Time evolution ($\tau=\beta_1 N_o \nu_o t$) of number and volume fraction for constant condensation ($I=\sigma_o$) and linear coagulation ($\beta=\beta_1(v+\tilde{v})$), $\Theta=0.1$ and (a) $\Lambda=0.1$, (b) $\Lambda=1.0$ and (c) $\Lambda=10.0$.

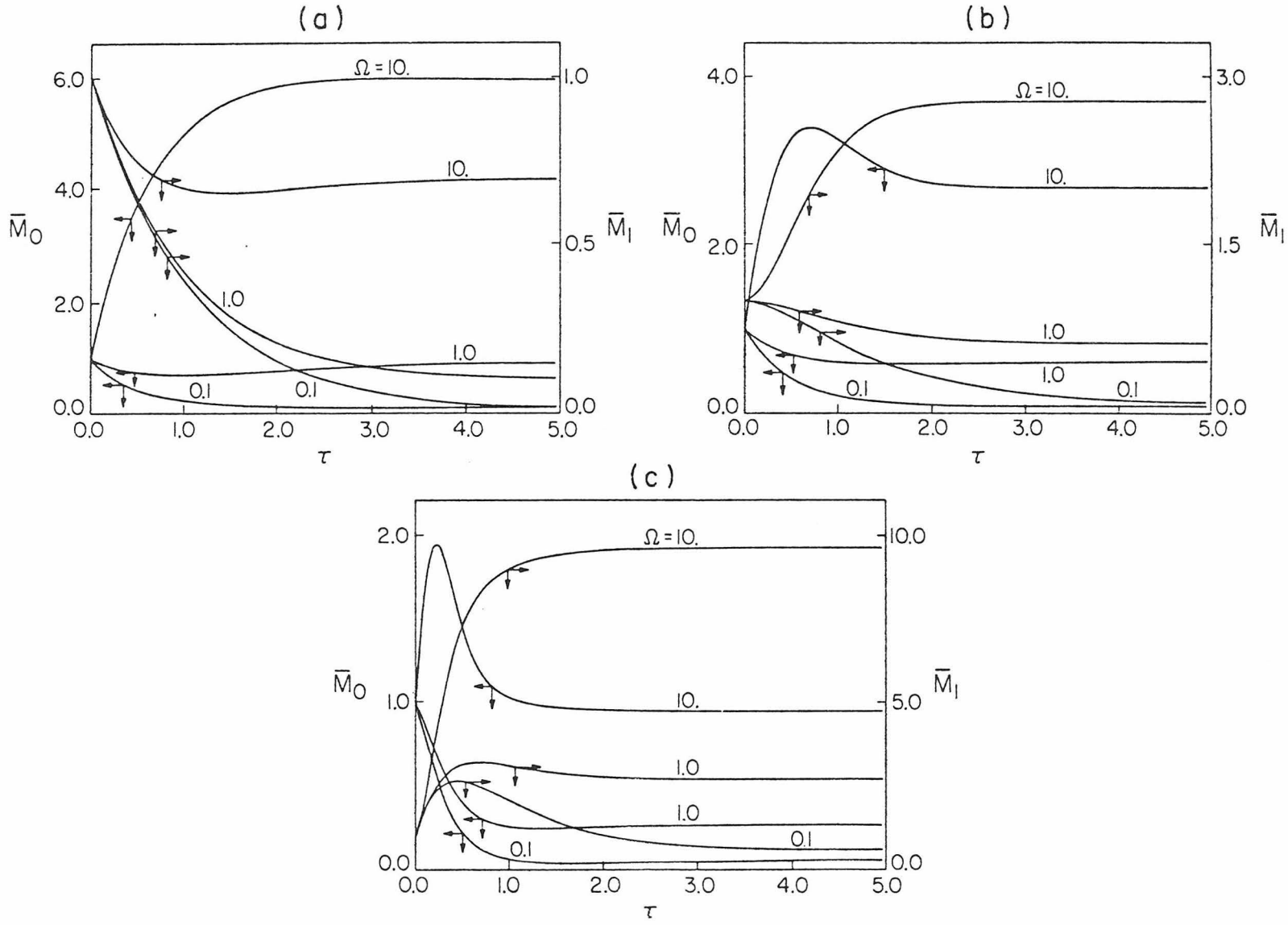

Figure 4.11

Time evolution ($\tau=\beta_1 N_o \nu_o t$) of number and volume fraction for constant condensation ($I=\sigma_o$) and linear coagulation ($\beta=\beta_1(v+\tilde{v})$), θ=1.0 and (a) Λ=0.1, (b) Λ=1.0 and (c) Λ=10.0 .

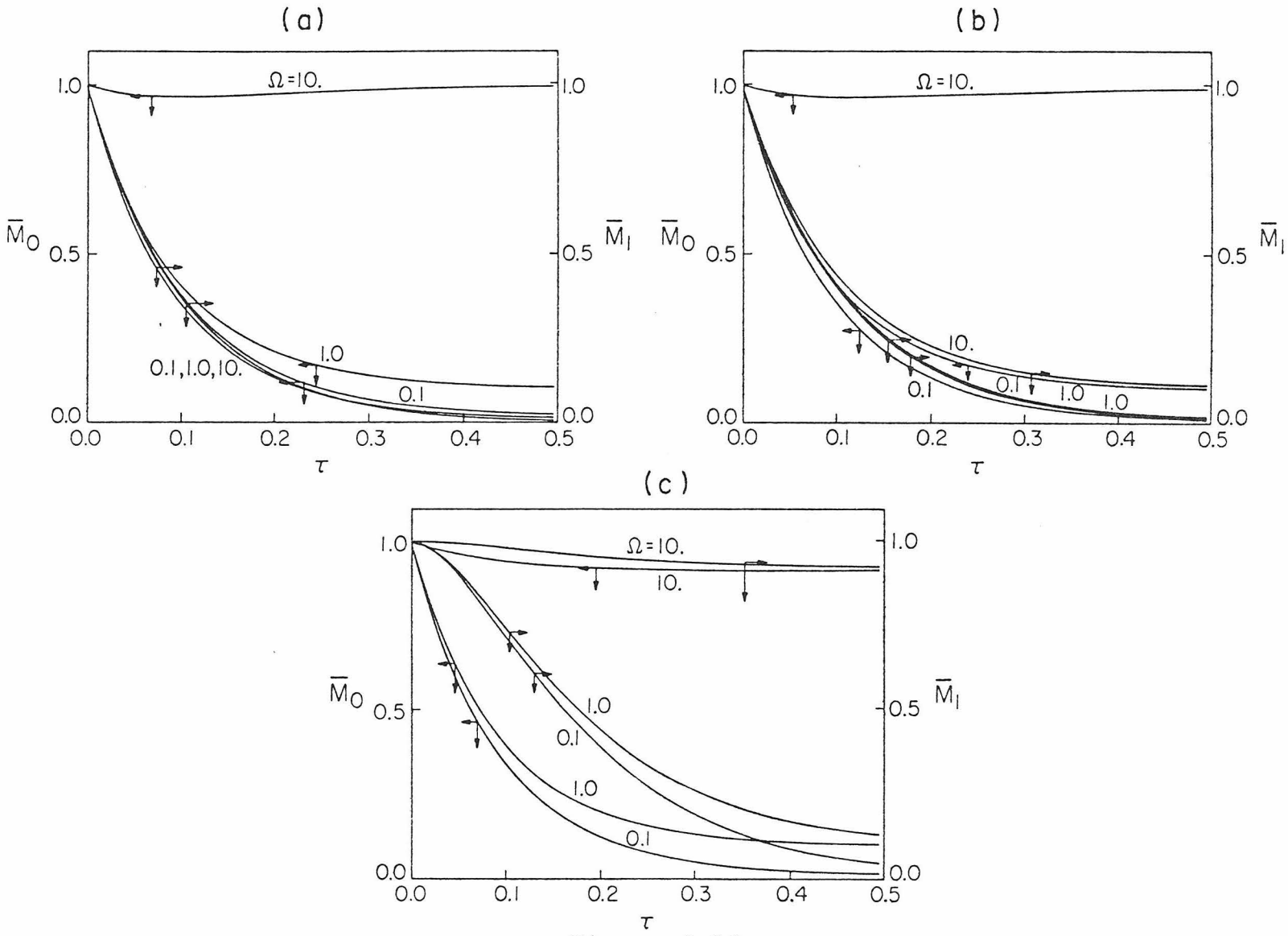

Figure 4.12

Time evolution ($\tau=\beta_1 N_o \nu_o t$) of number and volume fraction for constant condensation ($I=\sigma_o$) and linear coagulation ($\beta=\beta_1(v+\tilde{v})$), $\Theta=10.$ and (a) $\Lambda=0.1$, (b) $\Lambda=1.0$ and (c) $\Lambda=10.0$.

For large removal rates (Figure 4.12) and large nucleation rates (Ω=10), the total number falls off initially, reaches a minimum, and increases, in much the same way as $\bar{M}_0$ did for similar conditions in case 2.

Of interest in the behavior of $\bar{M}_1$ is the peak for large condensation rates and small nucleation rates. The large condensation rate causes the total volume to climb initially, until the distribution is biased to larger particles. This bias is strengthened by linear coagulation. Hence removal, which is homogeneous, removes a proportionally greater volume of large particles, causing the total volume to decrease. If the rate of condensation drops, the initial growth does not occur, and $\bar{M}_1$ decreases steadily. If nucleation increases, the volume and condensation site addition dominate removal for all times, and $\bar{M}_1$ steadily increases. By comparing these peaks with the curves for $\bar{M}_1$ for case 3 and the same values of the parameters, it is apparent that while coagulation obviously does not directly reduce total volume, linear coagulation, as compared to constant coagulation, coupled with a constant condensation process effectively reduces the total volume of the system. This is due to the larger decrease in condensation sites caused by linear coagulation.

4.5.5 Steady State Moments

The discussion on the moment distributions will be concluded by considering Figures 4.13 and 4.14, which plot the steady state values of $\bar{M}_0$ vs. θ, with Ω as a parameter. Λ is chosen to be 1.0 for convenience. Figures 4.13 and 4.14 show $\bar{M}_{0_{ss}}$ for cases 2 and 4, respectively. In both cases, which involve the mechanism of linear coagulation, we see the

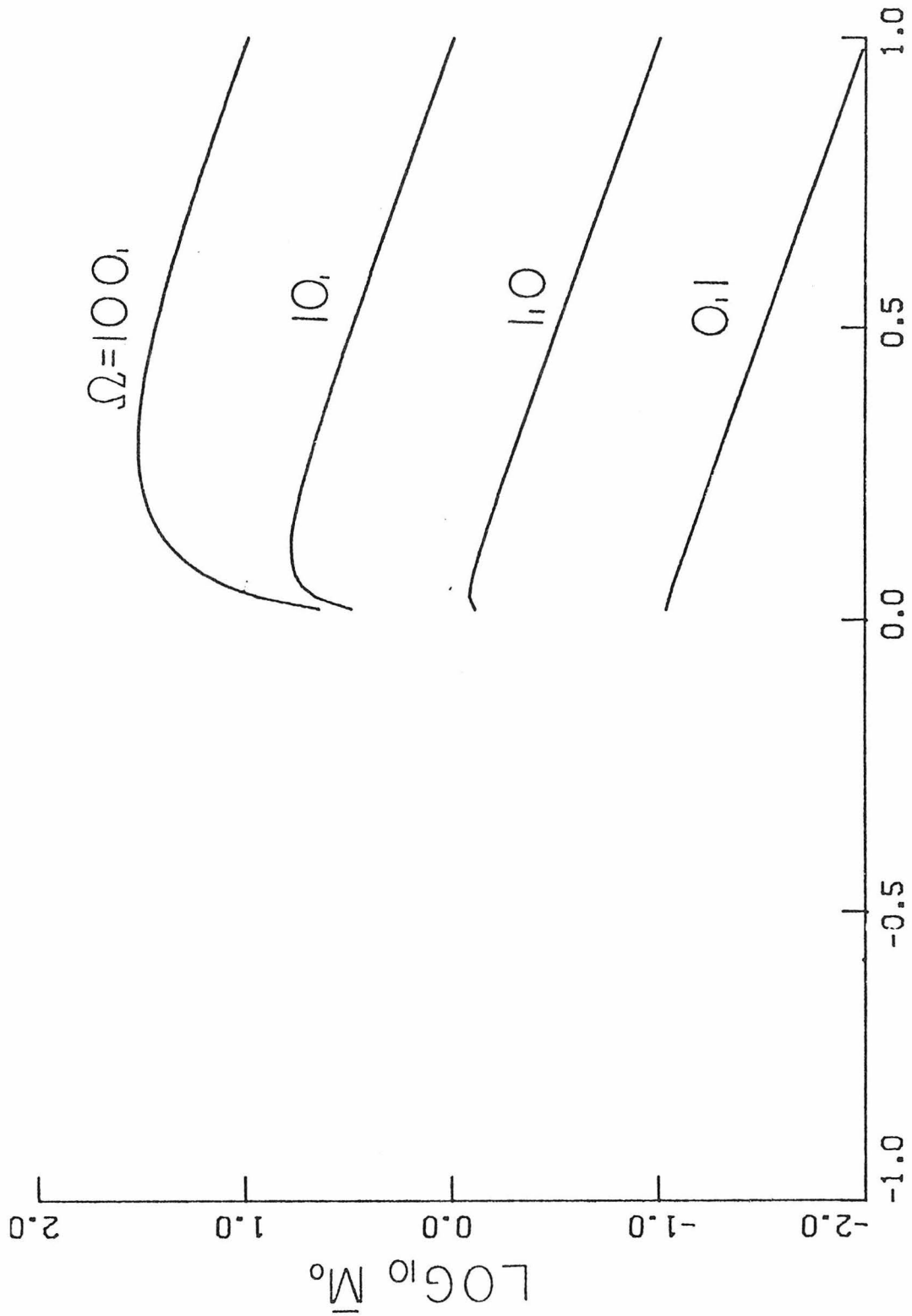

Figure 4.13
Steady state number fraction for linear condensation($I=\sigma_1 v$) and linear coagulation ($\beta=\beta_1(v+\tilde{v})$) , $\Lambda=1.0$.

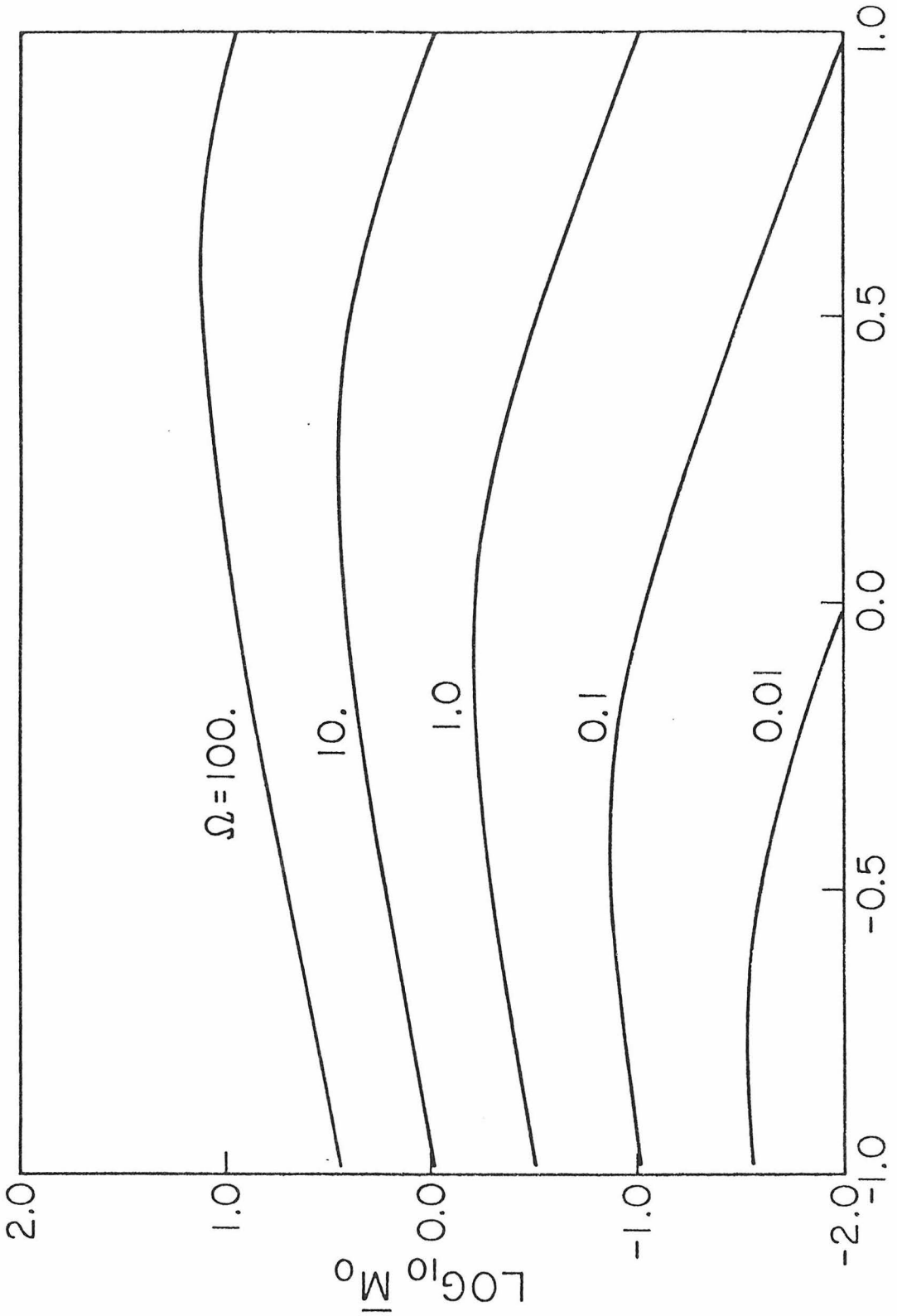

Figure 4.14

Steady state number fraction for constant condensation ($I=\sigma_o$) and linear coagulation ($\beta=\beta_1(v+\tilde{v})$) , $\Lambda=1.0$.

unexpected behavior of increased total number as the removal rate θ increases. For case 2, a non-zero steady state occurs only for $\theta > \Lambda$, hence the sharp decrease as θ approaches 1.0 (the value of Λ) from the right. Even under conditions such that $\bar{M}_{0_{ss}}$ goes to zero, the rate at which it goes to zero decreases as θ increases. For case 4, $\bar{M}_{0_{ss}}$ goes to zero only for certain parameters identically zero, and the peak is a much broader function of θ. The steady state equations for $\bar{M}_0$ and $\bar{M}_1$ for case 4 are given by

$$\bar{M}_{0_{ss}} = \frac{2\theta\Omega}{\Delta\Omega+\theta^2+\sqrt{(\Delta\Omega+\theta^2)^2+4\Lambda\Omega\theta}} \tag{4.30}$$

$$\bar{M}_{1_{ss}} = \frac{\Delta\Omega-\theta^2+\sqrt{(\Delta\Omega+\theta^2)^2+4\Lambda\Omega\theta}}{2\theta} \tag{4.31}$$

4.6 Solutions to the General Dynamic Equation for the Size Distribution

We now wish to consider the solution to the general dynamic equation describing the aerosol number distribution. As described previously, the method of approach is through the Laplace transformation with respect to volume, and the equations which result for the four separate cases considered are presented in Table 4.4. Were we able to solve analytically each of those equations, we would have but four solutions to deal with, each solution being a function of Λ, θ and Ω, the three dimensionless rate parameters. Such general solutions are not feasible however, and it is therefore necessary to consider specialized situations within each case. So too, considering that we have four cases and three rate parameters, each of which can assume any value, the necessity to approach systematically each example and minimize the number of examples considered

becomes paramount. We have therefore chosen to consider three major categories: processes with no coagulation, processes with no condensation and processes with both condensation and coagulation. Within each category there will be separate cases depending on the mechanisms of condensation and coagulation; two each for the no-condensation and no-coagulation catagories and four cases for the full condensation/coagulation category. Finally, within each case there will be four separate examples corresponding to the removal and nucleation mechanisms. For simplicity, we have chosen the nucleation and removal parameters (Ω and θ) to assume values of 0 or 1 only, hence the four examples.

Table 4.6 presents a summary of all the cases considered, as well as the final disposition of each case. For example, linear condensation, constant coagulation and removal (no nucleation) was solved analytically (hence the entry A), whereas only the Laplace transform of the solution was obtained for the constant coagulation, nucleation and removal case (hence the entry L). Finally, for simplicity we have assumed $\Lambda = 1$ for all cases in category 3. The analytic solutions and their derivations are not presented here, but may be found in the Appendix. We will discuss the results in each category based on their solutions as plotted in Figures 4.15-4.21. In order to minimize the range over which the abscissa varies, Figures 4.15-4.21 show $n(\bar{D})$ vs. $\bar{D}$, where,

$$\bar{D} = \frac{D}{D_o} = \left(\frac{v}{v_o}\right)^{1/3} \tag{4.32}$$

and

$$n(\bar{D}) = n(v)\,\frac{dv}{d\bar{D}} = 3v_o\bar{D}^2\,n(v) \tag{4.33}$$

Table 4.6 Summary of Cases Considered

NO	$\theta = 0$ $\Omega = 0$	$\theta \neq 0$ $\Omega = 0$	$\theta = 0$ $\Omega \neq 0$	$\theta \neq 0$ $\Omega \neq 0$
COAGULATION				
$I = \sigma_0$ (cases 3,4)	A	A	A	A
$I = \sigma_1 v$ (cases 1,2)	A	A	A	A
NO CONDENSATION				
$\beta = \beta_0$ (cases 1,3)	A	A	L,N	L*,N
$\beta = \beta_1(v+\tilde{v})$ (cases 2,4)	A	A	N	N
CONDENSATION AND COAGULATION ($\Lambda = 1$)				
$\beta = \beta_0$, $I = \sigma_1 v$ — case 1	A	A	N	N
$\beta = \beta_1(v+\tilde{v})$, $I = \sigma_1 v$ — case 2	A	A	N	N
$\beta = \beta_0$, $I = \sigma_0$ — case 3	L*	L*	L	L
$\beta = \beta_1(v+\tilde{v})$, $I = \sigma_0$ — case 4	-	-	-	-

A - Analytic solution obtained

N - Numerical solution obtained

L - Laplace transform obtained, intractable inversion

L* - Laplace inversion approximated.

Figures 4.15a-4.15d present the size distributions for aerosols undergoing constant condensation, removal and nucleation. Since the condensation rate is size independent, all particles grow at the same rate, and for a system with no sources the spectrum lacks particles below a certain diameter. This behavior is exhibited in Figure 4.15a. A rather unique situation occurs in Figure 4.15b, where removal is included. For $\theta = 1$, which is the case in Figure 4.15b, the number increase in the larger sizes is exactly offset by first order removal. Hence the distribution for subsequent times overlays all previous solutions for diameters above which particles still exist. For sizes below this diameter, no particles exist. Adding nucleation, on the other hand (Figure 4.15c) simply "fills in" the lower end of the spectrum (as compared to Figure 4.15a), again giving rise to an overlay of the distributions for successive times. However, due to the nature of the initial condition, which predicts a finite number of particles of infinitesimal size, and the mechanism of size independent condensational growth, we have a sharp peak, or "shock," at the edge of this characteristic moving wave. The peak decays very rapidly, not because the effect of the initial condition decays, but because the nucleation front decays. This can be better understood by visualizing what the distribution in Figure 4.15c would look like if there were initially no particles present. In that case, the number distribution would be identical to that in Figure 4.15c below the front, and would decay rapidly to zero (in exactly the same way as the peaks in Figure 4.15c decay to the shifted initial condition) past the front. A comparison of the nature of the distribution after the front in Figure 4.15c to the distribution in Figure 4.15a (no nucleation) indicates the obvious: that nucleation has little or no effect on the

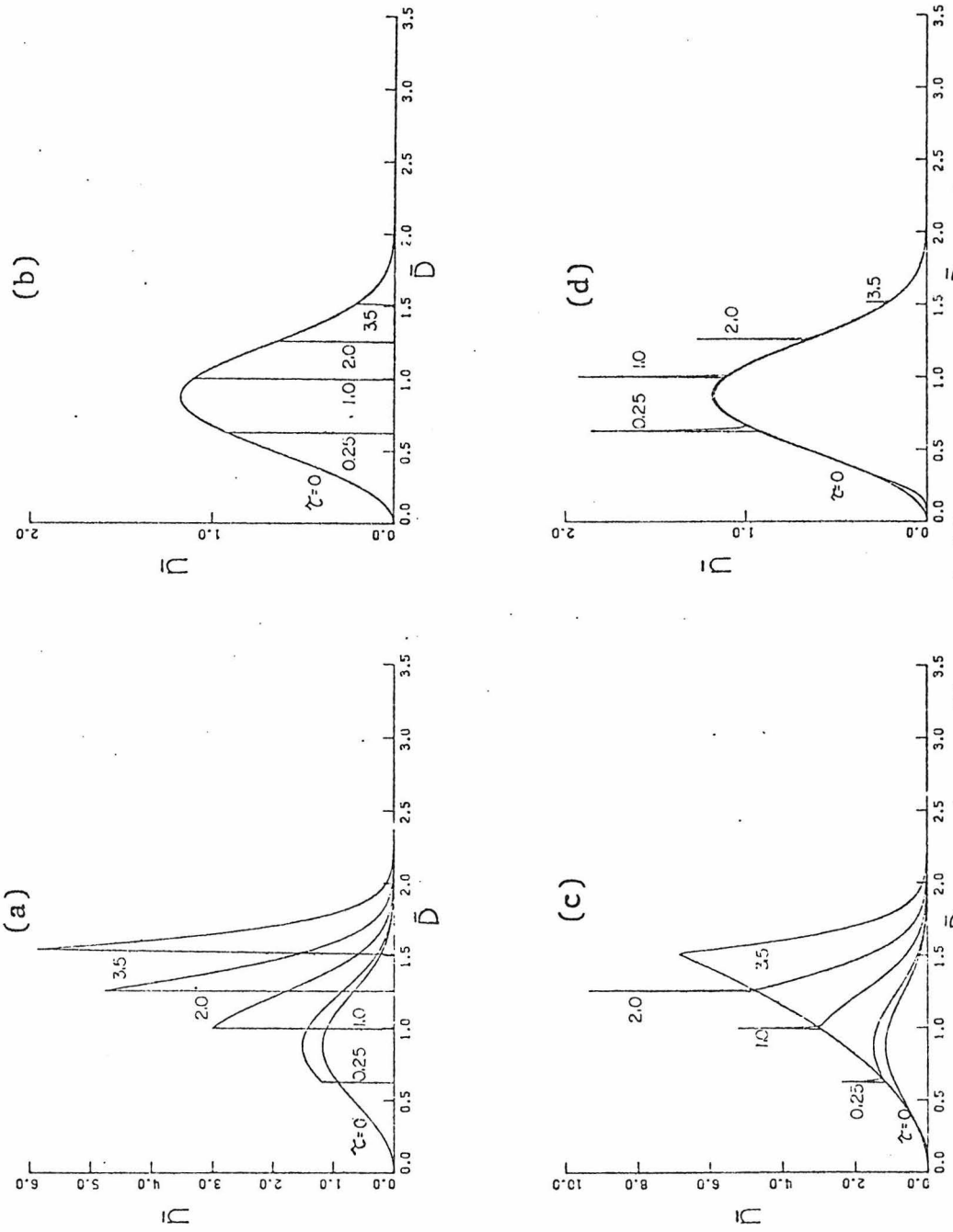

Figure 4.15

Particle size spectra for constant condensation ($I=\sigma_o$), $\tau=\sigma_o t/\nu_o$ and (a) $\Theta=\Omega=0$, (b) $\Theta=1,\Omega=0$, (c) $\Theta=0,\Omega=1$ and (d) $\Theta=\Omega=1$.

distribution past this front. It is important to emphasize that this peak is an artifact of two conditions: an initial condition which specifies a non-zero number distribution for particles of infinitesimal diameter, and a growth mechanism that is particle size independent. As we shall later show, linear condensation, or condensation with coagulation will not exhibit this behavior.

When both nucleation and removal are included (Figure 4.15d) we again find this overlay of distributions (a consequence of choosing $\theta = 1$) and the sharp spikes at the front of the characteristic (a consequence of size independent growth and the choice of initial condition). Interestingly, aside from small deviations near the lower end of the spectrum, near the top of the mode, and the large spiked peaks about the wave front, this particular distribution, with its accompanying mechanisms of nucleation and removal, is at "near-steady-state" from the outset.

For linear condensation processes, no such overlayed distributions or discontinuities occur, and the results are much more predictable. In Figure 4.16a, linear condensation without sources or removal rapidly spreads the distribution to the larger sizes. When removal is included, the distribution still shifts to the larger size, but is significantly reduced by removal. Nucleation (Figure 4.16c) produces the typical bimodal distribution, with the upper end (above $\bar{D} \approx 1.0$) almost identical to the upper end in Figure 4.16a, since nucleation has no effect on the larger sizes. Finally, inclusion of removal simply decreases the magnitude of the distribution for any time, and due to the first order nature of the removal mechanisms, tends to bring the bimodal peaks of the distribution closer in magnitude.

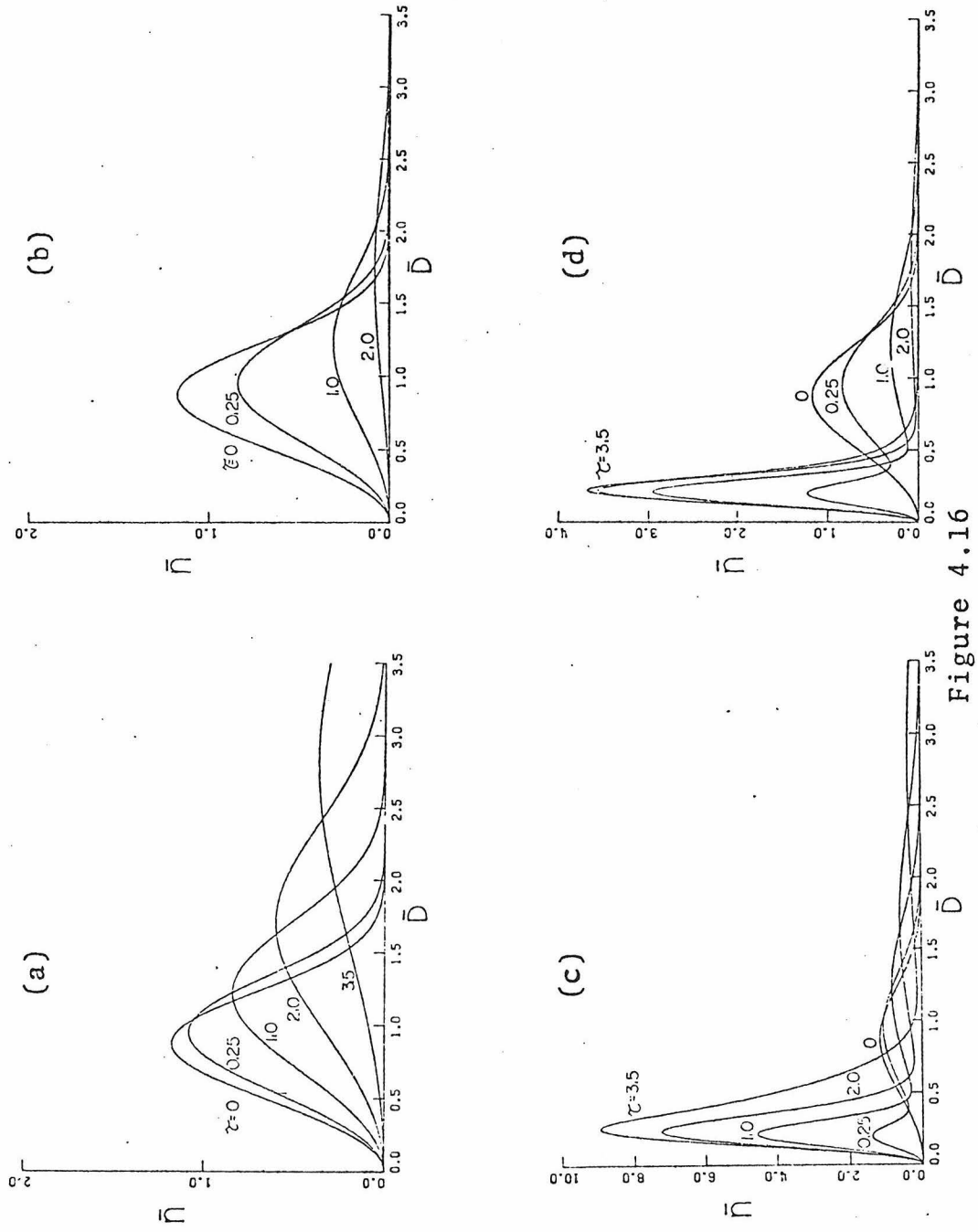

Figure 4.16

Particle size spectra for linear condensation ($I=\sigma_1 V$), $\tau=\sigma_1 t$ and (a) $\Theta=\Omega=0$, (b) $\Theta=1,\Omega=0$, (c) $\Theta=0,\Omega=1$ and (d) $\Theta=\Omega=1$.

Figures 4.17a-d present the size distributions for aerosols undergoing constant coagulation, removal and nucleation, with no condensation. Whereas Figures 4.15 and 4.16 for condensational growth processes showed no change in total number of particles (i.e. the area under the distribution curve) due to condensation alone, Figures 4.17 and 4.18 for aerosols undergoing coagulation do show a definite decrease in total number as time evolves. Comparing figures 4.17a and 4.15a, we can see that the second-order dependance of coagulation on aerosol number density prohibits the formation of a moving front, and therefore yields a continuous distribution. The coagulation process itself causes a decrease in total number, and coupled with first order removal (Figure 4.17b), leads to a rapid overall decrease in total number. Nucleation (Figure 4.17c) on the other hand, produces a distribution reminiscent of the linear condensation case, and nucleation with removal (Figure 4.17d) simply decreases the magnitude of the distribution overall. The size distributions in Figures 4.17c and 4.17d were generated numerically. However, Figure 4.17d includes an asymptotic approximation to the analytic solution, correct for large values of $\bar{D}$. As can be seen from Figure 4.17d, "large" values of $\bar{D}$ implies $\bar{D}$ greater than about 0.5. This asymptotic expansion was carried out in the Laplace domain in order to facilitate inversion. The details of this approach are given in the Appendix. In Figures 4.18a-d, coagulation varies linearly with particle volume. Because of the increase in coagulation rate with increasing particle size, total number is reduced more rapidly than for the constant coagulation situation. Smaller particles are less apt to coagulate, and therefore the peak in the distribution at each time interval is found for smaller particle diameters than experienced in Figure 4.17a. Again, removal (Figure 4.18b) causes a rapid decrease in number density. Due to

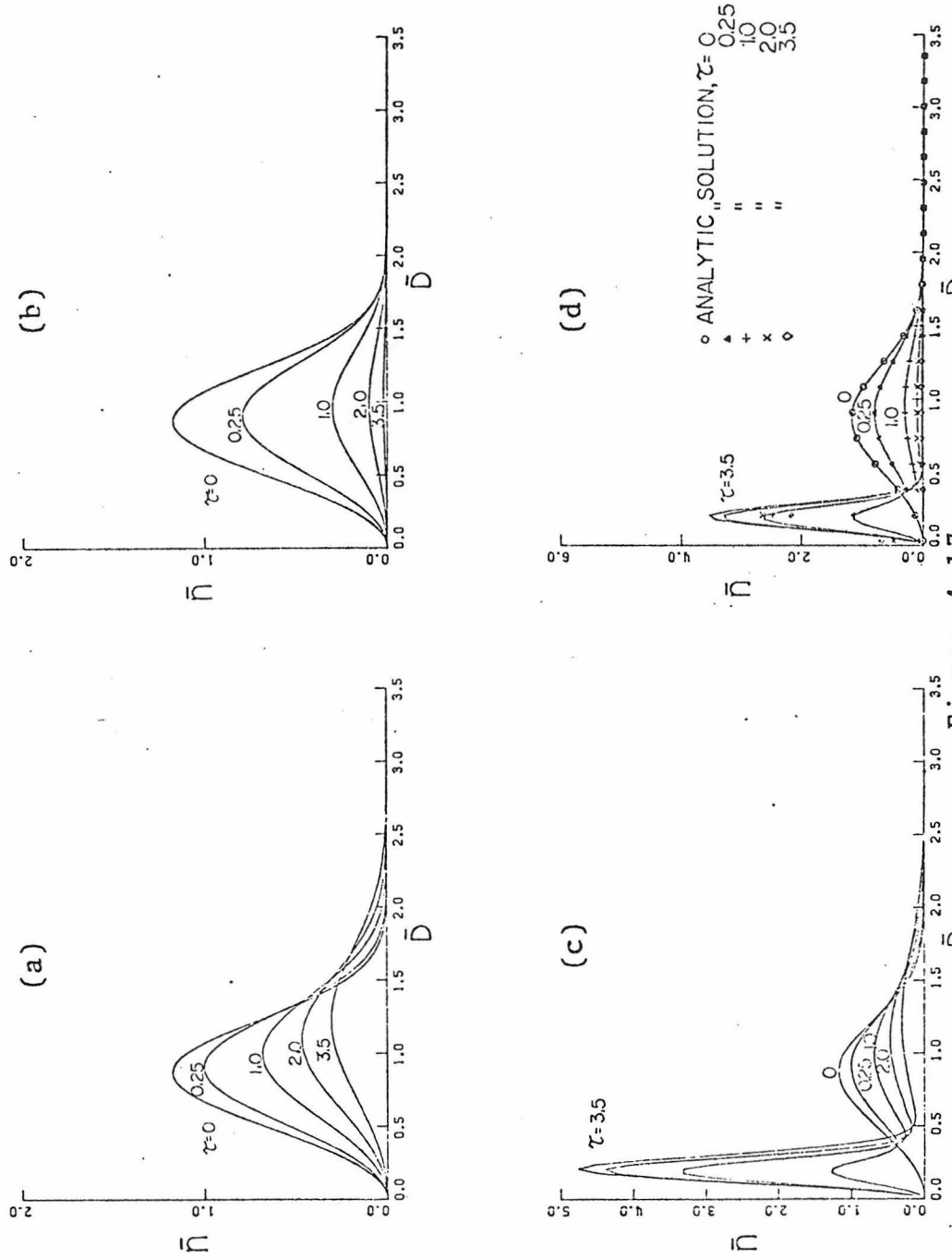

Figure 4.17

Particle size spectra for constant coagulation ($\beta=\beta_o$), $\tau=\beta_o N_o t$ and (a) $\theta=\Omega=0$, (b) $\theta=1, \Omega=0$, (c) $\theta=0, \Omega=1$ and (d) $\theta=\Omega=1$.

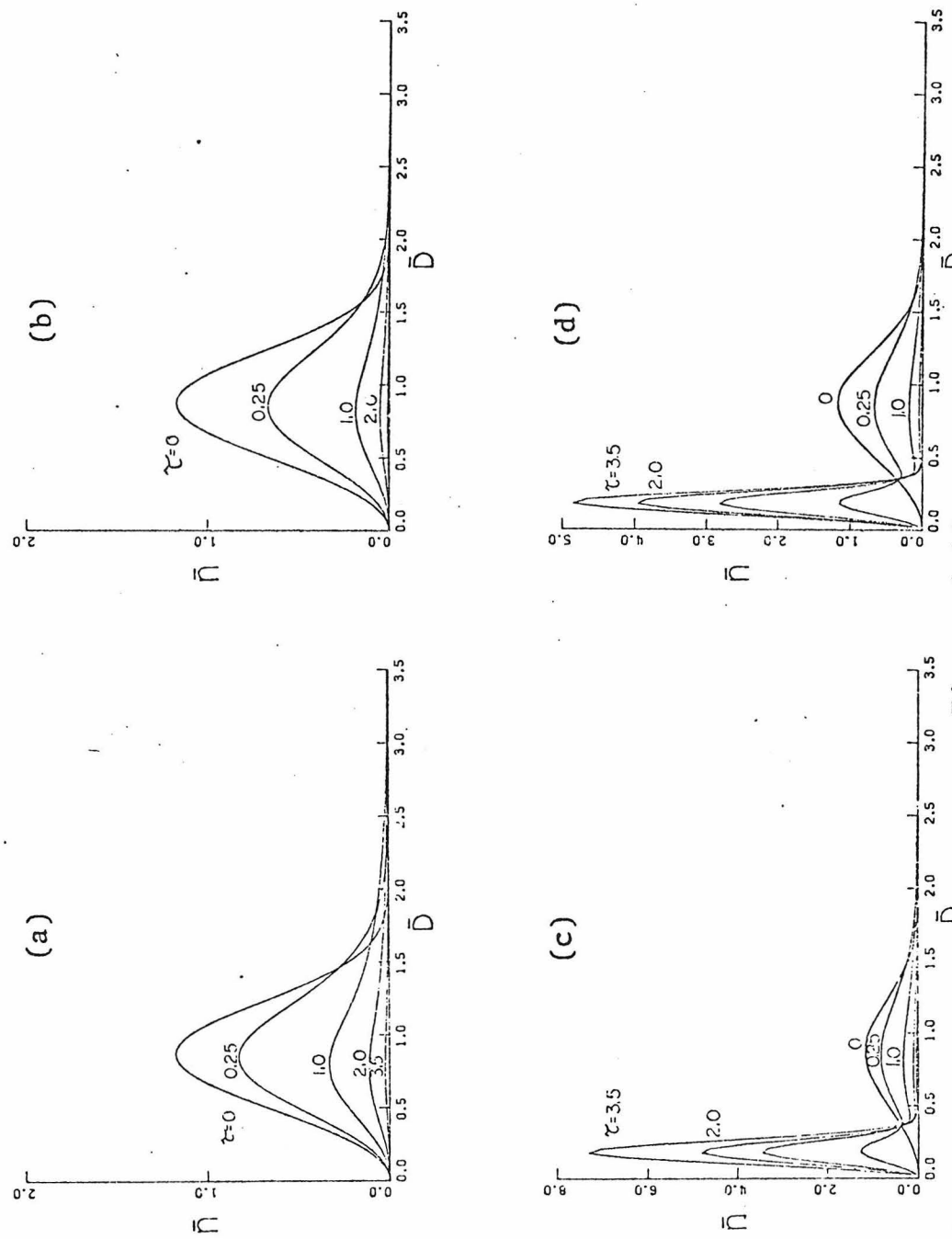

Figure 4.18

Particle size spectra for linear coagulation ($\beta=\beta_1(v+\tilde{v})$, $\tau=\beta_1 N_o v_o t$ and (a) $\theta=\Omega=0$, (b) $\theta=1,\Omega=0$, (c) $\theta=0,\Omega=1$ and (d) $\theta=\Omega=1$.

the small coagulation rates for small particles, nucleation (Figure 4.18c) yields much higher peaks for each time interval than found for constant coagulation (Figure 4.17c), since newly nucleated small particles are more hesitant to coagulate and move into larger size ranges. For the same reason, inclusion of removal causes the density to drop, but not to the same levels in the lower end that were experienced in Figure 4.17d.

Figures 4.19a-d present the aerosol size distribution for an aerosol undergoing linear condensation, constant coagulation, nucleation and removal. Figure 4.19a is obviously identical to case 1 of the previous chapter, since nucleation and removal are neglected. Whereas $n(\bar{D})/N_o$ is plotted here, recall that $n(\log_{10}\bar{D})/N_o$ was plotted previously. The process of linear condensation causes the distribution to spread into the larger sizes, while coagulation serves to reduce total number. Inclusion of removal (Figure 4.19b) reduces total number significantly with the peak values being lower than found in Figure 4.16b (due to coagulation) and the location of those peaks shifted to the right as compared to Figure 4.17b (due to condensation). Inclusion of nucleation (Figure 4.19c) essentially only effects the lower end of the distribution, with peak values reduced both by condensational growth and coagulation and to larger sizes. As one would obviously expect, nucleation and removal together produce a reduced distribution over all sizes.

By changing the coagulation mechanism to one linearly dependent on particle volume (Figures 4.20a-d) we obtain a distribution whose peaks are shifted to the smaller sizes, due to decreased coagulation rates for these particles. Nucleation (Figure 4.20c) produces much higher peaks than for constant coagulation (Figure 4.19c), again due to the mechanism of coagulation. For the full system (Figure 4.20d), it is apparent that the linear

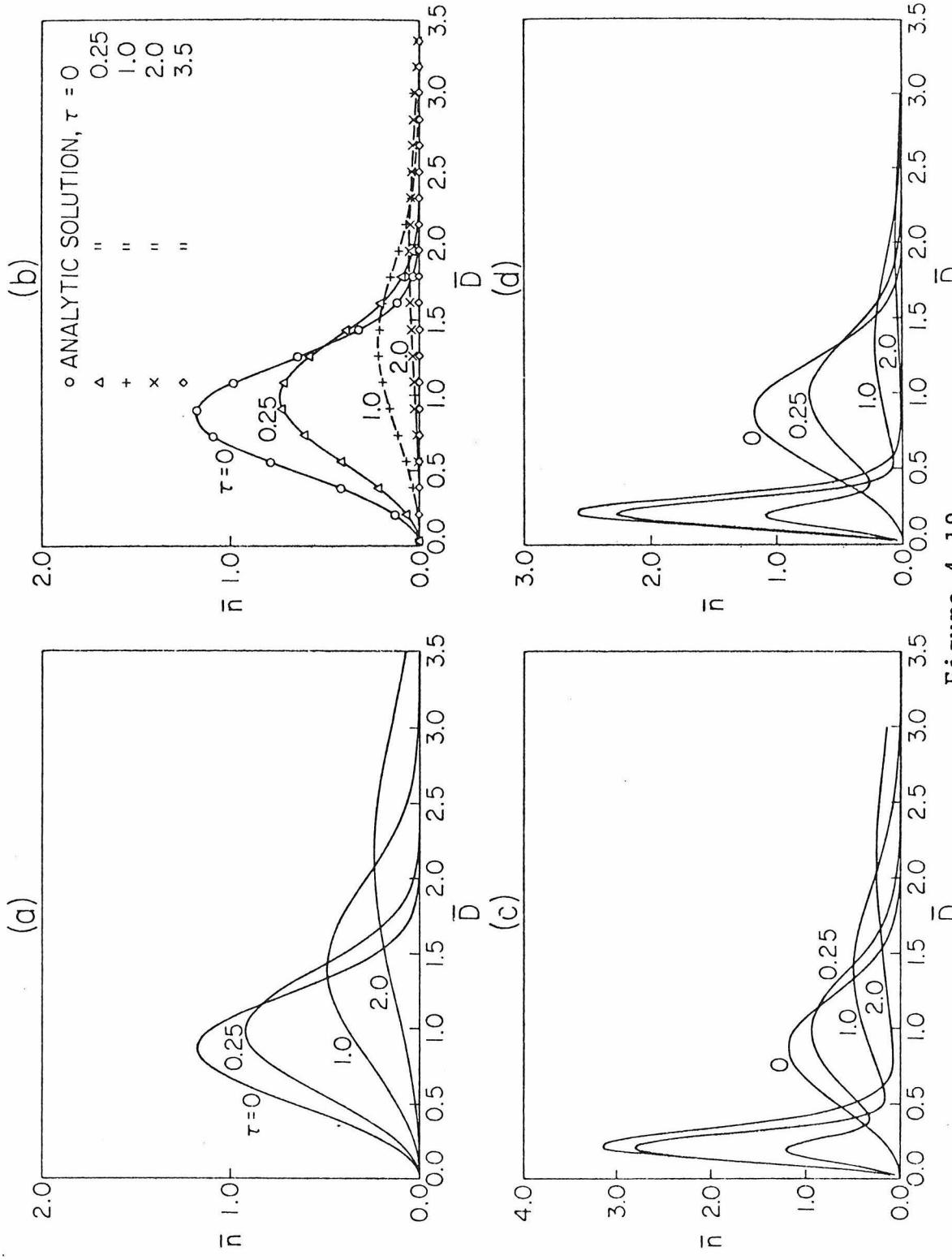

Figure 4.19

Particle size spectra for linear condensation ($I=\sigma_1 v$) and constant coagulation ($\beta=\beta_o$), $\tau=\beta_o N_o t$ and (a) $\Theta=\Omega=0$, (b) $\Theta=1,\Omega=0$, (c) $\Theta=0,\Omega=1$, and (d) $\Theta=\Omega=1$.

coagulation mechanism has the effect of increasing number density in the lower end of the spectrum, and decreasing number density in the upper end. (See Figure 4.19d for comparison.)

The final case we are able to consider is the case of an aerosol undergoing constant condensation and constant coagulation. Due to the discontinuous nature of the solution, the numerical routine of Gelbard (1978) is unable to examine constant condensation cases, and hence we have only the analytic solution with which to study the behavior of the aerosol. For no source or removal (Figure 4.21a) we see the discontinuous distribution or wave front characteristic of the constant condensation mechanism. By comparing Figures 4.21a and 4.15a, we see that coagulation serves to reduce the height of the discontinuity, and removal (Figures 4.21b and 4.15b) is reflected by an overall number reduction below the initial distribution.

4.7 Limiting Forms for n(v,t)

In addition to studying the dynamic behavior of n(v,t), it is worthwhile to examine the form of the distribution function for large sizes; i.e. the upper end of the particle spectrum. It is interesting to examine this end of the spectrum both from the standpoint of the analytic solutions obtained (which are dynamic solutions) and for steady state solutions of Equation (4.1) where they exist and are mathematically obtainable,

A number of investigators (Junge, 1955; Clark and Whitby, 1967; Blifford and Ringer, 1969; Blifford, 1970; Noll and Pilat, 1971) have reported that size distribution measurements for atmospheric aerosols can be approximated over a broad range of sizes by the power-law function, in terms of particle radius r,

$$n(r) \sim br^{-\nu} \tag{4.34}$$

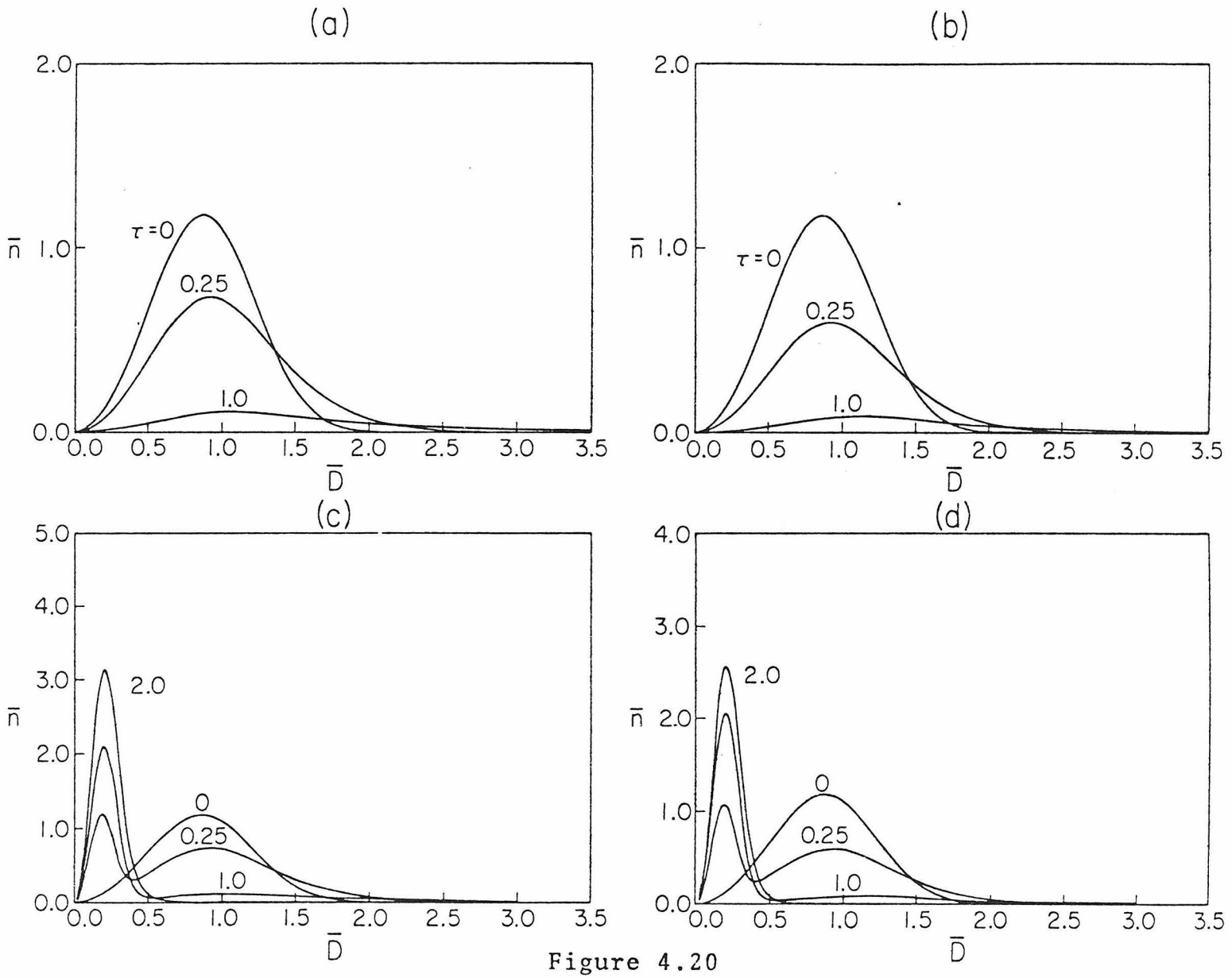

Figure 4.20

Particle size spectra for linear condensation ($I=\sigma_1 v$) and linear coagulation ($\beta=\beta_1(v+\tilde{v})$), $\tau=\beta_1 N_o \nu_o t$ and (a) $\theta=\Omega=0$, (b) $\theta=1, \Omega=0$, (c) $\theta=0, \Omega=1$ and (d) $\theta=\Omega=1$.

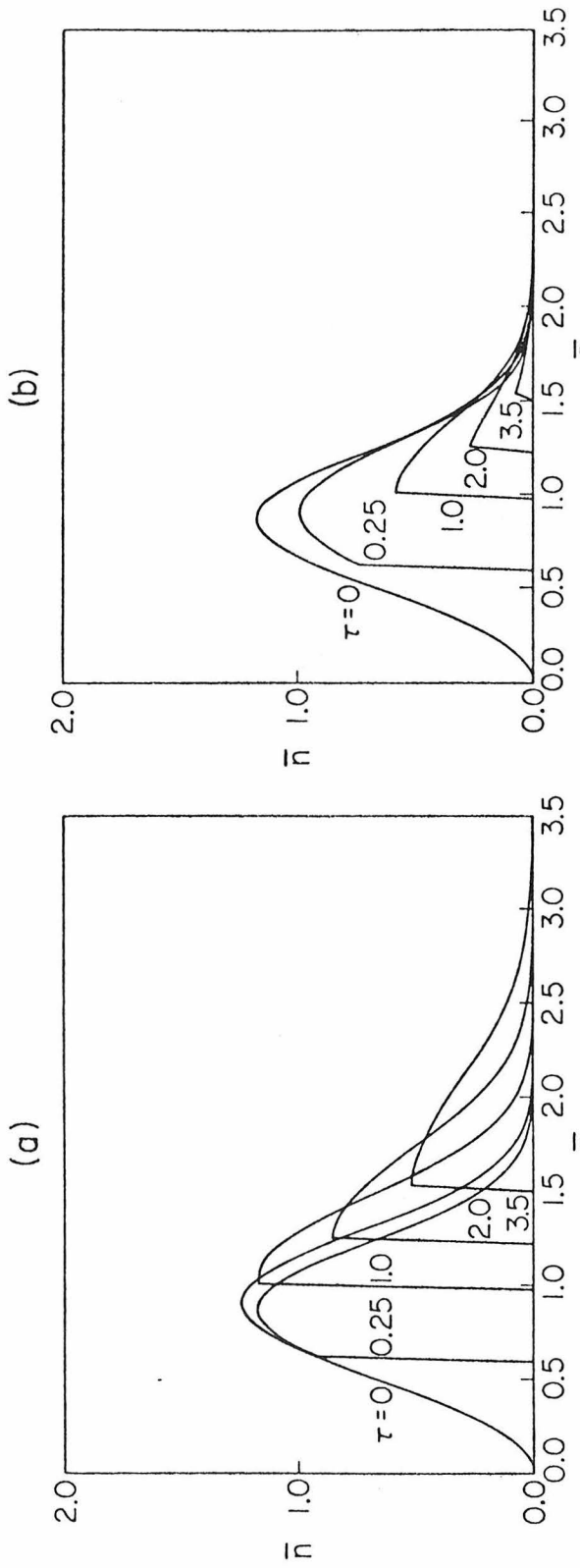

Figure 4.21

Particle size spectra for constant condensation ($I=\sigma_o$) and constant coagulation ($\beta=\beta_o$), $\tau=\beta_o N_o t$ and (a) $\Theta=\Omega=0$ and (b) $\Theta=1, \Omega=0$.

where b and ν are constants, with ν assuming values in the range 4 to 5. Many attempts have been made to explain the origin of the power-law distribution (4.34). Friedlander (1960ab, 1961) considered, as a possible explanation, a situation in which a source of small particles to a coagulating population is just balanced by a loss through sedimentation. Golovin (1963) showed that (4.34) is attained with $\nu = 5/2$ in non-stationary coagulation if β is proportional to the sum of the particle volumes. Takahashi and Kasahara (1968) showed that (4.34) is attained for larger particles for Brownian and turbulent coagulation with gravitational and diffusional deposition. Brock (1971, 1972) proposed that (4.34) results not from coagulation, but from a stationary balance between sources, condensational growth, and removal. Junge (1969) suggested that (4.34) may result purely from the mixing of particles entering the atmosphere from many independent sources. Burgmeier et al. (1973) extended Friedlander's earlier model to a continuous source of particles over the entire size spectrum to replace those lost by sedimentation. Klett (1975) obtained modulated power-law forms using coagulation kernels of the form $\beta = K_o v^a v_;^a$ where K_o and a are constant. He also included particle sources represented by gamma distributions. Lushnikov and Smirnov (1975) showed that (4.34) is achieved as the solution for the stationary equation for coagulation with a constant source of very small particles and a sink that removes all particles above a certain size.

In each of the above-mentioned studies, a special case of (4.1) was considered, generally either a coagulation-dominated or a condensation-dominated process. It does seem clear that the power-law form (4.34) has no special significance since a wide variety of physical situations lead to size distributions that roughly satisfy (4.34). We wish to conclude the

discussion of the analytic solutions obtained for (4.1) by examining the stationary or long-time form of n(v,t).

Table 4.7 presents the results of this examination. Except as where noted, all limiting forms for n(v,t) apply to the full case, including nucleation and removal. For cases 1 and 2, no coagulation, we obtain the power law form (4.34), as was also shown by Brock (1971). This result is a consequence of linear growth. For constant condensation, cases 3 and 4, the sum of exponential functions is obtained, one being due to the nucleation process, the other to the initial conditions. This is similar to the result of Drake (1976).

For processes excluding condensation we again obtain the exponential form (for constant coagulation). For linear coagulation (cases 2 and 4) we obtain a power law spectrum multiplied by an exponential term, arising from first-order removal. When no removal occurs, the power-law distribution is obtained, as already noted by Golovin (1963).

When both condensation and coagulation are present, it appears that the coagulation mechanism plays the dominant role in determining the large-volume distribution. In cases 1 and 3, both of which include constant coagulation, the exponential form predominates. In case 2, linear coagulation and condensation, we again see a power law leading term, multiplied by an exponential term.

Table 4.7 Stationary or Long-Time Solutions for $n(v,t)$, Large v

Case	No Coagulation	No Condensation	Condensation and Coagulation
1	$a_1 v^{-(1+\theta)}$	$a_1 \exp(-b_1 v)+a_2 \exp(-b_2 v)$ $a_3 \exp(-b_3 v)$ $\Omega = 0$; $\theta = \Omega = 0$	$a_1 \exp(-b_1 v)$ $\Omega = 0$; $\theta = \Omega = 0$
2	same as 1	$\frac{a_1}{v^{3/2}} \exp(-b_1 v)$ $\Omega = 0$ $\frac{a_1}{v^{3/2}}$ $\theta = \Omega = 0$	$\frac{a_1}{v^{3/2}} \exp(-b_1 v)$ $\Omega = 0$; $\theta = \Omega = 0$
3	$a_1 \exp(-b_1 v)+a_2 \exp(-b_2 v)$	same as 1	$a_1 \exp(-b_1 v) + a_2 \exp(-b_2 v)$ $\Omega = 0$; $\theta = \Omega = 0$
4	same as 3	same as 2	———

The a_i and b_i are constants or functions of time only, specific to each case.

REFERENCES

Blifford I.H., Jr. and Ringer L.D. (1969) The Size and number Distribution of Aerosols in the Continental Troposphere. J. Atmos. Sci. 26, 716-726.

Blifford I.H., Jr. (1970) Tropospheric Aerosols. J. Geophys. Res. 75(15), 3099-3103.

Brock J.R. (1971) On the Size Distributions of Atmospheric Aerosols. Atmos. Environ. 5,833-841.

Brock J.R. (1972) Condensational Growth of Atmospheric Aerosols. J. Coll. Int. Sci. 39(1),32-36.

Burgmeier J.W., Blifford I.H. Jr. and Gillette D.A. (1973) A Reinforced Coagulation-Sedimentation Aerosol Model. Water, Air and Soil Poll. 2,97-104.

Clarke W.E. and Whitby K.T. (1967) Concentration and Size Distribution Measurements of Atmospheric Aerosols and a Test of the Theory of Self-Preserving Size Distribution. J. Atmos. Sci. 24,677-687.

Drake R.L. (1976) Similarity Solutions for Homogeneous and Non-homogeneous Aerosol Balance Equations. J. Coll. Int. Sci. 57 (3),411-423.

Friedlander S.K. (1960a) On the Particle-Size Spectrum of Atmospheric Aerosols. J. Meteor. 17,373-374.

Friedlander S.K. (1960b) Similarity Considerations for the Particle-Size Spectrum of a Coagulating, Sedimenting Aerosol. J. Meteor. 17(5),479-483.

Friedlander S.K. (1961) Theoretical Considerations for the Particle-Size Spectrum of the Stratospheric Aerosol. J. Meteor. 18,753-759.

Friedlander S.K. (1977) Smoke, Dust and Haze. John Wiley and Sons, New York.

Gelbard F. (1978) Numerical Solution of the Dynamic Equation for Particulate Systems. Ph.D. Thesis, Calif. Inst. of Tech.

Golovin A.M. (1963) The Solution of the Coagulation Equation for Raindrops, Taking Condensation Into Account. Sov. Phys.-Dok. 8(2),191-193.

Junge C.E. (1955) The Size Distribution and Aging of Natural Aerosols as Determined from Electrical and Optical Data on the Atmosphere. J. Meteor. 12,13-25.

Junge C.E. (1969) The Physical and Chemical Properties of Atmospheric Aerosols and their Relation to the Condensation Process. Proc 7th Internat. Conf. on Cond. and Ice Nuclei, 1969 Suppl. Vol. 31.

Klett J.D. (1975) A Class of Solutions to the Steady-State, Source Enhanced Kinetic Coagulation Equation. J. Atmos. Sci. 32,380-389.

Lushnikov A.A. and Smirnov V.I. (1975) Stationary Coalescence and Particle Size Distribution of Atmospheric Aerosols. Atmos. and Ocean. Phys. 11(2),139-152.

Middleton P. and Brock J. (1976) Simulation of Aerosol Kinetics. J. Coll. Int. Sci. 54(2),249-264.

Noll K.E. and Pilat M.J. (1971) Size Distribution of Atmospheric Giant Particles. Atmos. Environ. 5,527-540.

Roberts G.E. and Kaufman H. (1966) Table of Laplace Transforms. W.B. Saunders, Philadelphia.

Scott W.T. (1968) Analytic Studies of Cloud Droplets Coalescence I.J. Atmos. Sci. 25,54-65.

Takahashi K. and Kasahara M. (1968) A Theoretical Study of the Equilibrium Particle Size Distribution of Aerosols. Atmos. Environ. 2,441-453.

Wadden R.A., Quon J.E. and Hulburt H.M. (1974) A Model of a Growing Coagulating Aerosol. Atmos. Environ. 8,1009-1028.

Willeke K. and Whitby K.T. (1975) Atmospheric Aerosols: Size Distribution Interpretation. J. Air Poll. Cont. Assoc. 25(5), 529-534.

APPENDIX. DERIVATION OF EQUATIONS

As in Chapter 4, the derivation of the solutions to the dynamic equation governing the aerosol density function will be divided into three categories: Category 1 for no coagulation, Category 2 for no condensation, and Category 3 for both condensation and coagulation. In Categories 2 and 3, the starting point for the derivations will be the equations in Table 4.4 of Chapter 4. For Category 1, however, the starting point will be the original equation (Eq. 4.1, Chapter 4) since the dimensionless equations of Table 4.4 are based on a characteristic coagulation time and a characteristic coagulation rate, and there is no coagulation in Category 1. Prior to the solution of the equations for the number distribution, the moment equations will be solved. Here, the starting point will be the equations of Table 4.3, Chapter 4.

Each case in each category will be examined. To facilitate possible further examination of these solutions, even the cases in which analytic solutions were not obtained are discussed. For those cases, the derivation is carried to the point where difficulties occurred. In this way, it is indicated why some solutions were not obtained in this work.

A.2.1 The Moments

A.2.1.1 Case 1

The governing equations are

$$\frac{d\bar{M}_0}{d\tau} = -\frac{1}{2}\bar{M}_0^2 - \theta\bar{M}_0 + \Omega \tag{A.1}$$

$$\frac{d\bar{M}_1}{d\tau} = (\Lambda-\theta)\bar{M}_1 + \Lambda\Omega \tag{A.2}$$

Since (A.1) and (A.2) are independent, they can be solved separately.

(A.1) yields

$$\frac{d\bar{M}_o}{(\bar{M}_o-r_1)(\bar{M}_o-r_2)} = -\frac{1}{2}\,d\tau \tag{A.3}$$

where

$$r_1 = -\theta + \sqrt{\theta^2+2\Omega} \tag{A.4}$$

$$r_2 = -\theta - \sqrt{\theta^2+2\Omega} \tag{A.5}$$

which upon integration produces

$$\bar{M}_o(\tau) = \frac{r_1-r_2F(\tau)}{1-F(\tau)} \tag{A.6}$$

where

$$F(\tau) = \frac{1-r_1}{1-r_2}\exp\left[-\left(\frac{r_1-r_2}{2}\right)\tau\right] \tag{A.7}$$

For $\Lambda \neq \theta$, (A.2) yields

$$\bar{M}_1(\tau) = \frac{\Omega\Delta}{\theta-\Lambda} + \left(1 - \frac{\Omega\Delta}{\theta-\Lambda}\right)\exp\left[(\Lambda-\theta)\tau\right] \tag{A.8}$$

For $\Lambda = \theta$, (A.2) yields

$$\bar{M}_1 = 1 + \Delta\Omega\tau \tag{A.9}$$

A.2.1.2 Case 2

The governing equations are

$$\frac{d\bar{M}_o}{d\tau} = -\bar{M}_o(\bar{M}_1 + \theta) + \Omega \tag{A.10}$$

$$\frac{d\bar{M}_1}{d\tau} = (\Lambda-\theta)\bar{M}_1 + \Delta\Omega \tag{A.11}$$

Since (A.11) is identical to (A.2), the solutions are given by (A.8) and (A.9). Equation (A.10) for $\bar{M}_0$ is coupled to the solution for $\bar{M}_1$. Dividing (A.10) by (A.11) yields

$$\frac{d\bar{M}_0}{d\bar{M}_1} = -\frac{1}{\Lambda-\theta}\left(\frac{\bar{M}_1+\theta}{\bar{M}_1+\beta}\right)\bar{M}_0 + \frac{\beta/\Delta}{\bar{M}_1+\beta} \tag{A.12}$$

where

$$\beta = \frac{\Omega\Delta}{\Lambda-\theta} \tag{A.13}$$

(A.12) can be solved by use of an integrating factor to yield

$$\bar{M}_0(\tau) = \left(\frac{1+\beta}{\bar{M}_1+\beta}\right)^{\frac{\theta-\beta}{\Lambda-\theta}} \exp\left(\frac{1-\bar{M}_1}{\Lambda-\theta}\right)\left\{1 + \frac{\beta}{\Delta}\int_1^{\bar{M}_1} \frac{\exp\left(\frac{\xi-1}{\Lambda-\theta}\right)}{\xi+\beta}\left(\frac{\xi+\beta}{1+\beta}\right)^{\frac{\theta-\beta}{\Lambda-\theta}} d\xi\right\} \tag{A.14}$$

Equation (A.14) for $\bar{M}_0$ holds only for $\Lambda \neq \theta$. When $\Lambda = \theta$ (which yields $\bar{M}_1$ given by (A.9)), $\bar{M}_0$ is given by

$$\bar{M}_0(\tau) = \exp[-(1+\theta)\tau]\exp\left[-\frac{\Omega\Delta\tau^2}{2}\right]\left\{1 + \Omega\int_0^{\tau} \exp[(1+\theta)\xi]\exp\left[\frac{\Omega\Delta}{2}\xi^2\right] d\xi\right\} \tag{A.15}$$

A.2.1.3 Case 3

The governing equations are

$$\frac{d\bar{M}_0}{d\tau} = -\frac{1}{2}\bar{M}_0^2 - \theta\bar{M}_0 + \Omega \tag{A.16}$$

$$\frac{d\bar{M}_1}{d\tau} = \Lambda\bar{M}_0 - \theta\bar{M}_1 + \Delta\Omega \tag{A.17}$$

The equation for $\bar{M}_0$ is identical to (A.1), and hence the solution is given by (A.6). Since $\bar{M}_1$ is coupled to $\bar{M}_0$ in (A.17), solution is obtained by dividing (A.17) by (A.16) to yield

$$\frac{d\bar{M}_1}{d\bar{M}_0} - \frac{2\theta}{(\bar{M}_0-r_1)(\bar{M}_0-r_2)}\bar{M}_1 = -\frac{2(\Lambda\bar{M}_0+\Delta\Omega)}{(\bar{M}_0-r_1)(\bar{M}_0-r_2)} \tag{A.18}$$

(A.18) can be solved by use of integrating factors to yield

$$\bar{M}_1(\tau) = \left(\frac{\bar{M}_0-r_1}{1-r_1}\frac{1-r_2}{\bar{M}_0-r_2}\right)^{\frac{2\theta}{r_1-r_2}}\left\{1-2\int_1^{\bar{M}_0}\frac{\Lambda\xi+\Delta\Omega}{(\xi-r_1)(\xi-r_2)}\left(\frac{\xi-r_2}{1-r_2}\frac{1-r_1}{\xi-r_1}\right)^{\frac{2\theta}{r_1-r_2}}d\xi\right\} \tag{A.19}$$

A.2.1.4 Case 4

The governing equations are given by

$$\frac{d\bar{M}_0}{d\tau} = -\bar{M}_0(\bar{M}_1+\theta) + \Omega \tag{A.20}$$

$$\frac{d\bar{M}_1}{d\tau} = \Lambda\bar{M}_0 - \theta\bar{M}_1 + \Delta\Omega \tag{A.21}$$

The analytic solutions of (A.20) and (A.21) could not be obtained in the general case. (A.20) and (A.21) were solved numerically.

A.2.2 Category 1: No Coagulation

The governing equation is given by

$$\frac{\partial n}{\partial t} + \frac{\partial}{\partial v}(In) = \frac{S_0}{v^*}\exp\left(-\frac{v}{v^*}\right) - \alpha n \tag{A.22}$$

For the cases of constant and linear condensation mechanisms, (A.22) yields

$$\frac{\partial n}{\partial t} + \sigma_o \frac{\partial n}{\partial v} = \frac{s_o}{v^*} \exp\left(-\frac{v}{v^*}\right) - \alpha n \tag{A.23}$$

and

$$\frac{\partial n}{\partial t} + \sigma_1 v \frac{\partial n}{\partial v} = \frac{s_o}{v^*} \exp\left(-\frac{v}{v^*}\right) - \alpha n - \sigma_1 n \tag{A.24}$$

respectively.

A.2.2.1 Case 1: Constant Condensation

If we define a characteristic condensation time τ and dimensionless ratios of nucleation to condensation Ω and removal to condensation θ as

$$\tau = \frac{\sigma_o}{\nu_o} t \tag{A.25}$$

$$\Omega = \frac{S_o \nu_o}{\sigma_o N_o} \tag{A.26}$$

$$\theta = \frac{\alpha \nu_o}{\sigma_o} \tag{A.27}$$

and further define dimensionless variables and characteristic nucleation volumes as

$$\bar{n} = \frac{n}{N_o/\nu_o} \tag{A.28}$$

$$\bar{v} = \frac{v}{\nu_o} \tag{A.29}$$

$$\Delta = \frac{v^*}{\nu_o} \tag{A.30}$$

Then (A.23) transforms to

$$\frac{\partial \bar{n}}{\partial \tau} + \frac{\partial \bar{n}}{\partial \bar{v}} = \frac{\Omega}{\Delta} \exp\left(-\frac{\bar{v}}{\Delta}\right) - \theta \bar{n} \tag{A.31}$$

If we let

$$\bar{p} = \bar{n} \exp(\theta \bar{v}) \tag{A.32}$$

we obtain

$$\frac{\partial \bar{p}}{\partial \tau} + \frac{\partial \bar{p}}{\partial \bar{v}} = \frac{\Omega}{\Delta} \exp\left(\left(\theta - \frac{1}{\Delta}\right) \bar{v}\right) \tag{A.33}$$

which can be solved by characteristics. If η is our characteristic variable, then (A.33) reduces to the ordinary differential system

$$\frac{\partial \tau}{\partial \eta} = 1 \tag{A.34}$$

$$\frac{\partial \bar{v}}{\partial \eta} = 1 \tag{A.35}$$

$$\frac{\partial \bar{p}}{\partial \eta} = \frac{\Omega}{\Delta} \exp\left[\left(\theta - \frac{1}{\Delta}\right) \bar{v}\right] \tag{A.36}$$

Solution for $\bar{p}$ and transformation back to $\bar{n}$ yields

$$\bar{n}(\bar{v},\tau) = \begin{cases} \left(\frac{\Omega}{\theta\Delta - 1}\right) \exp(-\theta \bar{v}) \left\{ \exp\left[\left(\theta - \frac{1}{\Delta}\right) \bar{v}\right] - 1 \right\} & \text{if } \bar{v} < \tau \quad (A.37) \\ \exp(-\theta\tau)\, \exp(-(\bar{v} - \tau)) + & \\ \left(\frac{\Omega}{\theta\Delta - 1}\right) \exp\left(-\frac{\bar{v}}{\Delta}\right) \left\{ 1 - \exp\left[\left(\frac{1}{\Delta} - \theta\right) \tau\right] \right\} & \text{if } \bar{v} > \tau \quad (A.38) \end{cases}$$

A.2.2.2 Case 2: Linear Condensation

We begin as in case 1, defining τ, Ω, and θ as

$$\tau = \sigma_1 t \tag{A.39}$$

$$\Omega = \frac{S_o}{\sigma_1 N_o} \tag{A.40}$$

$$\theta = \frac{\alpha}{\sigma_1} \tag{A.41}$$

which transforms (A.24) to

$$\frac{\partial \bar{n}}{\partial \tau} + \bar{v} \frac{\partial \bar{n}}{\partial \bar{v}} + (1+\theta)\bar{n} = \frac{\Omega}{\Delta} \exp\left(-\frac{\bar{v}}{\Delta}\right) \tag{A.42}$$

where $\bar{n}$, $\bar{v}$ and Δ are given by (A.28-A.30). If we let

$$\bar{p} = \bar{n} \exp((1+\theta)\tau) \tag{A.43}$$

we obtain

$$\frac{\partial \bar{p}}{\partial \tau} + \bar{v} \frac{\partial \bar{p}}{\partial \bar{v}} = \frac{\Omega}{\Delta} \exp\left(-\frac{\bar{v}}{\Delta}\right) \exp([1+\theta]\tau) \tag{A.44}$$

which can be solved by characteristics. Again, if η is our characteristic variable, then (A.44) reduces to the ordinary differential system

$$\frac{\partial \tau}{\partial \eta} = 1 \tag{A.45}$$

$$\frac{\partial \bar{v}}{\partial \eta} = \bar{v} \tag{A.46}$$

$$\frac{\partial \bar{p}}{\partial \eta} = \frac{\Omega}{\Delta} \exp\left(-\frac{\bar{v}}{\Delta}\right) \exp([1+\theta]\tau) \tag{A.47}$$

Solution for $\bar{p}$ and transformation back to $\bar{n}$ yields

$$\bar{n} = \exp\left(-\bar{v}\exp(-\tau)\right)\exp\left(-(1+\theta)\tau\right) +$$

$$\frac{\Omega\Delta^{\theta}}{\bar{v}^{1+\theta}}\left\{\Gamma\left(1+\theta, \frac{\bar{v}}{\Delta}\exp(-\tau)\right) - \Gamma\left(1+\theta, \frac{\bar{v}}{\Delta}\right)\right\} \tag{A.48}$$

where $\Gamma(a,x)$ is the incomplete gamma function.

A.2.3 Category 2: No Condensation

A.2.3.1 Case 1: Constant Coagulation

For constant coagulation, the governing equation is (from Table 4.4, Chapter 4)

$$\frac{\partial\bar{p}}{\partial\tau} = \frac{1}{2}\bar{p}^2 - (\bar{M}_o+\theta)\,\bar{p} + \frac{\Omega}{\Delta\bar{s}+1} \tag{A.49}$$

which is a Riccati equation. $\bar{M}_o$ is the solution of

$$\frac{d\bar{M}_o}{d\tau} = -\frac{1}{2}\left(\bar{M}_o^2 + 2\theta\bar{M}_o - 2\Omega\right) \tag{A.50}$$

By letting $T = \bar{M}_o$ and defining

$$y = \frac{\bar{p}}{T^2+2\theta T-2\Omega} \tag{A.51}$$

we obtain

$$\frac{\partial y}{\partial T} + y^2 = -\frac{2\Omega}{\Delta\bar{s}+1}\,\frac{1}{(T^2+2\theta T-2\Omega)^2} \tag{A.52}$$

Letting

$$y = \frac{1}{u(T)}\frac{du}{dT} \tag{A.53}$$

$$Z = \ell n \left(\frac{T-r_1}{1-r_1} \frac{1-r_2}{T-r_2} \right)^{\frac{1}{r_1-r_2}} \tag{A.54}$$

where r_1 and r_2 are given by (A.4) and (A.5), and

$$u = \sqrt{T^2+2\theta T-2\Omega}\; w(z) \tag{A.55}$$

we obtain

$$\frac{d^2w}{dz^2} - K^2 w(z) = 0 \tag{A.56}$$

where

$$K = + \sqrt{\frac{(\theta^2+2\Omega)\Delta\bar{s}+\theta^2}{\Delta\bar{s}+1}} \tag{A.57}$$

The solution of which is

$$w(z) = c_1 \exp(Kz) + c_2 \exp(-Kz) \tag{A.58}$$

Transformation to $\bar{p}$ and application of the initial condition

$$\bar{p}(t=0) = \frac{1}{\bar{s}+1} \tag{A.59}$$

yields

$$\bar{p} = \frac{[T+\theta+K]-C[T+\theta-K]\exp(-2Kz)}{1-C\exp(-2Kz)} \tag{A.60}$$

where

$$C = \frac{1-[1+\theta+K][\bar{s}+1]}{1-[1+\theta-K][\bar{s}+1]} \tag{A.61}$$

Due to the complex nature in which K (and hence C) depends on $\bar{s}$, exact inversion of (A.60) appears unlikely. Hence, (A.60) is inverted approximately in the following way. We seek an asymptotic solution for large volumes, and hence small values of $\bar{s}$. Both numerator and denominator

are expanded in Taylor series about $\bar{s} = 0$, retaining terms of $O(\bar{s})$ in the numerator and $O(\bar{s}^2)$ in the denominator. Using primes to denote differentiation with respect to $\bar{s}$, N and D to denote numerator and denominator, respectively, (A.60) can be written as

$$\bar{p} = \frac{N(\bar{s})}{D(\bar{s})} \approx \frac{N(0)+N'(0)\bar{s}}{D(0)+D'(0)\bar{s}+\frac{D''(0)}{2}\bar{s}^2} \tag{A.62}$$

If we let

$$a = \frac{N(0)}{N'(0)} \tag{A.63}$$

$$b = \frac{D'(0)}{D''(0)} + \sqrt{\left(\frac{D'(0)}{D''(0)}\right)^2 - \frac{2D(0)}{D''(0)}} \tag{A.64}$$

$$c = \frac{D'(0)}{D''(0)} - \sqrt{\left(\frac{D'(0)}{D''(0)}\right)^2 - \frac{2D(0)}{D''(0)}} \tag{A.65}$$

Then (A.62) can be inverted (Roberts and Kaufman, 1966) to yield

$$\bar{n} = \frac{2N'(0)}{D''(0)} \frac{1}{b-c} \left[(b-a)\exp(-b\bar{v})-(c-a)\exp(-c\bar{v})\right] \tag{A.66}$$

Setting $\theta = 0$ does not simplify the solution or the inversion, and therefore no further discussion is necessary. However, if $\Omega = 0$, (A.52) reduces to

$$\frac{\partial y}{\partial \bar{T}} + y^2 = 0 \tag{A.67}$$

which can be solved directly. Transformation to $\bar{p}$ and application of initial condition yields

$$\bar{p} = \frac{T^2+2\theta T}{1+2\theta} \quad \frac{1}{\left(\frac{T-1}{1+2\theta}\right) + \bar{s}+1} \tag{A.68}$$

which upon inversion produces

$$\bar{n} = \left(\frac{T+2\theta}{1+2\theta}\right) T \exp\left[-\left(\frac{T+2\theta}{1+2\theta}\right)\bar{v}\right] \tag{A.69}$$

If both θ and Ω are zero, (A.69) reduces to

$$\bar{n} = T^2 \exp(-T\bar{v}) \tag{A.70}$$

which is identical to the solution obtained by Scott (1968).

A.2.3.2 Case 2: Linear Coagulation

For linear coagulation, the governing equation is (from Table 4.4, Chapter 4)

$$\frac{\partial \bar{p}}{\partial \tau} + (\bar{p} - \bar{M}_0)\frac{\partial \bar{p}}{\partial \bar{s}} = -(\bar{M}_1 + \theta)\bar{p} + \frac{\Omega}{\Delta \bar{s}+1} \tag{A.71}$$

$\bar{M}_0$ and $\bar{M}_1$ are the solutions of

$$\frac{d\bar{M}_0}{d\tau} = -\bar{M}_0(\bar{M}_1 + \theta) + \Omega \tag{A.72}$$

and

$$\frac{d\bar{M}_1}{d\tau} = -\theta\bar{M}_1 + \Delta\Omega \tag{A.73}$$

If we define

$$T = \frac{\bar{M}_1 - a}{1-a} \tag{A.74}$$

where $a = \Delta\Omega/\theta$, and apply the change of variable

$$y = \frac{\bar{p}\ \exp\left(-\frac{1-a}{\theta}\,T\right)}{T^{1+a/\theta}} \tag{A.75}$$

we obtain

$$\frac{\partial y}{\partial \bar{T}} - \frac{1}{\theta\bar{T}}\left(y - \frac{\bar{M}_o(T)\exp\left(-\frac{1-a}{\theta}\,T\right)}{T^{1+a/\theta}}\right)\exp\left(\frac{1-a}{\theta}\,T\right)T^{1+a/\theta}\,\frac{\partial y}{\partial \bar{s}} =$$

$$-\frac{\Omega}{\theta\bar{T}}\ \frac{1}{\Delta\bar{s}+1}\ \ \frac{\exp\left(-\frac{1-a}{\theta}\,T\right)}{T^{1+a/\theta}} \tag{A.76}$$

which can, in principle, be solved by the method of characteristics. The system of ODE's produced is

$$\frac{\partial T}{\partial \eta} = 1 \tag{A.77}$$

$$\frac{\partial \bar{s}}{\partial \eta} = -\frac{1}{\theta\bar{T}}\exp\left(\frac{1-a}{\theta}\,T\right)T^{1+a/\theta}\left(y - \frac{\bar{M}_o(T)\ \exp\left(-\frac{1-a}{\theta}\,T\right)}{T^{1+a/\theta}}\right) \tag{A.78}$$

$$\frac{\partial y}{\partial \eta} = -\frac{\Omega}{\theta\bar{T}}\ \frac{1}{\Delta\bar{s}+1}\ \ \frac{\exp\left(-\frac{1-a}{\theta}\,T\right)}{T^{1+a/\theta}} \tag{A.79}$$

As can be seen, this system is highly non-linear and coupled. One approach is to realize that by (A.77) derivatives with respect to η are the same as derivatives with respect to T. Hence differentiating (A.78) once again with respect to T and eliminating y and its derivatives yields

$$\frac{\partial^2 \bar{s}}{\partial \bar{T}^2} - \left(\frac{1-a}{\theta} + \frac{a/\theta}{T}\right)\frac{\partial \bar{s}}{\partial \bar{T}} + \frac{\Omega}{(\theta\bar{T})^2}\ \frac{\Delta\bar{s}}{\Delta\bar{s}+1} = 0 \tag{A.80}$$

Even though we have succeeded in uncoupling the equations and considerably simplifying the system, (A.80) does not appear to be soluble analytically.

Setting $\theta = 0$ does not simplify the system appreciably, but if $\Omega = 0$, the governing equation is

$$\frac{\partial \bar{p}}{\partial \tau} + (\bar{M}_1 + \theta)\bar{p} + (\bar{p} - \bar{M}_0)\frac{\partial \bar{p}}{\partial \bar{s}} = 0 \tag{A.81}$$

If we let $T = \bar{M}_1$ and

$$y = \frac{1}{T} \exp\left(-\frac{(T-1)}{\theta}\right)\bar{p} \tag{A.82}$$

The governing equation becomes

$$\frac{\partial y}{\partial T} + \frac{1-y}{\theta} \exp\left(\frac{T-1}{\theta}\right)\frac{\partial y}{\partial \bar{s}} = 0 \tag{A.83}$$

which, by characteristics, transforms to

$$\frac{\partial T}{\partial \eta} = 1 \tag{A.84}$$

$$\frac{\partial \bar{s}}{\partial \eta} = \frac{1-y}{\theta} \exp\left(\frac{T-1}{\theta}\right) \tag{A.85}$$

$$\frac{\partial y}{\partial \eta} = 0 \tag{A.86}$$

the solution of which (in terms of $\bar{p}$) is

$$\bar{p} = \frac{2T \exp\left(\frac{T-1}{\theta}\right)}{\bar{s}+1+g(T)+\sqrt{(\bar{s}+1+g(T))^2-4g(T)}} \tag{A.87}$$

Here, $g(T) = 1 - \exp((T-1)/\theta)$, and we have selected the physically realistic positive square root in the denominator.

Inversion of (A.87) yields

$$\bar{n} = \frac{T \exp\left(\frac{T-1}{\theta}\right)}{\sqrt{g}\,\bar{v}} \exp\left[-(1+g)\bar{v}\right] I_1(2\sqrt{g}\,\bar{v}) \tag{A.88}$$

The function g is given by the expression below (A.87), and $I_1(x)$ is the modified bessel function of the first kind.

If both Ω and θ are zero, the solution must be rederived from (A.81). The starting equation is

$$\frac{\partial \bar{p}}{\partial t} + \bar{M}_1 \bar{p} + (\bar{p} - \bar{M}_o) \frac{\partial \bar{p}}{\partial \bar{s}} = 0 \tag{A.89}$$

If we let

$$T = 1 - \bar{M}_o \tag{A.90}$$

$$Y = \bar{p}/(T-1) \tag{A.91}$$

Then (A.89) reduces to

$$\frac{\partial y}{\partial T} - (1+y) \frac{\partial y}{\partial \bar{s}} = 0 \tag{A.92}$$

By characteristics, we have

$$\frac{\partial T}{\partial \eta} = 1 \tag{A.93}$$

$$\frac{\partial \bar{s}}{\partial \eta} = -(1 + y) \tag{A.94}$$

$$\frac{\partial y}{\partial \eta} = 0 \tag{A.95}$$

The solution of which (in terms of $\bar{p}$) is

$$\bar{p} = \frac{2(1-T)}{(\bar{s}+T+1)+\sqrt{(\bar{s}+T+1)^2-4T}} \tag{A.96}$$

Again, we have selected the physically realistic positive square root. Inversion yields

$$\bar{n} = \frac{1-T}{\sqrt{T}} \frac{1}{\bar{v}} \exp\left(-(1+T)\bar{v}\right) I_1(2\sqrt{T}\,\bar{v}) \tag{A.97}$$

which is identical to the results of Scott (1968).

A.2.4 Category 3

A.2.4.1 Case 1: Constant Coagulation, Linear Condensation

The governing equations are

$$\frac{\partial \bar{p}}{\partial \tau} + (\bar{M}_o+\theta)\bar{p} - \Lambda\bar{s}\,\frac{\partial \bar{p}}{\partial \bar{s}} = \frac{1}{2}\,\bar{p}^2 + \frac{\Omega}{\Delta\bar{s}+1} \tag{A.98}$$

$$\frac{d\bar{M}_o}{d\tau} = -\frac{1}{2}\,\bar{M}_o^2 - \theta\bar{M}_o + \Omega \tag{A.99}$$

$$\frac{d\bar{M}_1}{d\tau} = (\Lambda-\theta)\bar{M}_1 + \Delta\Omega \tag{A.100}$$

If we let $T = \bar{M}_o$, and

$$y = \frac{\bar{p}}{T^2+2\theta T-2\Omega} \tag{A.101}$$

we obtain

$$\frac{\partial y}{\partial T} + \frac{2\Lambda\bar{s}}{(T-r_1)(T-r_2)}\,\frac{\partial y}{\partial \bar{s}} = -y^2 - \frac{2\Omega}{\Delta\bar{s}+1}\,\frac{1}{(T-r_1)^2(T-r_2)^2} \tag{A.102}$$

where r_1 and r_2 are given by (A.4) and (A.5). By characteristics, we get

$$\frac{\partial T}{\partial \eta} = 1 \tag{A.103}$$

$$\frac{\partial \bar{s}}{\partial \eta} = \frac{2\Lambda \bar{s}}{(\bar{T}-r_1)(\bar{T}-r_2)} \tag{A.104}$$

$$\frac{\partial y}{\partial \eta} = -y^2 - \frac{2\Omega}{\Delta \bar{s}+1} \frac{1}{(\bar{T}-r_1)^2(\bar{T}-r_2)^2} \tag{A.105}$$

Equations (A.103) and (A.104) can be solved to yield

$$\bar{s} = \bar{s}_o \left(\frac{\bar{T}-r_1}{\bar{T}_o-r_1} \frac{\bar{T}_o-r_2}{\bar{T}-r_2} \right)^{\frac{2\Lambda}{r_1-r_2}} \tag{A.106}$$

which when substituted into (A.105) yields

$$\frac{\partial y}{\partial \bar{T}} + y^2 = \frac{-2\Omega}{(\bar{T}-r_1)^2(\bar{T}-r_2)^2 \left[1+\Delta \bar{s}_o \left(\frac{\bar{T}-r_1}{\bar{T}_o-r_1} \frac{\bar{T}_o-r_2}{\bar{T}-r_2} \right)^{\frac{2\Lambda}{r_1-r_2}} \right]} \tag{A.107}$$

Although (A.107) is a Riccati equation, the complex term on the right hand side makes analytic solution unlikely.

If $\Omega = 0$, (A.107) reduces to

$$\frac{\partial y}{\partial \bar{T}} + y^2 = 0 \tag{A.108}$$

which when solved and combined with (A.106) for $\Omega = 0$ yields (in terms of the transformed variable $\bar{p}$)

$$\bar{p} = \frac{\bar{T}^2+2\theta\bar{T}}{1+2\theta} \frac{1}{\left(\frac{1}{\bar{T}} \frac{\bar{T}+2\theta}{1+2\theta} \right)^{\Lambda/\theta}} \cdot \left[\bar{s} + \frac{\left(1 + \frac{\bar{T}-1}{1+2\theta} \right)}{\left(\frac{1}{\bar{T}} \frac{\bar{T}+2\theta}{1+2\theta} \right)^{\Lambda/\theta}} \right]^{-1} \tag{A.109}$$

which upon inversion yields:

$$\bar{n} = \frac{T^2+2\theta T}{1+2\theta}\left(\frac{1+2\theta}{T+2\theta}\,T\right)^{\Lambda/\theta}\exp\left[-\left(\frac{T+2\theta}{1+2\theta}\right)\left(\frac{1+2\theta}{T+2\theta}\,T\right)^{\Lambda/\theta}\bar{v}\right] \tag{A.110}$$

If $\theta = 0$ but $\Omega \neq 0$, the Riccati equation (A.107) is once again obtained. The only simplification is that $r_1 = \sqrt{2\Omega}$ and $r_2 = -\sqrt{2\Omega}$ (see (A.4) and (A.5)), and hence appears insoluble.

If $\theta = \Omega = 0$, (A.104) and (A.105) reduce to

$$\frac{\partial \bar{s}}{\partial \eta} = \frac{2\Lambda \bar{s}}{T^2} \tag{A.111}$$

$$\frac{\partial y}{\partial \eta} = -\,y^2 \tag{A.112}$$

which, with (A.103) yields (in terms of $\bar{p}$)

$$\bar{p} = \frac{T^2 \exp\left[2\Lambda\left(\frac{T-1}{T}\right)\right]}{\bar{s}+T\,\exp\left[2\Lambda\left(\frac{T-1}{T}\right)\right]} \tag{A.113}$$

Inversion yields

$$\bar{n} = T^2\,\exp\left(2\Lambda\left(\frac{T-1}{T}\right)\right)\exp\left(-\,T\exp\left(2\Lambda\left(\frac{T-1}{T}\right)\right)\bar{v}\right) \tag{A.114}$$

A.2.4.2 Case 2: Linear coagulation, Linear condensation

The governing equations are

$$\frac{\partial \bar{p}}{\partial \bar{\tau}} + (\bar{M}_1+\theta)\bar{p} + (\bar{p}-\bar{M}_0-\Lambda\bar{s})\,\frac{\partial \bar{p}}{\partial \bar{s}} = \frac{\Omega}{\Delta\bar{s}+1} \tag{A.115}$$

$$\frac{d\bar{M}_0}{d\tau} = -\,\bar{M}_0(\bar{M}_1+\theta) + \Omega \tag{A.116}$$

$$\frac{dM_1}{d\tau} = (\Lambda-\theta)\bar{M}_1 + \Delta\Omega \tag{A.117}$$

If we let $T = \bar{M}_1$, and perform the change of variables

$$y = h(T)\,\bar{p} \tag{A.118}$$

$$h(T) = \left(\frac{T+\beta}{1+\beta}\right)^{\frac{\theta-\beta}{\Lambda-\beta}} \exp\left(\frac{T-1}{\Lambda-\theta}\right) \tag{A.119}$$

where $\beta = \Delta\Omega/(\Lambda-\theta)$, then we obtain

$$\frac{\partial y}{\partial T} + \frac{1}{\Lambda-\theta}\,\frac{1}{T+\beta}\,\frac{1}{h(T)}\,(y-h(T)(\bar{M}_0(T) + \Lambda\bar{s}))\,\frac{\partial y}{\partial \bar{s}} =$$

$$\frac{\Omega}{\Lambda-\theta}\,\frac{1}{\Delta\bar{s}+1}\,\frac{h(T)}{T+\beta} \tag{A.120}$$

The ordinary differential system which results from application of the method of characteristics is analytically insoluble, as is the case when $\theta = 0$. However, if $\Omega = 0$ (and therefore $\beta = 0$) (A.120) reduces to

$$\frac{\partial y}{\partial T} + \frac{1}{\Lambda-\theta}\,\frac{1}{Th(T)}\,(y-h(T)(\bar{M}_0(T) + \Lambda\bar{s}))\,\frac{\partial y}{\partial \bar{s}} = 0 \tag{A.121}$$

where

$$h(T) = T^{\frac{\theta}{\Lambda-\theta}} \exp\left(\frac{T-1}{\Lambda-\theta}\right) \tag{A.122}$$

and, from (A.116)

$$\bar{M}_0(T) = h^{-1}(T) \tag{A.123}$$

The characteristic equations are

$$\frac{\partial T}{\partial \eta} = 1 \tag{A.124}$$

$$\frac{\partial \bar{s}}{\partial \eta} = \frac{1}{\Lambda-\theta}\,\frac{1}{Th(T)}\,[y-1-\Lambda h(T)\bar{s}] \tag{A.125}$$

$$\frac{\partial y}{\partial \eta} = 0 \tag{A.126}$$

The solution of the system (for $T_o = 1$) is (in terms of $\bar{p}$)

$$\bar{p} = \frac{T}{2\left(\exp\left(\frac{T-1}{\Lambda-\theta}\right)-1\right)}\left[\bar{s} + \frac{2-\exp\left(\frac{T-1}{\theta-\Lambda}\right)}{T^{\frac{\Lambda}{\Lambda-\theta}}} - \sqrt{\left(\bar{s} + \frac{2-\exp\left(\frac{T-1}{\theta-\Lambda}\right)}{T^{\frac{\Lambda}{\Lambda-\theta}}}\right)^2 - \left(\frac{2\sqrt{1-\exp\left(\frac{T-1}{\theta-\Lambda}\right)}}{T^{\frac{\Lambda}{\Lambda-\theta}}}\right)^2}\right] \tag{A.127}$$

which, when inverted, yields

$$\bar{n} = \frac{\exp\left(-\frac{1}{T^{\frac{\Lambda}{\Lambda-\theta}}}\left(2-\exp\left(\frac{T-1}{\theta-\Lambda}\right)\right)\bar{v}\right)}{T^{\frac{\theta}{\Lambda-\theta}}\exp\left(\frac{T-1}{\Lambda-\theta}\right)\sqrt{1-\exp\left(\frac{T-1}{\theta-\Lambda}\right)}}\,\frac{1}{\bar{v}}\,I_1\left(\frac{2\sqrt{1-\exp\left(\frac{T-1}{\theta-\Lambda}\right)}}{T^{\frac{\Lambda}{\Lambda-\theta}}}\bar{v}\right) \tag{A.128}$$

Finally, if both $\Omega = \theta = 0$, (A.128) reduces to

$$\bar{n} = \frac{\exp\left(-\frac{1}{T}\left(2-\exp\left(-\left(\frac{T-1}{\Lambda}\right)\right)\right)\bar{v}\right)}{\exp\left(\frac{T-1}{\Lambda}\right)\sqrt{1-\exp\left(-\left(\frac{T-1}{\Lambda}\right)\right)}}\,\frac{1}{\bar{v}}\,I_1\left(\frac{2}{T}\sqrt{1-\exp\left(-\left(\frac{T-1}{\Lambda}\right)\right)}\,\bar{v}\right) \tag{A.129}$$

A.2.4.3 Case 3: Constant coagulation, constant condensation

The governing equations are

$$\frac{\partial \bar{p}}{\partial \tau} = \frac{1}{2}\bar{p}^2 - (\bar{M}_o + \theta + \Lambda\bar{s})\bar{p} + \frac{\Omega}{\Delta\bar{s}+1} \tag{A.130}$$

$$\frac{d\bar{M}_o}{d\tau} = -\frac{1}{2}(\bar{M}_o^2 + 2\theta\bar{M}_o - 2\Omega) \tag{A.131}$$

As can be seen, (A.130) is an ordinary differential equation of the Riccati type. If we choose $T = \bar{M}_o$, and perform the variable transformation,

$$y = \bar{p}\, h(T) \tag{A.132}$$

$$h(T) = \left(\frac{1+2\theta-2\Omega}{T^2+2\theta T-2\Omega}\right)\left(\frac{T-r_2}{1-r_2}\,\frac{1-r_1}{T-r_1}\right)^{\frac{2\Lambda\bar{s}}{r_1-r_2}} \tag{A.133}$$

where r_1 and r_2 are given by (A.4) and (A.5), (A.130) transforms to the Riccati equation of the form

$$\frac{\partial y}{\partial T} + Q(T)y^2 = R(T) \tag{A.134}$$

where

$$Q(T) = \frac{1}{(1-r_1)(1-r_2)}\left[\frac{T-r_1}{1-r_1}\,\frac{1-r_2}{T-r_2}\right]^{\frac{2\Lambda\bar{s}}{r_1-r_2}} \tag{A.135}$$

$$R(T) = -\frac{2\Omega}{\Delta\bar{s}+1}\,\frac{(1-r_1)(1-r_2)}{(T-r_1)^2(T-r_2)^2}\left[\frac{T-r_2}{1-r_2}\,\frac{1-r_1}{T-r_1}\right]^{\frac{2\Lambda\bar{s}}{r_1-r_2}} \tag{A.136}$$

By the change of variable

$$y = \frac{1}{Q(T)} \frac{d}{dT} \ell n\, u(T) = \frac{1}{Q(T)} \frac{u'(T)}{u(T)} \tag{A.137}$$

we obtain the second order equation

$$u'' - \frac{2\Lambda\bar{s}}{(T-r_1)(T-r_2)} u' + \frac{2\Omega}{\Delta\bar{s}+1} \frac{1}{(T-r_1)^2(T-r_2)^2} u = 0 \tag{A.138}$$

By defining the new independent variable

$$\eta = \frac{T-r_1}{r_2-r_1} \tag{A.139}$$

and the dimensionless parameters

$$a_1 = \frac{\Lambda\bar{s}}{\sqrt{\theta^2+2\Omega}} \tag{A.140}$$

$$a_2 = \frac{\Omega}{2(\Delta\bar{s}+1)} \frac{1}{(\theta^2+2\Omega)} \tag{A.141}$$

and allowing over-dots to define derivatives with respect to η, we get

$$\eta^2(\eta-1)^2\ddot{u} + a_1\eta(\eta-1)\dot{u} + a_2 u = 0 \tag{A.142}$$

If we now perform the change of variables

$$u(\eta) = \eta^r(\eta-1)^s w(\eta) \tag{A.143}$$

where r and s are the roots of

$$r(r-1) - a_1 r + a_2 = 0 \tag{A.144}$$

$$s(s-1) + a_1 s + a_2 = 0 \tag{A.145}$$

we transform (A.142) to

$$\eta(1-\eta)\ddot{w} + \{(2r-a_1)-2(r+s)\eta\}\dot{w} - (r+s)(r+s-1)w = 0 \qquad (A.146)$$

which is precisely the hypergeometric differential equation, the general solution of which can be written as

$$w(\eta) = C_1 F(a,b;c;\eta) + C_2 \eta^{1-c}(1-\eta)^{c-a-b} F(1-a,1-b;2-c;\eta) \qquad (A.147)$$

where C_1 and C_2 are arbitrary constants, and

$$a = r + s \qquad (A.148)$$

$$b = r + s - 1 \qquad (A.149)$$

$$c = 2r - a_1 \qquad (A.150)$$

Transformation to $\bar{p}$ yields

$$\bar{p} = (r_1-r_2)\eta(1-\eta)\left\{\frac{r}{\eta} + \frac{s}{\eta-1} + \right.$$

$$\frac{ab}{c} F(a+1,b+1;c+1;\eta) + C_1\eta^{1-c}(1-\eta)^{c-a-b} \cdot$$

$$\left[\frac{(1-a)(1-b)}{(2-c)} F(2-a,2-b;3-c;\eta) + \left(\frac{1-c}{\eta} + \frac{c-a-b}{1-\eta}\right) \cdot \right.$$

$$\left.\left.F(1-a,1-b;2-c;\eta)\right]\right\} \Big/ \left\{F(a,b;c;\eta) + \right.$$

$$\left. C_1\eta^{1-c}(1-\eta)^{c-a-b} F(1-a,1-b;2-c;\eta)\right\} \qquad (A.151)$$

Application of the initial condition yields C_1, but analytic inversion seems impossible. Approximate inversion by asymptotic techniques also presents a formidable task, due to the necessity to successively differentiate

and evaluate the hypergeometric functions F. Assuming $\theta = 0$ does little to simplify the situation. However, if $\Omega = 0$, R(T) (A.136) becomes = 0, and (A.134) can be solved directly to yield

$$\bar{p} = \frac{(T^2+2\theta T)}{(1+2\theta)} \left(T\frac{1+2\theta}{T+2\theta}\right)^{\Lambda\bar{s}/\theta} \frac{1}{\bar{s}+1+F(T)} \tag{A.152}$$

where

$$F(T) = \int_1^T \left(\frac{\xi}{\xi+2\theta}\right)^{\Lambda\bar{s}/\theta} d\xi \tag{A.153}$$

We now seek to invert (A.152) by some approximate technique. If we arrange (A.152) into the form

$$\bar{p} = (T^2+2\theta T) \frac{N(\bar{s})}{D(\bar{s})} \tag{A.154}$$

where

$$N(\bar{s}) = \exp(g(T)\bar{s}) \tag{A.155}$$

$$D(\bar{s}) = (1+2\theta)(\bar{s}+1) + \int_1^T \exp\,(g(\xi)\bar{s})\, d\xi \tag{A.156}$$

$$g(T) = \frac{\Lambda}{\theta} \ell n \left(T\,\frac{1+2\theta}{T+2\theta}\right) \tag{A.157}$$

we can approximate $\bar{p}$ for small $\bar{s}$ as

$$\bar{p} \simeq \frac{[T^2+2\theta T]N(\bar{s})}{D(0)+D'(0)\bar{s} + \frac{D''(0)}{2}\bar{s}^2} \tag{A.158}$$

where

$$D(0) = T + 2\theta \tag{A.159}$$

$$D'(0) = 1 + 2\theta + \int_1^T g(\xi)\, d\xi \tag{A.160}$$

$$D''(0) = \int_1^T g^2(\xi)\, d\xi \tag{A.161}$$

$$D^{(n)}(0) = \int_1^T g^n(\xi)\, d\xi \qquad n \geq 2 \tag{A.162}$$

Inversion of (A.158) yields

$$\bar{n} \simeq \frac{T^2+2\theta T}{D''(0)} \; \frac{U(\bar{v}-\gamma(T))}{\beta}$$

$$\left\{\exp[(\alpha+\beta)(\bar{v}-\gamma(T))] - \exp[(\alpha-\beta)(\bar{v}-\gamma(T))]\right\} \tag{A.163}$$

where

$$\alpha = - D'(0)/D''(0) \tag{A.164}$$

$$\beta = \sqrt{(D'(0)/D''(0))^2 - 2D(0)/D''(0)} \tag{A.165}$$

$$\gamma(T) = \frac{\Lambda}{\theta} \ell n \left(\frac{T+2\theta}{T(1+2\theta)}\right) \tag{A.166}$$

$$D(0) = T + 2\theta \tag{A.167}$$

$$D'(0) = 1 + 2\theta + \frac{\Lambda}{\theta}\left\{T\ell nT - (T+2\theta)\, \ell n \left(\frac{T+2\theta}{1+2\theta}\right)\right\} \tag{A.168}$$

$$D''(0) = \left(\frac{\Lambda}{\theta}\right)^2\left\{T\ell nT[\ell nT-2] + (T+2\theta)\ell n \left(\frac{T+2\theta}{1+2\theta}\right)\left[\ell n \left(\frac{T+2\theta}{1+2\theta}\right) - 2\right] + 4(T-1) - 2\int_1^T \ell n(\xi)\, \ell n \left(\frac{\xi+2\theta}{1+2\theta}\right) d\xi\right\} \tag{A.169}$$

and $U(\cdot)$ is the unit step function.

Finally, the case where $\theta = \Omega = 0$ can be obtained either by taking the limit of (A.158) as $\theta \to 0$ (which requires applications of L' Hopital's rule) or by returning to the original equation (A.130). Either way, $\bar{p}$ is given by

$$\bar{p} \simeq \frac{T^2 \exp\left(- 2\Lambda\bar{s} \left(\frac{1-T}{T}\right)\right)}{[1+2\Lambda(T-1-\ell nT)]} \qquad \frac{1}{\bar{s} + \frac{1}{T}\frac{}{1+2\Lambda(T-1-\ell nT)}} \tag{A.170}$$

which upon inversion yields:

$$\bar{n} \simeq \frac{T^2 U\left(\bar{v}-2\Lambda\left(\frac{1-T}{T}\right)\right)}{1-2\Lambda(1-T+\ell nT)} \exp\left(- \frac{T\left(\bar{v}-2\Lambda\left(\frac{1-T}{T}\right)\right)}{1-2\Lambda(1-T+\ell nT)} \right) \tag{A.171}$$

where $U(\cdot)$ is the unit step function.

CHAPTER V
GROWTH OF AN
AEROSOL PARTICLE
BY
HETEROGENEOUS CONDENSATION AND CHEMICAL REACTION

INTRODUCTION

In this chapter we initiate a study of the detailed chemistry and physics of individual particles in the urban atmosphere. The overall object of the chapter is to develop a general framework for describing simultaneous chemical reaction and growth of multicomponent atmospheric aerosols. The general framework is then used to simulate secondary sulfate formation in aerosol droplets.

As discussed previously, particulate pollutants may be classed as primary or secondary, depending on whether they result from direct emission or chemical transformation of primary gaseous pollutants. Secondary aerosol constituents can be further divided into two classes, depending on their mechanism of transfer from gaseous to particulate phases. Homogeneous nucleation refers to any process by which a new particle is formed directly from vapor molecules. Depending on whether the initial cluster contains one or more chemical species, the process is referred to as homomolecular or heteromolecular homogeneous nucleation. If, on the other hand, the transfer of secondary species from gaseous to particulate phases occurs by diffusion of vapor molecules to an existing particle, the process is known as condensation. Again depending on whether the condensable vapor involves one or more species, the process is referred to homomolecular or heteromolecular condensation. The division between nucleation and condensation may be considered to be at the particle size corresponding to a stable growing embryo.

In this chapter we restrict our attention to particle growth by condensation. Thus, we begin with a collection of thermodynamically stable particles which may grow and change composition in response to gas- or aerosol-phase processes.

A full description of the processes by which vapor molecules transfer from the gas to particulate phase can be divided into three steps:

(1) Transport from the bulk (gas) phase to the particle surface (Section A)

(2) Transport across the gas-liquid interface (Section B)

(3) Transport and chemical reaction within the liquid phase (Section C)

Each of these steps is considered in the indicated section. Again, the primary object is to develop a general framework for describing the gas-to-particle conversion process.

A. Transport of Vapor Molecules from the Bulk Phase to the Particle Surface

The Continuum Regime

The rates of transfer of vapor molecules and energy to or from a droplet in the continuum regime* are governed by the continuum mass and energy conservation equations (Bird et al., 1960). It is generally assumed that steady state conditions prevail, that is, the time scales for heat and mass transfer to the particle are small when compared to those for changes in ambient conditions. This assumption is entirely valid for typical atmospheric conditions because, as we shall see later, characteristic diffusion times are the order of seconds or less.

The solutions of the steady state mass and energy conservation equations are

*The continuum regime is defined by the region where the Knudsen number $Kn \ll 1$. The Knudsen number is defined as $Kn = \lambda/r$ where λ is the mean fee path of the background gas, and r is a characteristic body length (e.g. particle radius).

$$\phi_i = \frac{4\pi r D_i}{RT_\infty} \left(p_{\infty_i} - p_{s_i}\right) \tag{5.1}$$

$$\psi = 4\pi k r \left(T_\infty - T_s\right) = \sum_i L_i' \phi_i \tag{5.2}$$

where

r = droplet radius, cm

D_i = diffusivity of species i through air, cm^2/sec

R = universal gas constant, cm^3 atm/mole ^oK

T_∞ = ambient temperature, ^oK

T_s = surface temperature, ^oK

p_{∞_i} = ambient pressure of species i, atm.

p_{s_i} = surface pressure of species i, atm.

k = gas conductivity, cal./cm sec ^oK

L_i' = heat of condensation/absorption of species i onto multicomponent droplet, cal/mole

ϕ_i = mass transfer rate, moles/sec

ψ = heat transfer rate, cal/second

The determination of the surface pressure p_{s_i} will be discussed in the next section. At this time it suffices to say that, in addition to a dependence on temperature (which is discussed below), p_{s_i} depends upon the droplet radius and the droplet composition of species i.

Also inherent in this formulation is the assumption that the diffusional processes of all species are independent. Since, in atmospheric applications, all transferring species are present in parts-per-million (ppm) concentrations, this assumption is quite reasonable. Thus, the diffusion coefficient D_i is that for species i in air, and all Stefan flow effects are negligible.

The temperature dependence of p_{s_i} enters via the Clausius-Clapeyron equation, which describes the temperature dependence of the saturation vapor pressure of a pure component above a flat surface as

$$p_{i_{sat}}(T_2) = p_{i_{sat}}(T_1) \exp\left(\frac{L_i}{RT_1T_2}(T_1-T_2)\right) \tag{5.3}$$

where

$p_{i_{sat}}$ = saturation vapor pressure at a given temperature, atm.

L_i = heat of condensation of species i over pure i, cal/mole

It will now be shown in a brief calculation that for general atmospheric conditions, the effects of temperature gradients can be neglected.

From eqs. (5.2) and (5.1)

$$(T_\infty - T_s) = \sum_i \frac{L_i'}{RT_\infty}\left(\frac{D_i}{k}\right)(p_{\infty_i} - p_{s_i}) \tag{5.4}$$

We seek to approximate the terms in (5.4) in order to estimate $T_\infty - T_s$.

If we assume as an <u>upper limit</u> on the pressure gradient:

$p_{\infty_i} - p_{s_i}$ = 10-100 ppm

L_i' = 10^4 cal/mole

D_i = 1 cm^2/sec

R = 1.987 cal/mole ^oK = 0.0821 liter atm/mole ^oK

k = 60×10^{-6} cal/cm sec ^oK

T_∞ = 298^oK

then

$$T_\infty - T_s = O(0.1\text{-}1.0)\ ^oK \tag{5.5}$$

A pressure gradient of 10-100 ppm is several orders of magnitude too high for all atmospheric pollutants, and is reasonable only for water vapor. It is quite evident that temperature differences can safely be neglected*.

If $\bar{v}_i$ is the molar volume (liter/mole) of species i in the liquid phase, and V is the particle volume, then the particle growth rate can be written as

$$\frac{dV}{dt} = \sum_i \bar{v}_i \frac{dm_i}{dt} = \sum_i \frac{4\pi r}{R\bar{T}_\infty} \bar{v}_i D_i (p_{\infty_i} - p_{s_i}) \tag{5.6}$$

Equation (5.6) adequately describes the growth of a spherical particle caused by diffusing pollutants and water vapor, provided the equations of continuum mechanics are valid. Such is not always the case in problems in aerosol physics.

Under normal ambient conditions, the mean free path of air is λ = 0.065 μm, and particle radii in an atmospheric aerosol can range from r = 0.001 - 1.0 μm or greater. Hence, for this range of particle sizes, the range of values of Kn is 0.06 to 65.

For Kn<<1, the continuum approach as given by Eq. (5.6) is valid. However, for Kn>>1, an approach based on gas kinetic theory can be taken, and for Kn=O(1) a suitable "transition regime" model must be employed.

*Heisler (1976) has also shown temperature effects to be negligible by a method that does not require an assumption for the pressure gradient. His results show that neglecting temperature gradients gives rise to errors of less than 0.1 percent.

First, the free molecular (or gas kinetic) regime will be discussed briefly, and then a rather detailed examination of this so-called "transition regime" will be taken.

The Free Molecule Regime

The rate of transfer of vapor molecules to a sphere in the free molecule regime is obtained as follows. Assuming a Maxwellian distribution for the velocities of the diffusing species, the radially directed flux is obtained by integration of the product of the molecular probability density distribution and radial velocity over all radial components of the velocity. Assuming evaporation and condensation accommodation coefficients of unity, the result is

$$\phi_i = \pi r^2 \bar{u}_i (n_- - n_+)/N_A \tag{5.7}$$

where $\bar{u}_i$ is the average velocity of vapor molecules of species i, N_A is Avogadro's number, and n_- and n_+ are the number concentrations (molecules/cm^3) of the inwardly and outwardly directed molecules, respectively.

The Transition Regime

While the continuum and free molecular approaches are valid for Kn<<1 and Kn>>1, respectively, neither equation adequately describes the growth process in the transition regime (Kn=O(1)). If we define ϕ_c and ϕ_{fm} as the rates of transfer (moles/sec.) to a sphere for the continuum and free molecular regimes respectively, then from Eqs. (5.1) and (5.7) for a single specie, we have

$$\phi_c = \frac{4\pi r D}{RT_\infty} (p_\infty - p_s) \tag{5.8}$$

$$\phi_{fm} = \frac{\pi r^2 \bar{v}}{RT_\infty} (p_- - p_+) \tag{5.9}$$

An early approach to condensation in the transition regime is the flux matching method of Fuchs (1959), the most general form of which is referred to as the boundary sphere method. The supposition inherent in the theory is that the continuum description is valid everywhere except in a region immediately surrounding the particle, wherein the free molecular theory must be employed. By defining a boundary layer thickness Δ, the flux predicted by the continuum theory to the boundary sphere is equated to the flux predicted by the free molecular theory through the boundary sphere to the particle surface. Thus,

$$\phi = \frac{4\pi(r+\Delta)D}{RT} (p_\infty - p_\Delta) = \frac{\pi r^2 \bar{v}}{RT} (p_\Delta - p_s) \tag{5.10}$$

One can solve for p_Δ from Eq. (5.10) and then use this expression for p_Δ to give ϕ. Assuming Δ is related to the mean free path by $\Delta = \alpha\lambda$, we obtain the ratio of the flux from Eq. (5.10) to the continuum flux, Eq. (5.8), as

$$\frac{\phi}{\phi_c} = \frac{1}{\frac{1}{1+\alpha Kn} + 4\beta Kn} \tag{5.11}$$

where the vapor diffusivity has been related to the mean free path by

$$D = \beta \bar{v} \lambda \tag{5.12}$$

and where β is a constant the value of which depends on the model chosen for the intermolecular potential forces between the vapor and the gas.* If the

*The most common representation is $\beta=1/3$, which reduces Eq. (5.12) to the well-known Meyer formula. Also seen is $\beta=1/4$, which represents a hard-sphere model.

the flux-matching takes place at the particle surface, then $\alpha = 0$, and

$$\frac{\phi}{\phi_c} = \frac{1}{1+4\beta Kn} \tag{5.13}$$

It is evident that ϕ/ϕ_c as given by Eq. (5.11) tends to unity as $Kn \to 0$. In order to determine the limit as $Kn \to \infty$, it is first necessary to convert Eq. (5.11) to ϕ/ϕ_{fm}. From Eqs. (5.8), (5.9) and (5.12), we deduce

$$\frac{\phi_c}{\phi_{fm}} = 4\beta Kn \tag{5.14}$$

Hence, from Eqs. (5.11) and (5.14)

$$\frac{\phi}{\phi_{fm}} = \frac{4\beta Kn}{\frac{1}{1+\alpha Kn} + 4\beta Kn} \tag{5.15}$$

As $kn \to \infty$, (5.15) tends to unity. However, the functional dependence of ϕ/ϕ_{fm} on Kn is not completely satisfactory as $Kn \to \infty$. For large Kn, Eq. (5.15) becomes

$$\frac{\phi}{\phi_{fm}} = \frac{1}{1 + \frac{Kn^{-2}}{4\alpha\beta}} \tag{5.16}$$

That is, only a second-order correction in Kn^{-1} is obtained. Other theories to be discussed shortly have first-order corrections in Kn^{-1}. An additional undesirable feature of the boundary sphere method is the unspecified nature of α.

A realistic transition regime model should evolve from the solution of the Boltzmann kinetic equation. Certain limiting solutions of the Boltzmann equation have been obtained that are applicable to the condensation

problem. Brock (1966) obtained a solution for Kn>>1 by using the BGK approximation (Bhatnagar et al., 1954) to the Boltzmann equation combined with the Knudsen iteration technque. His solution is of the form

$$\frac{\phi}{\phi_{fm}} = 1 - 0.2174 \left(x_v + x_g \left(\frac{m_v + m_g}{2m_g} \right) \left(\frac{D_{vv}}{D_{vg}} \right) \right) Kn^{-1} \qquad (5.17)$$

where x_v and x_g are the mole fractions of diffusing vapor and background gas, respectively, at infinite distance from the particle, and m_v and m_g are their molecular masses. The diffusivities D_{vv} and D_{vg} are the self and binary diffusivities of the vapor in the background gas. It is important to note that, in addition to the condition that Kn>>1, the use of the BGK linearization implies that $m_g >> m_v$. In atmospheric situations where the vapor species are, conceivably, high molecular weight organics and acids, this assumption may not be valid.

The similarity between some problems in neutron transport theory and those in transfer to aerosols has been exploited. The physical similarity between aerosol condensation and absorption of neutrons by a "black sphere" in a nuclear moderator suggests the applicability of one solution to another. Sahni (1966) obtained a solution to the steady state distribution of neutrons around a black sphere. In this solution the classical assumptions of one-speed transport theory and isotropic scattering are made. That is, all neutrons are assumed to have the same speed, and there is assumed to be an equal likelihood of velocities in any direction. This one-speed assumption is strictly valid only in the limit $m_v/m_g \to 0$, for it is only in this case that collisions with the moderating gas leave the neutron isotropically scattered with its previous velocity. Fuchs and Sutugin (1971) have fit Sahni's results by the formula

$$\frac{\phi}{\phi_c} = \frac{1}{1+\ell Kn} \tag{5.18}$$

where

$$\ell = \frac{4/3+0.71\ Kn^{-1}}{1+Kn^{-1}} \tag{5.19}$$

and $\beta = 1/3$ in Eq. (5.12).

In an attempt to remove the restrictions imposed by the one-speed assumption, Loyalka (1973) employed the variational method of Marshak (1947) to the linearized BGK model, as described by Brock (1966). Again, however, the BGK linearization implies that $m_v/m_g \ll 1$. The solution is presented as ϕ/ϕ_{fm} in tabular form as a function of Kn. Sampson and Springer (1969) applied the method of moments proposed by Lees (1959) to the Boltzmann equation. By assuming an inverse-fifth power force law (for reasons largely of mathematical tractability) and using $\beta = 1/4$ (hard sphere molecules), their results can be written in the form

$$\frac{\phi}{\phi_{fm}} = \frac{1}{1+Kn^{-1}} \tag{5.20}$$

Note that the form of Eq. (5.20) is identical to that of Eq. (5.15) obtained by the flux matching technique at the particle surface. Shankar (1970) has also studied the problem of steady condensation to a liquid droplet via the moment method proposed by Lees. His formulation, however, encompasses virtually all of the models previously discussed. In addition to describing properly the transition regime between free molecular and continuum mechanics, his model also reduces to the kinetic control limit when no background gas is present. This limit is, of course, of no interest in the current problem. Intermediate forms of the solution are identical to Fuch's flux-matching

model, Eq. (5.11), for various values of α. Again, however, the mathematically expedient assumption of an inverse-fifth power force law was made. It is apparent that this assumption, or the assumption that the mass of the diffusing species is small in comparison to the mass of the background gas, has been made in virtually all transition regime models. As mentioned previously, however, most diffusing species (e.g. high molecular weight organics, sulfuric acid and nitric acid) have molecular masses that are large in comparison to the molecular mass of air.

Figure 5.1 shows ϕ/ϕ_{fm} for the transition regime models: Fuchs' (1959) flux matching method (Eq. 5.15), the one-speed neutron transport solution of Sahni (1966) (Eqs. 5.18 and 5.19), and the BGK approximation of Loyalka (1973). The model of Sampson and Springer (1969) is identical to Eq. (5.15) for $\alpha = 0$ and $\beta = 1/4$, and hence corresponds to Fuchs' (1959) curve as well. Also presented in Figure 5.1 are the data of Chang and Davis (1976), who measured evaporation rates from suspended dioctyl phthalate droplets. As can be seen, the agreement between the various transition regime models and data is quite satisfactory, even though the assumptions under which the models were derived are likely to be in error. This important, and yet unsolved problem, in aerosol physics requires an approach based on kinetic theory, which is not restricted in applicability to the case $m_v \ll m_g$. It seems necessary to consider a simplified system (since full solution of the coupled Boltzmann equations for condensing vapor and background gas is quite impossible) in which the assumptions made are consistent with the physics of atmospheric aerosol growth. Until such a solution can be found, it is necessary to utilize the transition regime models presented here, which appear to correlate reasonably with existing data despite their basis on erroneous assumptions.

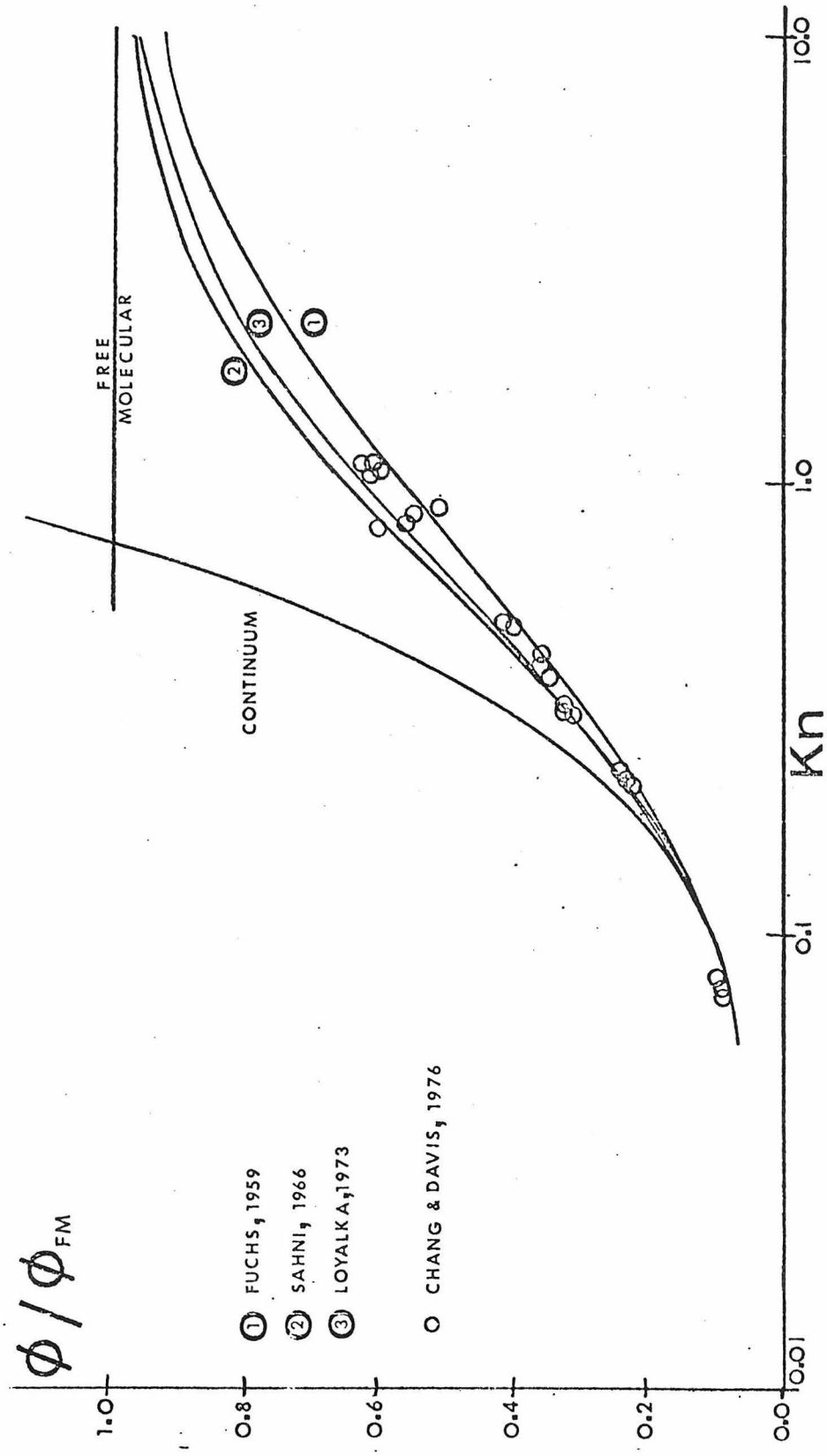

FIGURE 5.1
Normalized transfer rate vs. Knudsen number.

In the utilization of a diffusional growth mechanism for the model developed in this work, the transition regime approximation of Sahni (1966) (Eqs. (5.18) and (5.19) will be employed.

B. Equilibrium Conditions Across the Interface

In the continuum, free molecular and transition regime models discussed in the previous section, the transport rate ϕ has been expressed as a function of the partial pressure gradient between the bulk conditions and the conditions at the droplet surface. While bulk conditions are a "known" parameter in these models, surface equilibrium conditions depend upon the physics and chemistry of the droplet. In this section we discuss the two major factors influencing the equilibrium surface pressure; the Kelvin effect and the solute effect.

The Kelvin Effect

The Kelvin effect describes the relationship between the equilibrium vapor pressure of a component over a flat surface, and that over a curved surface. Its derivation is found in many references (Hamill (1975), Mirabel and Katz (1974), Nair and Vohra (1975), Skinner and Sambles (1972), Daniels and Alberty (1967)) and will not be repeated here.

From Nair and Vohra (1975) for a binary system

$$p_{c_i} = p_{f_i} \exp\left(\frac{2\sigma\bar{v}_i}{rRT}\left[1 + \frac{x_j}{\bar{v}_i}\frac{d\bar{v}_i}{dx_j} - \frac{3}{2}\frac{x_j}{\sigma}\frac{d\sigma}{dx_j}\right]\right) \tag{5.21}$$

where

p_{c_i} = vapor pressure of i over droplet of radius r, atm

p_{f_i} = vapor pressure of i over a flat surface, atm

σ = droplet surface tension, dyne/cm

$\bar{v}_i$ = liquid molar volume of species i, liter/mole

x_j = mole fraction of species j (=1-x_i).

The terms of Eq. (5.21) describing the surface tension and density changes with composition are often neglected, to yield a more compact form for Eq. (5.21):

$$p_{c_i} = p_{f_i} \exp\left(\frac{2\sigma\bar{v}_i}{rRT}\right) \tag{5.22}$$

Such an assumption is usually acceptable for dilute aqueous solutions, but becomes erroneous as solute concentration increases. For example, in the H_2O-H_2SO_4 system, the term involving the molar volume derivative assumes a value of 0.03, 0.17 and 0.5 for H_2SO_4 weight percents of 5, 25, and 70, respectively. The term involving the surface tension derivative assumes a value of 0.01, 0.06 and -0.4 at H_2SO_4 weight percents of 5, 25 and 70.

It is quite likely that these terms cannot be neglected for aerosols containing even trace amounts of organic compounds, due to the tendency of many organics to act as surfactants. For an aqueous droplet, we can estimate the relative effect of droplet curvature on the equilibrium surface pressure. Assuming σ = 72 dyne/cm, $\bar{v}_i$ = 0.03 liter/mole and T = 298^{o}K, we get almost a 600% increase in surface pressure over a 0.001 μm droplet as compared to the equilibrium pressure over a flat surface. The effect falls off rapidly as the droplet radius increases. The vapor pressure increases by 19%, 2% and 0.2% for droplets of radius = 0.01, 0.1 and 1.0 μm, respectively.

The Solute Effect

Until this point, all models for gas phase transport and interfacial equilibrium have contained as an unknown quantity the surface pressure. Through the Kelvin effect, we have reduced that unknown to the surface pressure above a flat liquid surface with composition identical to that of the droplet. It is through the solute effect, which will now be discussed, that the surface pressure is finally related to conditions within the aerosol droplet.

While the Kelvin effect serves to increase the equilibrium surface pressure over a droplet, the solute effect tends to decrease the surface pressure. The most general form of the solute effect relates the equilibrium surface pressure of a given component over a flat surface to the liquid fraction of that component by

$$p_{f_i} = \gamma_i x_i p_{sat_i} \tag{5.23}$$

where p_{sat_i} is the equilibrium saturation pressure of i over a flat surface of pure i, x_i is the mole fraction of i in the liquid phase and γ_i is the activity coefficient of i in the liquid phase.

While Eq. (5.23) is thermodynamically rigorous, and requires the experimental determination of only one parameter, γ_i, as a function of composition (under isothermal and isobaric conditions), other "one-parameter" models have been proposed to relate surface pressure to composition. All such models must, of course, be related, and Yue (1976) has given a thorough examination of these relationships. A summary of these relationships is presented here.

It is important to point out that when speaking of equilibrium conditions of gases and vapors other than water above aqueous (or nonaqueous) solutions, virtually all data are presented in the form of the activity coefficient as defined by Eq. (5.23), or an idealization thereof. However, when referring to the equilibrium vapor pressure of water above aqueous solutions, two parameters in addition to water activity are frequently reported, the van't Hoff factor and the osmotic coefficient.

Before discussing these parameters, it should be mentioned that even when the formulation of Eq. (5.23) is utilized for aqueous solutions, the water activity a_w, rather than the water activity coefficient γ_w, is usually reported. Their relationship is

$$a_w = \gamma_w x_w \tag{5.24}$$

and hence Eq. (5.23) becomes

$$p_{f_w} = a_w p_{sat_w} \tag{5.25}$$

In a solution of an electrolyte in water, some ambiguity arises as to the correct definition of the mole fraction of solute and solvent. If m is the molality (moles/kg. H_2O) of solute in water, then the mole fraction of water is

$$x_w = \frac{55.51}{m+55.51} \tag{5.26}$$

In an electrolye (specifically a strong electrolyte) each mole of electrolyte will split into ν_+ moles of cations and ν_- moles of anions. Hence Eq. (5.26) takes the form

$$x_w = \frac{55.51}{\nu m+55.51} \tag{5.27}$$

where $\nu = \nu_+ + \nu_-$.

Even when an electrolyte does not completely dissociate, the practical osmotic coefficient Φ is defined as if the electrolyte were completely dissociated. In this way Φ is related to the water activity by

$$\Phi = - \frac{55.51 \ \ell n \ a_w}{\nu m} \tag{5.28}$$

or, by analogy to Eq. (5.25),

$$p_{f_w} = p_{sat_w} \exp\left(- \frac{\nu m \Phi}{55.51} \right) \tag{5.29}$$

Finally, the van't Hoff factor i defined by McDonald (1953) is often used for equilibrium relationships of electrolyte solutions. It is related to water activity by

$$i = \frac{55.51}{m} \quad \frac{(1-a_w)}{a_w} \tag{5.30}$$

or, by analogy to Eq. (5.25),

$$p_{f_w} = p_{sat_w} \left(\frac{55.51}{im+55.51} \right) \tag{5.31}$$

Low (1969) presents a discussion of the uses of a_w, Φ and i in cloud physics problems, and present tables of a_w and i vs. molality of aqueous solutions of eight common electrolytes. Extensive data on water activities of binary electrolytes can be found in Robinson and Stokes (1965).

Given the fact that any one of these three parameters is subject to experimental error, it seems preferable to select a convention the single parameter of which varies as little as possible with composition. Tabulated

data for a number of electrolytes in Yue (1976) indicate that water activity is the parameter with least deviation with respect to composition. (In the ideal case a_w varies linearly with composition.)

This discussion of the solute effect on surface pressure will be concluded by considering the ideal cases of the above relationships. If the equilibrium vapor pressure of either solvent or solute varies linearly with composition, then $\gamma_i \equiv 1$ and is independent of composition, and Raoult's law results. Often, Raoult's law is applied to the solvent when a very weak solution of nonelectrolyte is considered. In this case, $\gamma_i \to 1$ as $x_i \to 1$ in Eq. (5.23).

If the concentration of an absorbed gas varies linearly with surface pressure at low gas phase concentrations, Henry's Law applies. In this case, the convention on γ_i for the solute is such that $\gamma_i \to 1$ as $x_i \to 0$ in Eq. (5.23). Such an assumption is often justifiably made for atmospheric problems, where the gaseous pollutants are found in ppm concentrations and lower.

In this work, either water activity or species activity coefficient will be used to describe deviations from ideal behavior. Any data reported in the form of practical osmotic coefficients or van't Hoff factors are converted to activities by equations (5.28) or (5.30).

C. Liquid Chemistry of the Aerosol Droplet

Once absorbed into the aerosol droplet, the vapor species may undergo chemical reaction. Before a general framework is constructed into which the various chemical pathways can be included, an important assumption is made. Considering that all aerosol particles of interest have radii of approximately 1 μm or less, it is assumed that the liquid phase is

well-mixed, and that diffusion within the droplet can be safely ignored. Considering a characteristic diffusivity of 10^{-5} $cm^2/sec.$, a characteristic diffusion time of $rx10^{-3}$ seconds is obtained, where r is the droplet radius in μm. Since the atmospheric processes of interest occur on the time scale of minutes to hours the assumption of well-mixedness is quite reasonable.

Chemical reactions within the droplet fall into two categories: those that can be considered to be in equilibrium and those not in equilibrium. If there exist n_e equilibrium reactions in the droplet, then the equilibrium equations can be written as

$$\sum_{i=1}^{N_R(j)} \rho_{ij} R_{ij}^{r_{ij}} \rightleftharpoons \sum_{i=1}^{N_P(j)} \psi_{ij} P_{ij}^{p_{ij}} \quad ; j = 1, n_e \tag{5.32}$$

where

ρ_{ij} = stoichiometric coefficient of reactant i in reaction j

ψ_{ij} = stoichiometric coefficient of product i in reaction j

R_{ij} = reactant i in reaction j

P_{ij} = product i in reaction j

r_{ij} = ionic charge on reactant i

p_{ij} = ionic charge on product i

$N_R(j)$ = number of reactants in reaction j

$N_p(j)$ = number of products in reaction j

n_e = number of equilibrium reactions

The equilibrium constant for each reaction can be written as

$$K_j = \frac{\prod_{i=1}^{N_P(j)} (\gamma_{p_{ij}} [P_{ij}])^{\psi_{ij}}}{\prod_{i=1}^{N_R(j)} (\gamma_{r_{ij}} [R_{ij}])^{\rho_{ij}}} \quad ; \quad j = 1, n_e \tag{5.33}$$

where $[\cdot]$ indicates the concentration in moles/liter, and $\gamma_{p_{ij}}$ and $\gamma_{r_{ij}}$ are the activity coefficients of products and reactants, respectively.

If there exist n_k non-equilibrium reactions in the droplet, these reactions can be expressed as

$$\sum_{i=1}^{N_R(j)} \rho_{ij} R_{ij}^{r_{ij}} \longrightarrow \sum_{i=1}^{N_P(j)} \psi_{ij} P_{ij}^{p_{ij}} \quad ; \; j = n_e+1, n_e+n_k \tag{5.34}$$

Consider as a simple example the following reaction scheme:

$$H_2O \rightleftarrows H^+ + OH^- \tag{5.35}$$

$$(SO_2)_\ell \rightleftarrows H^+ + HSO_3^- \tag{5.36}$$

$$HSO_3^- \rightleftarrows H^+ + SO_3^= \tag{5.37}$$

$$SO_3^= \xrightarrow{O_2} SO_4^= \tag{5.38}$$

Here, $n_e=3$, $n_k=1$ and the values of the other parameters are:

$$\rho_{11} = \rho_{12} = \rho_{13} = \rho_{14} = 1$$

$$\psi_{11} = \psi_{21} = \psi_{12} = \psi_{22} = \psi_{13} = \psi_{23} = \psi_{14} = 1$$

$$r_{11} = r_{12} = 0 \; ; \; r_{13} = -1 \; ; \; r_{14} = -2$$

$$p_{11} = p_{12} = p_{13} = 1 \; ; \quad p_{21} = p_{22} = -1 \; ; \quad p_{23} = -2$$

$$p_{14} = -2$$

Also necessary in the liquid chemistry formalism is the condition of electroneutrality. Should there be no ionic reactants or products, this condition reduces identically to zero*. Generally, however, it may be written as

$$\sum_{j=1}^{n_e+n_k} \left(\sum_{i=1}^{N_R(j)} r_{ij}[R_{ij}] + \sum_{i=1}^{N_P(j)} p_{ij}[P_{ij}] \right) = 0 \qquad (5.39)$$

The general model describing the growth of an aerosol droplet due to condensation of vapor is now complete, at least in principle. There are many parameters (most notably activity coefficients and water activities) that must be experimentally determined before an actual system can be simulated. In the next section, this model will be applied to a simple but realistic situation in a polluted urban atmosphere.

D. Sulfate Formation in Aerosol Droplets

The atmospheric oxidation of SO_2 to particulate sulfate represents a problem of much current interest. It is now recognized that such oxidation may occur by gas-phase as well as particulate-phase processes. Gas-phase processes are felt to involve the homogeneous oxidation of SO_2 to H_2SO_4, followed by homogeneous nucleation or condensation of the sulfuric acid vapor. Particulate-phase processes involve the absorption of SO_2 followed by liquid-phase oxidation or, in some instances, may involve the catalytic oxidation of SO_2 or particle surfaces. A review of studies

*Care must be taken to avoid duplication of species that appear in more than one reaction. For example, in the simple reaction scheme of Eqs. (5.35)-(5.38), the hydrogen ion appears three times ($p_{11}=p_{12}=p_{13}=1$). However, it must only be included once in the electroneutrality condition of Eq. (5.39).

related to the atmospheric oxidation of SO_2 to sulfate is beyond our scope. A thorough review of studies on the homogeneous atmospheric oxidation of SO_2 can be found in Sander and Seinfeld (1976). Homogeneous nucleation of sulfuric acid vapor and water has been considered by Reiss (1951), Mirabel and Katz (1974), Nair and Vohra (1975), and McMurry (1977). Catalytic oxidation of SO_2 by particulate surfaces has been discussed by Burke et al. (1973) and Novakov et al. (1974). Table 5.1 presents a summary of aqueous phase SO_2 oxidation mechanisms (Harrison, 1976).

While the chemistry of SO_2 oxidation has been studied extensively, there exist relatively few studies of the simultaneous chemistry and growth that occur in atmospheric particles. Foster (1969) used curves for the vapor pressure lowering effects of H_2SO_4 and $MnSO_4$ on H_2O to calculate the growth of a droplet in which dissolved SO_2 is catalytically oxidized to sulfate by metal ions. Similar calculations were carried out by Freiberg (1974, 1976). Wadden et al. (1974) considered simultaneous growth and coagulation, using a vapor pressure lowering calculation similar to that of Foster.

In selecting a specific atmospheric situation to study, we seek a problem which involves growth by diffusion and chemical equilibria and kinetics within the droplet. Table 5.2 lists a number of situations of atmospheric interest for potential simulation. If possible, the simulation of the system of category 4b in Table 5.2 would be undertaken, since this is the problem of immediate interest in photochemical air pollution. However, thermodynamic data (e.g. surface tension, water activity, molar volumes, etc.) for aqueous solutions of complex organics, such as found in the Los Angeles airshed, are simply unavailable. Power plant plume

Table 5.1. Summary of Aqueous Phase SO_2 Oxidation Mechanisms

Author	Type of Mechanism	Elements of Mechanism	Rate Coefficients and/or Expressions	Comments
Fuller and Crist, 1941	Sulfite oxidation by O_2 with no catalyst; Cu^{2+} catalyst; mannitol inhibitor	Very long chain reaction	$-\frac{d(O_2)}{dt} = k(SO_3^{--})$ $k=.013+2.5(Cu^{2+})$ with Cu^{2+} catalyst; $k=.013+6.6(H^+)^{1/2}$ with acid added	25^oC; rate coefficient with acid added assumes second dissociation of H_2SO_3 equals $5x10^{-6}$ (too large)
Basset and Parker 1951	Sulfurous acid oxidation by metal salts and O_2	uncatalyzed; formation of complexes such as $[O_2 \cdot SO_3]^{--}$; catalyzed: formation of complexes such as $[O_2 \cdot Mn(SO_3)_2]^{--}$ and rapid oxidation		
Junge and Ryan 1958	SO_2 oxidation catalyzed by Fe^{2+}, with and without ammonia		conversion rate $= 1.8x10^{-4}$ %/min	sulfate formation asymptotic to a certain pH; maximum formation varies linearly with SO_2 partial pressure
Van den Heuvel and Mason 1963	SO_2 oxidation catalyzed by NH_3	$2SO_2+O_2 \rightarrow 2SO_3$ $SO_3+H_2O \rightarrow H_2SO_4 \rightarrow 2H^+ + SO_4^=$ $NH_3+H_2O \rightarrow NH_4OH \rightleftarrows NH_4^+ + OH^-$	conversion rate $= 2.5$ %/min	extrapolation to atmospheric conditions used to estimate conversion rate

Table 5.1. Summary of Aqueous Phase SO_2 Oxidation Mechanisms (Continued)

Author	Type of Mechanism	Elements of Mechanism	Rate Coefficients and/or Expressions	Comments
Espenson and Taube 1965	SO_2 oxidation by ozone	$SO_2+O_3+H_2O \rightarrow HSO_4^- + H^+ + O_2$ (in acid solution) $SO_3^= + O_3 \rightarrow SO_4^= + O_2$ (in basic solution)	not determined	
Scott and Hobbs 1967	SO_2 oxidation catalyzed by NH_3	SO_2, NH_3, CO_2 in equilibrium with ions and gas $SO_3^= + 1/2\ O_2 \rightarrow SO_4^=$	$\frac{d[SO_4^=]}{dt} = k[SO_3^=]$ $k=.0017\ sec^{-1}$	25°C only; k estimated from Van den Heuvel and Mason
Beilke and Georgii 1968	Washout and rainout of SO_2 and sulfate aerosols		assumed instantaneous oxidation of all SO_2 incorporated into droplet	calculated $SO_4^=$ concentrations from 0.3 to 36.5 mg/ℓ depending on rain rate and assumed SO_2 gas phase concentration
Foster 1969	SO_2 oxidation catalyzed by metal salts	$2SO_2+2H_2O+O_2 \xrightarrow{\text{catalyst}} 2H_2SO_4$	SO_2 conversion rate= .09%/min for Mn, .15 to 1.5%/min for Fe for typical input parameters	theoretical study; rates for Mn and Fe are functions of many factors; rate for Fe catalyzed oxidation is pH dependent

Table 5.1. Summary of Aqueous Phase SO_2 Oxidation Mechanisms (Continued)

Author	Type of Mechanism	Elements of Mechanism	Rate Coefficients and/or Expressions	Comments
Matteson, Stober, and Luther 1969	SO_2 oxidation catalyzed by metal salts	$Mn^{2+}+SO_2 \rightleftharpoons Mn\cdot SO_2^{2+}$ $2Mn\cdot SO_2^{2+}+O_2 \rightleftharpoons [(Mn\cdot SO_2^{2+})_2\cdot O_2]$ $\rightleftharpoons 2Mn\cdot SO_3^{2+}$ $Mn\cdot SO_3^{2+}+H_2O \rightleftharpoons Mn^{2+}+HSO_4^- +H^+$ $HSO_4^-+H^+ \rightleftharpoons H_2SO_4$	$-\frac{d(SO_2)}{dt} = k_1\left[Mn^{2+}\right]_0^2$ $k_1=2.4\times10^5\ M^{-1}s^{-1}$	negligible $SO_4^=$ formation for RH<95%; similar mechanism may be responsible for catalyst by other metal salts
McKay 1971	SO_2 oxidation catalyzed by NH_3	same as Scott and Hobbs	$\frac{d[SO_4^=]}{dt} = k[SO_3^=]$ $k=(.013+59[H^+]^{1/2})\ sec^{-1}$ $= .032\ sec^{-1}$ at neutrality (25^oC)	considered variation with temperature; k estimated from Fuller and Crist; found large negative temperature rate correlation
Cheng, Corn, and Frohliger 1971	SO_2 oxidation catalyzed by NH_3	$2SO_2+2H_2O+O_2 \xrightarrow{\text{catalyst}} 2H_2SO_4$	SO_2 conversion rate $\sim$.03%/min with Mn^{2+} levels typical of urban industrial atmosphere; $\sim$.33%/min with levels typical of plume from coal powered plant	oxidation rate estimated by extrapolation to atmospheric conditions
Miller and de Pena 1972	SO_2 oxidation catalyzed by NH_3	similar to Scott and Hobbs	$\frac{d[SO_4^=]}{dt} = k[SO_3^=]$ $k\sim.003\ sec^{-1}(25^oC)$	k estimated by fit of experimental data to theoretical curves

Table 5.1. Summary of Aqueous Phase SO_2 Oxidation Mechanisms (Continued)

Author	Type of Mechanism	Elements of Mechanism	Rate Coefficients and/or Expressions	Comments
Penkett 1972	SO_2 oxidation by ozone	$HSO_3^- + O_3 \rightarrow HSO_4^- + O_2$	$\frac{d(O_3)}{dt} = k_2(O_3)(HSO_3^-)$ $k_1 = 3.32 \pm .13 \times 10^5 M^{-1} s^{-1}$ SO_2 conversion rate $\sim .21\%/min$	9.6^oC; SO_2 oxidation rate extrapolated from data; much faster than Scott and Hobbs
Chen and Barron 1972	Sulfite oxidation catalyzed by cobalt ions	free radical mechanism; Co(III) reduced	$-\frac{d(O_2)}{dt} = k[Co(H_2O)_6^{3+}]^{1/2} [SO^{3=}]^{3/2}$	could not determine specific value for k
Penkett and Garland 1974	SO_2 oxidation by ozone	$HSO_3^- + O_3 \rightarrow HSO_4^- + O_2$	$-\frac{d(SO_2)}{dt} = k[SO_3^=]$ $k = 4.18 \times 10^{-4} + 1.77[H^+]^{1/2} sec^{-1}$	pH range from 4 to 7 10^oC; .1 ppm SO_2, .05 ppm O_3 in fog water
Brimblecombe and Spedding 1974	SO_2 oxidation by O_2 with trace Fe catalyst	complex	$-\frac{d\,S(IV)}{dt} = k[Fe(III)][S(IV)]$ $k = 100\ M^{-1} s^{-1}$ SO_2 conversion rate $\sim 3.2\%$/day in fog assuming 28 $\mu g/m^3$ SO_2 and 10^{-6} M Fe(III)	Possibility of Fe(III) contamination discussed

Table 5.1. Summary of Aqueous Phase SO_2 Oxidation Mechanisms (Continued)

Author	Type of Mechanism	Elements of Mechanism	Rate Coefficients and/or Expressions	Comments
Freiberg 1974	SO_2 oxidation catalyzed by Fe	complex	$\frac{d[SO_4^{=}]}{dt} = K_0 K_S^2 [H_2SO_3]^2 [Fe^{3+}]/[H^+]^3$ k_s = 1st dissociation constant of H_2SO_3	Rate increases rapidly with RH and decreases by about one order of magnitude with 5^0C increase in temperature
Freiberg 1975	SO_2 oxidation catalyzed by Fe	complex	Same as above, except K_0 a complex function of $[Fe^{3+}]$	Rate dependence changes from $[SO_2]^2/[H^+]^3$ to $[SO_2]/[H^+]$ as pH or $[SO_2]$ increases.

Table 5.2 Atmospheric Situations Involving Heterogeneous Chemical Reactions

System	Primary Species and Dissolved Vapor Species	Representative References
1. Dissolved salt aerosols (e.g. sea salt aerosol)	$NaC\ell$, $MnC\ell_2$, $MgC\ell_2$, $CaC\ell_2$	El Golli et al. (1974, 1977) Tang (1975)
2. Washout/Rainout In Polluted Regions	SO_2, NH_3	Scott and Hobbs (1967) McKay (1971) Miller and dePena (1972)
3. Power Plant Plumes	SO_2, NH_3, Mn^{2+}, Fe^{3+}	Foster (1969) Matteson et al. (1969) Cheng et al. (1971) Freiberg (1974, 1975, 1976)
4. Photochemical Aerosol		
a. Marine Background	SO_2, NH_3, NO, NO_2, $NaC\ell$, $MgC\ell_2$, H_2SO_4	Orel and Seinfeld (1977) Moskowitz (1977)
b) Full Photochemical	SO_2, NH_3, NO, NO_2, $NaC\ell$, $MgC\ell_2$, H_2SO_4, Fe^{3+}, Mn^{2+}, = Organics	Grosjean and Friedlander (1975)

particle dynamics are of interest in many regions, particularly those with coal-fired utility plants. Oxides of nitrogen play an important role in smog photochemistry as well as in power plant plumes, and do indeed contribute to particulate nitrate levels. As in the case of photochemical aerosols, their inclusion requires thermodynamic information not generally available.

While both the plume problem and the nitrate problem are situations we wish to study eventually by using the general aerosol growth mechanism constructed here, it is felt that as an initial application of this growth mechanism, a simpler system should be considered.

We consider the formation of sulfate and the accompanying growth of an aqueous atmospheric aerosol. Initially the aerosol is assumed to consist of an aqueous solution of NaCℓ and $MgCℓ_2$, the dominant salts in sea water. (Thus, the particle is typical of those advected into the Los Angeles area from the ocean.) The ratio of NaCℓ to $MgCℓ_2$ in the particle is taken to be that in sea water, and the initial size of the droplet is the equilibrium size corresponding to the given quantities of NaCℓ and $MgCℓ_2$ and the prevailing relative humidity. The particle is then assumed to be exposed to typical ambient (Los Angeles) levels of SO_2, NH_3, sulfuric acid vapor, and water. The sulfuric acid vapor is assumed to be the result of homogeneous gas phase oxidation of SO_2, a process not accounted for in detail here. The SO_2, NH_3, and H_2SO_4 gases are absorbed into the particle, with the subsequent liquid phase chemistry resulting in particle growth.

This situation can be viewed as an approximation to the process of growth of a marine aerosol as it passes over a region polluted by SO_2, NH_3 and H_2SO_4. Although oxides of nitrogen play an important role in the

photochemical process, the process which we are to study is similar to the situation experienced in the Los Angeles airshed. Here, marine aerosol is advected into the basin, where it passes over regions of high industrial pollution.

Table 5.3 lists the equilibria relevant for this situation. As evidenced by conditions 3, 6, and 10, we have assumed Henry's law to be applicable for SO_2, NH_3, and $HC\ell$.* Henry's law can be taken to be valid because of the low vapor pressures (ppm levels) and low liquid concentrations of the dissolved gases. The activity coefficients of the ions (γ_+, γ_- and γ_{2-}) are calculated according to the Davies approximation

$$\log_{10}(\gamma_z) = - AZ^2 \left(\frac{\sqrt{I}}{1+\sqrt{I}} - 0.2I \right) \tag{5.40}$$

where z is the ionic charge, A = 0.5085 for water at 25°C, and I is the ionic strength, defined by

$$I = \frac{1}{2} \sum_i [c_i] z_i^2 \tag{5.41}$$

where $[c_i]$ is the concentration of ionic species i and z_i is its ionic charge. The validity of Eq. (5.40) is uncertain for ionic strengths larger than 0.5 mole/liter.

The final parameter which must be estimated is the water activity a_w. This parameter is the single most difficult one to estimate, and, unfortunately, the most important one in the simulation. It is a_w which

*Note that $HC\ell$ is desorbed after formation from H^+ and $C\ell^-$. It is not assumed to be present initially in the gas phase.

Table 5.3 Equilibrium Chemistry

Reaction	Equilibrium Constant	Value at 25°C	Reference
1. $H_2O_{(g)} \rightleftarrows H_2O_{(\ell)}$	$1/p_{sat_w} = a_w/p_{H_2O}$	31.99 atm^{-1}	a
2. $H_2O_{(\ell)} \rightleftarrows H^+ + OH^-$	$K_w = [H^+][OH^-]\gamma_+\gamma_-$	10^{-14} $moles^2 \ell^{-2}$	b
3. $SO_{2(g)} \rightleftarrows SO_{2(\ell)}$	$K_{hs} = [SO_{2(\ell)}]/p_{SO_2}$	1.24 molesℓ^{-1} atm^{-1}	c,d
4. $SO_{2(\ell)} \rightleftarrows H^+ + HSO_3^-$	$K_{1s} = [H^+][HSO_3^-]\gamma_+\gamma_-/[SO_{2(\ell)}]$	0.0127 molesℓ^{-1}	e
5. $HSO_3^- \rightleftarrows H^+ + SO_3^=$	$K_{2s} = [H^+][SO_3^=]\gamma_+\gamma_{2-}/[HSO_3^-]\gamma_-$	6.24×10^{-8} moles ℓ^{-1}	e
6. $NH_{3(g)} \rightleftarrows NH_{3(\ell)}$	$K_{hA} = [NH_{3(\ell)}]/p_{NH_3}$	57. moles ℓ^{-1} atm^{-1}	f
7. $NH_{3(\ell)} \rightleftarrows NH_4^+ + OH^-$	$K_{1A} = [NH_4^+][OH^-]\gamma_+\gamma_-/[NH_{3(\ell)}]$	1.774×10^{-5} moles ℓ^{-1}	b
8. $MgC\ell_{2(\ell)} \rightleftarrows Mg^{++} + 2C\ell^-$	$K_{1M} = [Mg^{++}][C\ell^-]^2\gamma_{2+}\gamma_-^2/[MgC\ell_{2(\ell)}]$	∞	assumed
9. $NaC\ell_{(\ell)} \rightleftarrows Na^+ + C\ell^-$	$K_{1N} = [Na^+][C\ell^-]\gamma_+\gamma_-/[NaC\ell_{(\ell)}]$	∞	assumed
10. $HC\ell_{(g)} \rightleftarrows HC\ell_{(\ell)}$	$K_{hH} = [HC\ell_{(\ell)}]/p_{HC\ell}$	19. moles ℓ^{-1} atm^{-1}	g
11. $HC\ell_{(\ell)} \rightleftarrows H^+ + C\ell^-$	$K_{1H} = [H^+][C\ell^-]\gamma_+\gamma_-/[HC\ell_{(\ell)}]$	1.3×10^6 moles ℓ^{-1}	h

a. Perry (1974)
b. Robinson and Stokes (1965)
c. Johnstone and Leppla (1934)
d. Hales and Sutter (1973)
e. Yui (1940)
f. Morgan and Maass (1931)
g. International Critical Tables (1928)
h. Robinson (1936)

determines the water content of the droplet, and therefore (to a great extent) the droplet size.

There are numerous experimental results reported in the literature for a_w for binary systems. The most extensive of these tabulations for electrolytes are probably those of Robinson and Stokes (1965) and Teng and Lenzi (1974). Data on ternary aqueous solutions are far more scarce, and data for multicomponent aqueous solutions are practically non-existent.

Table 5.4 lists the anions, cations and a few possible combined compounds that could be found in an aerosol droplet with the equilibrium chemistry of Table 5.3. As can be seen, there are at least 10 possible compounds that could be found in the droplet.

What is needed, therefore, is an approximation of a_w for a multicomponent aerosol droplet, based on binary data for each component in water. Before such an approximation is useful, however, we must decide just <u>which</u> components are present in the droplet. This is quite difficult (or impossible) since most electrolytes remain in their ionic form in solution, and there is no way of correctly identifying what cations and anions will combine to form neutrally charged species. Some assumption concerning these species must be made.

The assumption made is the following: For purposes of calculation of a_w <u>only</u>, it is assumed that

1.) All oxides of sulfur are dissociation products of H_2SO_4

2.) All ammonium ions are dissociation products of NH_4OH

3.) All Na^+ ions are dissociation products of $NaC\ell$

4.) All Mg^{++} ions are dissociation products of $MgC\ell_2$

Table 5.4. Ions and Possible Compounds in Aerosol Droplet

Cations	Anions	Some Possible Compounds
H^+, NH_4^+, Mg^{++}, Na^+	OH^-, HSO_3^-, $SO_3^=$, $C\ell^-$, $SO_4^=$	H_2SO_4, $HC\ell$, NH_4OH, $(NH_4)HSO_4$, $(NH_4)_2SO_4$, $NH_4C\ell$, $MgSO_4$, $MgC\ell_2$, Na_2SO_4, $NaC\ell$.

Under these assumptions, we must determine water activity for the system H_2O-H_2SO_4-NH_4OH-NaCℓ-$MgCℓ_2$. Robinson and Stokes (1965) present binary data for the aqueous solutions of H_2SO_4, NaCℓ and $MgCℓ_2$ as a function of molality (moles/kg H_2O) of solute. Table 5.5 lists the maximum molality (and corresponding minimum water activity) reported by these data. No data are reported for the H_2O-NH_4OH system. However, for many compounds up to molalities as high as 2.0, the following relationship holds:

$$a_w = x_w^2 \tag{5.42}$$

where x_w is the mole fraction of water in the binary system. Since, as will be seen, NH_4^+ levels rarely exceed 2.0 moles/liter, Eq. (5.42) is probably a reasonable assumption for the H_2O-NH_4OH system.

There are a number of methods proposed for predicting thermodynamic properties of multicomponent systems. Sangster and Lenzi (1974) provide an excellent critical examination of various methods of predicting water activities for multicomponent aqueous solutions. Based upon their recommendations, the correlation proposed independently by Zdanovskii (1936) and Stokes and Robinson (1966) for solutions of electrolytes is utilized. This relation is

$$1 = \sum_i \frac{m_i}{m_{bi}(a_w)} \tag{5.43}$$

where m_i is the molality of species i in the multicomponent solution, and $m_{bi}(a_w)$ is the binary molality of species i at the given water activity a_w. The summation is over all components in the droplet.

Table 5.5 Binary Activity Data*

System	m_{max}	$a_{w_{min}}$
H_2O-H_2SO_4	10.0	0.3616
H_2O-NaCℓ	6.0	0.76
H_2O-$MgCℓ_2$	5.0	0.44

*From Teng and Lenzi (1974) and Robinson and Stokes (1965).

The formulation of Eq. (5.43) implies semi-ideal solutions. That is, the binary solutions are not ideal (non-ideal solute-solvent interactions) but there are no solute-solute interactions that alter the binary interactions. Hence, the solution is assumed to be composed of a series of "binary" solutions, each unaffected by the presence of the other components. Such an assumption is no doubt reasonable under dilute conditions of a few components. Hence, by knowing the binary relationships between m_{bi} and a_w one can either:

a.) Calculate molalities of each solute given a_w, or

b.) Calculate a_w given the moles of each solute in the droplet.

A final relationship required for equilibrium calculations is given by the electroneutrality condition of Eq. (5.39).

In addition to the equilibria of Table 5.3, the ammonia-catalyzed reaction of McKay (1971) is proposed for the homogeneous oxidation of $SO_3^=$ to $SO_4^=$. This mechanism is given (for a variable volume droplet) by

$$\frac{d(SO_4^=)}{dt} = V\left(0.013 + 59.[H^+]^{1/2}\right)[SO_3^=] \tag{5.44}$$

where $(SO_4^=)$ is the moles of sulfate in the droplet, $[H^+]$ and $[SO_3^=]$ are concentrations (moles/liter) of H^+ and $SO_3^=$, and V is the total particle volume. Units of $d(SO_4^=)/dt$ are moles sec^{-1}.

Two diffusional processes are included. First, there is diffusion of gaseous HCℓ desorbed from the droplet, given by

$$\frac{d(C\ell_{(\ell)})}{dt} = \frac{4\pi r}{RT} D_{HC\ell}\left(- \frac{P_{surf(HC\ell)}}{1+\ell Kn}\right) \tag{5.45}$$

where $(C\ell_{(\ell)})$ is the total chlorine in the liquid (moles), Kn is the Knudsen number and ℓ is given by Eq. (5.19), $D_{HC\ell}$ is the binary diffusivity of $HC\ell$ in air, and $p_{surf(HC\ell)}$ is the surface pressure, related to the equilibrium partial pressure by the Kelvin equation,

$$p_{surf(HC\ell)} = p_{HC\ell} \exp\left(\frac{2\sigma\bar{v}_{HC\ell}}{rRT}\right) \tag{5.46}$$

It is assumed that the ambient level of $HC\ell_{(\ell)}$ is zero.

Second, there is diffusion of H_2SO_4 vapor from the gas phase to the particle, and subsequent condensation. Further, it is assumed that complete dissociation of H_2SO_4 to H^+ and $SO_4^=$ takes place in the droplet. The diffusion equation is written as

$$\frac{d}{dt}(H_2SO_4) = \frac{4\pi r}{RT} D_{H_2SO_4} \left(\frac{p_\infty(H_2SO_4)}{1+\ell Kn}\right) \tag{5.47}$$

where (H_2SO_4) is the total moles of condensed H_2SO_4 in the droplet. Since the equilibrium vapor pressure of H_2SO_4 is negligible, it is assumed that its surface pressure is zero.

The surface pressures of H_2O, SO_2, and NH_3 are related to the equilibrium partial pressures by

$$p_{surf}(H_2O) = p_{H_2O} \exp\left(\frac{2\sigma\bar{v}}{rRT} H_2O\right) \tag{5.48}$$

$$p_{surf}(SO_2) = p_{SO_2} \exp\left(\frac{2\sigma\bar{v}}{rRT} SO_2(\ell)\right) \tag{5.49}$$

$$p_{surf}(NH_3) = p_{NH_3} \exp\left(\frac{2\sigma\bar{v}}{rRT} NH_3(\ell)\right) \tag{5.50}$$

and the surface pressures are assumed equal to the ambient pressures of each of these three components.

$$p_{surf(H_2O)} = p_{\infty(H_2O)} \tag{5.51}$$

$$p_{surf(SO_2)} = p_{\infty(SO_2)} \tag{5.52}$$

$$p_{surf(NH_3)} = p_{\infty(NH_3)} \tag{5.53}$$

We note that it is not necessary that the vapor phase diffusion equation be written for H_2O, SO_2 and NH_3, as it has been for HCℓ and H_2SO_4. It can be assumed that surface conditions and ambient conditions are identical. The time required to reach equilibrium (that is, for Eqs. 5.51 - 5.53 to be satisfied) is the order of 10^{-3} sec. or shorter. On the other hand, since the surface pressure of H_2SO_4 and the ambient pressure of HCℓ are so low (assumed zero), the time-scales needed to reach equilibrium are much longer.

The general method of solution is to integrate Eqs. (5.44), (5.45) and (5.47), solving the equilibrium conditions of Table 5.3 and Equations (5.39), (5.40), and (5.41) iteratively at each time step. Table 5.6 lists miscellaneous parameters required for the simulation.

E. Results

Seven cases were considered. Case A is considered the "base" case against which all other cases are to be compared. With the exception of case F, only one parameter has been changed between each case and case A. Table 5.7 lists the parameters that were altered and their values for each run.

Table 5.6 Necessary Parameters for Simulation

Parameter	Value	Reference
$\bar{v}_{H_2O}$	0.018 liter/mole	a
$\bar{v}_{SO_{2(\ell)}}$	0.054	a
$\bar{v}_{NH_{3(\ell)}}$	0.039	a
$\bar{v}_{HC\ell(\ell)}$	0.045	a
$\bar{v}_{H_2SO_{4(\ell)}}$	0.054	a
$D_{H_2SO_4}$	0.54 cm^2/sec	calculated
$D_{HC\ell}$	0.185	calculated
$(NaC\ell/MgC\ell_2)_o$	13.7	b
λ	0.055 μm	c
T	298 ^oK	assumed
$P_{sat(H_2O)}$	23.76 mm Hg	a
σ	72 dyne/cm	a

a. Perry (1974)

b. Molar ratio of sea water

c. For air at 25^{o}C

Table 5.7 Simulations Performed

RUN	RH, %	r_o,[a] μm	$p_\infty(H_2SO_4)$,[b] ppm	$p_\infty(NH_3)$, ppm
A	90	0.1	$5.x10^{-6}$	0.01
B	85	0.1	$5.x10^{-6}$	0.01
C	95	0.1	$5.x10^{-6}$	0.01
D	90	0.01	$5.x10^{-6}$	0.01
E	90	0.1	10^{-5}	0.01
F	99	0.1	10^{-6}	0.01
G	90	0.1	$5.x10^{-6}$	0.001

(a) Initial particle radius. Composition of NaCℓ (and hence $MgCℓ_2$) are determined by assuming droplet is in equilibrium initially.

(b) Estimated by Jerskey et al. (1976) by equating rate of production in gas phase to rate of conversion to aerosol phase.

Since, at equilibrium, the water activity must approximately equal the relative humidity (depending upon the magnitude of the Kelvin effect), the humidity range which can be considered is limited by the available water activity data. From Table 5.5, a_w must be greater than approximately 0.75. Hence, the relative humidities considered must be greater than 75 percent. Another factor that must be considered is that total ionic strength, given by Eq. (5.41), must be less than about 1.0, in order to minimize the errors of extrapolation of Eq. (5.40).

The results of the seven simulations are presented in Figures 5.2-5.6. Plotted are particle radius, moles of total sulfate, pH, sulfate and ammonia concentrations vs. time in Figures 5.2-5.6, respectively.

It should be mentioned from the outset that in all cases studied, the sulfate contributed by the liquid phase oxidation reaction (Eq. 5.44) is insignificant in comparison to condensed H_2SO_4. Hence, the NH_4^+ levels (which change pH and hence the reaction rate of Eq. (5.44)) had no effect on sulfate levels.

From Figure 5.2, it is evident from cases A, B and C that radius increases with relative humidity. While particle radius is lower initially for smaller initial radius (case D), the differences between cases A and D become negligible after about 90 minutes. Particle size increases dramatically with increased $p_{H_2SO_4}$ (E), due to the solute effect. Increasing RH and decreasing $p_{H_2SO_4}$ (F) increases radius, but not to as great an extent as would be obtained were $p_{H_2SO_4}$ held constant (compare cases C and F). Finally, increasing p_{NH_3} has little effect on radius, since the ammonia levels in the liquid do not drastically reduce water activity, and, in this model, have no effect on the diffusion rate of H_2SO_4.

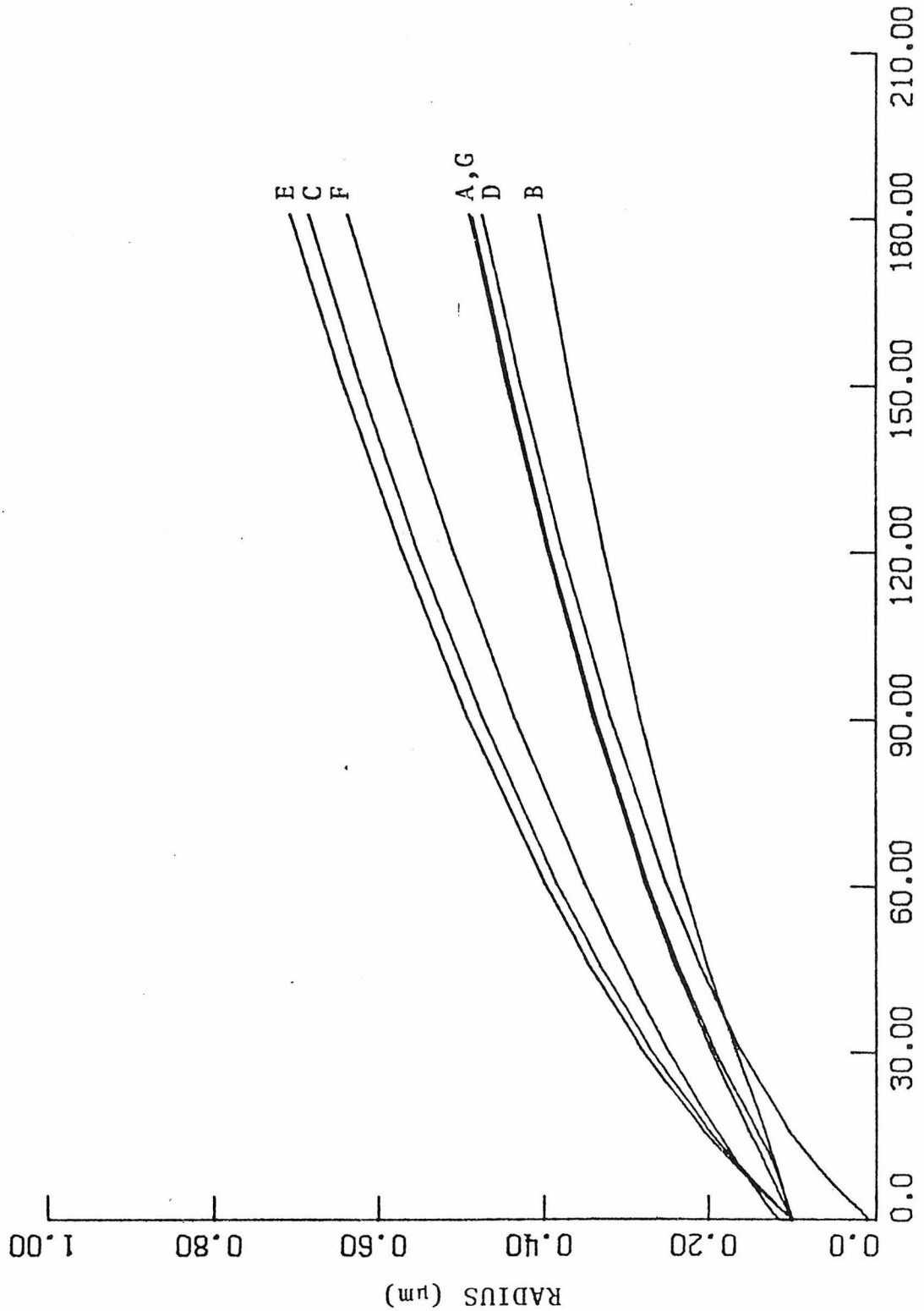

FIGURE 5.2

Particle radius (μm) vs. time (minutes).
See Table 5.7 for parameter definitions.

From Figure 5.3, we again see similar trends to those observed in Figure 5.2. As RH increases (B,A,C) total sulfate loading (μμ moles) increases slightly, since as particle radius increases H_2SO_4 condensation increases (by Eq. 5.47). For the same reason, total sulfate loading drops slightly with smaller initial radius (D). A significant increase in sulfate loading is seen for increased $p_{H_2SO_4}$ (E), as expected from Eq. (5.47), while p_{NH_3} does not affect sulfate loadings (G). When RH is increased and $p_{H_2SO_4}$ decreased (F), we obtain a decrease in total sulfate loading. This is obviously a situation where the effect of decreased $p_{H_2SO_4}$ dominates an increase in particle radius in Eq. (5.47).

Some interesting results are seen for the time dependence of pH (Fig. 5.4). As is expected, pH increases with increasing RH. Since we are dealing with a strongly acidic solution, any dilution will favor less acidic conditions. Of interest is the effect of decreasing initial particle radius (D), where the pH drops dramatically, bottoms out and then levels off. The minimum in pH is a result of the Kelvin effect, where a given ambient RH yields an equilibrium water activity that is lower than what would be experienced were the Kelvin effect unimportant. Hence, the pH drops dramatically and reaches a minimum at the radius where the Kelvin effect no longer dominates. The equilibrium a_w is then a function of RH only, and the pH levels off. As expected, increasing $p_{H_2SO_4}$ (E) lowers pH initially, but due to water equilibrium, it also eventually levels off. Increasing RH and decreasing $p_{H_2SO_4}$ (F) both act to increase pH significantly, while lowering p_{NH_3} (G), the only base in the equilibrium system, obviously decreases pH significantly.

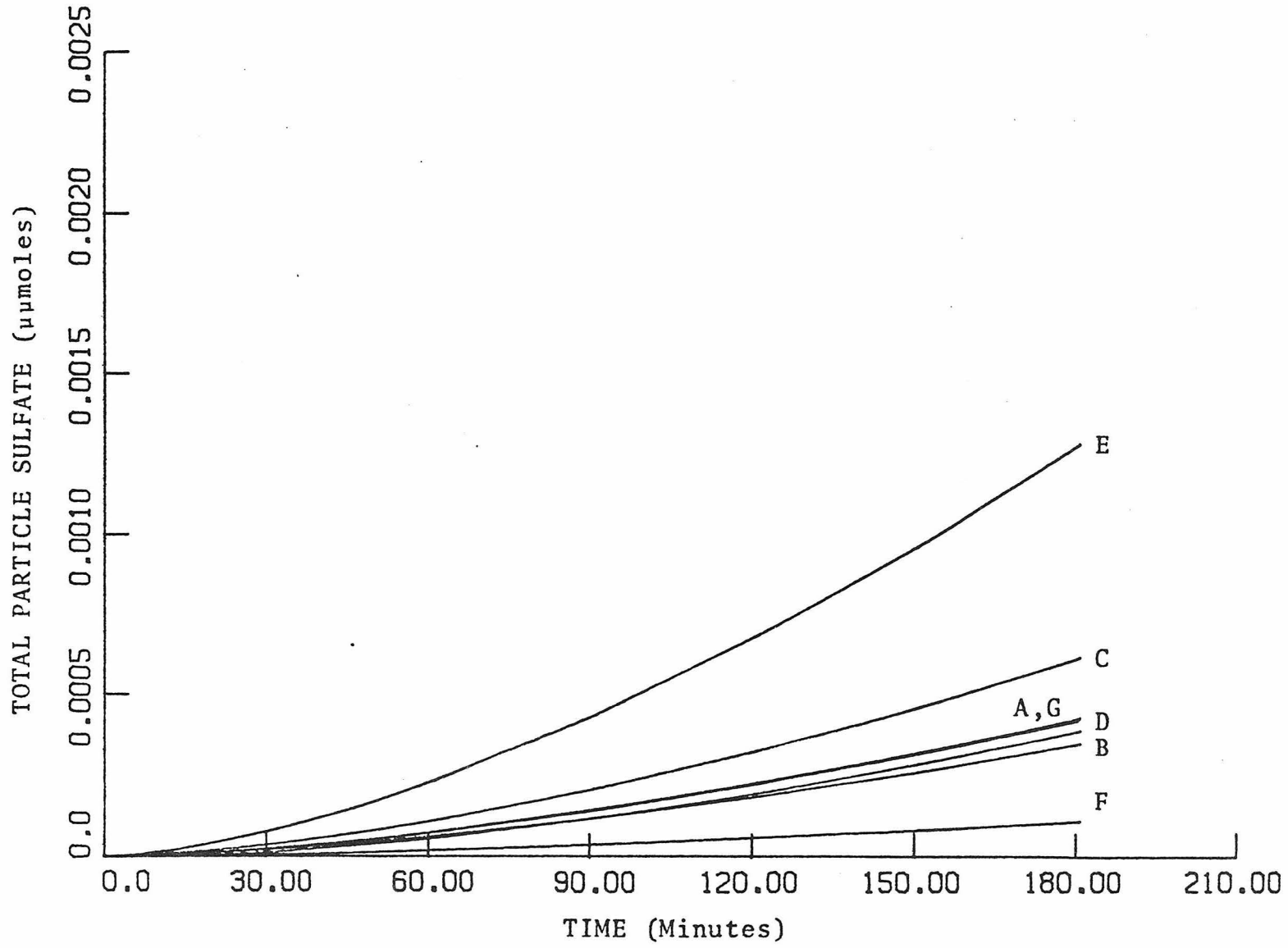

FIGURE 5.3

Total particle sulfate (μμmoles) vs. time (minutes).
See Table 5.7 for parameter definitions.

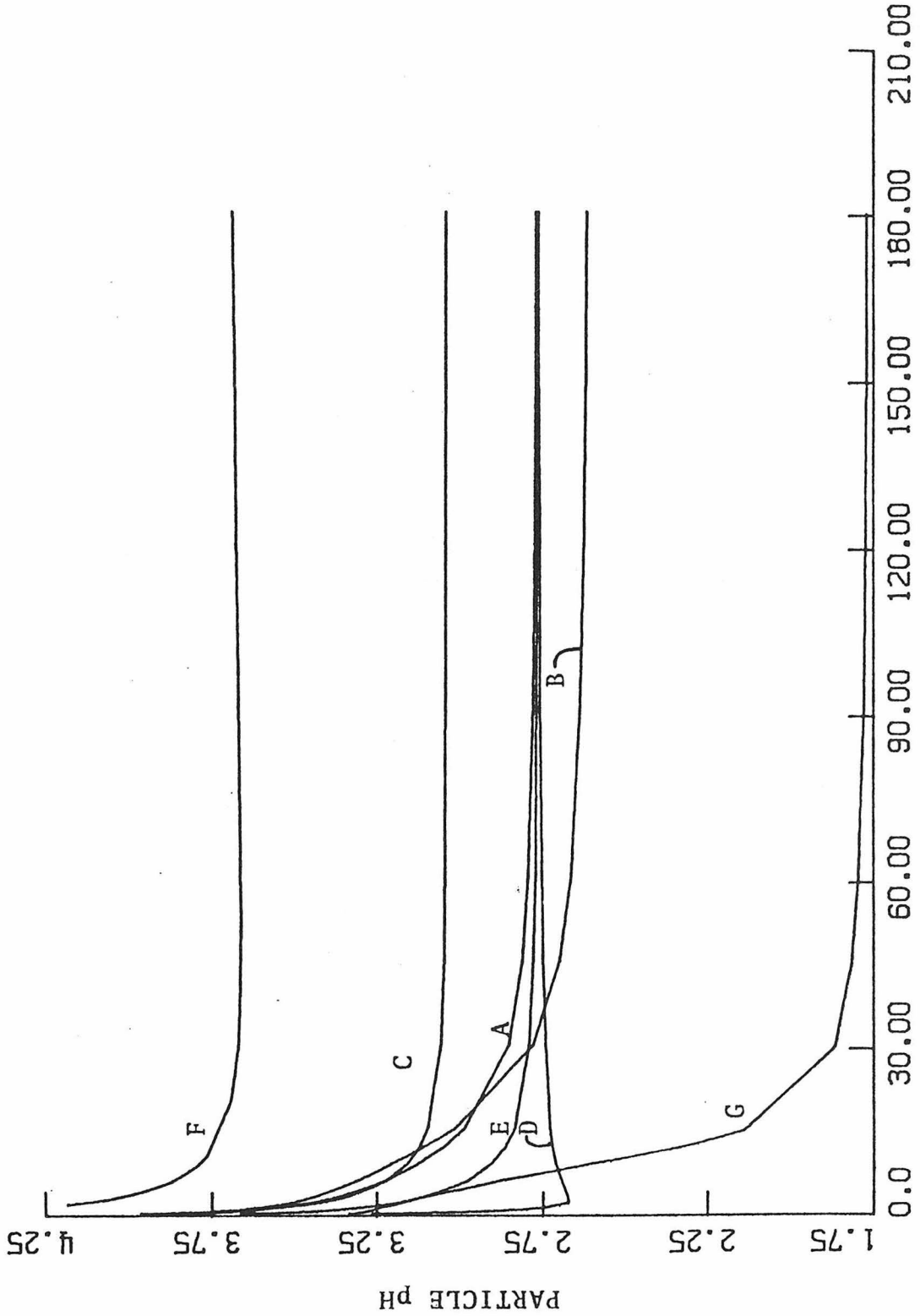

FIGURE 5.4

Particle pH vs. time (minutes)
See Table 5.7 for parameter definitions.

For long times, it is evident that for constant p_{NH_3} (A-F) pH is a function of RH only, and is independent of initial particle radius or $p_{H_2SO_4}$. Similar results are seen in the temporal variation of $[SO_4^=]$ in Figure 5.5. Increasing RH causes higher dilution and hence lower concentrations. A peak in $[SO_4^=]$ is seen for r_o = 0.01 μm(D), again due to the Kelvin effect as explained in the discussion of Figure 5.3. Increasing $p_{H_2SO_4}$ (E) causes an initial increase in $[SO_4^=]$, but the difference becomes negligible after about 30 minutes. Simultaneously lowering $p_{H_2SO_4}$ and increasing RH causes $[SO_4^=]$ to decrease dramatically as expected (F), whereas decreasing p_{NH_3} causes $[SO_4^=]$ to rise slightly initially because the equilibrium particle size is initially slightly smaller (compare curves A and G of Figure 5.2 for times less than 30 minutes).

For long times, $[SO_4^=]$ is dependent only on RH, and not on r_o, $p_{H_2SO_4}$ or p_{NH_3}.

Finally, Figure 5.6 describes the variation of $[NH_4^+]$ with time. As with $[SO_4^=]$, $[NH_4^+]$ increases as RH decreases, due to dilution. We again see the peaked behavior characteristic of the Kelvin effect for smaller particles (D), and an initial increase in $[NH_4^+]$ as $p_{H_2SO_4}$ increases (E). This is a consequence of the proportional dependence of $[NH_4^+]$ on $[H^+]$ (reactions 2 and 7 of Table 5.3). Decreasing $p_{H_2SO_4}$ and increasing RH both act to reduce $[NH_4^+]$ (F) mainly by dilution, and whereas decreasing p_{NH_3} intially lowers $[NH_4^+]$, the effect is negligible after about 60 minutes.

As with $SO_4^=$, NH_4^+ is dependent only on RH for long times, and is independent of r_o, $p_{H_2SO_4}$ or p_{NH_3}.

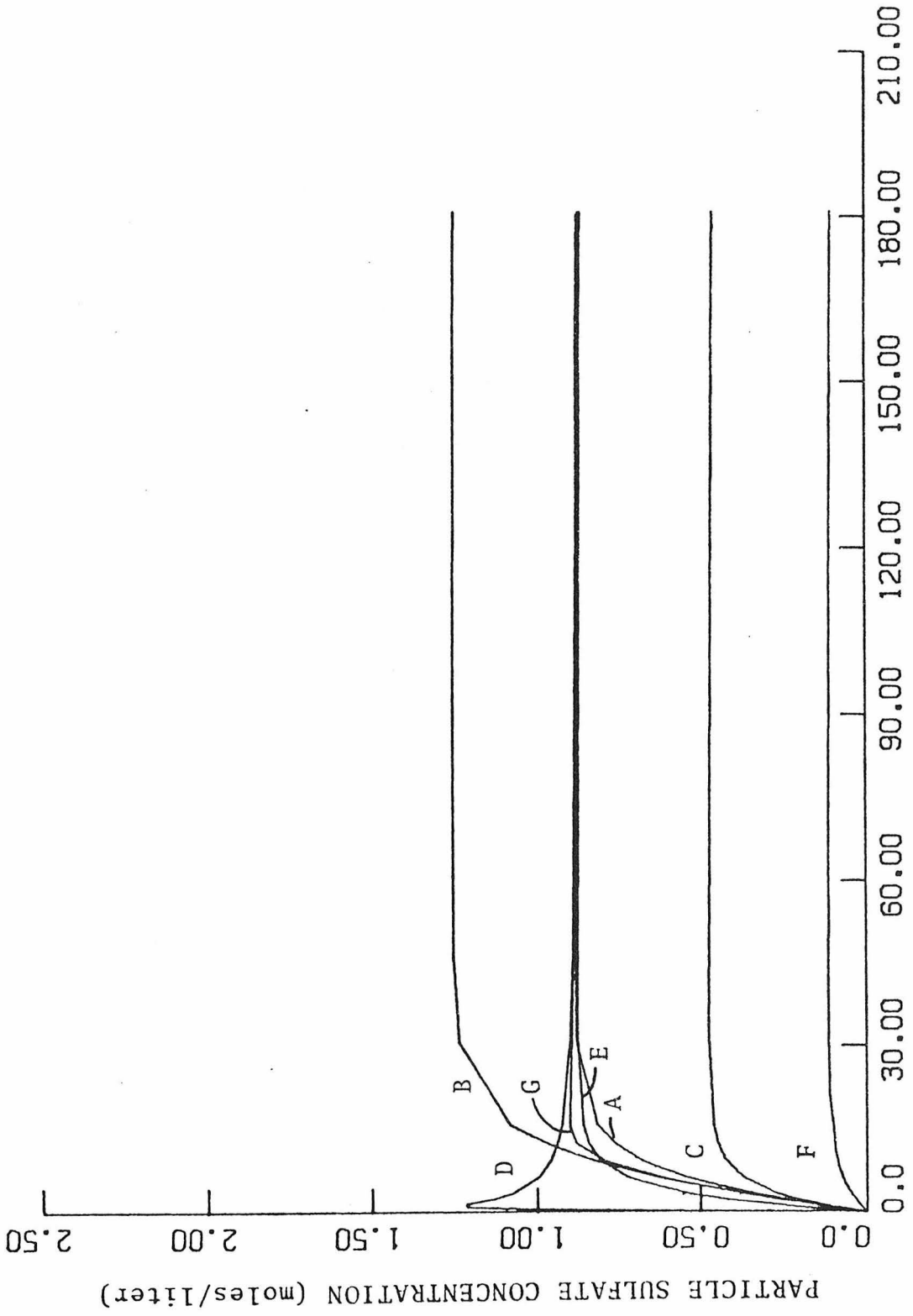

FIGURE 5.5

Particle sulfate concentration (moles/liter)vs. time (minutes).
See Table 5.7 for parameter definitions.

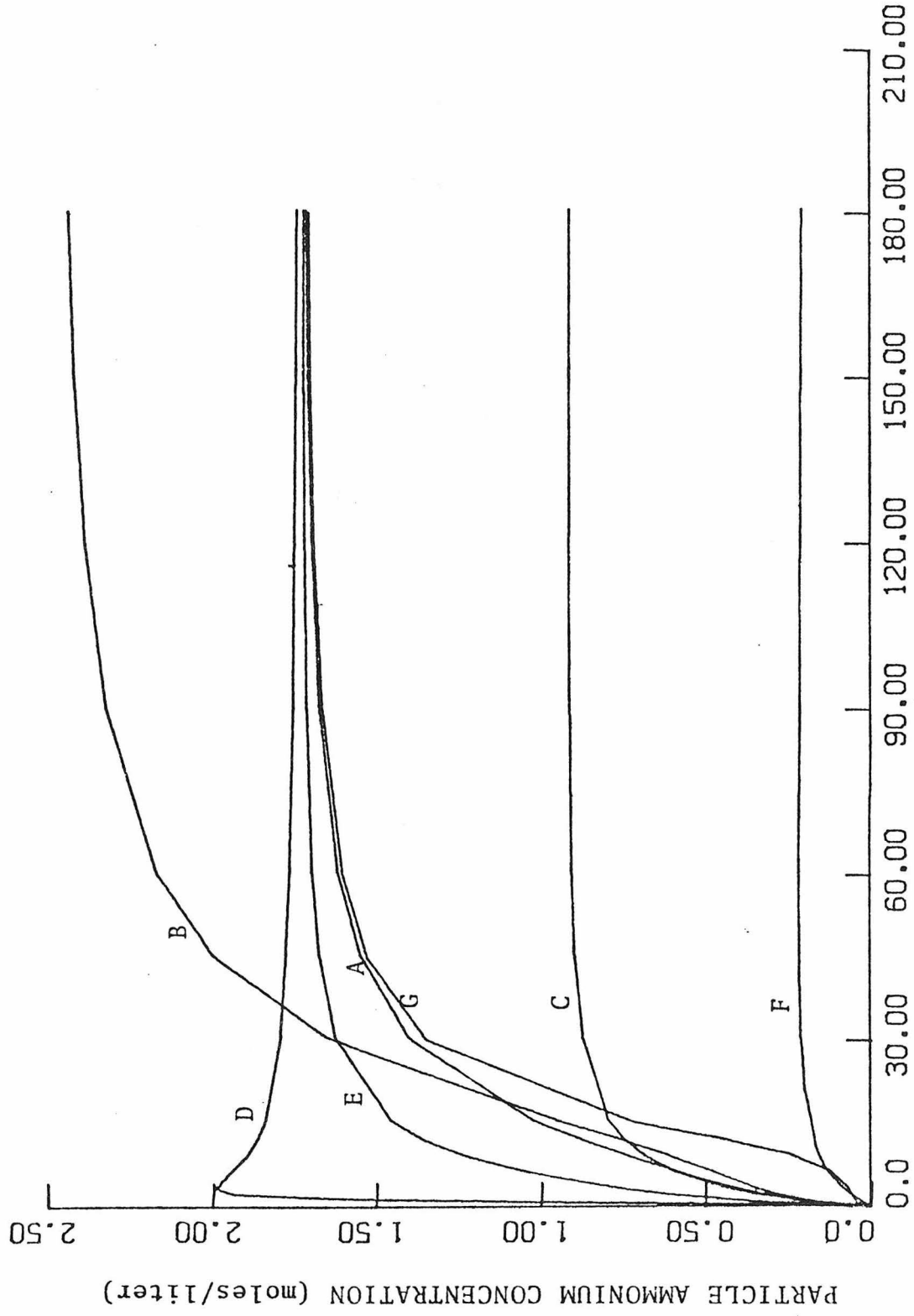

FIGURE 5.6

Particle ammonium concentration (moles/liter) vs. time (minutes)
See Table 5.7 for parameter definitions

It is difficult to determine by comparison with atmospheric data whether the particular mechanism chosen correctly models what happens in an urban airshed like Los Angeles. One very interesting point, however, is that for long times, the ratio of sulfate to ammonium concentration for all runs, regardless of RH, $p_{H_2SO_4}$ or p_{NH_3}, is very near the stoichiometric ratio of 1:2 found in the atmospherically prevalent salt $(NH_4)_2SO_4$.

F. Summary and Conclusions

In this chapter we have developed a model that describes aerosol growth including: (1) transport of vapor molecules in the gas phase, (2) transport of vapor molecules across the gas-lqiuid interface, and (3) liquid phase chemistry involving dissolved species. In principle, the model can be used to describe the detailed growth dynamics of atmospheric particles under a wide variety of circumstances, such as in power plant plumes and photochemical air pollution. An important feature of the development has been the elucidation of the parameters necessary to perform such a detailed calculation. The lack of data required to perform multicomponent aerosol growth calculations has been pointed out.

The model was applied to the growth of aqueous, salt-containing aerosols in the presence of SO_2, NH_3 and H_2SO_4. This simple system was studied first because of the relatively low ionic strength of the resultant equilibrium solution. This permitted calculation of activity coefficients with the Davies relationship, given by Eq. (5.40). The systems to be examined next are the power plant plume, (where liquid phase oxidation to sulfate proceeds by a metal-catalyzed mechanism), and the photochemical problem including dissolved oxides of nitrogen. The latter system will

require careful examination of predicted ionic strengths and activity coefficients, due to the limited applicability of Eq. (5.40), and the significant effect of dissolved NO_x on pH.

Although this work has focused on the growth of a single droplet, the extension to aerosol particles with a discrete distribution of sizes is straightforward. It is also possible to allow all gas phase concentrations of pollutants to vary with time and to allow for gas phase reactions to form condensable species. For example, in this study, we have assumed that ambient levels of both SO_2 and H_2SO_4 are time invariant, but it is also possible to allow SO_2 to vary with time, and H_2SO_4 to be a product of gas phase oxidation of SO_2.

Aside from the limitations of applicability of the equations used to predict activity coefficients and water activities (which are, to be sure, important limitations) the main drawback in performing more complete atmospheric simultations is the lack of data for systems of interest. Thermodynamic data (such as water activity) are particularly needed for the aqueous solution of a select class of organics (di-acids, organic salts, etc.) found in the atmosphere and discussed in Chapter 2.

Finally, given the fact that it is clearly impossible to experimentally validate the predictive equations for water activity of all multicomponent systems of atmospheric interest, it is recommended that experimental work be done on selected systems (such as H_2O-H_2SO_4-HNO_3-NaCℓ) to estimate the error involved in using these equations.

REFERENCES

Bassett H. and Parker W.G. (1951) The Oxidation of Sulfurous Acid. J. Chem. Soc. Pt.2,1540-1560.

Beilke S. and Georgii H.W. (1968) Investigation on Incorporation of SO_2 into Fog and Rain Droplets. Tellus 20,435-442.

Bhatnagar P.L., Gross E.P. and Krook M. (1954) A Model for Collision Processes in Gases. Phys. Rev.94(3),511-525.

Bird R.B., Stewart W.E. and Lightfoot E.N. (1960) Transport Phenomena. John Wiley and Sons, New York.

Brimblecombe P. and Spedding D.J. (1974) The Catalytic Oxidation of Micromolar Aqueous SO_2--I. Oxidation in Dilute Solutions Containing Iron (III). Atmos. Env. 8,937-945.

Brock J.R. (1966) Diffusion to Particles in the Near Free Molecule Region. J. Coll. Int. Sci. 22,513-516.

Burke M.F., Baker R.K. and Moyers J.L. (1973) Interaction of SO_2 with airborne Particulate Matter. J. Chrom. Sci. 11(11), 575-578.

Chang R. and Davis E.J. (1976) Knudsen Aerosol Evaporation. J. Coll. Int. Sci. 54(3),352-363.

Chen T. and Barron C.H. (1972) Some Aspects of the Homogeneous Kinetics of Sulfite Oxidation. Ind. Eng. Chem. Fund. 11,446-470.

Cheng R.T., Corn M. and Frohliger J.O. (1971) Contribution to the Reaction Kinetics of Water Soluble Aerosols and SO_2 in Air at ppm Concentrations. Atmos. Env. 5,987-1008.

Daniels F. and Alberty R.A. (1967) Physical Chemistry, 3rd Ed., John Wiley and Sons, New York.

El Golli S., Bricard J., Turpin P.Y. and Treiner C. (1974) The Evaporation of Saline Droplets. Aerosol Sci. 5,273-292.

El Golli S., Arnaud G., Bricard J. and Treiner C. (1977) Evaporation of Volatile Solvent from Saline Multi-Component Droplets Carried in a Stream of Air. J. Aerosol Sci. 8,39-54.

Espenson J.H. and Taube H. (1965) Tracer Experiments with Ozone as Oxidizing Agent in Aqueous Solution. Inorg. Chem. 4,704-709.

Foster P.M. (1969) The Oxidation of SO_2 in Power Station Plumes. Atmos. Env. 3,157-175.

Freiberg J. (1974) Effects of Relative Humidity and Temperature on Iron-Catalyzed Oxidation of SO_2 in Atmospheric Aerosols. Env. Sci. Tech. 8(8),731-734.

Freiberg J. (1975) The Mechanism of Iron Catalyzed Oxidation of SO_2 in Oxygenated Solutions Atmos. Env. 9,661-672.

Freiberg J. (1976) The Iron Catalyzed Oxidation of SO_2 to Acid Sulfate Mist in Dispersing Plumes. Atmos. Env. 10,121-130.

Fuchs N.A. (1959) Evaporation and Droplet Growth in Gaseous Media. Pergamon Press, Oxford.

Fuchs N.A. and Sutugin A.G. (1971) High Dispersed Aerosols, in Topics in Current Aerosol Research (G.M. Hidy and J.R. Brock, Eds.) Pergamon Press, Oxford.

Fuller E.C. and Crist R.H. (1941) The Rate of Oxidation of Sulfite ions by Oxygen. J. Am. Chem. Soc. 63,1644-1650.

Grosjean D. and Friedlander S.K. (1975) Gas-Particle Distribution Factors for Organic and Other Pollutants in the Los Angeles Atmosphere. J. Air Poll. Cont. Assoc. 25(10),1038-1044.

Hales J.M. and Sutter S.L. (1973) Solubility of SO_2 in Water at Low Concentrations. Atmos. Env. 7,997-1001.

Hamill P. (1975) The Time Dependent Growth of H_2O-H_2SO_4 Aerosols by Heteromolecular Condensation. J. Aerosol Sci. 6, 475-482.

Harrison H. (1976) Private Communication to J.H. Seinfeld.

Heisler S.L. (1976) Gas-to-Particle Conversion in Photochemical Smog: Growth Laws and Mechanisms for Organics. Ph.D. Thesis, Calif. Inst. of Tech.

International Critical Tables (1928) First Edition, 3,258.

Jerskey T.N., Seinfeld J.H., Gelbard F. and Reid L.E. (1976) Continued Research in Mesoscale Air Pollution Simulation Modelling: Vol. VII -- Mathematical Modelling of Urban Aerosol Dynamics. Cont. No. 68-02-2216,EF76-144, U.S.E.P.A.

Johnstone H.F. and Leppla P.W. (1934) The Solubility of SO_2 at Low Partial Pressures. J. Am. Chem. Soc. 56,2233-2238.

Junge C.E. and Ryan T.G. (1958) Study of the SO_2 Oxidation in Solution and Its Role in Atmospheric Chemistry. Q.J.R. Met. Soc. 84,46-55.

Lees L. (1959) A Kinetic Theory Description of Rarfied Gas Flows. GALCIT Hyper. Res. Proj. No. 51, Calif. Inst. Tech.

Low R.D.H. (1969) A Generalized Equation for the Solution Effect in Droplet Growth. J. Atmos. Sci. 26,608-611.

Loyalka S.K. (1973) Condensation on a Spherical Droplet. J. Chem. Phys. 58(1),354-356.

Marshak R.E. (1947) The Variational Method for Asymptotic Neutron Densities. Phys. Rev. 71(10),688-697.

Matteson J.J., Stober W. and Luther H. (1969) Kinetics of the Oxidation of SO_2 by Aerosols of Manganese Sulfate. Ind. Eng. Chem. Fund. 8,677-687.

McDonald J.E. (1953) Erroneous Cloud-Physics Applications of Raoult's Law.J. Meteor. 10,68-70.

McKay H.A.C. (1971) The Atmospheric Oxidation of SO_2 in Water Droplets in Presence of Ammonia. Atmos. Env. 5,7-14.

McMurry P.H. (1977) On the Relationship Between Aerosol Dynamics and the Rate of Gas-to-Particle Conversion. Ph.D. Thesis, Calif. Inst. Tech.

Miller J.M. and de Pena R.G. (1972) Contribution of Scavenged SO_2 to the Sulfate Content of Rain Water. J. Geophys. Res. 77,5905-5916.

Mirabel P. and Katz J.L. (1974) Binary Homogeneous Nucleation as a Mechanism for the Formation of Aerosols. J. Chem. Phys. 60(3),1138-1144.

Morgan O.M. and Maass O. (1931) Investigations of the Equilibria Existing in Gas-Water Systems Forming Electrolytes. Can. J. Res. 5,162-199.

Moskowitz A.H. (1977) Particle Size Distribution of Nitrate Aerosols in the Los Angeles Air Basin. EPA Rpt. EPA-600/3-77-053.

Nair P.V.N. and Vohra K.G. (1975) Growth of Aqueous H_2SO_4 droplets as a Function of Relative Humidity. J. Aerosol Sci.6, 265-271.

Novakov T., Chang S.G. and Harker A.B. (1974) Sulfates in Pollution Particulates: Catalytic Oxidation of SO_2 on Carbon Particles. Science 186,259-261.

Orel A.E. and Seinfeld J.H. (1977) Nitrate Formation in Atmospheric Aerosols. Submitted for publication, Env. Sci. Tech.

Penkett S.A. (1972) Oxidation of SO_2 and other Atmospheric Gases by Ozone in Aqueous Solution. Nature, Phys. Sci. 240, 105-106.

Penkett S.A. and Garland J.A. (1974) Oxidation of SO_2 in Artificial Fogs by Ozone. Tellus 26,284-290.

Perry J.H. (1974) Chemical Engineer's Handbook, 4th Ed. McGraw-Hill, New York.

Reiss H. (1951) The Kinetics of Phase Transitions in Binary Systems. J. Chem. Phys. 18(6),840-848.

Robinson R.A. (1936) The Dissociation Constant of HCl. Trans. Farad. Soc. 32,743-744.

Robinson R.A. and Stokes R.H. (1965) Electrolyte Solutions. Butterworths, London.

Sahni D.C. (1966) The Effect of a Black Sphere on the Flux Distribution in an Infinite Moderator. J. Nucl. En. A/B 20, 915-919.

Sampson R.E. and Springer G.S. (1969) Condensation on and Evaporation From Droplets by a Moment Method. J.F.M. 36(3), 577-584.

Sander S.P. and Seinfeld J.H. (1976) Chemical Kinetics of Homogeneous Atmospheric Oxidation of SO_2. Env. Sci. Tech. 10 (12),1114-1123.

Sangster J. and Lenzi F. (1974) On the Choice of Methods for the Prediction of the Water-Activity and Activity Coefficient for Multicomponent Aqueous Solutions. Can. J. Chem. Eng. 52, 392-396.

Scott W.D. and Hobbs P.V. (1967) The Formation of Sulfate in Water Droplets. J. Atmos. Sci. 24,54-57.

Shankar P.N. (1970) A Kinetic Theory of Steady Condensation. J.F.M. 40(2),385-400.

Skinner L.M. and Sambles J.R. (1972) The Kelvin Equation -- A Review. Aerosol Sci. 3,199-210.

Stokes R.H. and Robinson R.A. (1966) Interactions in Aqueous Nonelectrolyte Solutions I. Solute Solvent Equilibria. J. Phys. Chem. 70(7),2126-2131.

Teng T.T. and Lenzi F. (1974) Water Activity Data Representation of Aqueous Solutions at 25° C. Can. J. Chem. Eng. 52,387-391.

van den Heuvel A.P. and Mason B.J. (1963) The Formation of Ammonium Sulfate in Water Droplets Exposed to Gaseous SO_2 and NH_3. Q.J.R. Met. Soc. 89,271-275.

Wadden R.A., Quon J.E. and Hulburt H.M. (1974) A Model of a Growing Coagulating Aerosol. Atmos. Env. 8,1009-1028.

Yue G.K. (1976) A Better Parameter for the Solution Effect in Droplet Growth. Atmos. Sci. Res. Cntr., S.U.N.Y., Albany.

Yui T. (1940) On the Electrolytic Dissociation Constant of Sulfurous Acid. Tokyo Inst. Phys. Chem. Res. Bull. 19,1229-1236.

Zdanovskii A.B. (1936) Trudy Solyanoi Laboratorii Akad, Nauk SSSR,6.

CHAPTER VI

SUMMARY

In this work, we have solved three preliminary problems that will serve to initiate the development of a general mathematical model to describe the dynamics of an urban aerosol particle distribution. First, we have analytically solved the steady-state diffusion equation including settling, deposition and first order removal, which allowed us to predict expected levels of gaseous and particulate pollutants from pollutant emissions inventories. This enabled us to perform material balance calculations, the main purpose being to determine the relative roles of conversion and removal in governing gaseous and particulate concentration levels. The model was then applied to the prediction of gaseous and particulate pollutant material balances in the Los Angeles airshed and downwind. In so doing, the following areas of further study (for the L.A. region) were delineated:

1.) Detailed study is needed of the mechanisms of conversion of NO_x to nitrate in urban atmospheres.

2.) The specific hydrocarbons that are organic aerosol precursors need further identification; their emission rates from urban sources require elucidation; and the specific mechanisms for their conversion to particulate organics require study.

Second, the dynamic behavior of an aerosol size distribution undergoing coagulation, condensation, nucleation and removal was studied analytically. These analytic solutions aided in determining the characteristics

of the particle size distribution as it was influenced by these mechanisms, and contributed valuable insight into the importance of these mechanisms in the urban atmosphere. This work also provided exact solutions against which numerical routines to solve the general dynamic equation can be tested.

Finally, we studied the problem of particle growth by heterogeneous condensation and chemical reaction. Here, the major objective was to develop a general framework through which one can describe the simultaneous processes of condensation on and chemical reaction within growing aerosol particles. By applying this model to a realistic atmospheric problem, the thermodynamic data and important parameters necessary to perform such a detailed calculation were elucidated. From this, we concluded that there was a need for more extensive data on water activities for multicomponent solutions typical of the polluted atmosphere.

The development of a general mathematical model to describe aerosol dynamics in a polluted atmosphere is a very difficult task. The inclusion of physical as well as chemical processes governing the distribution, in addition to the inherent heterogeneity of a particle size distribution, considerably complicates the already significant numerical problems of atmospheric modeling. It is hoped that this work has contributed to the initial stages of development of an aerosol model, and that the contributions herein will further that goal.